https://theses.gla.ac.uk/

Theses Digitisation:

https://www.gla.ac.uk/myglasgow/research/enlighten/theses/digitisation/

This is a digitised version of the original print thesis.

Copyright and moral rights for this work are retained by the author

A copy can be downloaded for personal non-commercial research or study, without prior permission or charge

This work cannot be reproduced or quoted extensively from without first obtaining permission in writing from the author

The content must not be changed in any way or sold commercially in any format or medium without the formal permission of the author

When referring to this work, full bibliographic details including the author, title, awarding institution and date of the thesis must be given

Enlighten: Theses
https://theses.gla.ac.uk/
research-enlighten@glasgow.ac.uk

ASPECTS OF ARTICULATED COLUMN DESIGN INCLUDING RIGID BODY AND ELASTIC VIBRATION

BY

ALAN B.HILL BSc MEng MICE

A THESIS SUBMITTED FOR THE DEGREE OF MASTER OF SCIENCE IN THE DEPARTMENT OF NAVAL ARCHITECTURE AND OCEAN ENGINEERING AT THE UNIVERSITY OF GLASGOW

MAR 1988

© A.B.HILL, 1988

ProQuest Number: 10997910

All rights reserved

INFORMATION TO ALL USERS
The quality of this reproduction is dependent upon the quality of the copy submitted.

In the unlikely event that the author did not send a complete manuscript
and there are missing pages, these will be noted. Also, if material had to be removed,
a note will indicate the deletion.

ProQuest 10997910

Published by ProQuest LLC (2018). Copyright of the Dissertation is held by the Author.

All rights reserved.
This work is protected against unauthorized copying under Title 17, United States Code
Microform Edition © ProQuest LLC.

ProQuest LLC.
789 East Eisenhower Parkway
P.O. Box 1346
Ann Arbor, MI 48106 – 1346

ABSTRACT

The work contained in this thesis mainly relates to aspects of the dynamic behaviour of articulated column production platforms. However, the work can be applied in a more general sense to certain other compliant structures which share some of the dynamic characteristics of articulated columns.

After an introductory chapter on the characteristics and uses of articulated columns, some time is devoted to the examination of fundamental aspects which will have an important bearing on the feasibility of the articulated column concept. Such features as the amount of buoyancy required in terms of payload and static heel considerations, space utilisation within the structure, installation procedure and human awareness to motion responses are, discussed. Data are provided which are intended to give general guidance to designers and also establish the inter-dependence of certain parameters.

Chapters 4 and 5, are concerned with the rigid body motion response in the time domain. Computer programs have been developed to solve the equations of motion on a time incremental basis, using the modified Morison equation as the forcing function. Once developed, the programs have been applied to examine certain of the non-linear behaviour characteristics of articulated columns in regular waves. Chapter 5 is devoted to examining those aspects of dynamic instability which are readily examined in a time series analysis. Instability mechanisms examined are those due to regular waves and wave groups. Experimental results have been obtained and comparisons with theory are made.

The slenderness of the construction of articulated columns gives rise to elastic vibration characteristics which may result in undesirable resonant vibrations. Chapter 6 is concerned with an examination of this aspect, in terms of free vibration analysis, and of those parameters which have the greatest influence on vibration. The finite element method has been used for the free vibration analysis.

In Chapter 7, the development of programs to examine the full vibration analysis of articulated columns, in the time domain, is described. The programs have been used to examine, in the time domain, certain of those parameters which were examined in the free vibration analysis presented in Chapter 6. Some experimental results for a very flexible structure are presented and the programs have been adapted to simulate the model construction and test conditions. These results give credibility to the use of a full vibration analysis in the time domain and comparisons of observed non-linear behaviour and predicted non-linear behaviour are made.

The non-linear behaviour of articulated columns is shown to play a major part in concept feasibility as are elastic vibration characteristics. However, the concept comprising a lower column of relatively straightforward structural section is shown to be feasible in water depths up to 300 metres. Thereafter, greater flexural rigidity is required.

ACKNOWLEDGEMENT

The author expresses his gratitude both to Professor D Faulkner, for the opportunity to undertake and continue this work, and to the Scientific and Engineering Research Council who provided the necessary funding.

My express gratitude is to Mr N S Miller whose vigilant supervision and unstinting discussion have contributed greatly to the endeavours during the research period.

Thanks are also recorded to Dr A M Ferguson for allowing the use of the testing facilities which has been an essential aspect of this work.

Mr and Mrs E Peters are thanked for all their help during the final months in the typing of this work and their selfless endeavours in this respect are acknowledged.

Thanks are also recorded to all the laboratory technicians for their assistance in manufacturing models and providing the necessary instrumentation.

Mr J McCallum is also thanked for his impeccable work in the production of drawings and illustrations.

Last, but by no means least, my thanks go to my wife Cecilia for her support, both moral and material, and encouragement throughout the period of research.

DECLARATION

Except where reference is made to the work of others, this thesis is believed to be original

* *

CONTENTS

LIST OF FIGURES

NOMENCLATURE

a	variable in vibration analysis $=\sqrt{EI/\rho As}$
a_a	apparent amplitude of group waves
a_i, i=1,2	group wave amplitude
a_o	regular wave amplitude
A	equivalent shape functions for beam element displacements
A_a	amplitude of wave group envelope
A_o	arbitrary constant
A_p	projected area
A_s	cross section area
B	appropriate derivative of shape functions [A]
B_F	buoyancy force
B_o	arbitrary constant
c	wave celerity
C	damping matrix
C_A	added virtual mass coefficient
C_D	drag coefficient
C_{DC}	current drag coefficient
C_{DW}	wind drag coefficient
C_{DL}	equivalent linearisation of drag = $8u_0/3\pi$ x C_D
C_{DW}	wind drag coefficient
C_M	inertia coefficient
CVR_1,CVR_2, etc	added mass coefficients for cylinder of radius R_1 and length L_1, etc
d	water depth
D	diameter of cylinder
DC	deck clearance
DW	deck width
E	Young's modulus of elasticity
F	force vector
F_D	drag component of force
F_{eq}	equivalent nodal load force vector

F_I	inertia component of force
F_o	maximum steady state force
F_T	total force vector
g	gravitational constant
$H(\omega)$	frequency response function
I	second moment of area of section
I	identity matrix = $M^{-1}M$ (Chapter 6)
I_{AV}	added mass moment of inertia about articulation
I_M	mass moment of inertia about articulation
I_T	total mass moment of inertia about articulation
J	three dimensional flow coefficient = 0.635
J_1'	derivative of Bessel function of first order
k, k_1, k_2	wave numbers = $2\pi/L$
K	elastic stiffness coefficients
K_{DS}	Dieckmanns sensitivity coefficient
K_G	geometric elastic stiffness coefficients
K_s	pendulum stiffness of articulated column
ℓ	length of beam column element
L	wave length
L_1	submerged depth of upper support column
L_2	length of buoyancy chamber
L_3	length of lower column
L_p	distance from SWL to deck
m	mass per unit length of element
M	mass of element
M_1 etc	lumped mass (Chapter 6)
M_D	moment of drag forces about articulation
MF	full width matrice
M_I	moment of inertia forces about articulation
MS	semi-band width of matrice
M_θ	total moment of forces about articulation
M_ψ	moment of forces about vertical axis

n	n^{th} vibration mode
N	total number of degrees of freedom
p	fluid pressure distribution
P	axial load on element
q	Eigen vectors
r	radius from articulation
r_i, i=1-4	finite elemental degree of freedom notation
r^*	internal displacements
$r_s(t)$	rigid body steady state response at time t
R	plan radial distance from centre of cylinder
R_o	rigid body maximum steady state response
R_1	radius of upper support column
R_2	radius of buoyancy chamber
R_3	radius of lower column
RKC	distance from articulation to centre of current forces
RKB	distance from articulation to centre of buoyancy
RKG	distance from articulation to centre of gravity
RKW	distance from articulation to centre of wind pressure
s	integration variable along length of finite element
S	surface force vector
t	instantaneous time
$\bar{T}$	total heave force
$\bar{T}_D$	drag heave force
$\bar{T}_I$	inertia heave force
$\bar{T}_o$	excess buoyancy force
u	horizontal water particle velocity
u	horizontal water particle acceleration
U	displacement vector
U_s	strain energy for virtual displacement
v	vertical water particle velocity
v	vertical water particle acceleration
V	volume displaced
V_c	current velocity
V_w	wind velocity

$w_{i,\ i=1-3}$	weighting functions for Gauss quadrature integration
W	weight of structure
W_E	external work done due to virtual displacement
x	horizontal co-ordinate scalar quantity
$\dot{x}$	first derivative of x wrt time
$\ddot{x}$	second derivative of x wrt time
$x_{i,\ i=1,3}$	value of function f(x) to integrate function between specified limits using Gauss quadrature
X	normal function
$\bar{X}_D$	drag component of pitching force
$\bar{X}_I$	inertia component of pitching force
$\bar{X}_o$	amplitude of forced oscillation
y	depth measured from still water level (SWL)
Y_n	generalised co-ordinates
Y_1	derivative of Bessel function of 2nd order
z	horizontal co-ordinate
Z	body force vector
α	coefficients in Newmark integration
α	element inclination (Chapter 6)
β	percentage critical damping
γ	damping coefficient
γ	element co-ordinate transformation coefficients (Chapter 6)
γ_1	nodal co-ordinate transformation coefficients (Chapter 6)
δ	coefficient in Newmark integration algorithm
δ	logarithmic decrement of damping (Chapter 5)
ε	elastic strain
ξ	phase angle between excitation and response
η_t	wave profile

θ	coefficient in Newmark-Wilson algorithm (Chapter 7)
θ	pitch rotation about vertical axis
$\dot{\theta}$	first derivative of wrt time
$\ddot{\theta}$	second dervative of wrt time
μ	damping coefficient
π	constant = 3.142
ρ	water density
σ	elastic stress
ϕ	mode shape vector
Φ_G	velocity potential for generated or radiated wave
Φ_I	velocity potential for undisturbed incident wave
$\Phi_{j,j=1,n}$	velocity potential for generated wave for mode j
Φ_S	velocity potential for undisturbed incident wave
$\omega, \omega_1, \omega_2$	wave frequency
ω_n	natural frequency in pitch of structure
ω_a	frequency of apparent group wave

CHAPTER 1

INTRODUCTION AND OVERVIEW

1. INTRODUCTION

Forecasting the demand for, and availability of, offshore hydrocarbons is fraught with uncertainty. However, certain references (1) indicate that approximately two thirds of estimated future potential crude oil discoveries will be made offshore. One third will be within the continental shelf regions in water depths not exceeding 200 metres, while the other third will be in deep water and polar regions.

Other references (2, 3) indicate that as water depths increase there will be considerably more attention given to production platforms of a more cost effective genre than conventional fixed platforms. In addition to costs, technical limits in respect of fundamental vibration modes are reached with fixed platforms as water depths increase. Figure 1.1 indicates that deep water hydrocarbon extraction will be possible by 1985 to 1990. The chronology is suspect and at present the fixed platform technology available will only allow extraction in maximum water depth of approximately 300 metres. The relatively long lead times associated with the development of new concepts make it necessary that research be undertaken well in advance of anticipated requirements.

Floating production systems based either on semi-submersibles or large tankers are attractive alternatives to fixed platforms. The

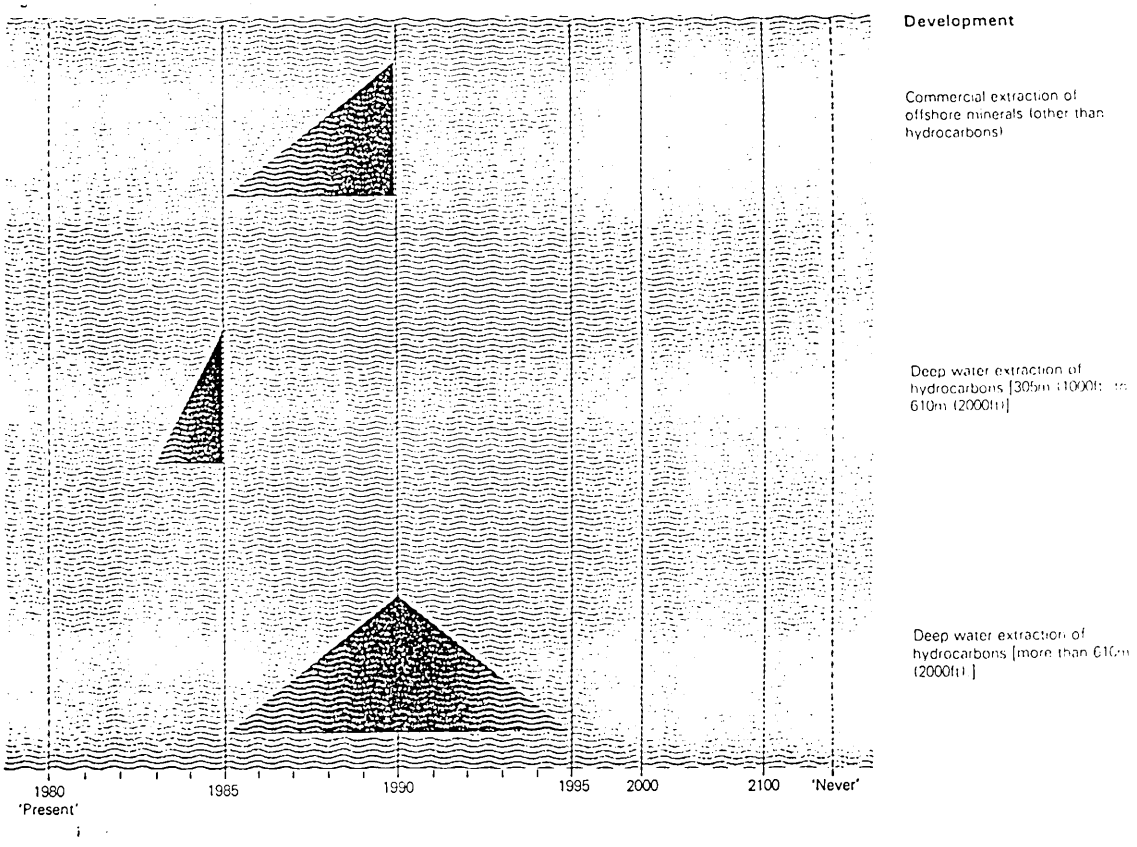

OFFSHORE PRODUCTION SYSTEMS REF (3)
FIG 1.1

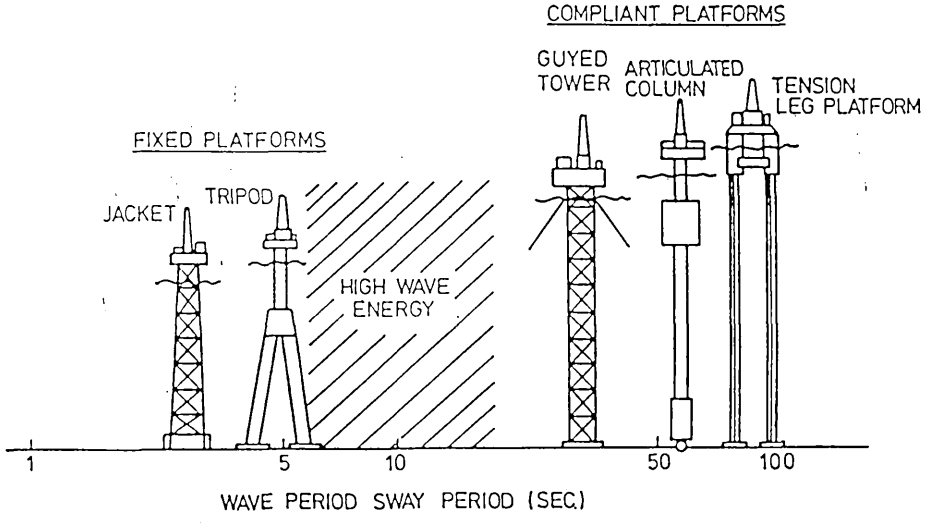

FIG 1.2

former are generally moored in a 'fixed' position and orientation and only move within the restraints imposed by their moorings. The most serious of these from the riser design point of view is the vertical (heave) movement although this is being overcome by flexible risers. In deeper water the problem of mooring becomes very severe due to the mass of cable or chain involved and unless some new material such as KEVLAR can be brought into use, will impose a definite limit on this type of vessel. Its other great weakness is the lack of storage capacity. This is overcome by using a tanker but in this case it is impossible to moor the vessel in a fixed position and it must be allowed to rotate to be substantially head on to the sea and wind forces. This is achieved by mooring to a buoy or articulated column which must incorporate the risers plus a swivel to allow the vessel to rotate while accepting a continuous flow of oil and gas. These tanker mooring towers are one of the widest uses of articulated columns at present. The large storage in the tanker means that the export vessel need only call at intervals of a few days and there is little downtime on the export side. Floating production systems in the form of a tanker permanently moored and containing all of the processing equipment is another alternative. One such system is the CADLAO FPS in the Phillipines (4) which is operated by the Amoco oil company. The system has been operational since 1981 and has a minimum record of downtime.

Fixed jacket structures are limited by technical considerations in respect of fundamental sway periods, to maximum water depths of the order of 300 metres. The transition from one side of the spectrum to the other, as shown in fig. 1.2, is effected by allowing compliancy of the structure with waves. Compliant structures allow some lateral sway motion with waves while keeping vertical

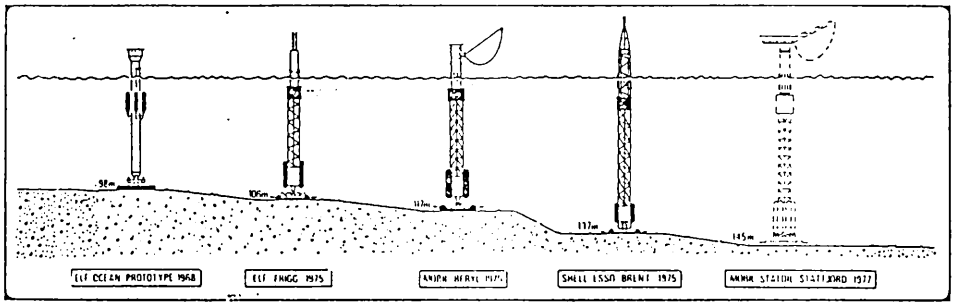

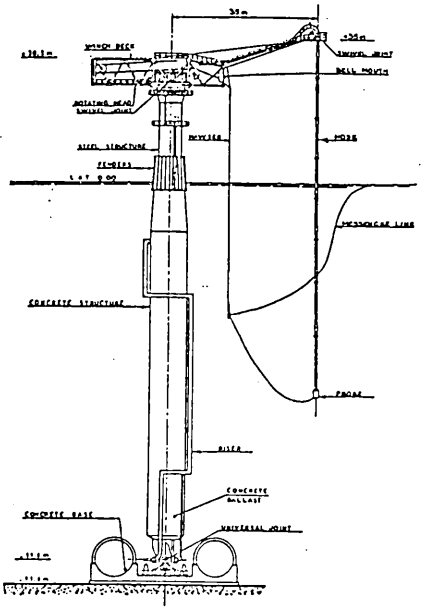

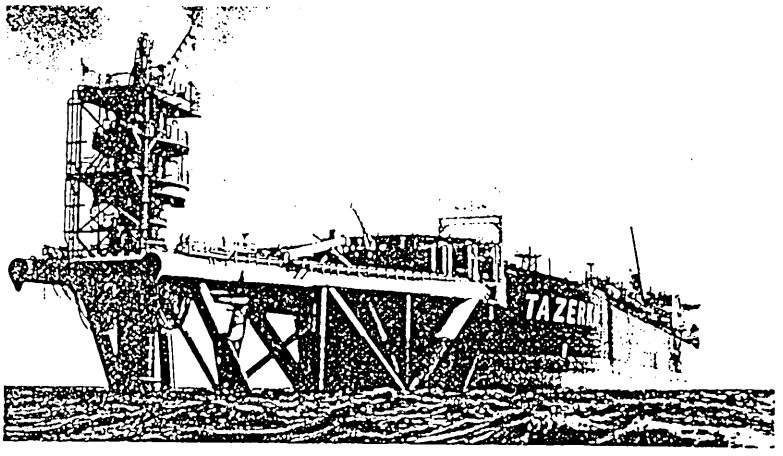

Gravity-Base SALS At Tazerka

SOME EXISTING APPLICATIONS

DEEP WATER GRAVITY TOWER

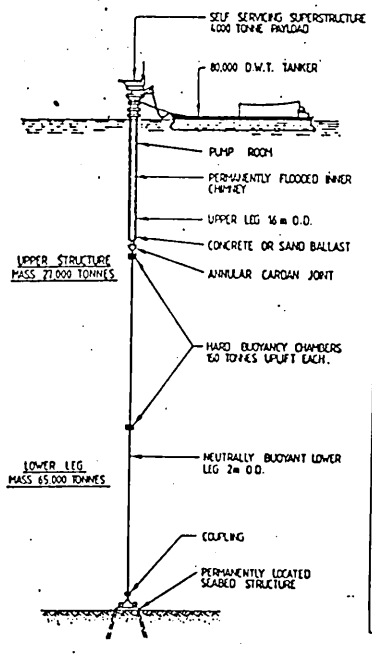

– General arrangement of deepwater towers.

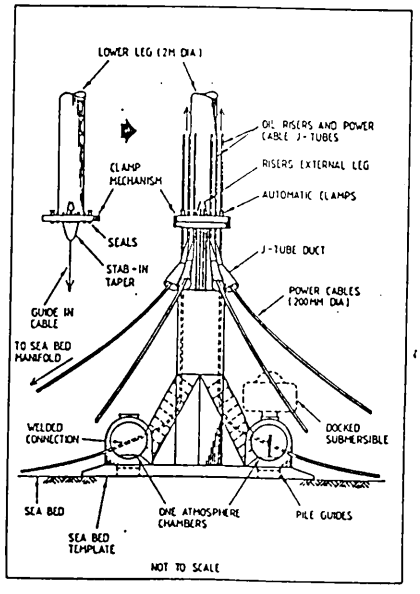

– Seabed structure.

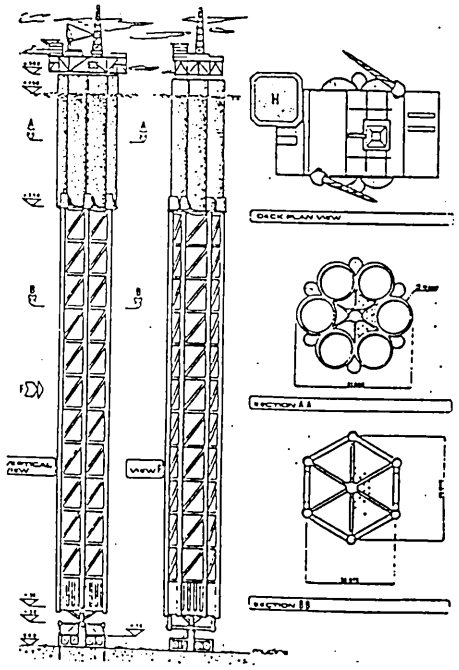

FIG 1.3

PROPOSED APPLICATIONS

movements to a very low level. This avoids overloading drill stems and risers and achieves the transition from one side of the spectrum to the other in respect of fundamental vibration modes. However, while the fundamental natural frequencies may decrease, other vibration considerations in respect of higher modes become increasingly important as is shown in subsequent chapters.

A deepwater compliant riser system is proposed by the Mobil company (5). This system basically comprises a central structural core to which are attached the peripheral rigid risers. Buoyancy support for the central core is provided by a chamber which is at a depth of some 200 feet beneath the still water level. Flexible pipes complete the transition from the subsurface buoyancy chamber to the moored tanker, which contains the production equipment. The depth of submergence of the buoyancy chamber greatly reduces exciting forces and so motion responses on the lower structure will be very small. The array of flexible pipes, on the other hand, are in the most active wave region and will have to sustain considerable loads.

Guyed towers (GT), Tension Leg Platforms (TLP) and Articulated Columns (AC), are those structures generally associated under the broader term 'compliant systems'. A review of the relative merits of each is given in Reference 6.

2. EXISTING APPLICATIONS

Articulated columns have been successfully used in the North Sea and elsewhere, for a number of years, mainly as loading terminals and flare columns, and their suitability has been established.

The articulated column ELFOCEAN (5), was installed in 100 metres of water in the bay of Biscay in 1968. Buoyancy tanks are provided near to the surface of the 7 metre diameter steel column and ballast is provided near to the base of the structure. ELFOCEAN was operational for 3 years during which time extensive tests confirmed the suitability of the concept in application as a mooring column for oil tankers and as flare stacks. The studies concluded, in part, that loading of tankers in the bay of Biscay could continue for 85-90% of the time compared to 70-75% of the time in the case of conventional mooring terminals.

Articulated columns have also been successfully used in the Beryl; Statfjord and Maureen fields as loading columns. The Maureen column is placed in approximately 100 metres of water (8). The main column is constructed of pre-stressed concrete and is 9 metres diameter with a wall thickness of 300 mm. The Statfjord C articulated loading column (9) recently commissioned is 196m long overall and is probably the largest articulated column commissioned so far. This is a significant step in terms of water depths and is an indication of the increased awareness among operators as to the potential of the articulated column concept. Some examples of the structures mentioned are shown in fig. 1.3.

However, not all of the existing applications have enjoyed unmitigated success and the double articulated column servicing the Thistle field suffered a failure at the uppermost articulated joint in 1979 (10). The upper column was found to be attached to the lower column by the two flexible risers across the joint. Attempts to sever the connection using explosives caused damage to the lower column. The

structure was re-commissioned but broke away from its mooring in January 1983 and has since been taken out of service.

The articulated column concept can be applied also to a combined mooring and riser device in which the column contains all the risers. The heavy processing equipment is then carried by a support vessel such as a tanker, barge or semi-submersible. The tanker is connected to the column by means of a rigid yoke which attaches to the tanker and the column by way of a horizontal hinge and universal joint, respectively. This concept is illustrated in fig. 1.3 and is currently used in the development of the Tazerka field in the Mediterranean (11). This system incorporates a complex manifold chamber and swivels which are located on the yoke and are designed to allow for tanker rotation roll, pitch and heave. Such a complex arrangement may be responsible for a substantial portion of the overall structural costs.

3. POTENTIAL APPLICATIONS

In addition to the uses already mentioned, it is envisaged that the concept could be applied as a production unit servicing a number of sub-sea wells (12) each well being connected to separate inlet manifolds on the column deck by individual high-pressure risers. Oil storage capacity of approximately 12,600 barrels could be provided at the base of the column so that production would not be interrupted when switching from one tanker to another. This amount would allow several hours production in the absence of a vessel moored to the structure. However, greater amounts of storage may be provided at the base of the column as necessary.

The concept might also be used as a relay column installed remote to sub-sea wells. In this case, the function would be remote production control in addition to well-killing capabilities and pump down operations.

The Howard-Doris deep water gravity tower concept (12) is proposed as a production platform for a site in the Mediterranean in 490m of water. The buoyancy chamber is to be constructed of concrete and the lower column member is to be constructed as a lattice steel structure. This structure has a total topside payload of 15,000 tonnes and is capable of producing 50,000 BPD of oil. Risers and conductors would be 'clumped' and located within the lower column lattice framework.

An all concrete articulated column Arcolprod is proposed in Reference 13 and this concept includes for extension and retraction of the lower column telescopically. The articulated joint connection for Arcolprod comprises an array of synthetic tendons thus eliminating the need for a mechanical articulation device. Access through the joint into the base of the structure is provided by means of non structural flexible access tubes.

Guyed towers can be considered as a special type of articulated column with the buoyancy providing support to a fraction of the total mass of the structure. The remaining stiffness is provided by attached catenary guy lines anchored to the sea bed. The Exxon guyed tower (14) is situated in 300 metres of water and supports a payload of 240,000 KN. The total weight of the structure is 470,000 KN and approximately 120,000 KN of buoyancy is provided. The remaining restoring stiffness is provided by twenty guy lines equally

spaced around the structure. The guy lines therefore constitute the major contribution to the restoring stiffness in this case. This means that the tower itself has to be designed to support very substantial compression loads. The provision of more buoyancy will reduce the compression loads on the tower and make an increased contribution to the restoring stiffness.

It is considered that buoyancy can be provided in such amounts as to provide support for the complete structure or a substantial proportion of the total weight of the structure, thus reducing the design and construction problems of the lower column.

4. DESIGN GUIDANCE

In order to promote the adoption of new concepts in a manner in keeping with the safety provisions necessarily imposed to ensure minimal risk to both personnel and the environment, it is essential that design guidance of an adequate and accredited quality be available to designers. This means that the formulation of proper design codes be undertaken by the relevant certification authorities.

Novel concepts lack the benefits of established, tried and tested technology and so the philosophy fundamental to the evolution of the design code must be sufficiently pragmatic to ensure that design considerations are rigorous. The DnV approach to the certification of novel concepts (15) is to provide guidance rules which ensure that proper procedures are adopted. DnV draw particular attention to the following aspects relating to the certification of articulated columns:-

a. Dynamic Behaviour: the need to have a thorough understanding of the compliant motions the structure will undergo both at wave and resonant response frequencies. Time series analysis including rigid body and elastic modes should be completed.

b. Universal Joints: movements of joints and attendant forces at these must be understood in order that adequate provision be made for the transfer of flexible riser pipes either through or adjacent to the joints.

c. Inspection and Maintenance: the need to provide for comprehensive inspection and maintenance procedures in respect of all critical items of structural importance.

In respect of the latter item, there are indications that existing trends point to maintenance and repair costs for fixed platforms of the same order as the capital cost of the structure (15,16). It is estimated that approximately 100 diver inspection hours is required to inspect one node on a typical jacket structure (16).

Quite apart from the technical design problems associated with jacket structures in water depths greater than 300 metres, diver inspection/maintenance costs could conceivably become extremely high by virtue of the number and complexity of joints. Moreover, physical limitations mean that diver access is not possible beyond about 300 metres water depth. This means that inspection must be remote and structural details for components at these depths must either be kept simple or allow retrieval to within diver depths for maintenance

purposes. From these points of view constraints may also be imposed on articulated columns, although it is envisaged that the construction will be simpler in detail thereby reducing maintenance requirements. Therefore, considerably more attention has to be given to inspection and maintenance at the concept evaluation stage, research and development, to ensure good directional control of efforts and, finally, design.

Research has an important contribution to make to the development of codes and to ensuring that the strengths and weaknesses of numerical techniques as applied to the dynamic analysis of compliant or fixed structures is rigorously and realistically assessed.

From this point of view, experimental work should continue hand in hand with the analytical work either as confirmation of analytical reliability and/or to highlight areas which require more rigorous analytical research. There are, of course, scaling problems with experimental work and a dearth of available and adequate deep water facilities. Nevertheless, it is an essential aspect of research into compliant structures.

5. PREVIOUS WORK

Articulated columns, as a consequence of the small restoring stiffness attributed to the displacement volume, have very small pitching frequencies. The slender nature of the construction means also that they will possess very little damping when excited at low frequencies. The steady drift forces which can be induced (17,18) require understanding and accurate assessment.

Drake et al (19) have studied the steady drift of articulated columns subject to regular waves by the formulation of far field (17) and near field (18) surface disturbance forces set up by the presence of the structure. They found that the analytical expressions for both approaches were identical and that a numerical boundary procedure based on both methods yielded results within 1% of the exact solution. The mean drift force was also found to increase with increasing water depth and inertias for a given wave frequency.

Kirk and Jain (20,21) have investigated the response of both single and double articulated columns in the time domain. They were primarily concerned with the response such structures can undergo when subject to exciting forces which are multi-directional. They predicted complex swirling trajectories when such forces prevail. An understanding of the swirling motion of loading columns is essential from the tanker hook up operational aspects and the predictions augment the value of the time domain approach to the solution of the equations of motion.

Kirk (22) has presented an approximate frequency domain analytic solution to the problem of a single anchor leg storage system (SALS) with attached tanker, similar in concept to the Tazerka structure. The complete tanker/column and yoke analysis predicts that the riser would have to sustain compression loads during part of the loading cycle for a 20 metre wave, thus possibly sustaining dynamic snatch loads.

Chakrabarti (23) has completed work on the transverse oscillations which can be generated in waves as a consequence of vortex shedding on the body of the cylinder and found that the

transverse motions couple with the inline motions to form swirling trajectories.

The dynamic instabilities which compliant structures may experience has been examined in the frequency domain (24,25) and found to exist in the form of a transient oscillation when the structures are excited at twice their natural frequency in pitch.

The elastic vibrations of articulated columns were described by Bishop (26) using Timoshenko beam theory and a linearised quadratic drag term as part of the forcing function. He describes the vibration response as being analogous to that of ships in waves despite the differences in mode shapes obtained. McNamara et al (27) have presented a finite element analysis procedure to predict the time domain response of an articulated loading tower and found good agreement with predicted rigid body motion responses.

Eatock Taylor et al (28) have investigated the elastic vibration of articulated columns by extracting the first three response modes in the absence of tension forces and fluid inertial contributions. They include diffracted and radiated potentials in the formulation of the problem and noted the magnitude of the first resonant flexural response mode.

6. AIMS OF THIS WORK

Although there is a certain amount of general literature available on proposed uses for articulated columns, there appears to be very little available in the form of design guidance in respect of some of those aspects which are fundamental to any conceptual design

appraisal. Chapter 2 addresses certain aspects which would probably determine the feasibility of a project and is intended as general design guidance.

The rigid body motion response of articulated columns has received a certain amount of attention (20,21,23) and some of this has been in the time domain (20,21). However, it appears that certain of the more salient features of the motion response of such compliant systems have not been treated in a manner most suitable to accommodate the non-linearities which give rise to them. Such features include the transient response harmonic with the natural pitch frequency, steady drift responses, dynamic instabilities, resonant response excitation at the natural pitch frequency and other non-linear sources such as non-linear waves and currents. In respect of rigid body motion responses, Chapters 4 and 5 of this work address certain of the aforementioned features by advancing the solution of the equations of motion in the time domain. The importance of certain of the features is noted and the implications of these in the design of articulated columns is assessed. The question of dynamic instabilities which may develop, resonant with the pitch frequency and at twice the pitch frequency is also examined in the time domain. The role of viscous damping in limiting responses is assessed and this is only feasible with a time domain solution.

Work on the elastic vibration of articulated columns, in the main, has been confined to a frequency domain analysis and has noted the importance of the first resonant flexural mode. Chapter 6 addresses the elastic vibration problem in attempting to give a parametric treatment to those factors which have the greatest effect upon the frequency of the first flexural vibration mode. This is done

on the basis that the structural components of the articulated column are comprised of circular cylindrical steel sections of annular construction. The importance of accounting for the axial loads in the determination of vibration frequencies is also addressed.

Further work on the elastic vibration problem is given in Chapter 7 using an incremental solution to solve the equations of motion in the time domain, thus incorporating the full vibration time history. Such a procedure is necessary to fully understand the interaction of structural vibrations, acting in combination with significant compliant motions. Adequate structural analysis in combination with time simulation procedures must be assessed in order to validate the quality of the results. This approach and its ability to predict certain non-linear behaviour is vindicated by certain experimental results obtained for a model articulated column.

CHAPTER 2

CONCEPTUAL DESIGN CONSIDERATIONS

1. INTRODUCTION

As discussed in Chapter 1 articulated columns have been successfully implemented in a number of practical applications. These are, in the main, restricted to lighter structures in water depths not exceeding 150 metres. A proposed production platform may have a payload requirement of the order of 100,000KN and may well be situated in water depths in excess of 250 metres. The payload will be a function of the field characteristics, which will determine the amount of separation and processing necessary. In this respect, trends are towards much lighter deck components (29). The analysis presented in this chapter relates to a heavier structure and exemplifies the versatility of the articulated column. Lighter payloads will improve the efficacy of the concept.

The extrapolation of existing designs to deeper water and heavier structures is not straighforward and it is essential to make a fundamental appraisal of those factors which will determine the feasibility of any particular design.

Hence, the aim of this chapter is to examine those factors which have the greatest influence on basic design considerations. Those factors which are examined include static stability due to wind and currents, ballasting the structure, deck clearances required, access to the buoyancy chamber and damage stability. Having made an examination of these separate aspects, the interdependence of certain parameters is established and their optimisation is considered.

Installation and relocation problems for this type of structure are examined and possible procedures are outlined. Finally, the human awareness to motion response is assessed.

The structure used for these initial studies has a deck payload of 100,000KN and the length from the seabed to the deck is 285 metres. The water depth is 270 metres and the top of the buoyancy chamber is some 30 metres below the still water level (SWL). The structure is shown in fig. 2.1.

2. STATIC STABILITY

2.1 Wind and Steady Currents

Tension leg platforms, by virtue of their design, will surge under the action of steady current and wind forces. However, the deck will remain essentially horizontal in these circumstances and so steady drift forces will have no real impact on operational constraints. On the other hand, articulated columns by virtue of their design, will pitch under the action of steady drifting forces and the deck, therefore, will not remain horizontal, possibly imposing constraints on activities at deck level. It is necessary, therefore, to make an assessment of the amount of pitch the structure is likely to experience under the action of steady drift sources such as wind and current.

For any given structural configuration and distribution of mass it is possible to evaluate the amount of buoyancy which will be required in order to maintain a specified angle of heel under the actions of a steady current and wind speed.

TABLE 1

COMPONENT	MASS (TONNES)
DECK	10,000
DECK SUPPORT COLUMN	500
BUOYANCY CHAMBER	3,000
LOWER TENSION MEMBER	1,000
BALLAST	8,500

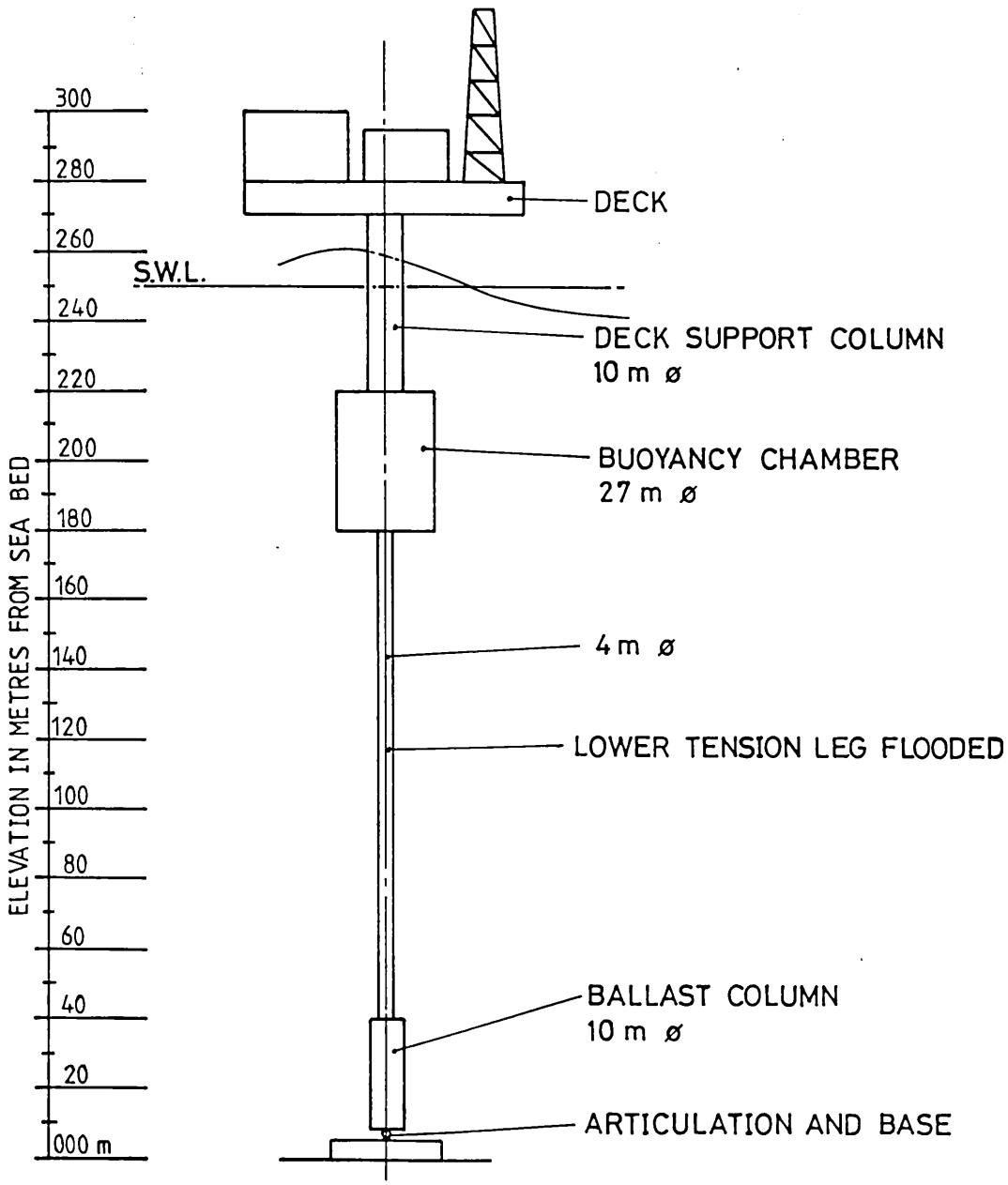

GENERAL ARRGT. OF ARTICULATED COLUMN STRUCTURE

FIG. 2.1

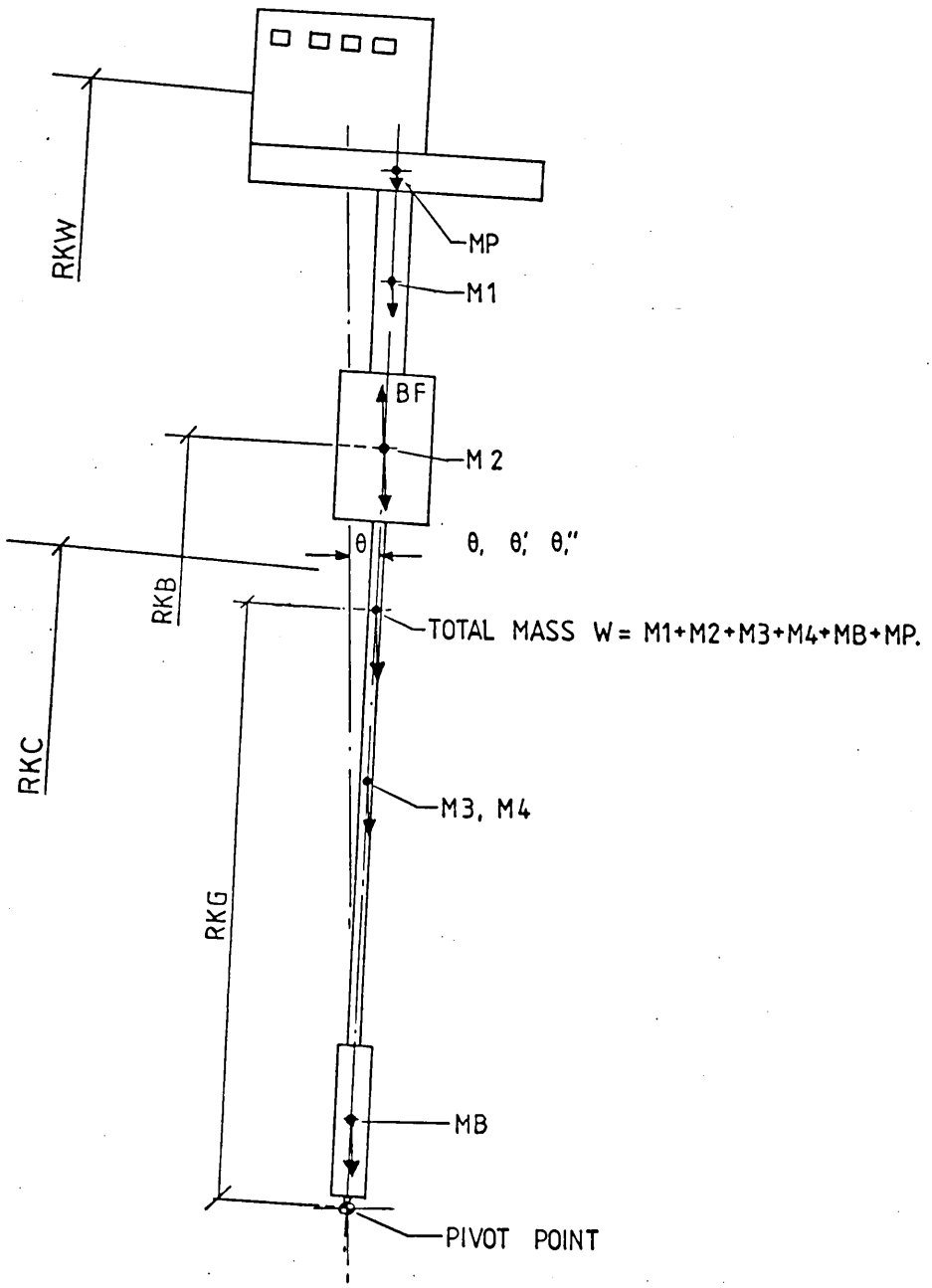
RKW
MP
M1
BF
M 2
θ
θ, θ', θ,"
RKB
TOTAL MASS W = M1+M2+M3+M4+MB+MP.
RKC
M3, M4
RKG
MB
PIVOT POINT

FIG. 2.2

The static stability of the structure, shown in fig. 2.1, is calculated on the basis of equilibrium of the sums of the moments of the overturning and restoring forces taken about the pivot point or articulated joint. With reference to fig. 2.2 and by taking moments about the pivot, then:-

$$\text{Total moments of forces about the pivot} = 0. \tag{2.1}$$

$$\Sigma \text{ Overturning moments} = \Sigma \text{ Wind forces} + \Sigma \text{ Current forces} + \Sigma \text{ Self-weight forces} \tag{2.2}$$

$$\Sigma \text{ Restoring forces} = \Sigma \text{ Buoyancy forces}$$

where Self-weight forces $= W.RKG.\sin\theta$

Buoyancy forces $= B_F.RKB.\sin\theta$

Wind forces $= \frac{1}{2}.\rho_{air}.C_{DW}.A_P.V_W^2.RKW$

Current forces $= \frac{1}{2}.\rho_{water}.C_{DC}.A_P.V_C^2.RKC$

and $C_{DC} = 1.0$

$C_{DW} = 1.5$

A_p = projected area

V_w = wind speed

V_c = current speed.

RKG, RKB, RKW and RKC refer to the height of the centres of gravity, buoyancy, wind force and current force above the pivot point, respectively.

The value of $C_{DC} = 1.0$ may be somewhat high for a smooth cylinder in the supercritical Reynolds number range. However, an allowance must be made for increased surface roughness as a consequence of marine growth and a value of 1.0 is not unreasonable.

Equating moments:-

$$\Sigma \text{ wind forces} + \Sigma \text{ current forces} + \Sigma \text{ self-weight forces} - \Sigma \text{ buoyancy forces} = 0 \qquad (2.3)$$

Figure 2.3 has been prepared in accordance with the form of equation 2.3. For the structure shown in fig. 2.1, it shows the amount of buoyancy chamber volume required as a function of the static angle of heel for given wind and current velocities as shown and in this case the wind speed is zero. There are two curves shown, one for the case of the lower column being flooded and the other assuming that the lower column is watertight. The trends for both curves are the same and they both display optimum points after which very little improvement in the angle of heel is achieved for fairly large increases in the amount of buoyancy required. It is obvious that considerably more buoyancy is required in the case of the flooded column.

Figure 2.4 shows the same plots but in this case, the wind speed is 35 metres per second. The buoyancy required is very considerably increased and, on the basis that the weights of the structural components are as shown in the table in fig. 2.1, then the amount required to maintain an angle of heel of 1^{o} is approximately 1.5 times the total weight of the structure for the case where the lower column is flooded. To maintain a 2^{o} angle of heel the buoyancy required is 1.35 times the total weight. It is clear, therefore, that the lower column for this particular design would have to sustain considerable tensile loads in order to satisfy the static heel requirements mentioned. An angle of heel of 2^{o} corresponds to a horizontal excursion of the platform of approximately 3.5% of the water depth. The lower column can be designed to withstand the tension

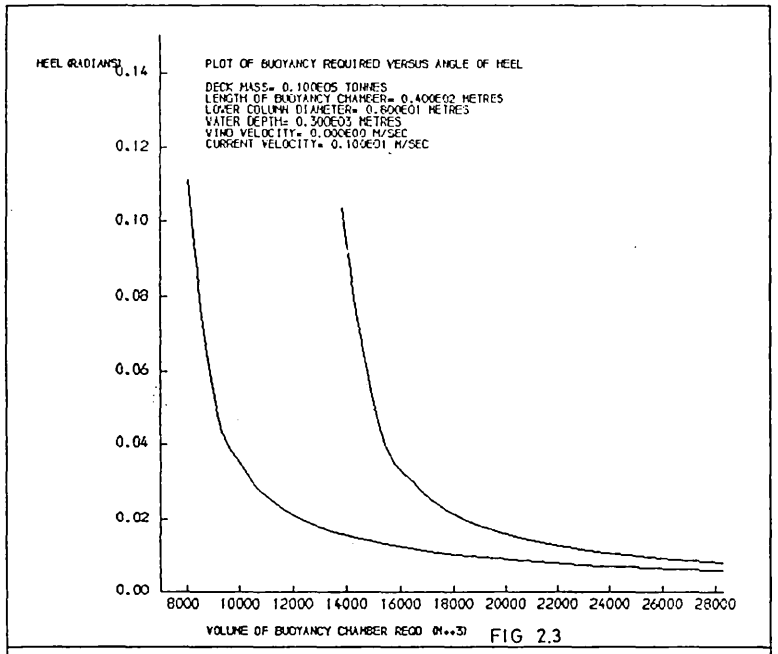

FIG 2.3

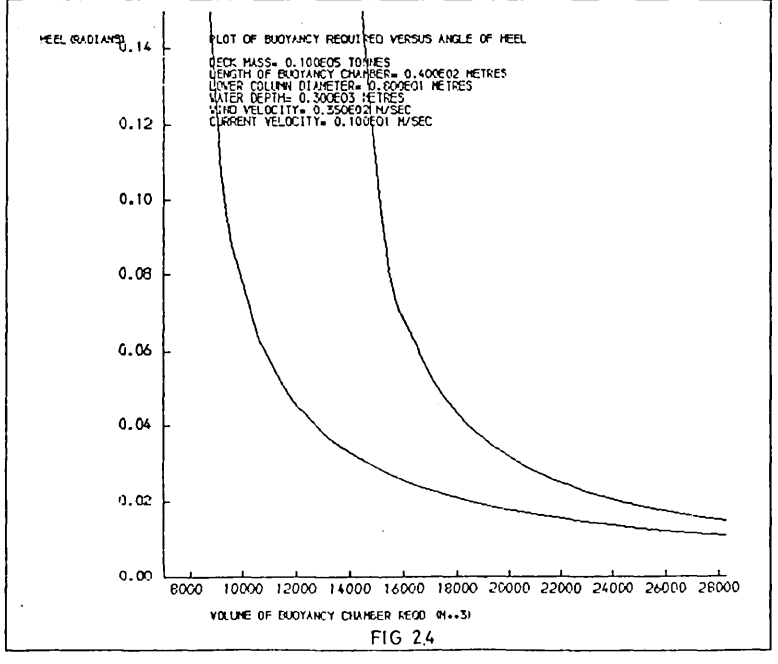

FIG 2.4

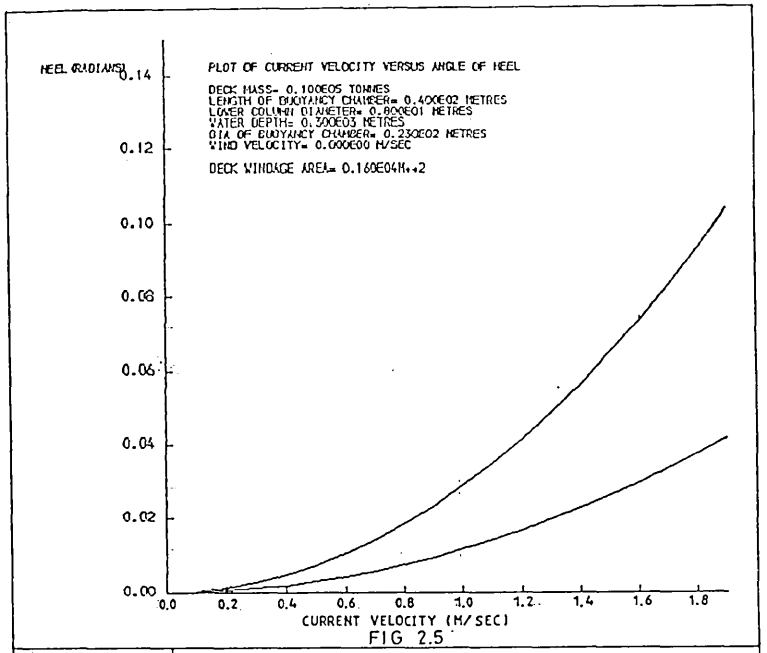

FIG 2.5

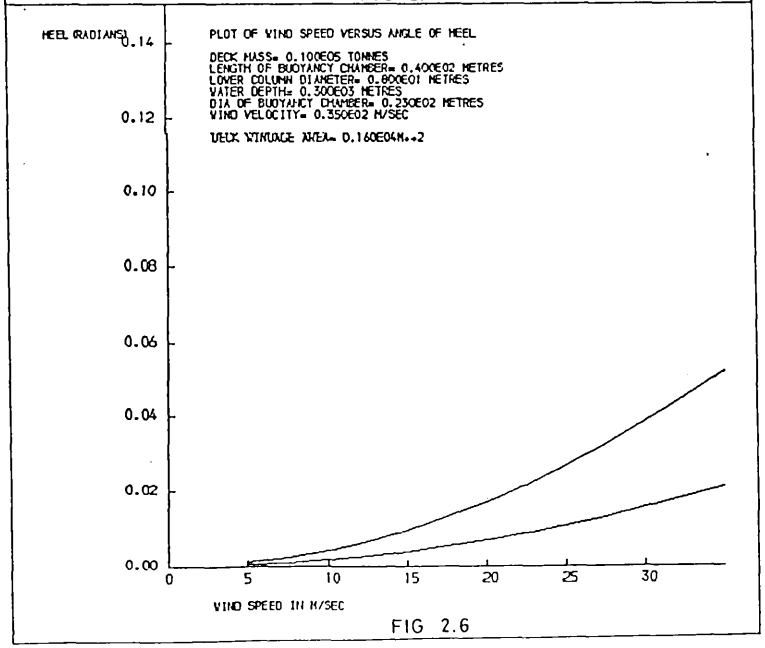

FIG 2.6

envisaged but there may be difficulty with the articulated joint. To overcome this it is necessary to have ballast at the foot of the lower column in order to put the articulated joint into compression.

For a fixed amount of buoyancy the angle of heel as a function of current velocity for zero wind speed is shown in fig. 2.5. The structure with the lower column flooded displays the most pronounced increase in heel as the current velocity is increased as would be expected. The increase in the angle of heel is fairly gradual for current velocities up to about 1 metre per second and thereafter increases quite rapidly.

Figure 2.6 shows the angle of heel as a function of the windspeed for zero current velocity. The trend is similar but less pronounced than for the previous figure and displays the influence of the speed squared term in each case. For a combination of wind and current the sum of the two components will sensibly be correct with minor adjustments for the small variation in buoyancy as the pitch increases.

It should be noted that the pitching moment due to wind on the deck and superstructures will increase as a function of the pitch angle, as the frontal area exposed to wind increases, and the wind force lever arm changes.

It should also be noted, however, that as the depth of water increases, the buoyancy required to maintain the same angle of heel will reduce as a consequence of the increased lever arm of the buoyancy, as will the excess tension loads on the lower leg. For example in 550 metres of water the buoyancy force required to maintain the same angle of heel for a platform of similar payload, ie

100,000KN, would be approximately 200,000KN so that the lower leg would be subject to tensile loads of about 25% of the total weight of the platform. However, the extra weight of the lower column, to some extent, will offset the benefits of reduced tensile loads, so that the situation with regard to static stability will improve with depth.

Vibration aspects are shown to play a dominant role in the design of the lower column in chapters 6 and 7 of this thesis. The order of magnitude of the tensile loads in the lower column, therefore, are likely to be somewhat less than discussed here. However, increased tensile loads contribute to improved vibration characteristics and this is discussed in chapter 6.

2.2 Ballasting the Structure

Problems associated with the design of an articulated joint capable of withstanding the tensile loads anticipated calls for difficult engineering with a potentially dangerous situation developing if the structure breaks loose from its base. For this reason, it would be desirable to reduce the tensile loads at the articulated joint and, if possible, make it a compression load.

This can be achieved by the addition of an amount of ballast to the lower end of the lower tension leg and just above the joint so that the tensile load in the joint is reduced.

For the articulated column investigated the weight of ballast is of the order of 8500 tonnes. If concrete were to be used as ballast material this would result in a 'cylinder' of ballast with possible dimensions 40m long and 10m in diameter. However, problems associated with the removal of concrete render its use untenable and, therefore,

it is thought that high density drilling mud which has a density of 2300Kg/m^3 would be used as ballast material since it may be placed and removed by pumping more readily than concrete.

2.3 Deck Clearance

Maximum responses will generally lag maximum wave forces by 180^o so that the maximum pitch, for a linear response, will occur at a wave node. This means that were the structure to be subject to linear waves and respond linearly then the amount of deck clearance between the mean surface level and the underside of the deck would need to be at least equal to the maximum wave amplitude expected during the life of the structure. However, it will almost certainly be necessary to allow for some amount of static heel as discussed in the previous section so that this must enter into the considerations in respect of adequate deck clearance.

If we assume, in an extreme situation, that the wave crest is directly beneath the tilted deck when the pitch is maximum then an approximate formula to determine the deck clearance is given as follows:-

$$DC = L_p - d - a_o - 0.5.DW.\sin\theta \qquad (2.4)$$

where DC = deck clearance

L_p = distance from bottom to underside of deck

d = water depth

a_o = wave amplitude

DW = deck width

θ = steady angle of heel

This approximate formula would serve to determine requirements if the structure responded in a linear fashion about the steady heel caused by waves and currents. In subsequent chapters it is shown that the motion response of articulated columns, generally speaking, is not linear and further considerations will inevitably enter into the rigorous assessment of adequate deck clearance. The main consideration in this respect is the transient response harmonic with the natural period in pitch of the structure and the combined effects of current plus wave. This is discussed in greater detail in Chapters 4, 5 and 7.

The deck mass location will significantly affect the centre of gravity and, consequently, the static angle of heel. This is also a function of the windage area of the deck superstructure in that the centre of gravity of the deck can be assumed to increase in approximate proportion with the height of the deck superstructure. Wind profiles increase with elevation above sea level and the API code (30) indicates that a sustained wind speed at an elevation of 50 metres above SWL is some 23% greater than that 10 metres above SWL. This, in combination with the raised centre of gravity, would suggest that low profiles are preferred. However, lower profiles will require greater lateral distribution of deck mass with consequent influences on deck support structure, deck clearances, etc.

2.4 Access to Buoyancy Chamber

In order to lower the centre of gravity it is desirable that the buoyancy chamber be used to accommodate certain items of machinery and plant which would otherwise be located on the deck of the structure. Therefore, it is essential that access from the deck to the buoyancy chamber be provided in a manner which will satisfy damage stability considerations and this should allow for ventilation duct

requirements. A typical minimum access dimension of about 4 metres diameter is thought to be adequate. However, this dimension will be a function of the design of production or other equipment which will be located in the chamber and will only be critical where the deck support structure is other than a single circular cylindrical member. The diameter of the deck support column is likely to be of the order of 8-10 metres so that access should not be a problem. The main advantages of utilising the buoyancy chamber as accommodation for machinery rooms and stores are thought to be:-

a. The total deck weight can be reduced by the amount of plant relocated in the chamber: this will result in a more slender and lighter deck structure.

b. Lighter deck support column structure.

c. Deck windage area will be reduced - decreased wind loads.

d. Lowering of the C.G. of the structure thus improving the restoring moment.

The buoyancy chamber could be split on three levels, possibly even four levels and in available floor space this could amount to 30% to 40% of the area available on a 60m x 60m deck. Personnel accommodation is most likely to be situated at deck level. However, it is envisaged that the chamber would accommodate certain production equipment and other materials not required on the deck. Regulations may impose restrictions on activities within the chamber in regard to ventilation requirements. These may dictate a high rate of change of air so that it may only be possible to conduct low air requirement activities within the chamber, certain of the more hazardous activities being conducted at deck level. Nevertheless, in view of the possible gains to be achieved in using the chamber, emphasis is stressed on achieving maximum utilisation of the available space.

2.5 Riser Accommodation

The riser flowlines conveying oil from the wellhead to the surface are central to the continued and uninterrupted production of oil. The early floating production systems such as the semi-submersibles in Argyll and Buchan used rigid risers with heave compensators. The proposed Balmoral development will use flexible risers with a buoy into an S configuration. Most of the tanker FPS use some form of articulated column which contains a rigid riser terminating in a swivel before entering the tanker. Thus many systems are in use and this is still considered one of the areas of greatest risk in 'compliant' operations. The penalties as a consequence of riser failure and/or downtime may run into millions of dollars per day and, therefore, it is essential that adequate provision is made for risers. A review of the technology is presented in Reference (31).

The risers can be accommodated inside the bulkheaded annulus of the lower column along its entire length from the seabed to the buoyancy chamber. Alternatively, separate accommodation could be provided within the inner annulus of the lower column, see fig. 2.7.

In some cases it may be necessary to use cooling water and this presents no problem to utilising the bulkheaded annulus section. Risers can be supported at intervals along the length of the lower column, thus eliminating any requirement for top tensioning support or heave compensators as required in a conventional FPS. Ventilation requirements at the riser terminations will be a function of the capacity of the risers. It may be necessary to provide temporary ventilation to the riser accommodation in the lower column in the event of maintenance operations being necessary.

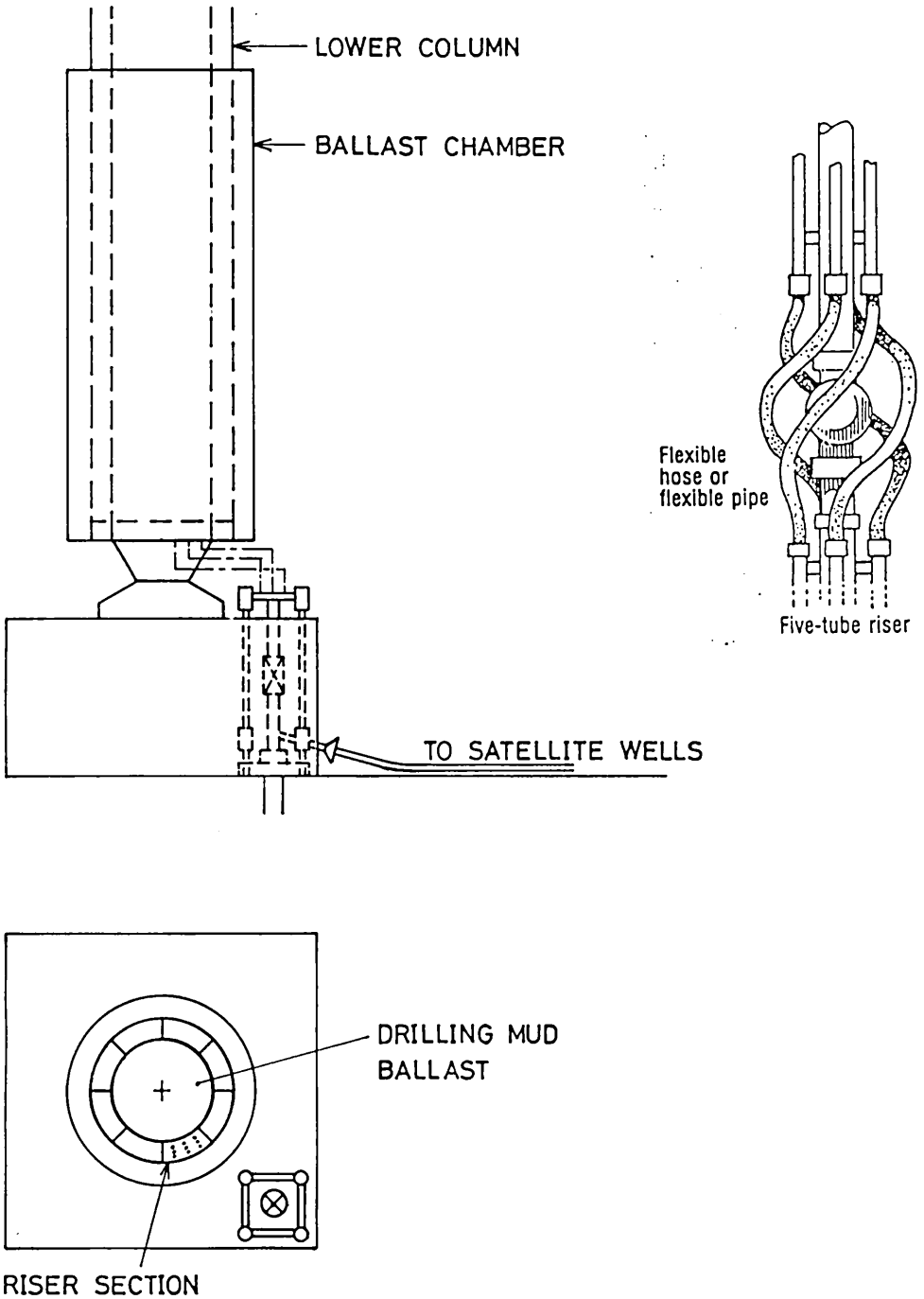

RISER ACCOMMODATION

FIG. 2.7

Articulated production risers (32) utilise flexible hose connectors at articulations to provide continuity between rigid risers on either side of the articulated joint (see fig. 2.7). Similar methods can be employed to effect the transition from the wellhead passing around the outside of the articulated joint and into a location in the lower column above the articulated joint.

2.6 Damage Considerations

The overall integrity and stability of the structure will be a function of both its structural strength and its buoyancy characteristics. Fundamental to its integrity is the ability to remain buoyant and stable, assuming that the lower joint remains intact. Therefore, it is essential that the structure is capable of maintaining a satisfactory damage stability in the event of a major buoyancy device such as the buoyancy chamber and/or the submerged portion of the deck support column sustaining an impact which might render the skin of either or both to flood.

Therefore, the incorporation of an adequate arrangement of watertight subdivision will be necessary in the design of both the buoyancy chamber and the deck support column. Similar arrangements will be necessary for the lower column if it is to be designed as watertight. This is unlikely to make increased demands on the structural mass of the lower column since vibration considerations will require substantial second moments of area and this will aid the design to withstand the hydrostatic pressures. This aspect is discussed in greater detail in Chapter 6.

One such possible arrangement is shown in fig. 2.8 although this might be subject to alteration depending on other requirements as might be determined by the possible uses for the space within the buoyancy chamber.

In the event of a bulkhead sustaining a fracture and a bulkhead compartment flooding, the effect will be to subject the column to an additional mass, equal to the flooded mass, acting at a lever arm approximately equal to the radius of the buoyancy chamber. From fig. 2.8 it can be seen that the centre of buoyancy will move away from the centreline of the chamber resulting in a reduced restoring moment.

For the arrangement shown in fig. 2.8 the static angle of heel would be increased to 3.5^{o} for flooding of a bulkhead compartment to the full height of the buoyancy chamber ($1200m^3$ of water). A more extensive arangement of bulkheads which would reduce the flooded volume is necessary and, for example, if a bulkhead arrangement as shown in fig. 2.8 were adopted then in the event of chamber number 1 becoming flooded this would increase the static heel to 1.86^{o}. This arrangement of bulkheads is especially feasible if the buoyancy chamber is provided with split level decks. Figure 2.8 shows angle of heel versus flooded volume.

Two compartment flooding will be a mandatory requirement for the upper support column to provide against surface ship collision. This requirement may be relaxed for the buoyancy chamber which is some 25-30 metres beneath the SWL and one-compartment flooding will probably suffice for the buoyancy chamber.

The bulkhead arrangements shown in fig. 2.8 conform with rules

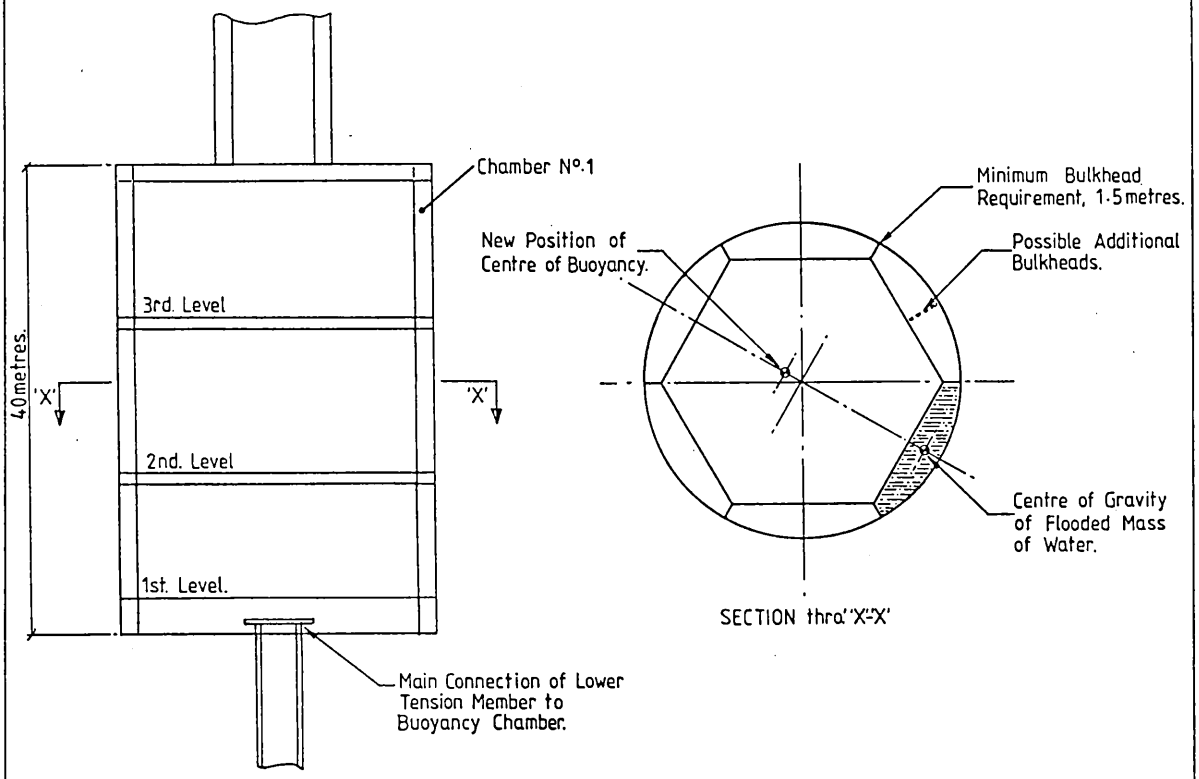

ARRANGEMENT OF BUOYANCY CHAMBER AND BULKHEAD ARRANGEMENT.
(arrangement for upper column similar.)

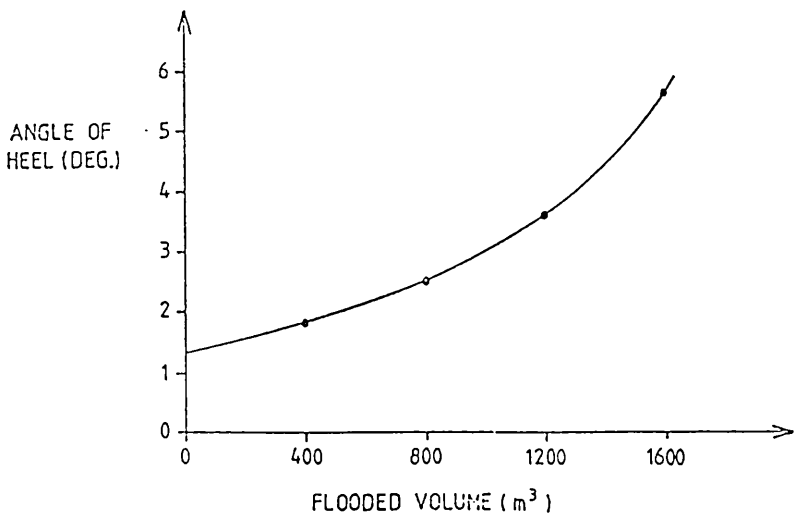

PLOT OF FLOODED VOLUME VERSUS ANGLE OF HEEL

FIG. 2.8

C300 and C305 of the DnV (33) requirements in respect of possible collision/impact damage in that the minimum penetration dimension of 1.5 metres is satisfied. It should be noted, however, that this requirement is intended to account for possible damage as a consequence of impact from, say, a supply vessel or other such source. While the upper support column is clearly susceptible to damage of this nature, the buoyancy chamber, by virtue of its submergence depth of some 30 metres, is less likely to sustain damage of a similar nature. Double bulkheading will be necessary but the requirement in respect of the penetration dimension may be somewhat less stringent. Some degree of extra protection from impact to the top of the buoyancy chamber resulting from dropped objects from the platform above would be prudent and some extra bulkheading may be necessary.

The possibility of the structure breaking loose from the articulated connection must be considered. This is most likely to happen, if at all, in a storm situation and in such circumstances production will probably be very limited or even terminated. Wellkill procedures will almost certainly have been implemented to minimise the risk of environmental pollution. It will be essential to provide some form of emergency mooring between the lower end of the lower column and the foundation which will prevent the structure from drifting off location in the event of a breakaway. This emergency mooring should be of sufficient length to allow the drifting structure to clear such wellhead equipment, etc as may be located in the vicinity of the base in order to minimise the risk of damage to wellheads as a consequence of the structure fouling these.

The free floating stability of the structure will be ensured by the mass of the ballast at the lower end of the lower column. However, heave amplitudes must be assessed to determine the

possibility of bottom fouling. In this respect, a connection point at the base sufficiently elevated from the sea bed to allow for maximum heave in a storm situation should be provided.

3. INSTALLATION AND RELOCATION

The installation and relocation are major factors in the assessment of both technical and economic feasibility. In the final design process a detailed structural analysis will be necessary for the installation and relocation stages.

Site restoration regulations now in force may in certain fixed platform applications jeopardise the economic viability of the project. Therefore, it is important that sufficient detailed conceptual planning be undertaken so that restoration costs can be accurately and reasonably estimated and accounted for in the economic model for the project. In this respect, articulated columns have definite advantages over fixed platforms or other compliant structures such as TLPs which require tensile load bearing foundations.

The articulated column can be so ballasted, as discussed in section 2.2, in order to render a gravity foundation feasible. This is attractive to the foundation designer and may preclude the necessity for piling the foundation. This arrangement, in principle, would reduce the termination problems to that of effective disconnect of risers. Removal of wellheads remains a problem irrespective of the platform type.

3.1 Installation

It is pertinent to assess conceptually the feasibility of the

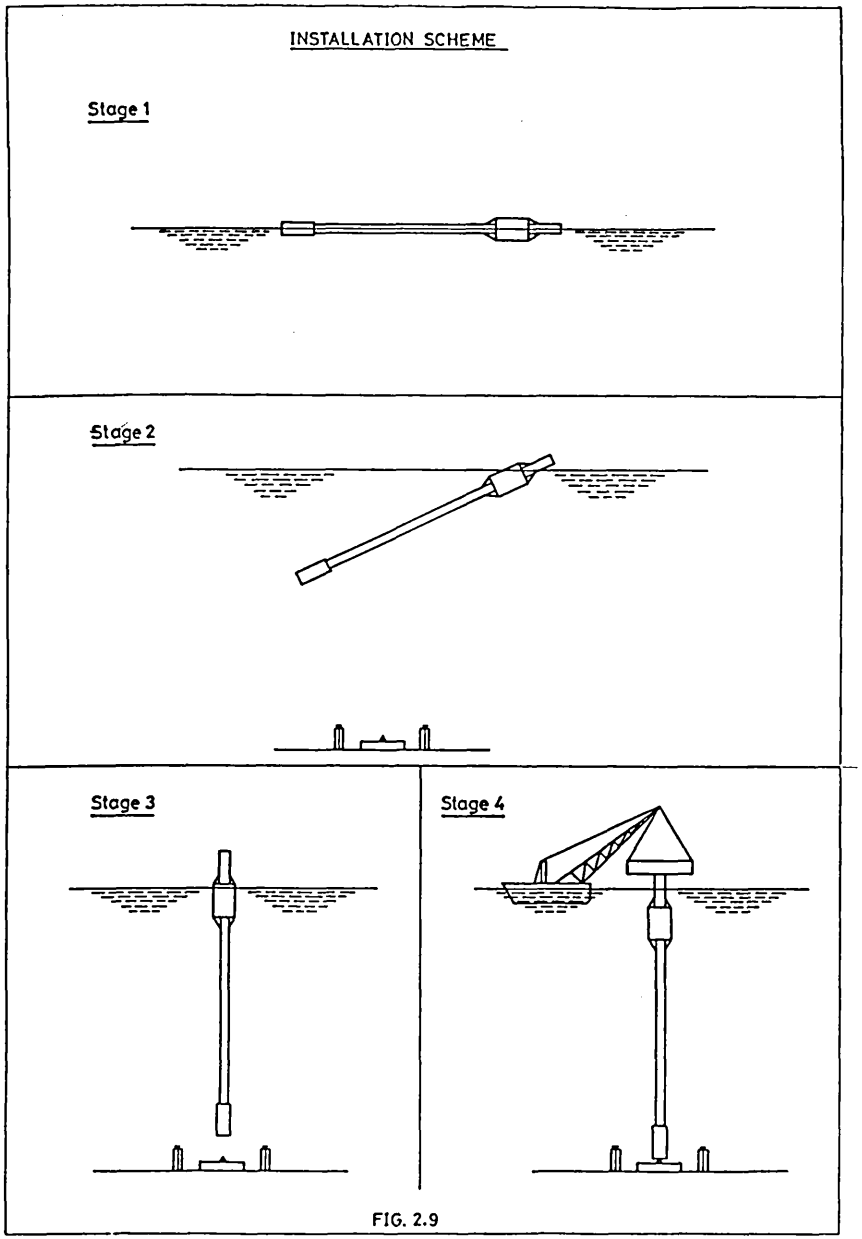

FIG. 2.9

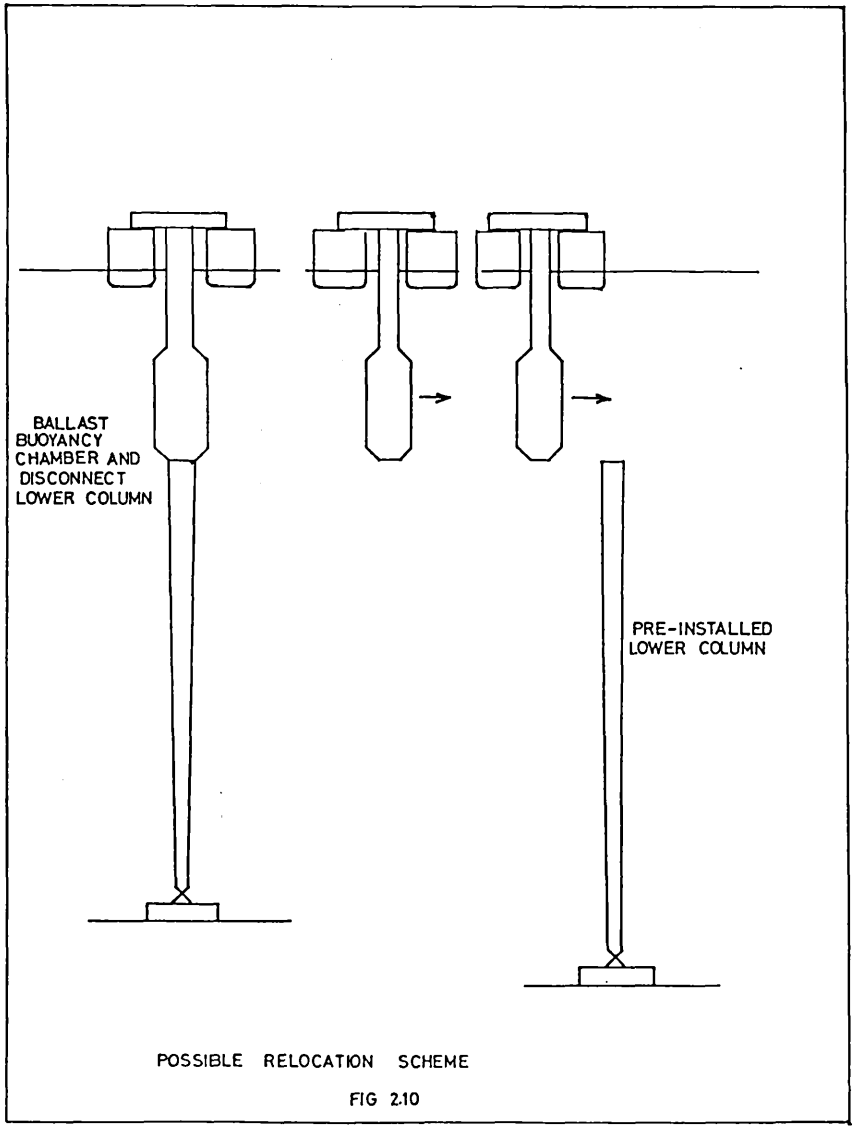

POSSIBLE RELOCATION SCHEME

FIG 2.10

installation and relocation process and, accordingly, a possible installation scheme is presented, together with a possible relocation scheme.

Scheme 1

This is shown diagramatically in fig. 2.9 and basically comprises preassembly of the three major component parts, ie the lower column, the buoyancy chamber and the upper support column. The deck structure would be added later. The preassembly would be towed to the location.

The foundation for the structure having been pre-positioned, the structure is control ballasted using the bulkheaded compartments until it locates with the connection joint assembly on the base. It may be necessary to fix the complete articulated joint to the column assembly and to effect a connection with the base at the lower end of the articulated joint rather than to effect a connection at the swivel point of the articulated joint.

Controlled deballasting of the buoyancy chamber would be necessary and this would continue concurrently with the addition of mud ballast to the bottom of the lower column and the addition of deck masses.

3.2 Relocation

The economic viability of a structure of this nature will be a function of a number of different considerations but probably the most important single consideration will be that of possible re-use of the structure in another field. Therefore, it is essential that the concept should show promise in terms of the feasibility of re-locating

the structure to another site.

The inherent buoyant stability of the ballasted structure in the free floating situation will be of considerable merit in terms of ancillary re-location operations such as ballasting, etc.

In the event that relocation of the structure to deeper water is necessary, a procedure as outlined below and shown in fig. 2.10 could be utilised. This procedure is based on the assumption that the lower column may be disconnected from the buoyancy chamber. Such an arrangement is thought to be technically feasible.

a. Partially ballast the buoyancy chamber and decouple the lower column from the buoyancy chamber. It may be necessary to reduce deck loads. However, since lifting capacity has improved considerably in the past decade this should not present major problems.

b. Float buoyancy chamber to a new location and ballast the assembly on to a pre-installed lower column.

4. PARAMETERS FOR OPTIMISATION

The deck mass and superstructure are supported by the buoyancy chamber and static stability requirements will usually determine that the buoyancy exceeds the total mass by a substantial amount in the case where the lower column is flooded. As discussed in section 2.1, the lower leg of the structure, generally, will be subject to a net tension force, allowing for cyclic heave forces and this will help to reduce the structural requirements for the lower tension leg and simplify its design. In some cases, designers may wish to have the articulated joint in compression and to do this a large mass is added

immediately above the joint. Such a procedure does not alter the above arguments.

The lower leg may be left flooded but it is doubtful if this is a major attraction. The vibration aspects of the lower column will probably determine structural requirements since the vibration frequencies are proportional to $\sqrt{EI/m\ell^4}$. Therefore, it is desirable to keep the unit mass of the lower column to a minimum. In order to maintain vibration frequencies which are higher than expected wave spectrum frequencies, to avoid resonant excitation, wall thicknesses are likely to be substantial so that the lower column can probably be designed to withstand the water pressures. This aspect is the subject of a more rigorous analysis and is discussed in more detail in Chapter 6.

It is envisaged that risers and associated equipment would be located within the lower leg. This feature has advantages in that such equipment will not be subject to wave and current actions. The advantages are much enhanced in the case of a dry lower leg.

Minimising the variation in the heave force on the buoyancy chamber is desirable and can be achieved by the judicious choice of buoyancy chamber radius and those of the upper and lower columns. Cancellation of heave forces is possible for a particular wave frequency and this aspect will play a major part in the design of the articulated joint. This aspect is given further consideration in Chapters 4 and 5.

The elevation of the buoyancy chamber will determine not only the overall stability of the structure but also the structural requirements and, therefore, the dimensions of the upper support

column. A deeper immersion increases the external pressure on the chamber and reduces the buoyancy lever about the joint but also leads to reduced wave loading and it is the optimum combination of these factors which is being sought.

Dynamic response will depend on the pendulum stiffness and, therefore, on the buoyancy chamber dimensions and on the distribution of the mass of the structure and these aspects are considered in more detail in Chapter 4. The provisions to be made in respect of the deck clearance required also will be a function of the dynamic response.

Therefore, an adequate design must make an appraisal of the interdependence of the parameters discussed and an optimisation procedure may be undertaken.

The optimisation of the parameters mentioned will be greatly influenced by the operational requirements and performance specifications for a particular project and a sufficiently general approach is not feasible. In principle, however, an optimisation procedure similar to that shown in fig. 2.11 would be necessary.

5. HUMAN RESPONSE TO STRUCTURE MOTIONS

The human response to induced motions of the structure is of importance and perception levels have been established and need to be borne in mind. Perception thresholds are found to be insensitive to small amplitude vibrations with frequencies in the range 1-5Hz (34,35) and it has been suggested that for frequencies less than 1 Hz the rate of change of acceleration, ie 'jerk' is an appropriate measure of human awareness.

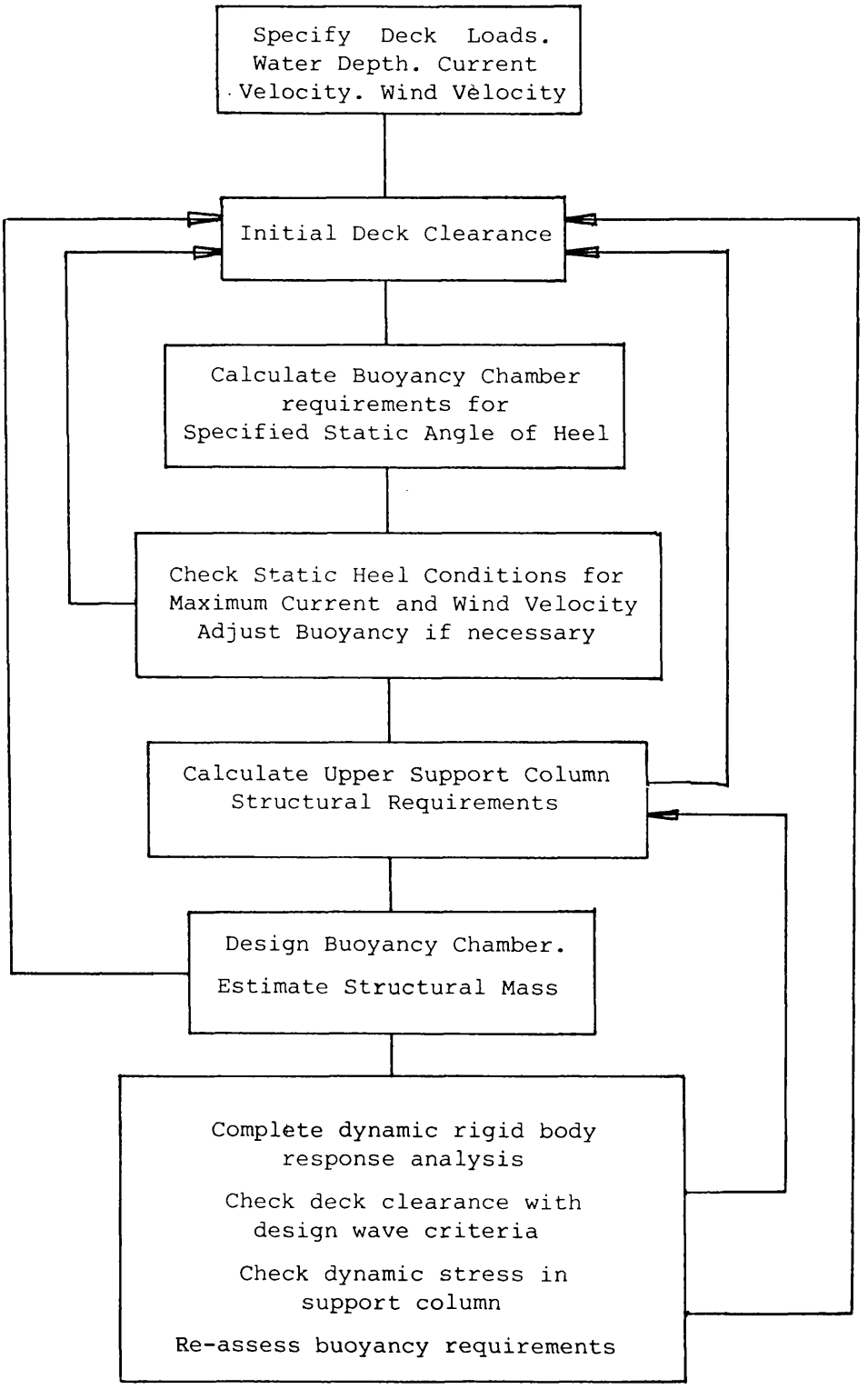

Fig.2.11 Design Optimisation Chart for Articulated Columns

EFFECT ON WORK OF ACCELERATION LEVELS

Class of Human Reaction	Effect on Work
Very weak	Unhindered
Perceptible; unpleasant for long exposure	Slightly hindered
Decidedly perceptible	Hindered
Unpleasant; tolerable for one hour	Much hindered
Very unpleasant; tolerable for 10 minutes	Practically impossible
Extremely unpleasant; tolerable for one min	Impossible
Unbearable	Impossible

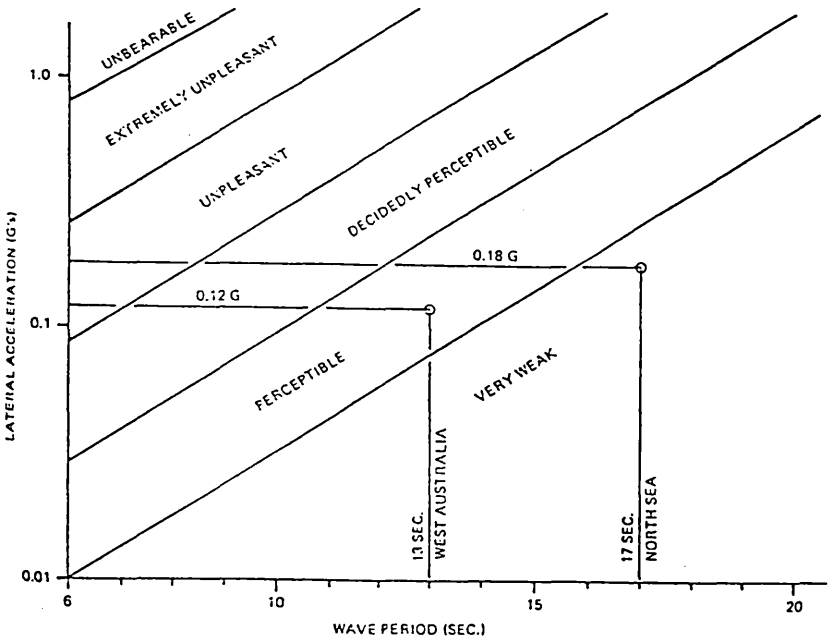

Reference "Criteria for Human Reaction to Environmental Vibration on Naval Ships" by E. Suommann, Ph.D., Department of Navy, David Taylor Model Basin.

FIG 2.12

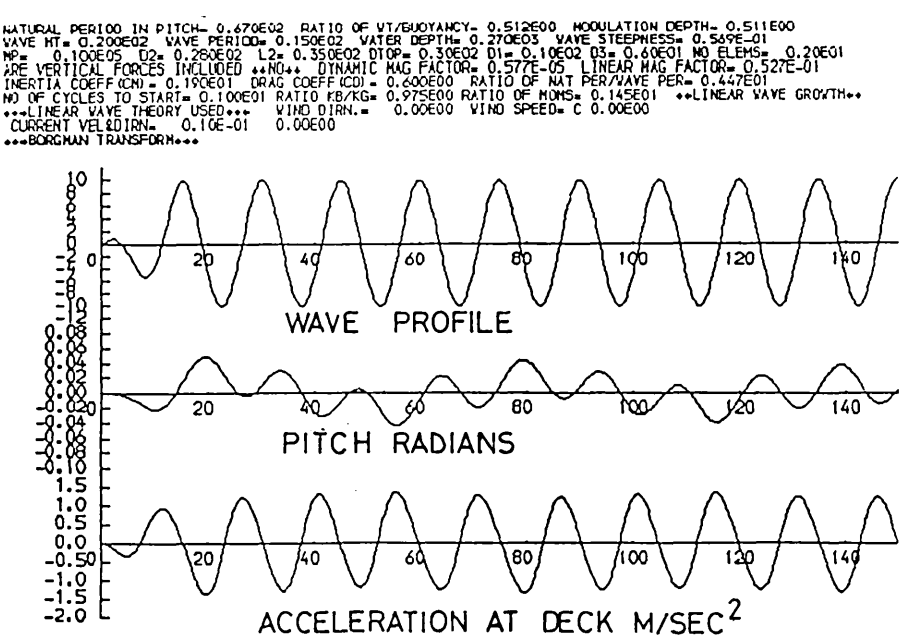

FIG 2.13

The effects of levels of accelerations on the ability of personnel to perform satisfactorily has been suggested as shown in fig. 2.12 (36). This also shows the various bands of awareness to acceleration levels in terms of accelerations and wave periods. The structure considered in fig. 2.1 experiences an acceleration level at the deck of approximately 1.5 m/sec^2 (0.153 G's) for a 20 metre high wave, with a period of 15 seconds. This value falls within the 'perceptible' band. The response of the structure is shown in fig. 2.13 as a function of time. The acceleration at the deck level in m/sec^2 is shown as the bottom plot in the figure. Dynamic response is discussed in greater detail in subsequent chapters.

A 20 metre high, 15 second wave is likely to be experienced only in severe storm conditions. In such circumstances, operational constraints in respect of production and processing are likely to be imposed in any case.

An alternative measure of human awareness is commonly expressed in terms of Dieckmann's Sensitivity coefficient K_{DS} and a relationship between K_{DS} and the 'jerk' is proposed in reference (35).

For the structure shown in fig. 2.1 the maximum 'jerk' was of the order of 20 cms/sec^3 for a wave of height 20 metres and 15 second period. This corresponds to a Dieckmann coefficient K_{DS} of just greater than 1 and just higher than the classification of 'distinctly perceptible but not objectionable'. Potential applications are most likely to be in water depths in excess of 250 metres. Therefore, natural pitch frequencies will decrease as water depth increases. For this wave in greater water depths, the ratio of wave frequency to natural frequency will increase and the dynamic magnification factor for response will decrease since the peak occurs at resonance.

It is thought unlikely that major objections in terms of human response to acceleration levels will arise, although there may be misgivings in respect of non-preferential directional response as a consequence of multi-directional forces and this is investigated further in Chapters 4 and 5.

6. CONCLUDING REMARKS

The amount of buoyancy required to maintain an acceptable level of static heel is noted to be sensitive to both steady currents and wind speed. In respect of the latter, greater attention should be given to minimising the windage drag on the deck superstructure. The size and form of the superstructure are obviously important and it is this aspect which strongly suggests that a greater use be made of the buoyancy chamber to accommodate plant and machinery which would otherwise have to be placed on the deck, thereby contributing to the windage area at the deck level and raising the centre of gravity.

Relocation of deck masses to the buoyancy chamber considerably improves the static stability of the articulated column and this is a very important aspect in terms of the feasibility of the structure. It also plays a major role in the optimisation of other important parameters and is believed to be a central factor in many respects, not least of which will be the design of the deck support column and the deck structure itself.

Damage provisions must be made but the structural requirements in terms of providing adequate bulkheading are not onerous since utilisation of the buoyancy chamber will necessitate structural provisions to accommodate plant, etc on different levels. Some form of

ring and/or stringer stiffeners would be required for the buoyancy chamber in any case and there is scope here for optimising the design.

Installation and relocation have been shown to be feasible in principle and these will play an important part in determining the economic viability of the concept.

CHAPTER 3

WAVE FORCE EVALUATION

1. INTRODUCTION

The evaluation of wave forces on any structure, fixed or floating, reduces to the determination of the distribution of pressure over the wetted surface of the body. The complete fluid motion can be said to comprise two parts, one of which is associated with the irrotational inviscid flow which satisfies specified boundary conditions and the other which is associated with the vorticity of the fluid shed from the body.

This chapter first describes the forces attributed to the irrotational inviscid flow (potential flow) and then describes the effects of diffraction which increases as typical body dimensions increase. The limitations of the Morison approach to fluid loading are discussed and finally the drift forces which can affect floating structures are discussed in the context of articulated columns.

2. IRROTATIONAL FLOW AND LINEAR DIFFRACTION

The equation of motion for a fluid domain is uniquely defined by the Bernoulli equation:-

$$-\frac{\partial \Phi}{\partial t} + \tfrac{1}{2}(u^2 + v^2) + \frac{p}{\rho} + gy = 0 \qquad (3.1)$$

where Φ = velocity potential describing the flow field.

U,V = horizontal and vertical velocities.

p = pressure distribution.

ρ = density of fluid.

y = elevation of point considered.

g = gravitational constant.

The incompressibility of flow in two dimensional motion (x,y) states that:-

$$\frac{\partial u}{\partial x} + \frac{\partial v}{\partial y} = 0 \qquad (3.2)$$

If in addition the flow is irrotational, then the velocity must satisfy the conditions that:-

$$U = -\frac{\partial \Phi}{\partial x} \quad \text{and} \quad V = -\frac{\partial \Phi}{\partial y} \qquad (3.3)$$

The combination of these relations gives rise to :-

$$\frac{\partial^2 \Phi}{\partial x^2} + \frac{\partial^2 \Phi}{\partial y^2} = 0 \qquad (3.4)$$

which is the Laplace equation

The solution of this partial differential equation in conjunction with the specified boundary conditions constitutes the derivation of the velocity potential Φ.

3. BOUNDARY CONDITIONS

In boundary value problems it is common to define the condition of zero normal velocity at the fluid boundaries.

a. The boundary condition to be satisfied at the sea bed is:-

$$V = -\frac{\partial \Phi}{\partial y} = 0 \quad \text{on } y = -d \text{ where } d = \text{water depth} \qquad (3.6)$$

b. The free surface kinematic boundary condition states that

the rate of increase of the hydrostatic component of pressure at the surface is equal to the rate of decrease of the transient component of pressure.

The height of the free surface increases at a rate equal to the vertical component of fluid velocity or the vertical gradient of the velocity potential, ie $\partial\Phi/\partial y$. Thus the boundary condition to be satisfied is:-

$$-\rho g\frac{\partial\Phi}{\partial y} = \rho\frac{\partial^2\Phi}{\partial t^2} \text{ at } y = 0 \qquad (3.7)$$

where d = water depth

The solution of the Laplace equation with the boundary conditions proceeds to yield the velocity potential Φ :-

$$\Phi = a_o g\frac{\cosh\{k(y + d)\}}{k\sinh kd}\cos(kx - \omega t)$$

where a_o = wave amplitude.

k = wave number = $2\pi/L$

ω = frequency.

It follows that the dispersion relationship between ω and k can be stated as:-

$$\omega^2 = gk\tanh kd \qquad (3.9)$$

For deep water (d > L/2), equations (3.8) and (3.9), take the form:-

$$\Phi = a_o\omega e^{ky}\cos(kx - \omega t) \qquad (3.10)$$

and $\omega^2 = gk$ (3.11)

The velocity potential thus described is referred to as the undisturbed incident wave velocity potential and is henceforth denoted by a subscript I, ie Φ_I.

The ability of the body to 'resist' the incident wave manifests itself in the generation of a scattered wave emanating from the surface of the body and in a direction away from the body (see fig. 3.1). This diffracted wave potential must, in addition to the boundary on the incident wave potential, satisfy the kinematic boundary condition on the surface of the body of zero normal velocity, ie:-

$$\frac{\partial \Phi_A}{\partial n} = 0 \quad \text{at the body surface} \tag{3.12}$$

$$\text{Now, since } \Phi_A = \Phi_I + \Phi_S \tag{3.13}$$

$$\text{then } \frac{\partial \Phi_A}{\partial n} = \frac{\partial \Phi_I}{\partial n} + \frac{\partial \Phi_S}{\partial n} \tag{3.14}$$

$$\text{so that } \frac{\partial \Phi_I}{\partial n} = - \frac{\partial \Phi_S}{\partial n} \tag{3.15}$$

It is also necessary to specify a radiation boundary condition which states that the scattered waves associated with the potential Φ_S are travelling outwards from the body (37).

$$\lim_{R \to \infty} R^{\frac{1}{2}} \left(\frac{\partial \Phi_S}{\partial r} - \frac{i\omega}{c} \Phi S\right) = 0 \tag{3.16}$$

where $R = \sqrt{x^2 + z^2}$ = the radial distance

and $\omega = 2\pi/T$

$c = L/T$

The Laplace equation, solved in accordance with the additional boundary condition, constitutes the derivation of the scattered or diffracted potential Φ_S. The scattered potential Φ_S is derived in terms of Hankel functions of the first kind, whilst the new incident potential Φ_I can be expressed as a series expansion of Bessel functions. McCamy and Fuchs (38) have developed this theory and

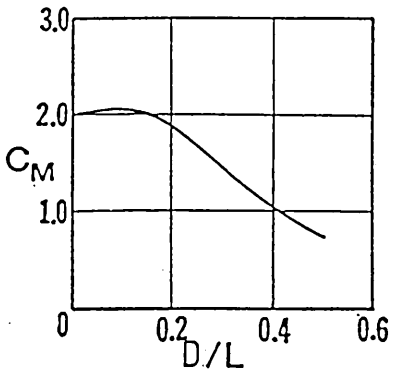

Inertia coefficient for a pile computed from diffraction theory

D—Pile diameter
L—Wave length

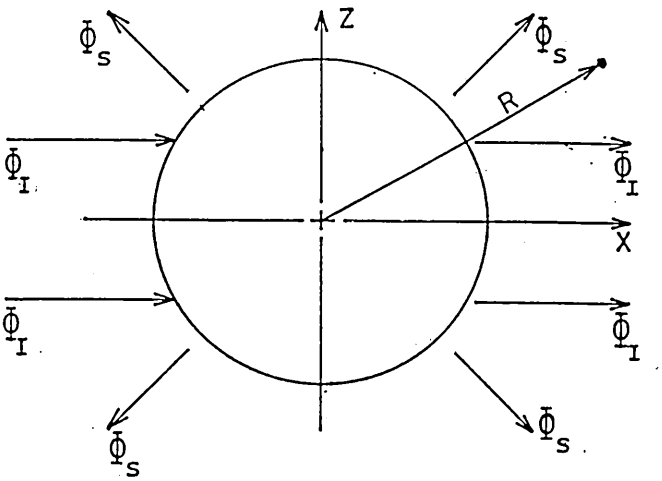

$$\Phi_A = \Phi_I + \Phi_S$$

AT THE BODY SURFACE

$$\frac{\partial \Phi_S}{\partial n} = -\frac{\partial \Phi_I}{\partial n}$$

VELOCITY POTENTIALS

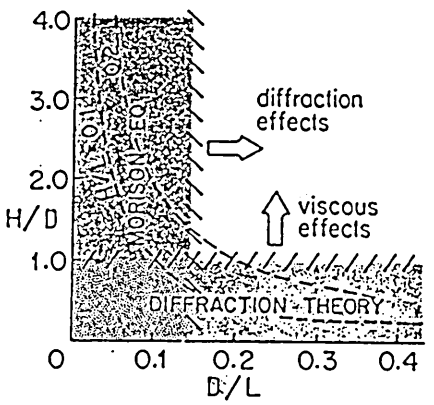

Regions of validity—wave interaction with a pile

H—Wave height = 2
D—Pile diameter
L—Wave length

FIG. 3.1 REGIONS OF VALIDITY OF MORISONS EQUATION

express the inertia coefficient:-

$$C_M = 1 + C_A = \frac{4}{\pi} \frac{1}{(\pi D/L)^2} \frac{1}{\sqrt{J_1'(\pi D/L)^2 + Y_1'(\pi D/L)^2}} \qquad (3.17)$$

where J_1' and Y_1' are derivatives of Bessel functions of the first and second order, respectively.

Values of C_M based on equation (3.17) are shown in fig. 3.1 and shows that the diffraction theory results approach those of the inertia term in the Morison equation as the ratio of D/L tends to zero.

Bodies free to respond to waves will themselves generate waves as a consequence of the induced motions and these can be expressed as additional to the incident and scattered potentials in the form:-

$$\Phi_A = \Phi_I + \Phi_S + \Phi_G \qquad (3.18)$$

$$\text{where } \Phi_G = \sum_{j=1}^{N} \Phi_j \qquad (3.19)$$

and Φ_j represents the potential of waves generated by movement in the j^{th} mode in otherwise calm water. The surface foundary condition must reflect the motion of the body.

The general form of the velocity potential is then written as:-

$$\Phi_A = \Phi_I + \Phi_S + \sum_{j=1}^{N} \Phi_j \qquad (3.20)$$

The pressure distribution is then obtained using the Bernoulli equation.

The total forces on the system will comprise those attributed to the incident and scattered potentials and those attributed to the radiated potential. The latter is decomposed into added mass and damping components and the equation of motion can then be written:-

$$(M + M_A)\ddot{x} + C\dot{x} + Kx = F_E \tag{3.21}$$

where F_E is the force due to incident and diffracted potentials.

4. MORISON'S EQUATION AND ITS LIMITATIONS

The Morison (39) approach to fluid loading assumes that the total force can be expressed as a sum of two components, ie:-

$$F_T = \rho.V.C_M.\dot{u} + \tfrac{1}{2}\rho.C_D.D.u|u| \tag{3.22}$$

The first inertial term reduces to $2\rho V\dot{u}$ as the ratio of D/L tends to zero with $C_M = 2$, when diffraction effects are unimportant see fig. 3.1. The first term is associated with the irrotational part of the flow.

The second term is meant to account for forces associated with the velocity of the flow and takes the form of a steady flow drag force, such as would represent the drag force in steady unbounded flow.

This semi-intuitive form infers that the flow is such as would prevail were the body removed from the fluid, ie that the flow field remain undisturbed. There must therefore be misgivings as to the adequacy of the expression when the ratio of characteristic dimension to wave length D/L increases.

Figure 3.1 (40) gives an indication as to the regions of applicability of the diffraction theory and Morison's equation. This suggests that there is an overlap region banded by $2a_o/D = 1.0$ and $D/L = 0.15$ where both theories are applicable. It also suggests that at large values of both $2a_o/D$ and D/L then both diffraction and viscous effects are important simultaneously so that neither theory would be valid. However, this region is never realised as a consequence of the maximum breaking wave height limit of $2a_o/L = 0.14$ which is shown on the figure.

Lighthill (41) has demonstrated that it is necessary to make corrections to the Morison equation to account for three extra contributions of force as follows:-

a. The linearisation of the free surface boundary condition ignores a quadratic potential which would account for the rate of change of surface elevation. This potential generates a contribution of force associated with the dynamic pressure at the free surface.

b. A second order component of force associated with the linear velocity potential attributed to the distribution of pressure over the complete wetted surface of the structure up to the instantaneous water surface.

c. A second order component of force associated with the linear velocity potential attributed to a fluctuating velocity or extensional velocity term.

Lighthill has shown that the inclusion of the three extra terms as a correction to the Morison equation has the effect of increasing the forces by 12% over and above that predicted by the

Morison equation. In fact for small ratios of D/L the quadratic term is not significant and it is the other two terms, ie (2) and (3) which contribute to the increase. However, as D/L increases so does the quadratic term.

It is evident that the contribution of forces deriving from the complete immersion of the surface piercing cylinder play a significant part in the determination of the forces.

4.1 Choice of Coefficients C_D and C_M

The question of realistic values for inertia and drag coefficients has received considerable attention in the past decade. Keulegan and Carpenter (42) postulated that the coefficients were a function of the period parameter, or Keulegan-Carpenter number, KC,

where $KC = U_m T/D$

and U = maximum horizontal particle velocity

T = wave period

D = diameter of cylinder.

Amongst other things, their observations were that C_D and C_M had maximum and minimum values respectively, corresponding to a KC number of 15. Most of the available experimental data relates to small diameter members in the sub-critical Reynolds number range, ie $R_n < 2.10^5$, and little data at supercritical Reynolds numbers, ie $R_E > 2.10^6$, exists.

Steady flow drag coefficients for a smooth circular cylinder at supercritical Reynolds numbers are likely to have values in the region of 0.66 - 0.8 and possibly greater.

The structures investigated in this study have a minimum diameter of approximately 10 metres, typical structural velocities will be of the order of 3-4 metres per second, so that the structures will be operating at supercritical Reynolds numbers most of the time. A time independent value for C_D of 0.9 has been used for most of the analysis. However, the effects of varying the drag coefficient is the subject of a parameter study in chapter 4. A time independent value for the inertia coefficient of 1.9 has been used throughout the analysis, This is not unreasonable as suggested in References (43,44) for small values of KC, ie <5.

Plots of C_D and C_M as a function of KC and Reynolds numbers for harmonically oscillating flow are shown in fig. 3.2. It is apparent that there is little variation in C_M at the lower values for KC. Values of C_D for small KC are in the region of 1.0 to 1.6 but these are also for very small Reynolds numbers.

4.2 Non Linear Wave Theory

Since the evaluation of wave forces by the use of the Morison equation essentially reduces to the determination of particle velocities and accelerations, it is pertinent to examine the effects of non linear waves. This is discussed in greater detail in Chapters 4 and 5 of this thesis.

It is essential to have an understanding of the shortcomings of any wave loading estimation techniques in order to make a pragmatic assessment of the resulting forces and motions. Notwithstanding, it is believed that the Morison approach to wave loading on articulated columns is valid so long as there is no violation of the

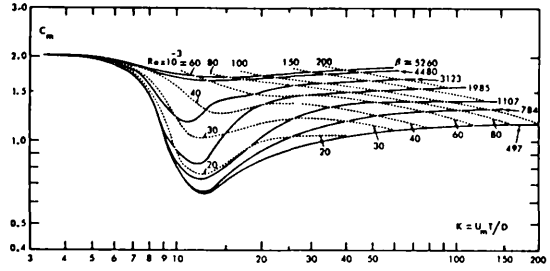

Fig. 3.20. C_m versus K for various values of the Reynolds number and the frequency parameter (Sarpkaya

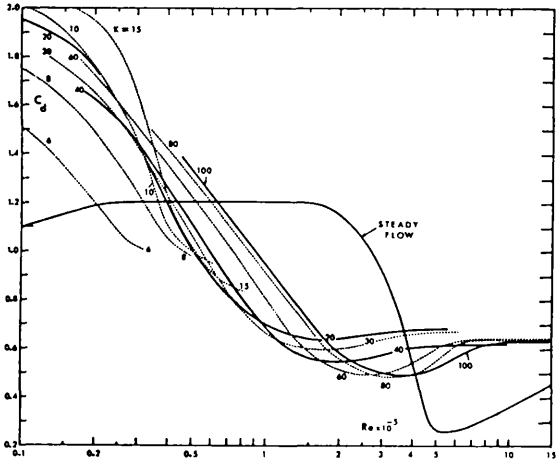

Fig. 3.21. C_d versus Reynolds number for various values of K (Sarpkaya

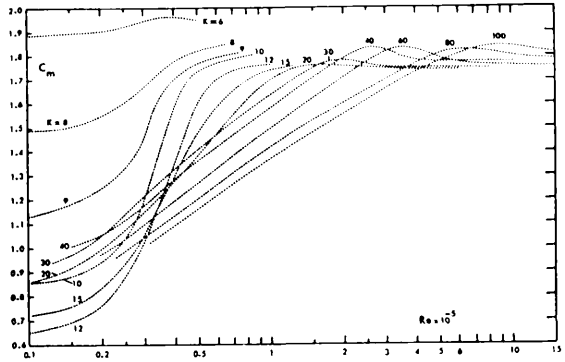

Fig. 3.22. C_m versus Reynolds number for various values of K (Sarpkaya

DRAG AND INERTIA COEFFICIENTS AS A FUNCTION OF REYNOLDS NUMBER AND KEULEGAN- CARPENTER NUMBER

FIG 3.2

characteristic dimension and wave parameter relationships as put forward and shown in fig. 3.1.

5. SECOND ORDER FORCES

The preceeding analysis relates to first order forces and assumes a linear relationship between forces and responses. It is known that floating structures can experience drift forces, either steady or slowly varying. The latter are associated with wave grouping effects and this aspect is further discussed in Chapter 5.

Steady drift can arise as a consequence of second order forces not accounted for in the linearised analysis aforementioned (45). It is an important aspect of motion response and its effects on a structure's performance require understanding.

Drag and diffraction forces contribute to mean drift forces whereas inertia forces do not. The drag contribution is attributable to the integration of these forces to the free surface level, whereas integration of the inertia forces to the free surface levels produces a nett zero inertia component of force.

Diffraction forces contribute to mean drift forces by virtue of the change in momentum of the wave train as a consequence of the diffracted and radiated waves. However, linear diffraction theory will not predict mean drift forces since small amplitude linear waves are used and the velocity potential is also linear, resulting in linear sinusoidally varying forces with the same period as the wave.

Havelock (46) and Newman (17) have presented different approaches to the estimation of mean drift forces. The former is more suited to situations where the waves have a high frequency content whilst the latter which is based on slender body formulations is more suitable to greater wave lengths.

Mean drift forces can be derived in two ways, ie the Far Field (wave momentum) method and the Near Field method.

The Near Field method (18) postulates that the mean force comprises the sum of 6 separate components. These are shown diagramatically in fig. 3.3 and can be interpreted physically as:-

a. A contribution to the first order force as a consequence of pressures on the body between the SWL and the free surface.

b. Second order dynamic pressure term $1/2\rho u^2$

c. A contribution by virtue of the displaced position of the structure.

d. This represents the change in direction of the force vector as a consequence of the rotation of the body.

e. This represents the change in buoyancy by virtue of induced motions.

f. Second order wave contribution, due to the set down of the regular wave train.

A more comprehensive description of these components is given in Reference (45) in which it is noted that the computational task involved in accounting for all the components is considerable.

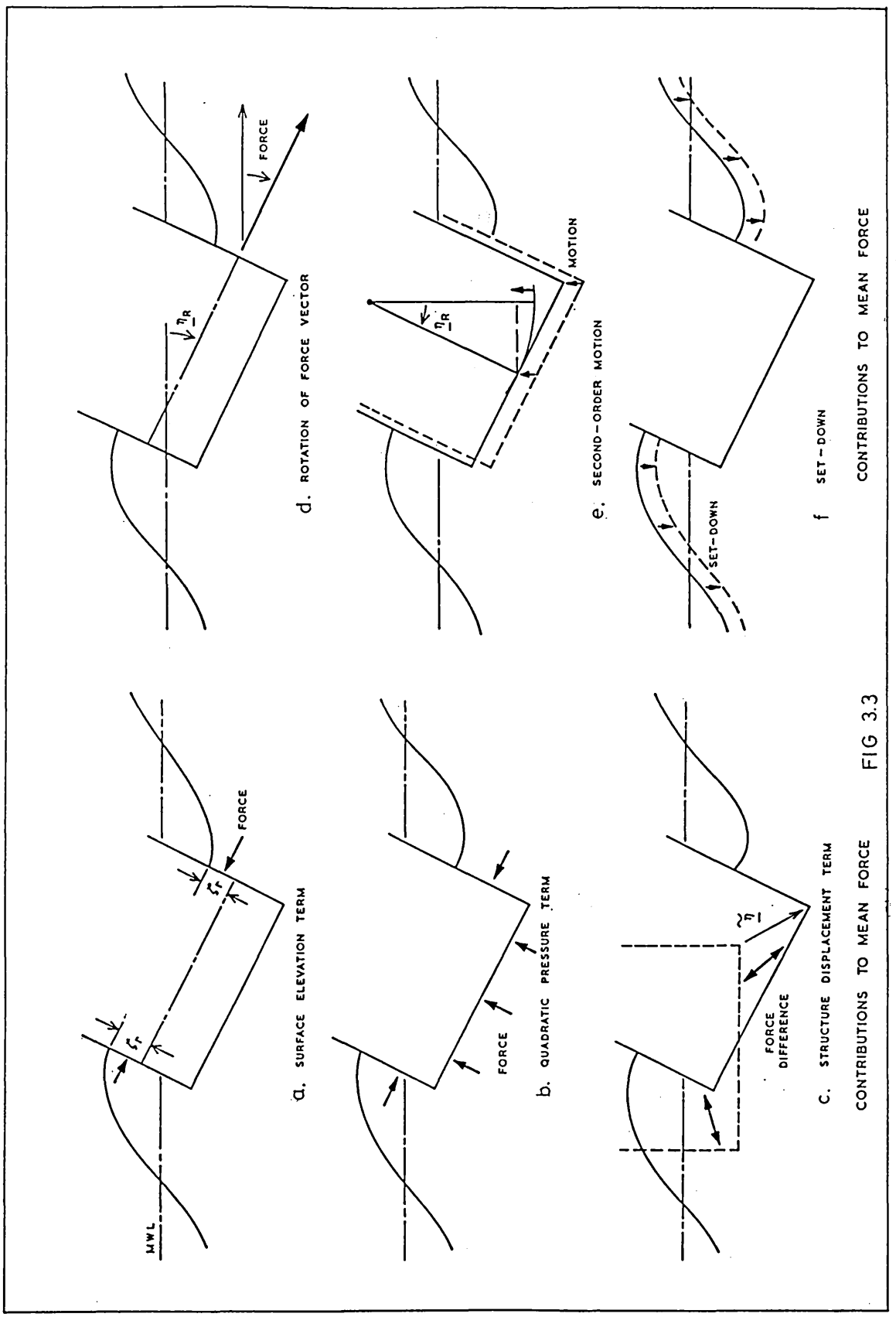
MWL
FORCE
a. SURFACE ELEVATION TERM
FORCE
b. QUADRATIC PRESSURE TERM
FORCE DIFFERENCE
c. STRUCTURE DISPLACEMENT TERM
FORCE
d. ROTATION OF FORCE VECTOR
MOTION
e. SECOND-ORDER MOTION
SET-DOWN
f SET-DOWN
CONTRIBUTIONS TO MEAN FORCE
CONTRIBUTIONS TO MEAN FORCE

FIG 3.3

In the analysis which follows in subsequent chapters the procedure adopted, albeit based on a Morison approach, is believed to account, in principle, for components a. to e. The second order set down wave component has not been modelled but its contribution is confined to slowly varying drift forces and this aspect is further considered in Chapter 5, Section 5.

CHAPTER 4

DYNAMIC ANALYSIS OF ARTICULATED COLUMNS

1. INTRODUCTION

The dynamic analysis of the motion response of compliant structures can, in general, be made either in the frequency domain or in the time domain. The former type of analysis is adequate for linear systems which respond linearly and is generally more efficient in computation time.

In researching the dynamic response of compliant structures, analysis in the time domain is considered both feasible and valuable. Feasible in that modern processors render the very considerable arithmetic computations much less onerous than was the case even a few years ago. Valuable in that non linear behaviour, such as transient response is readily evaluated and investigated. Time varying stiffness properties may also be readily accommodated and examples of this are the varying pendulum stiffness of articulated columns and guyed tower catenary stiffness.

This chapter examines the importance of certain parameters which either contribute to non linear response behaviour or are non linear by nature. The single degree of freedom (SDOF) rigid body equation of motion is described and the modified Morison equation is included as the forcing function. Some features of dynamic response are then examined and these include transients, effects of drag coefficient C_D, effects of relocating deck masses in the buoyancy chamber, alternative geometries of buoyancy chamber, effects of

Stokes 5th order wave theory and the effects of waves and currents. The effects of the variation in the heave forces is given a rigorous examination in Chapter 5 and the contribution of this, in respect of dynamic instabilities, is assessed.

Some experimental results are presented and these are examined in the light of the analytical results obtained. Finally, the action of forces which are not acting colinearily on the structure are examined and the implications assessed.

The calculation of wave loading should properly allow for incident, diffracted and radiated potentials as discussed in Chapter 3. These become increasingly important for the shorter waves where the structure may experience steady drift forces (45). Such analysis is more appropriately conducted in the frequency domain although it can be adapted to time incremental solutions subject to limitations on computation time.

A simplified method of calculating the wave forces by strip theory can, however, be utilised, the assumption being that the structure leaves the flow field undisturbed. One such appropriate method is by the use of the Morison equation (39) which comprises an inertia term and a steady flow drag term. The non-linear drag component, which would require linearisation for a frequency domain analysis, is amenable to and readily accounted for in time simulation analysis.

As discussed in Chapter 3, it is considered that the Morison approach to the evaluation of wave loads is reasonable in the investigation of the maximum response of articulated column

structures where typically ratios of member diameter to wave length (D/L) will be less than 0.2. This ratio determines a lower limit of about 10 seconds on the wave period for structures considered herein. For smaller periods, the dynamic pitch response is not of any great technical significance. Vibration considerations are important for wave periods of this order and less and this is discussed in more detail in Chapter 6.

2. STRUCTURE SUBJECT TO COLINEAR EXCITING FORCES

In general, maximum responses will occur when the exciting forces are acting colinearly with one another on the structure. Accordingly, the motion response of an articulated column can be described by the pitching motion of the structure about the articulated joint. It is assumed, for the time being, that rigid body deformations predominate so that the system can be considered as a single degree of freedom system (SDOF).

2.1 Equation of Motion

Single degree of freedom

With reference to Fig. 4.1; the equation of motion for the articulated column can be written:-

$$I_T\ddot{\theta} + C\dot{\theta} + K_S\theta = M \qquad (4.1)$$

where $I_T = I_M + I_{AV}$

I_M = Mass moment of inertia

I_{AV} = Added mass moment of inertia

C = Damping coefficient

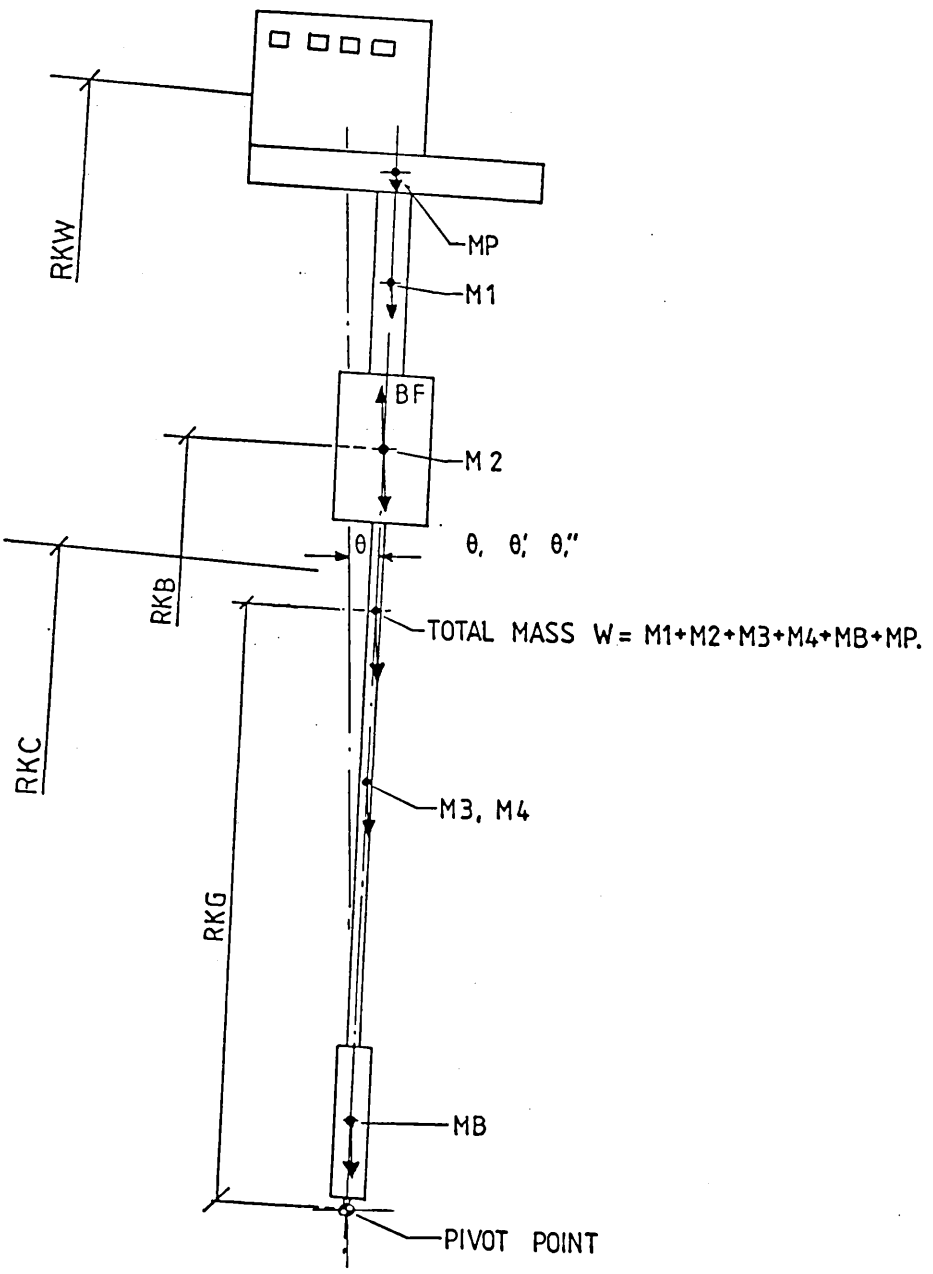
RKW
MP
M1
BF
M 2
θ
θ, θ', θ,"
RKB
TOTAL MASS W = M1+M2+M3+M4+MB+MP.
RKC
M3, M4
RKG
MB
PIVOT POINT

FIG. 4.1

M = Sum of exciting moments about the pivot

K_S = Pendulum stiffness of column in ϑ direction

= B_F.RKB - W.RKG

B_F = Buoyancy force

W = Total weight of structure

RKB = Distance from pivot to centre of buoyancy

RKG = Distance from pivot to centre of gravity.

The natural frequency of the column in pitch for free undamped vibration, therefore, is given by:-

$$\omega_n = \left[\frac{(B_F.RKB - W.RKG)}{I_M + I_{AV}}\right]^{\frac{1}{2}} \qquad (4.2)$$

Linear Equations of motion

If we assume a linear system and that excitation and response may be written in the form:-

$$F(t) = F_o \exp(j\omega t) \qquad (4.3)$$

and $$r_s(t) = R_o \exp(j\omega t) \qquad (4.4)$$

then the steady state response is given by

$$r_s(t) = |H(\Omega)|F(t) \qquad (4.5)$$

where $$H(\Omega) = \frac{1}{I_T(\omega_n^2 - \Omega^2 + 2j\beta\omega_n\Omega)} \qquad (4.6)$$

Now $H(\Omega)$ is complex and can be written in the form $|H(\Omega)| K_s \exp(j\,\xi)$ where $|H(\Omega)|$ is the real amplitude of response due to a unit amplitude excitation at frequency Ω and ξ is the phase angle between the excitation and the response.

$$\text{Hence,} \quad |H(\Omega)| = \frac{1}{I_T \omega_n^2 \left[\left(1 - \left(\frac{\Omega}{\omega_n}\right)^2\right)^2 + 4\left(\frac{\beta\Omega}{\omega_n}\right)^2\right]^{\frac{1}{2}}} \tag{4.7}$$

where $|H(\Omega)|$ is the dynamic magnification factor.

The peak response can be written,

$$r_{PK} = |H(\Omega)| M_{PK}$$

where the subscript PK refers to peak values.

Modified Morison Equation

The RHS of the equation can be written in the Morison form as:-

$$M = M_I + M_D \tag{4.9}$$

where M_D = Moment attributed to viscous effects

$= \frac{1}{2}\rho . C_D . D . u|u| r$ per unit length

M_I = Moment attributed to inertia effects

$= \rho . V . C_M . \dot{u} . r$ per unit length

V = Volume of member

D = Diameter of member

r = Radius from articulation

d_i = Immersed depth

ρ = Water density

C_M = Inertia coefficient = $(1 + C_A)$

C_A = Added Mass Coefficient

C_D = Drag coefficient

$u, \dot{u}$ = Horizontal particle velocity and acceleration

The stiffness term K_s must allow for the contribution of the submerged portion of the upper support column and its variation as a

function of wave profile.

$$\text{Hence, } M = \int_{-di}^{o} [\tfrac{1}{2}.\rho.C_D.D.u|u|.r + \rho.V.C_M\dot{u}.r]dr \qquad (4.10)$$

This may be rewritten to account for the motions of the structure relative to the waves, wind and current.

$$\text{ie, } M = \int_{-di}^{o} [\rho.V.(C_M - 1).r.(\dot{u} - r\ddot{\theta}) + \rho.V.\dot{u}.r$$

$$+ \tfrac{1}{2}\rho.C_D.D.(u - r\dot{\theta})|u - r\dot{\theta}|.r]dr \qquad (4.11)$$

The first term is the added mass term; the second term is the Froude-Krylov component and the third term is the non-linear drag term.

Rewriting equation (4.11):-

$$M = \int_{-di}^{o} [\rho.V.r.(C_M - 1)\dot{u} - \rho.V.r.(C_M - 1)r.\ddot{\theta} + \rho.V.\dot{u}.r$$

$$+ \tfrac{1}{2}.\rho.D.C_D(u - r\dot{\theta})(u - r\dot{\theta})r]dr \qquad (4.12)$$

Now I_{AV} = Added mass moment of inertia

$$= \int_{-di}^{o} [\rho.V.r^2.(C_M - 1)\ ]dr \qquad (4.13)$$

This term can be transferred to the LHS of the equation of motion so that:-

$$(I + I_{AV})\ddot{\theta} + C\dot{\theta} + K_s\theta = \int_{-di}^{o} [\rho.V.C_M.r.\dot{u} + \tfrac{1}{2}.\rho.C_D.D.(u - r\dot{\theta}).|u - r\dot{\theta}|]dr \qquad (4.14)$$

The non-linear quadratic drag term is not amenable to linear analysis and is frequently equivalently linearised (47). This introduces an error term which can be minimised in the least squares sense. So that an equivalent linear drag force term can be substituted, viz,

$$\text{Drag force} = \tfrac{1}{2}\rho C_{DL}.D.u_n \qquad (4.15)$$

where,

$$C_{DL} = C_D.\frac{8}{3\pi}.u_o \qquad (4.16)$$

u_o = the amplitude of the oscillatory resultant normal velocity and u_n = resultant normal velocity

This assumption has the basis that the drag term does not constitute a major portion of the forcing function and is, therefore, not responsible for any significant instability phenomenon which is not also contained in the linear approximation.

Response amplitude operators of pitch per unit wave height versus wave excitation frequency can thus be obtained. This approach is valuable in the design and appraisal of the motion characteristics of offshore vessels and structures and is commonly utilised.

2.2 Time Domain Solution of the Equations of Motion

The non-linear drag term as discussed in the previous section

together with the time varying pendulum stiffness of an articulated column as a function of the immersed depth, position of the structure relative to the wave and the heaving forces renders an analysis in the time domain desirable.

There are, essentially, two approaches to the time incremental solution of the equations of motion, viz direct integration methods and multi-step methods[48]. Both methods have been found to be satisfactory in the solution of the SDOF equation of motion and both have been used in obtaining the results presented.

A computer program was written to solve the equation of motion (4.14) on a time incremental basis. The direct integration procedure used was the Wilson-θ operator with $\theta = 1.0$ and this is basically a linear acceleration method. More details of this integration procedure are given in Chapter 7 and Appendix 4.1.

Program development was on the assumption that the lower column would remain flooded. The buoyancy restoring force attributed to the displacement volume of the buoyancy chamber and the submerged portion of the upper support column was considered to act at the centre of buoyancy as shown in fig. 4.1.

The LHS of equation (4.14) contains terms for the mass plus added mass, damping and stiffness in respect of acceleration, velocity and displacement respectively. The calculation of forces attributed to these terms is carried out up to the instantaneous or temporal water surface level. Thus the added mass and stiffness terms reflect the variation in the water surface level as a function of time.

2.3 Transient Responses

The equation, $M\ddot{x} + C\dot{x} + K_s x = F_o \sin\omega t$ has the full solution (49),

$$x(t) = e^{\frac{C}{2M}.t} \left(A_o \sin\omega_n t + B_o \cos\omega_n t\right) + \frac{F_o}{K_s} . \left|H(\omega)\right| \sin(\omega t - kx) \qquad (4.17)$$

where A_o and B_o are arbitrary constants and can be evaluated for any given starting conditions.

The first term is the transient response and the second term is the steady state response. The first term is generally considered to decay rapidly with small amounts of damping ($\beta\omega_n = C/2M$). The second term is the steady state response as a consequence of the steady state excitation at frequency ω.

Inoue (50) has given a solution to the above equation as,

$$x(t) = X_o \frac{\omega}{\omega_n} e^{-\frac{C}{2M} t} \sin\omega_n t - \sin\omega t$$

where X_o is the amplitude of the forced oscillation.

This equation implies that the transient response is proportional to the frequency of excitation ω. Inoue presents results in support of the equation which shows that with increasing ω the ratio of the amplitude of the transient response to the amplitude of the forced oscillation also increases.

The results of this investigation do not concur with those of Inoue and, in fact, tend to display an attenuation of the ratio of the

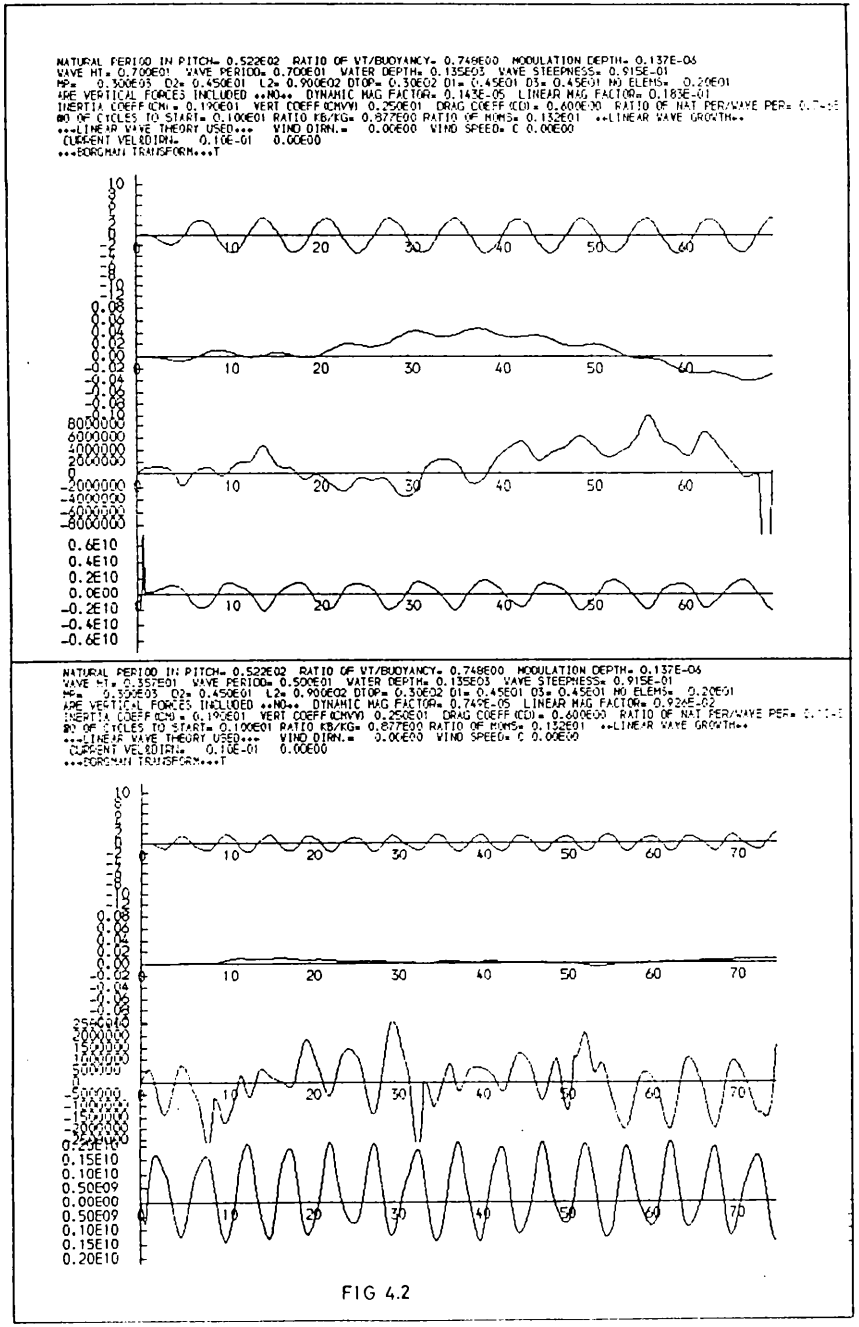

FIG 4.2

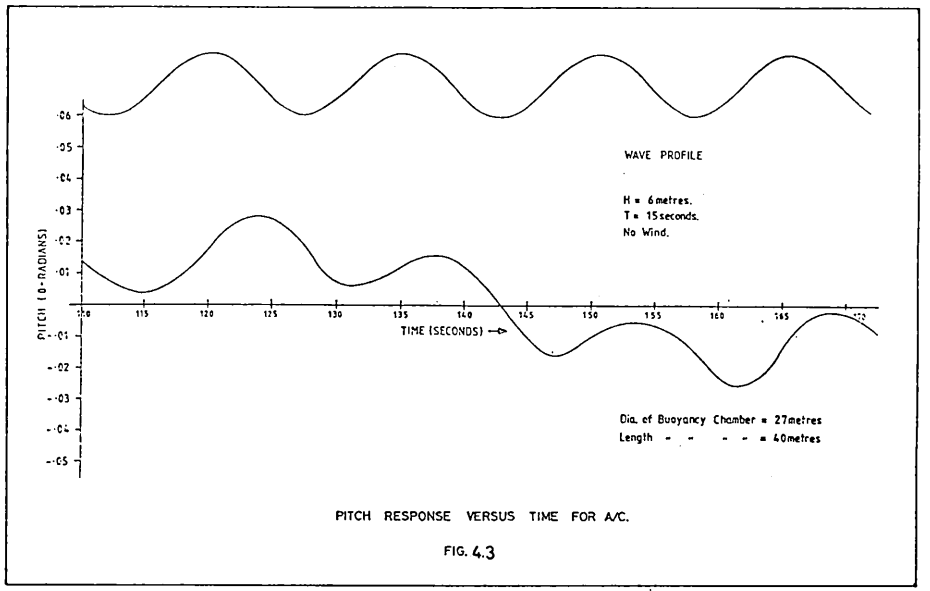

PITCH RESPONSE VERSUS TIME FOR A/C.

FIG. 4.3

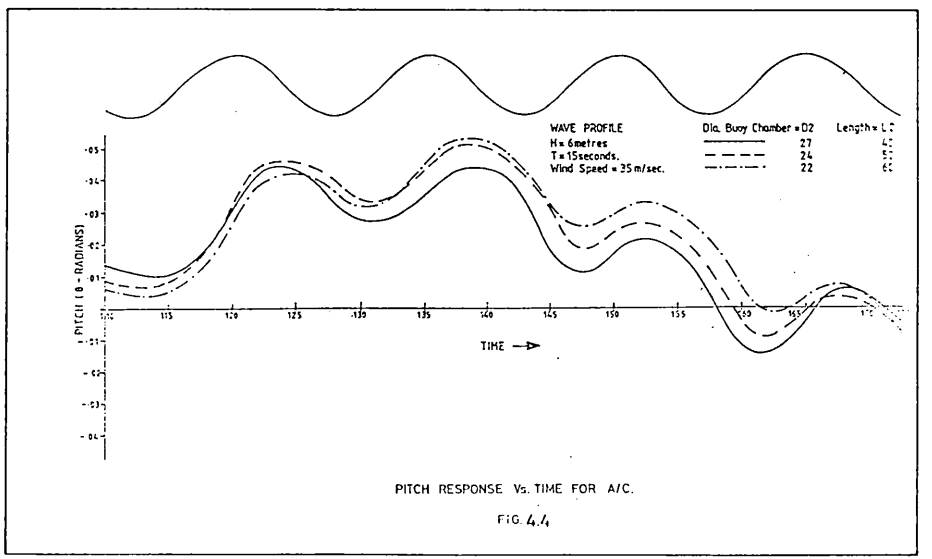

PITCH RESPONSE Vs. TIME FOR A/C.

FIG. 4.4

amplitude of the transient oscillation to that of the frequency oscillation for increasing forcing frequency ω. Figure 4.2 is a comparison of curves showing the response at two different frequencies but for the same amplitude of forced oscillation. The attenuation of the transient oscillation is apparent.

Kokkinowrachos (51) has predicted transient oscillations in the case of articulated columns and these have been observed on a full scale prototype articulated column. Some analytical results are presented in section 2.4 of this chapter.

Relative Velocity Term

The modified Morison equation approach to fluid loading which allows for the inclusion of the non linear relative velocity drag terms and its effect on the response merits consideration.

The wave forces on the structure are calculated on the basis that the evaluation of particle velocities and accelerations is valid for elevations above the still water level, up to the instantaneous water surface level. The calculation of forces up to the instantaneous water surface will result in a nett cancellation of the inertia forces in a wave cycle. This will not be the case in respect of the drag forces which will display some proportionality with the wetted length of the structure in a wave cycle. On a fixed structure the drag force would have a nett component in the direction of the wave travel and this component would be maximum for a Keulegan-Carpenter number (KC) of approximately 15.0. (42). The Keulegan-Carpenter number (KC) is defined as $KC = U_m T/D$ or $\pi H/D$ where U_m is the maximum horizontal particle velocity.

In the case of articulated columns, or compliant structures in general, the situation with regard to nett drag forces is somewhat less straightforward in view of the phase of the response with respect to the wave forces. In general the wave frequency ω will be much greater than ω_n and the inertia forces will predominate, so that the response will lag the maximum wave inertia forces by approximately 180^o, ie the response will be positive when the wave forces are negative and vice-versa. This means that the structures velocities will generally be in phase with wave particle velocities. This will tend to reduce the damping effects of the viscous component of force. However, this would not be the case in respect of motions due to slowly varying drift forces for example when the body motions may lag the wave inertia forces by 90^o.

Nonetheless, the drag component will affect the motion response and may, in fact, contribute to the transient part of the response.

2.4 Analytical and Experimental Results

Analytical results

The computer program developed, first calculates the static angle of heel of the column subject to a steady 35 metres per second wind force and/or a specified current velocity and uses this value together with the initial condition that the column is stationary to start the time series solution.

A particular version of the program allows for the excursion of the elemental section in the wave in calculating the particle

velocities and accelerations pertaining to the section. In the calculation of forces on elemental sections, components normal to the axis of the structure are taken. The results of this version of the program for the column subject to a 6m, 15 sec wave and zero wind speed are shown in fig. 4.3. This figure also shows response curves for different buoyancy chamber dimensions - in this case the displacement volume and centre of buoyancy are maintained as constant and the length and diameter of the chamber are varied. The closer proximity of the top of the 22 metre diameter chamber to the water surface explains the increased response for that particular structure.

Figures 4.3 and 4.4 show what appears to be a harmonic transient oscillation, about which is superimposed a higher frequency oscillation of the column at the wave exciting frequency. This transient oscillation, although locked on to a multiple of the wave frequency, is of the order of the natural period of oscillation of the column in pitch as calculated from equation (4.2), ie T_n = 72 seconds, $T_{transient}$ = 75 seconds.

Results for 17 second and 25 second waves show the transient oscillation period at 68 seconds and 75 seconds, respectively, and in phase with wave oscillation, ie the structure tends to lock on to a multiple of the wave period.

Transient phenomena will be more pronounced in compliant structures and the question of authenticity naturally is posed. In order to examine the transient the programs were run for 2000 seconds model time. Figure 4.6 shows the results of the extended run time for the column subject to a 6 metre high, 15 second wave plus a wind speed

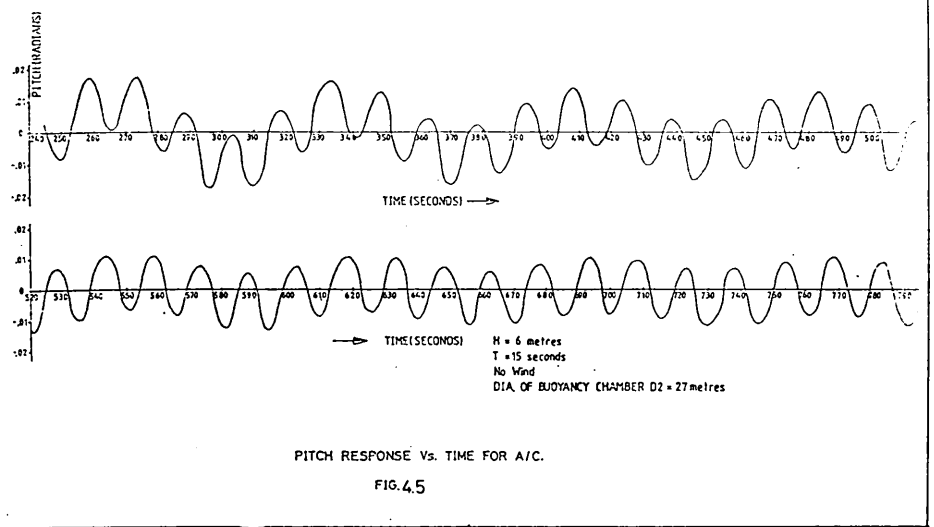

PITCH RESPONSE Vs. TIME FOR A/C.

FIG. 4.5

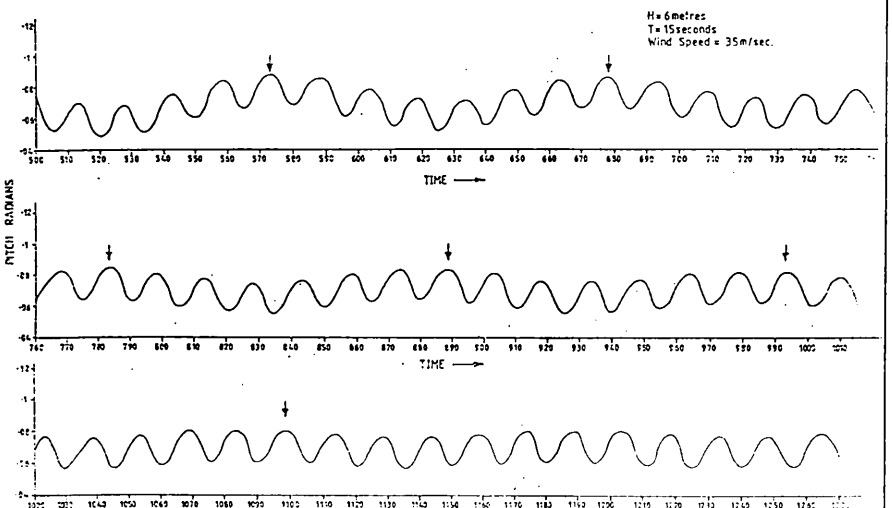

PITCH RESPONSE Vs. TIME FOR A/C

(DAMAGE CONDITION, BULKHEAD FLOODED)

FIG 4.6

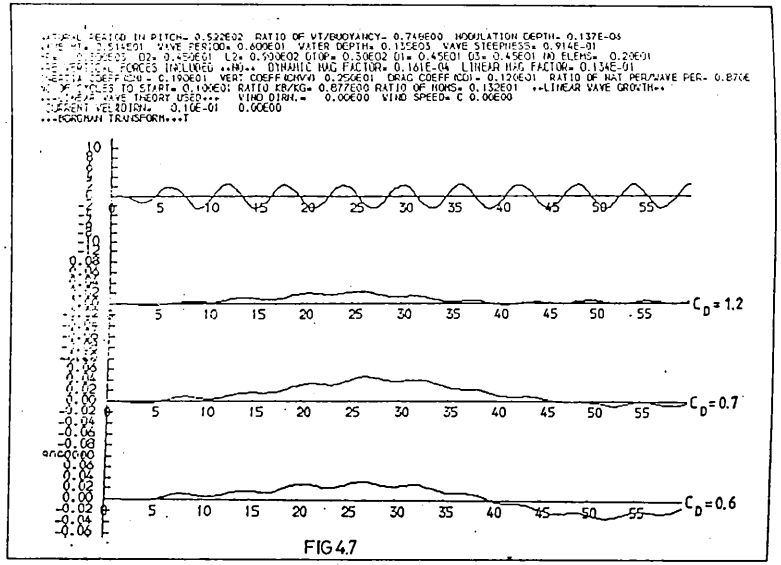

FIG 4.7

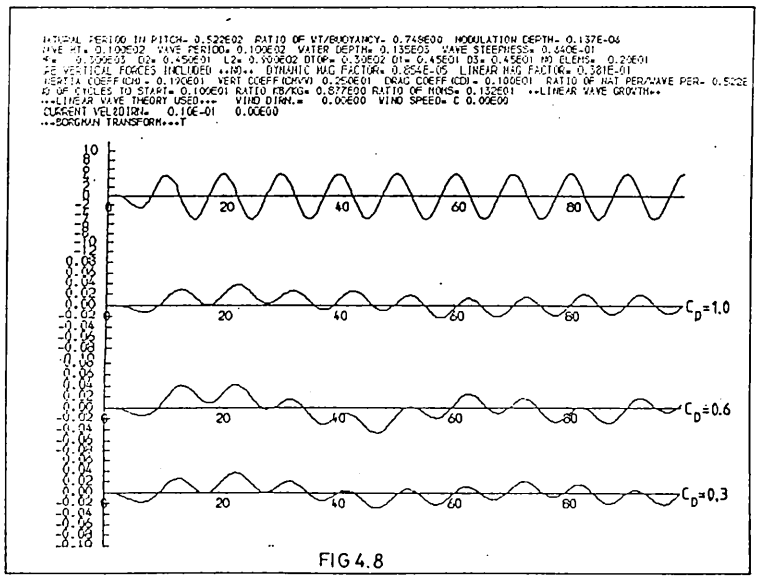

FIG 4.8

of 35 metres per second and a watertight compartment flooded. The extra mass due to the flooded compartment has the effect of reducing the natural frequency of the column in pitch, ie the period of the transient is increased and the pitch response is reduced. Figure 4.6 shows the decay in the transient to be more rapid and this may be attributed to the extra damping provided by the wind force.

The steady state linear peak response in pitch for a 6 metre high, 15 second wave as given by equation (4.5) is equal to 0.0135 radians. This is to be compared with the peak response as shown in fig.4.3, of 0.028 radians, ie a 107% increase in response. Allowing for the decay in the transient, the responses calculated by both methods are of the same order of magnitude, ie the wave frequency oscillatory responses are the same.

Effect of C_D on response

Figure 4.7 shows the response for a structure subject to the same wave for different values of drag coefficient C_D. The bottom plot is that for a C_D value of 0.6. It is apparent that the transient part of the response increases to a maximum for a value of $C_D = 0.7$ and thereafter decreases to a minimum for the value of $C_D = 1.2$ where the transient is eventually completely damped out. The damping effect of the drag component is evident for values of C_D greater than 0.7. Close inspection of the plots shows that the responses have different phases for the different values of C_D. It would appear therefore that, for this relatively small structure, the value of drag coefficient can affect the phase of the motion response and, in turn, affect the damping contribution of the relative speed squared term. These results are for a 6 second wave 5.14 metres high. A

similar trend is observed for a larger and longer wave ie 10 metres high with a period of 10 seconds, as shown in fig. 4.8.

The transient may be attributable, in part, to the integration procedure used and it is noted that the results for figs. 4.2 to 4.6 were obtained by a direct integration procedure, whereas the results in figs. 4.7 to 4.8 were obtained by a multi-step integration procedure, ie Runge-Kutta-Merson. Transients are further investigated in the context of dynamic instabilities and discussed in Chapter 5. It is also noted that at the full scale, Reynolds numbers are likely to be in the supercritical region ie $> 10^6$. Values of C_D are likely to be of the order of 0.5 to 0.7 and it would therefore not be unreasonable to expect maximum transient responses at the full scale. However, these values relate to smooth cylinders and it must be borne in mind that marine growth will make a contribution to increasing roughness values over a period of time, so that corresponding values of C_D could well be of the order of 1.0-1.2.

Effects of Relocating Deck Masses in Buoyancy Chamber

As discussed in Chapter 2, it is envisaged that the accommodation inside the buoyancy chamber could be used to contain certain items of plant and machinery which would otherwise be located on the platform deck. The structural provisions necessary to achieve this aim are not considered to be excessive compared to those to be made for the buoyancy chamber not containing plant, ie some form of lateral bracing will probably be necessary and the proposed flooring on three levels will help in this respect.

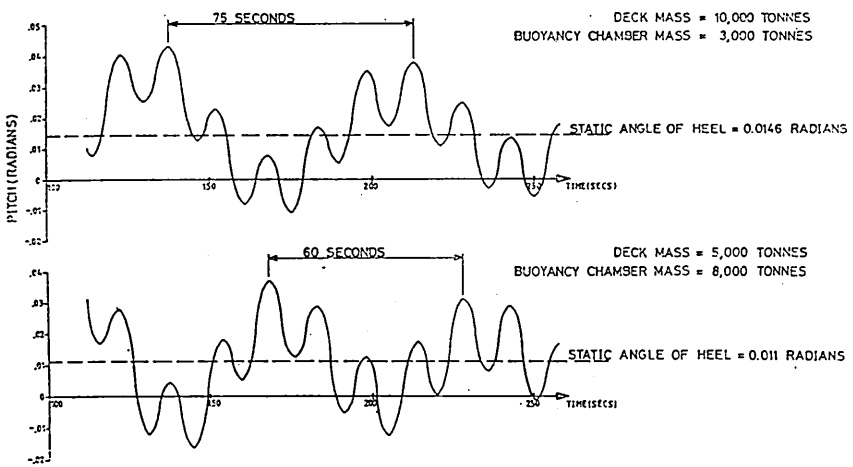

PITCH RESPONSE VERSUS TIME FOR PLATFORMS WITH VARYING DECK MASS.

FIG. 4.9

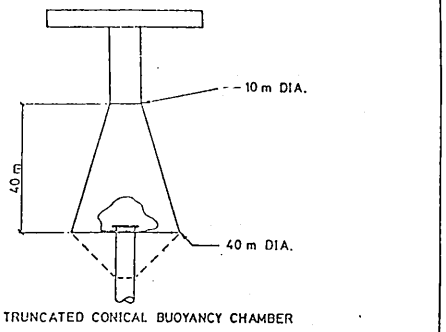

TRUNCATED CONICAL BUOYANCY CHAMBER

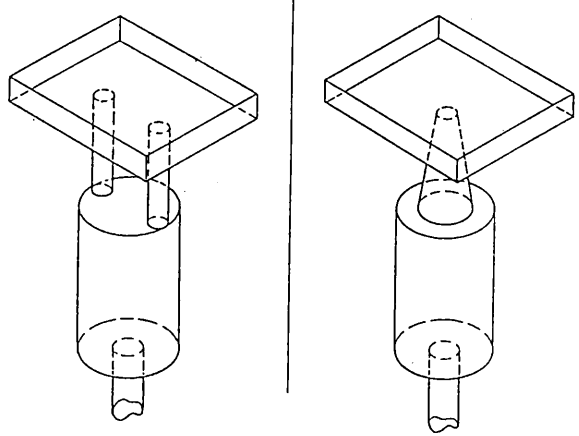

POSSIBLE ALTERNATIVE ARRGTS. FOR
BUOYANCY CHAMBER & DECK SUPPORT COLUMNS

FIG. 4.10

The effects of varying the deck mass and payload have been examined in the context of dynamic response. The platform deck and payload was reduced by an amount which was added to the buoyancy chamber. This reduces the mass moment of inertia of the structure and, therefore, increases the natural frequency in pitch. For the case of a reduction in the platform deck weight from 100,000 KN to 50,000 KN there is an accompanying reduction in the pitch response of the order of 10%. This is a modest reduction and is, in the main, attributable to the increased pitch stiffness (see fig. 4.9).

Alternative Geometries for the Buoyancy Chamber

The buoyancy chamber and the upper support column are in the most active wave loading region and it is essential that means of reducing loading are investigated.

A spherical buoyancy chamber is probably the most efficient buoyancy device from the hydrodynamic point of view, although it may suffer from lateral instabilities (52), but highly impracticable in terms of construction and accommodation. From this point of view, plane surfaces are desirable. The circular cylinder as proposed is a reasonable compromise in consideration of construction, accommodation and hydrodynamic efficiency.

The truncated conical buoyancy chamber as shown in fig. 4.10was investigated and, using inertia and drag coefficients C_M and C_D as for the circular cylindrical section, a reduction in response of 25% was achieved.

Effect of Stokes Fifth Order wave

The use of linear wave theory in the calculation of wave forces has obvious attractions but may result in under/over predictions (53) of these forces. Non-linear wave lengths are generally greater than the linear wave length of the same period and as the horizontal inertia force decreases as $2\pi a/L$ increases, above a given value, then a decrease in $2\pi a/L$ as a consequence of the increased wave length may give rise to an increased horizontal load (40).

The non-linear wave profile will also display differences to the linear profile, in that wave amplitudes and troughs are generally greater than and less than, respectively, half the wave height. This effect is more pronounced in the higher frequency waves and, for example, the Stokes fifth order wave theory calculates a crest height above mean level of 11.9 metres for a 10 second wave 20 metres high - an increase of almost 20% on the wave crest over that of a linear wave. In consideration of the drag component of force, this non-linearity warrants quantification and comparison with the linear case.

Hogben and Standing (53) have compared the forces on surface piercing cylinder by both linear theory and Stokes fifth order theory. They found that differences in velocity and acceleration profiles by both methods were small for deep water waves (ie $H/d = 0.2$, $H/gT^2 = 0.015$, $d = 150m$, $H = 30m$, $T = 14$ secs). Also that inertia components of force by Stokes theory were slightly greater than by linear theory when integrated to the free surface and slightly less than linear theory when integrated to the SWL. Drag

components by Stokes theory were less than by linear theory when integrated to the SWL but were greater when integrated to the free surface.

The solution to the Stokes fifth order wave theory as presented by Skjelbria and Hendrikson (54) is outlined in Appendix 4.2 and the constants given for various ratios of d/L. The procedure is readily programmed and requires the solution of two simultaneous equations for wave height, wave length and lambda. This has been done in the form of two subroutines; the first subroutine solves the simultaneous equations and calculates the constants, iterating the solution on a bisection procedure. The second routine calculates the wave profile and the particle velocities and accelerations.

The regions of validity of the various wave theories are suggested as shown in fig. 4.11 (55) and indicates that for deeper water the Stokes fifth order wave theory is applicable.

At intermediate and shallow water depths the wave profile and velocity and acceleration profiles may contain unrealistic 'bumps' and this suggests a limitation to the application of the theory as per Skjelbria and Hendrikson. Ebbesmeyer (56) has suggested these limitations graphically as shown in fig. 4.11.

By way of illustration of the presence of the so called 'bumps', fig. 4.12 shows the surface profile and velocity and acceleration profile for a 5.69 metre wave with period 7.72 seconds in water depth 9.25 metres. The H/gT^2 and d/gT^2 values are 0.0097 and 0.0157, respectively. The wave profile does not possess any irregularities. However, velocity and acceleration profiles do

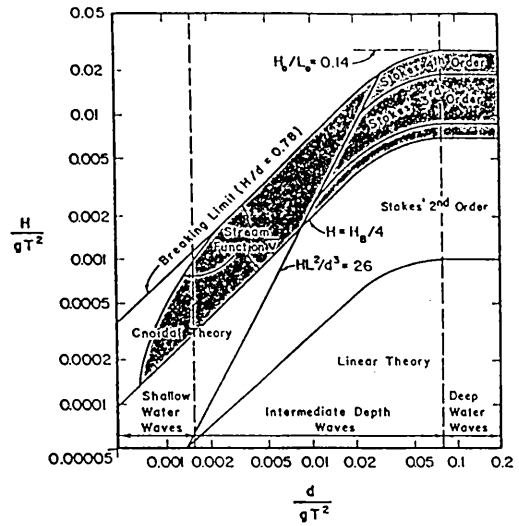

Ranges of suitability for various wave theories as suggested by Le Méhauté

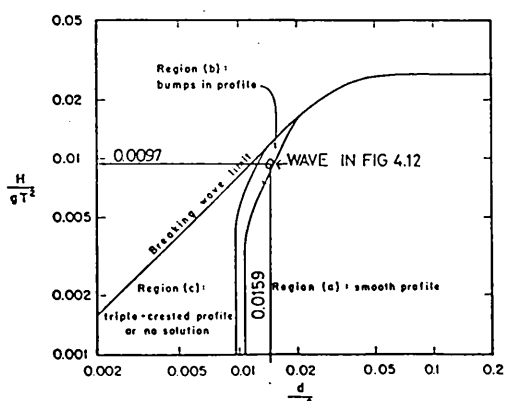

Regions of characteristic wave profiles predicted by Stokes fifth order wave theory (Ebbesmeyer

FIG 4.11

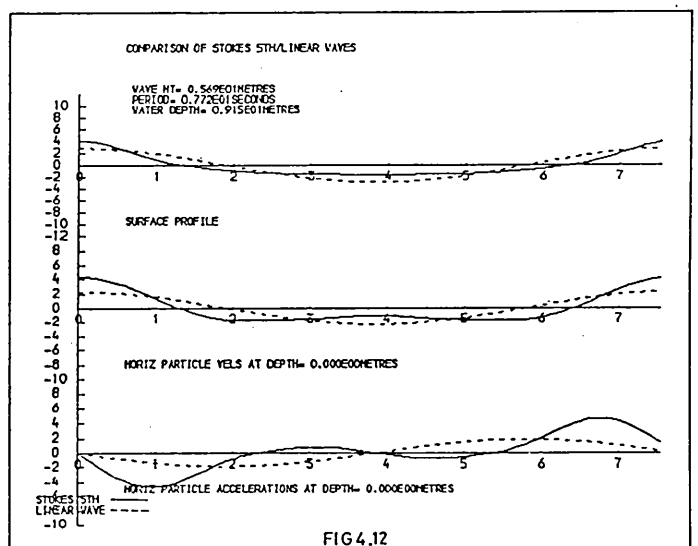

FIG 4.12

display undulations. This example is the same as that presented by Skjelbria and Hendrikson and corresponds to an intermediate depth wave. The horizontal particle velocities at the mean surface level are approximately 21% greater as calculated by Stokes fifth order theory than by linear wave theory.

As water depths increase the differences in particle kinematics as predicted by both theories also decreases. As an example of a deep water wave, ie H/gT^2 and d/gT^2 equal to 0.02 and 0.137, respectively, fig. 4.13 shows the variation of velocity and acceleration with depth as a comparison for the linear wave theory and Stokes fifth order wave theory. Stokes theory appears to predict velocities and accelerations about 9% less than those predicted by linear theory at the still water level. The difference decreases with depth to about 25 metres below the SWL and, thereafter, Stokes theory predicts values somewhat higher than linear theory but only of the order of 2% to 3%.

Figure 4.14 shows results obtained for a wave at the upper limit of the definition of intermediate water depth, ie $d/gT^2 = 0.068$. Velocity distributions are similar to those of the deep water wave except that the Stokes theory displays an asymptotic minimum value of about 0.75 metres per second at the sea bed. Accelerations by the Stokes theory are less than those by linear theory over the whole depth.

It is also instructive to compare velocity and acceleration distributions by both theories as a function of the wave phase angle. Figure 4.15 gives distributions for one wave cycle at a depth of 5m below the SWL. The Stokes theory predicts velocities less than those

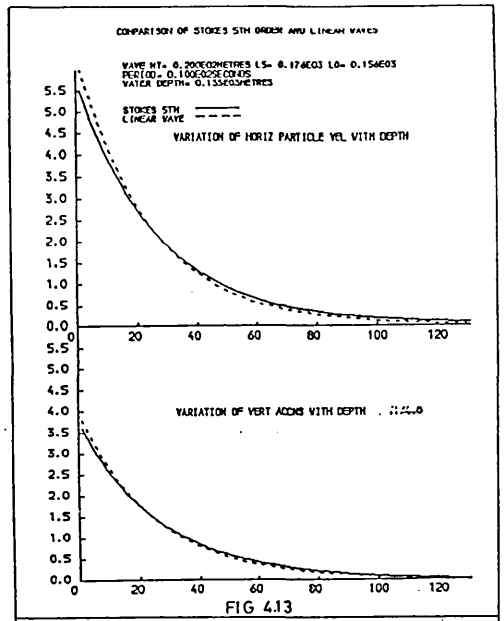

FIG 4.13

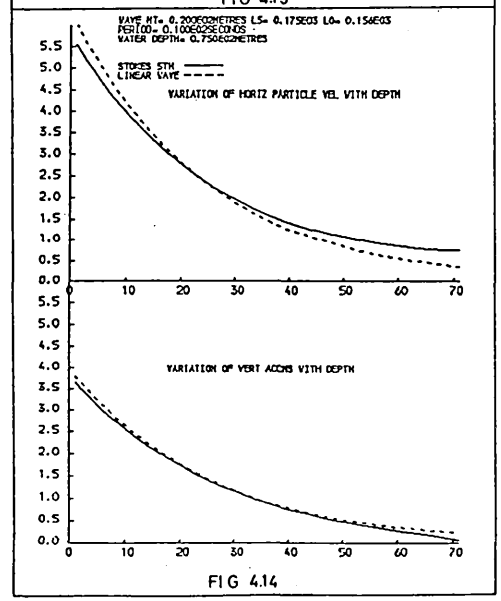

FIG 4.14

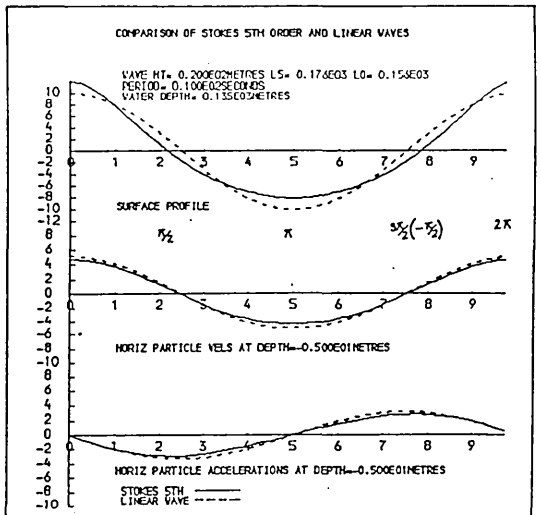

FIG 4.15

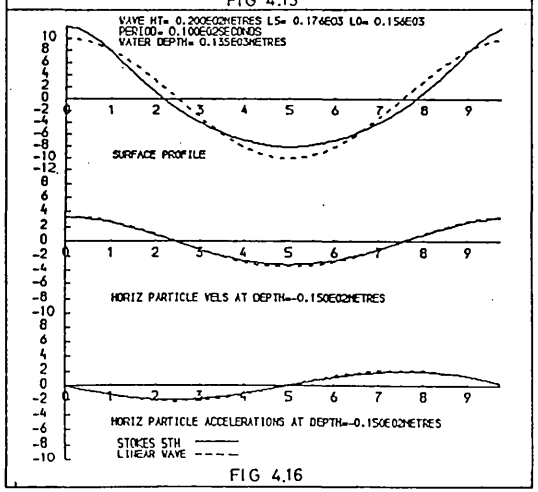

FIG 4.16

of linear theory between $-\pi/2$ and $\pi/2$ radians and greater velocities between $\pi/2$ and $3\pi/2$ radians. Accelerations predicted by Stokes appear to be less throughout the wave cycle, the maximum difference occurring at approximately 0.7π radians and 1.3π radians. For comparison, fig. 4.16 shows the distribution of velocity and acceleration for the same wave at a depth of 15 metres beneath the SWL.

Ohmart and Gratz[57] have compared velocity and acceleration distributions by Stokes fifth order, Deans stream function and linear theory with measured distributions from a site in the Gulf of Mexico and their findings indicate that results of Stokes theory and stream function theory were almost indistinguishable. The distributions were qualitatively similar to those in fig. 4.15, ie the Stokes theory predicted values somewhat less than those predicted by linear theory.

Comparison of responses

For figs. 4.17 to 4.26, the top plot is the wave profile; the second plot is the pitch response; the third plot is the damping force and the fourth plot is the restoring moment.

Figure 4.17 shows the response for a structure subject to a 20 metre high 15 second period wave, the wave particle kinematics being calculated by linear theory. Figure 4.18 shows the response for the same wave, the particle kinematics being calculated by Stokes fifth order theory. The responses for figs. 4.17 and 4.18 are very similar and this is not unreasonable considering the similarity of the velocity and acceleration distributions for this relatively long wave which are shown in fig. 4.19.

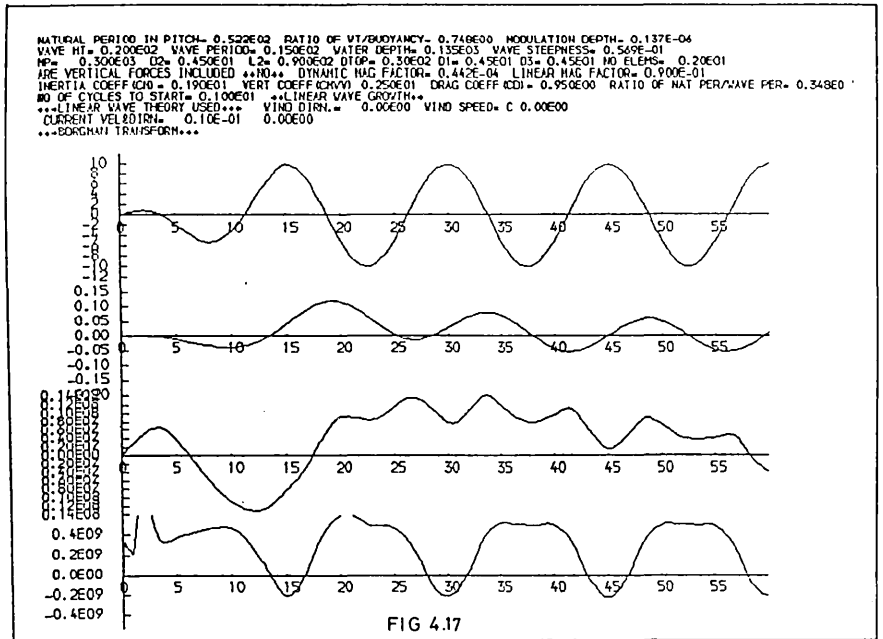

FIG 4.17

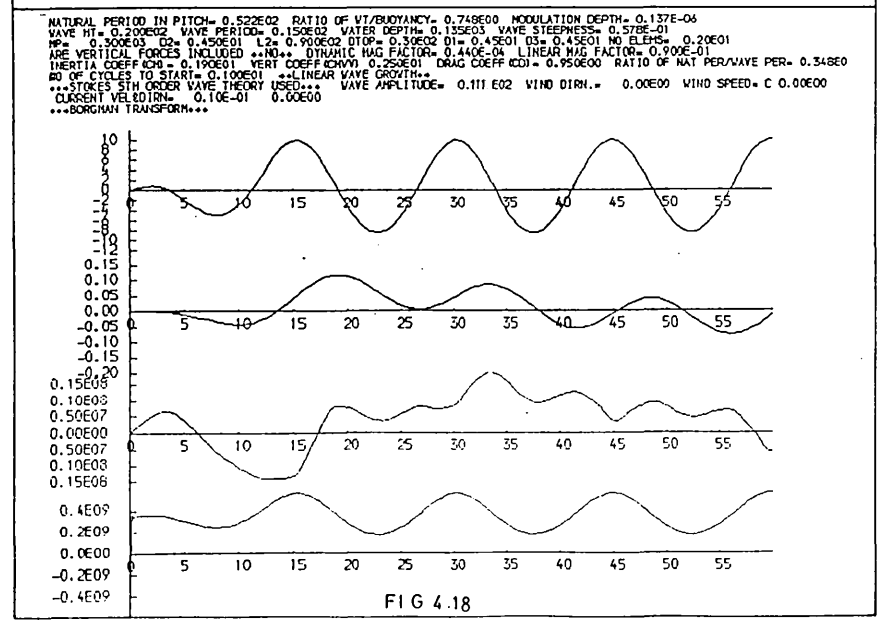

FIG 4.18

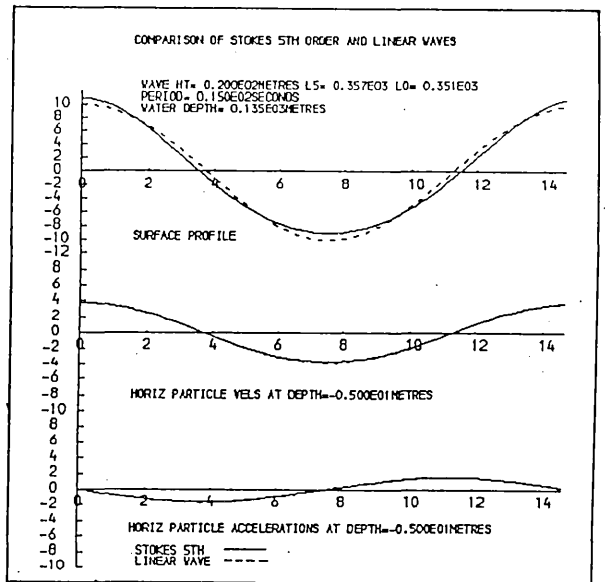

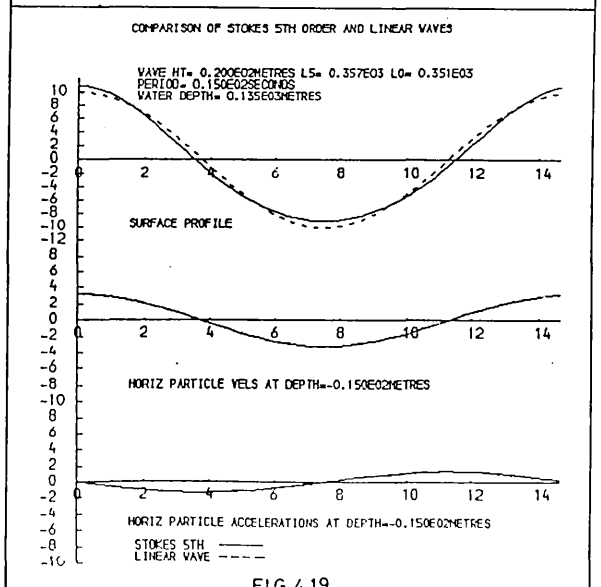

FIG 4.19

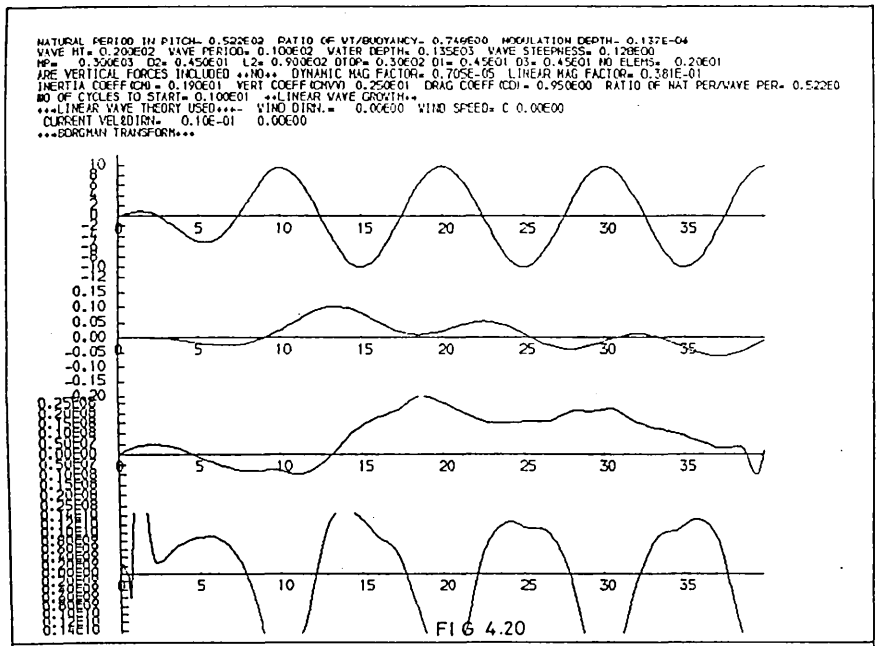

FIG 4.20

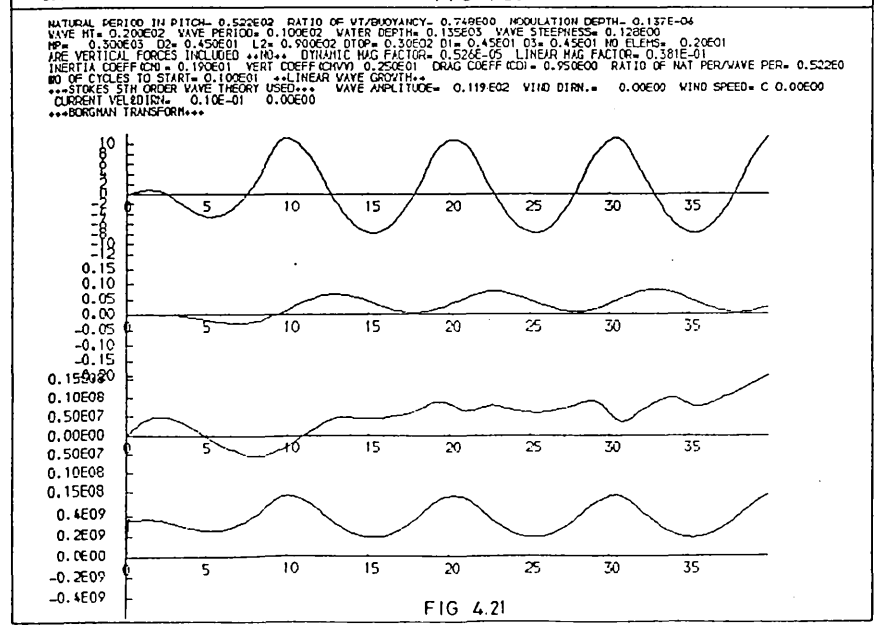

FIG 4.21

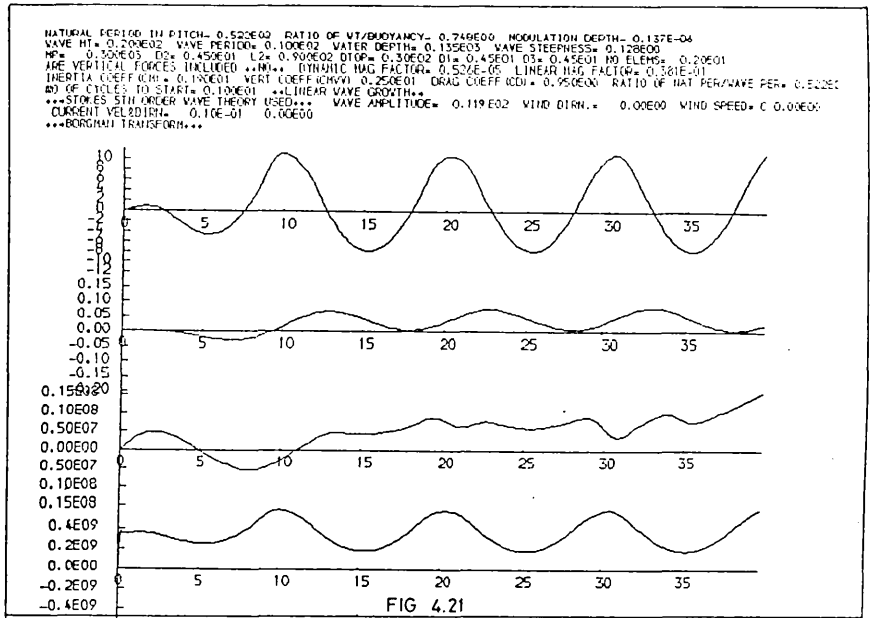

FIG 4.21

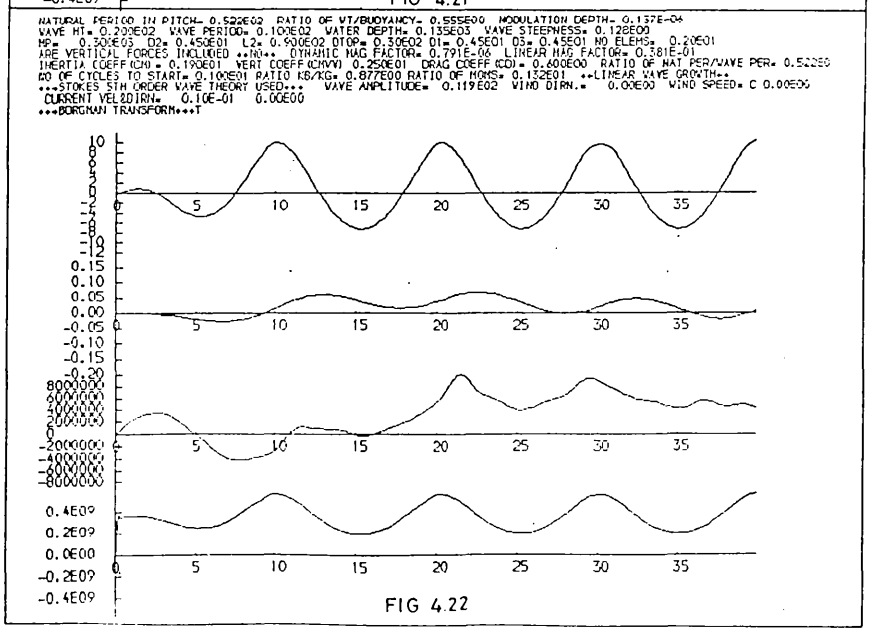

FIG 4.22

Figures 4.20 and 4.21 show the responses obtained for the structure subject to a 20 metre high 10 second period wave (ie 80% of maximum wave steepness), the particle kinematics being calculated by linear theory and Stokes fifth order theory, respectively. Apart from transient responses, the wave frequency oscillatory responses are of the same magnitude. The response for Stokes theory in fig. 4.21 stays positive after the first cycle, whereas the response for linear theory oscillates about zero. The difference is considered in the main to be attributable to the drag component of force and by way of illustration of the effects of the drag coefficient, fig. 4.22 shows the response for a drag coefficient C_D = 0.6, whereas the drag coefficient for fig. 4.21 was equal to 0.95. The response eventually oscillates about zero, presumably as a consequence of the reduction in drag component.

Effects of co-linear waves and currents

Waves travelling on currents will undergo changes in the wave length (58), that is to say that waves travelling in the same direction as the current will undergo elongation whereas waves travelling in the opposite direction to the current will become shorter and steeper. The wave particle kinematics will be somewhat altered and can be determined theoretically.

An approximation of the particle velocities as a linear combination of the current velocity and the wave particle velocity is considered reasonable in assessing the overall effects of currents and waves acting co-linearily.

Figures 4.23 and 4.24 show responses for a structure subject

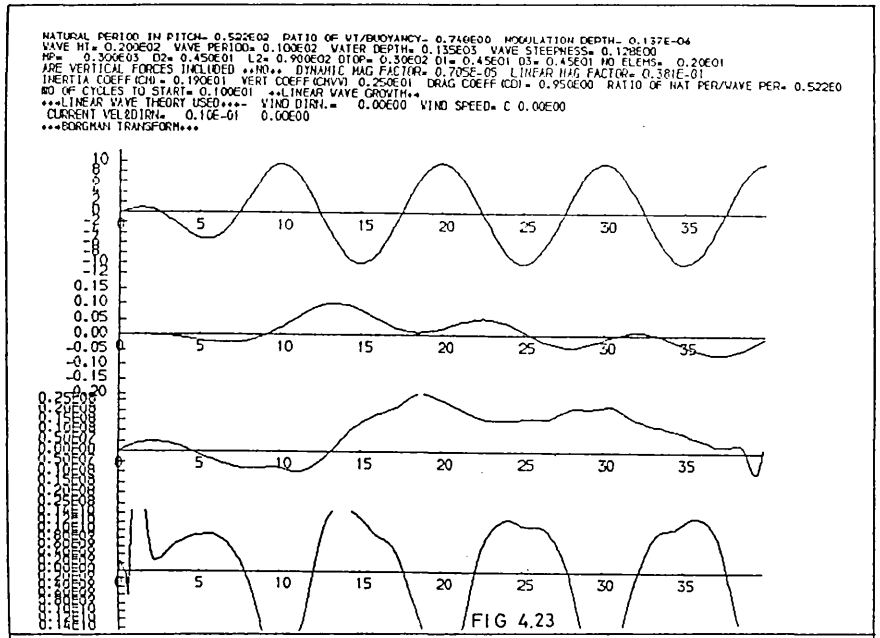

FIG 4.23

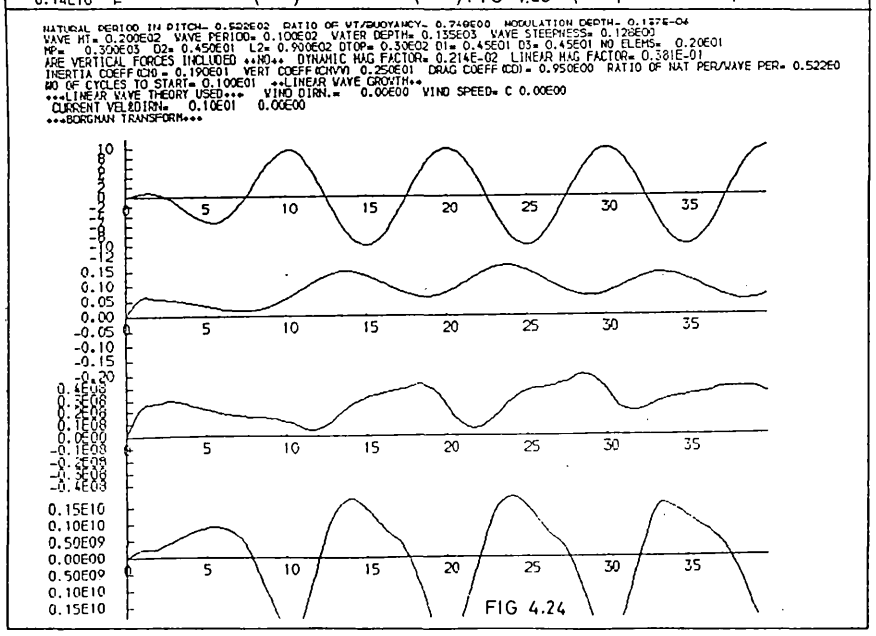

FIG 4.24

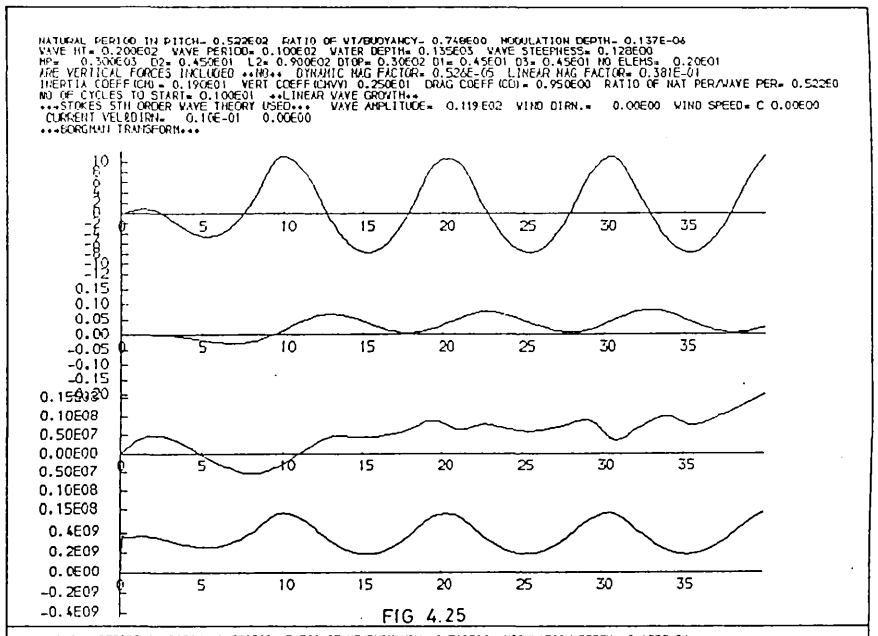

FIG 4.25

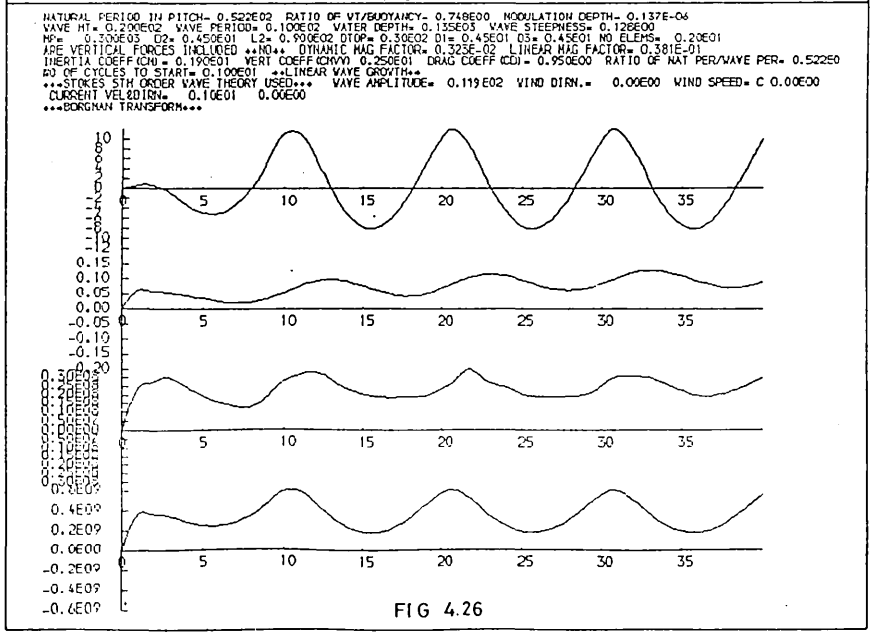

FIG 4.26

to a 20 metre high 10 second period wave with zero current and 1 metre per second current, respectively, the wave particle kinematics being calculated by linear wave theory. The current is responsible for a mean static heel of approximately 0.06 radians and it is noted that this value does not constitute a new mean about which the structure oscillates. The new mean has a value of approx 0.12 radians so that mean dynamic responses are increased by approximately 100%.

Figures 4.25 and 4.26 show responses for the same wave and current, the particle kinematics being calculated by Stokes theory. The new mean has a value of 0.075 radians, an increase of 25%.

Experimental Results

In order to assess the validity of some of the results obtained from the mathematical analysis of the articulated column structure, some limited amount of experimental observations were made in the experiment tank at the University of Glasgow, Department of Naval Architecture and Ocean Engineering

A model articulated column was constructed to an approximate scale of 1/100 of a full scale prototype. The diameter of the buoyancy chamber used was 0.32 metres and the length 0.286 metres. The main concern with these dimensions was the possible violation of the validity of the use of Morison's equation where D/L should be less than 0.2. However, some limited number of tests were completed and the results obtained correlate well qualitatively with those of the mathematical analysis and are presented here.

Movement of the model was monitored with the use of a light

emitting diode fitted to the model. This method of observing translations avoids the attachment of any other monitoring device to the model and, thus, eliminates any possible damping as a consequence of such attachments. Unfortunately, in order to simulate wind loading, a constant force was applied to the platform deck by means of a weight attached via a system of pulleys. The experimental arrangement of the model and equipment is shown in fig. 5.1.

The natural frequency of the model in pitch which was measured by means of a free oscillation test was found to be 0.11Hz. The trace of the free oscillation is shown in fig. 5.34.

Figure 4.27 shows pen recordings of the fore and aft displacement of the model subject to a wave 0.086 metres high and period 1 second. Note that the plots shown here are not phase compensated in that the recording pens have staggered positions. The simulated wind loading is in the same direction as the waves. The existence of a harmonic transient oscillation is very evident at a frequency equal to the pitch frequency of the model. Oscillations at the wave frequency are fairly uniform.

Figure 4.28 shows the displacement for a 1.5 sec wave 0.093 metres high. The transient oscillation is evident but is very much reduced to that shown in fig. 4.27.

The experimental observations do not suggest any tangible relationship between the magnitude of the transient oscillation and any other significant wave paramater such as period or height. Accordingly they are not considered to be conclusive in this respect. However the phenonema has been observed experimentally and is noted.

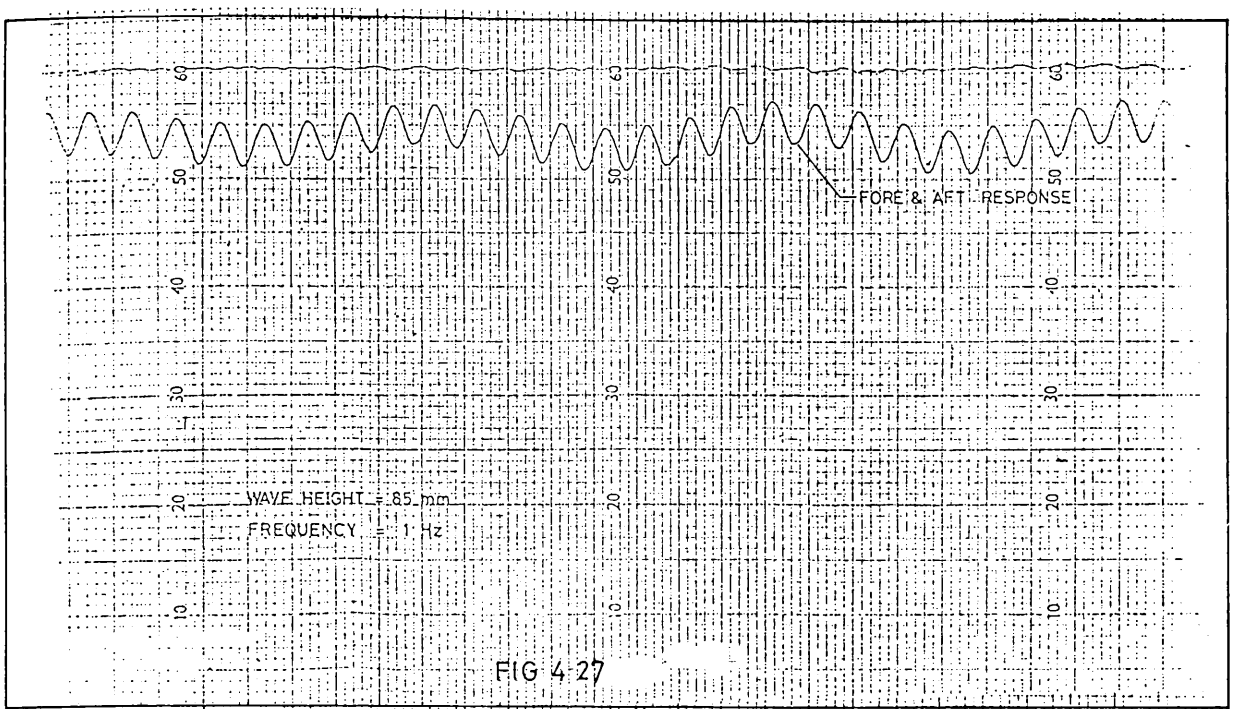

FIG 4.27

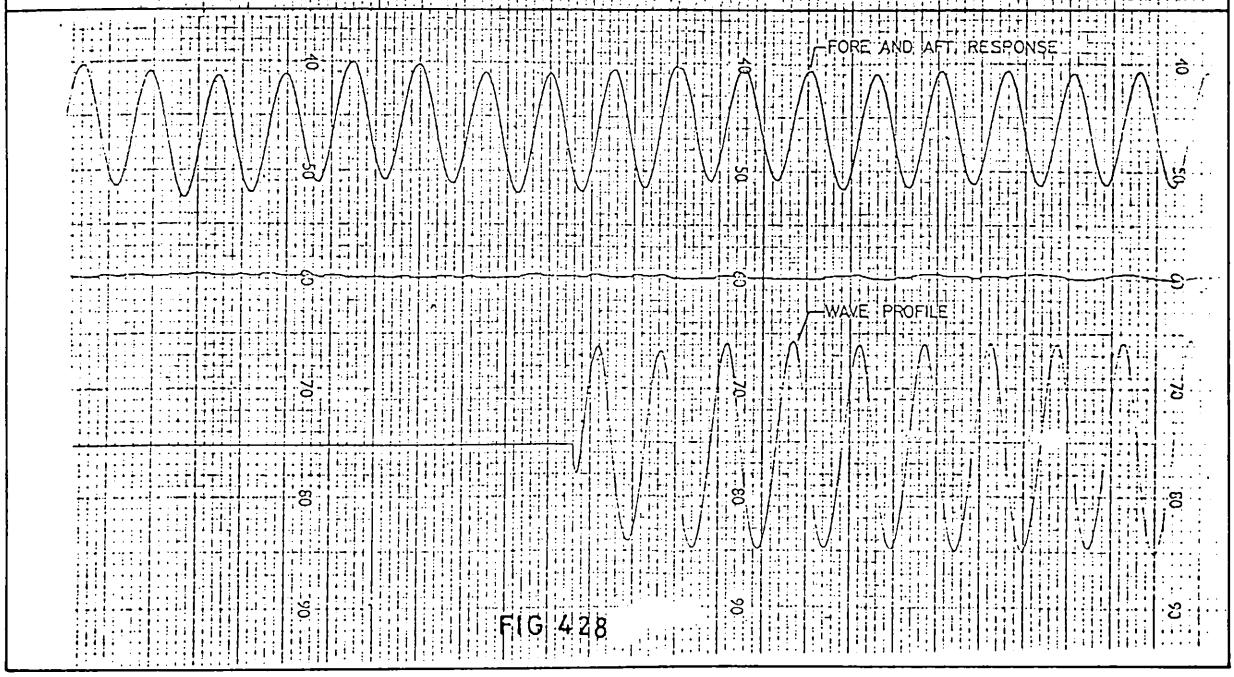

FIG 4.28

3. STRUCTURE SUBJECT TO NON CO-LINEAR EXCITING FORCES

The assumption that exciting forces in the form of waves, currents, winds, etc are acting co-linearly renders the SDOF model, described in section 2, most suitable and adequate in the investigation of the motion response and the determination of maximum response. It is well known, however, that this is not always the case in the real situation and, therefore, a more adequate and rigorous analysis which will allow for multi-directional exciting forces is desirable to examine the response of a structure subject to such a system of forces.

Kirk and Jain (20) and Kokkinowrachos (51) have investigated the response of articulated columns in spherical co-ordinates (2 degrees of freedom) and both have found that under certain non-colinear actions of waves and currents, the platform performed a complex swirling motion.

In addition to wind, waves and currents, the articulated column may, under certain circumstances, experience lift forces as a consequency of the action of vortex shedding. Lift forces on cylinders has been the subject of many investigations and there is a certain amount of data available for cylinders both horizontal and vertical in steady flow (43,59).

In the case of horizontal cylinders subject to sinusoidal oscillating flow, the alternating lift forces can be well correlated (59,60). In the case of an articulated column structure, a steady current may be sufficient to correlate the vortex shedding lift forces on either the buoyancy chamber or the upper column.

Chakrabarti (23) has obtained experimental data on lift forces on an articulated column and found these to be well correlated in some circumstances. Appendix 4.3 contains a table listing some vortex shedding frequencies, current velocities and member diameters.

In consideration of the possible combinations of non-linear exciting forces, the investigation of the response of the structure in two degrees of freedom is considered of value and beneficial to an understanding of the physical problem and to future research.

The equations of motion for the column are derived by the Lagrange (61) method for a combination of conservative and non-conservative forces and the development of the equations together with the evaluation of the forces is given in Appendix 4.4. The equations of motion are:-

$$I_T\ddot{\theta} - I\dot{\psi}^2\sin\theta\cos\theta + K_S\sin\theta = M_\theta \qquad (4.19)$$

$$I_T\ddot{\psi}\sin^2\theta + 2I\dot{\psi}\dot{\theta}\sin\theta\cos\theta = M_\psi \qquad (4.20)$$

3.1. Solution of the Equations of Motion

Equations (4.19) and (4.20) are solved simulataneously on an incremental time basis. The $\sin^2\theta$ term in the second equation gives rise to a singularity in the region of small θ and care needs to be taken in the solution. This is of particular importance in the case of small structures with very small mass moments of inertia about their central axis. In such cases, errors may accumulate as θ becomes small and it is necessary to place a stringent bound on error controls.

For larger structures the problem is less acute as generally these will possess significant mass moments of inertia about their

central axis and the $I\ddot{\psi}\sin^2\theta$ term will be replaced with an equivalent I_{EQIV} term, thus, reflecting the structures own inertia about the central axis.

The equations of motion have been solved by two methods ie direct integration method, ie Wilson-θ, and a Multi-Step method.

The direct integration method solves the two equations independently having first made a substitution for $\ddot{\theta}$ and $\ddot{\psi}$ in terms of θ and ψ in the equations of motion. By this means it was necessary to account for the moment of inertia of the structure about its own centroid as already mentioned. The results thus obtained were for larger structures and there was no evidence of any instability in the solutions obtained. The results obtained by this method are presented in figs. 4.30 to 4.33.

The Multi-Step methods basically comprise the Runge-Kutta Merson, Adams and Gear methods(48). These are available as standard NAG routines and in various stages of sophistication depending upon the degree of accuracy required for the solution (62).

The Gear Method is most suitable for systems of equations having rapidly decaying time components ie a stiff system of equations. A preliminary check on the stiffness properties of the equations by means of the Runge-Kutta Merson routine D02BDF indicated stiffness values of the order of 0.4-0.5. The recommendation is that for low values of stiffness, the Gear routines are not appropriate.

Accordingly the Runge-Kutta Merson routine D02BDF was used but this did not prove to be sufficiently general in terms of error

controls and subsequently the Runge-Kutta Merson routine D02PAF which allows for a wide range of error controls was used.

The NAG routines solve the equations on an iterative basis and consequently call the main program, supplied by the user, a number of times per successful iteration. Routine D02PAF did so approximately 15-20 times per successful iteration. This is obviously computationally time consuming and the recommendation in such cases is that the Adams routines are used. The Adams routine D02QAF was subsequently used to solve the equations and this routine allows for the implementation of any one of five different error control bounds. Routine D02QAF calls the main program approximately 2-3 times per successful iteration.

Although guidance is available on the most appropriate error control for any particular problem the choice must be subjective and trials made. The error control test which displayed the most consistency in results was the 'Mixed Error Test applied componentwise'. Nevertheless, some difficulties were encountered in the solution of the equations in the region of small values of θ particularly for the smaller structures with smaller inertias about their centroids.

However, satisfactory results were obtained when there was sufficient damping available in the form of a steady current to counter the tendency for the structure to respond through the origin. The results obtained are considered reasonable in reflecting the complex responses in these circumstances (see figs 4.34 to 4.35).

3.2 Analytical Results

The motion response of the structure as shown in fig. 4.1 for 6 metre high 15 second period waves at zero degrees orientation together with a steady wind speed of 35 metres per second with an orientation of $+20^{o}$, is shown in fig. 4.30. This is the plan trajectory in terms of the X and Z co-ordinates as defined in fig. 4.29. The starting point is the point marked 'O' and it is observed that a figure of eight pattern emerges with the column travelling in the opposite direction in the opposite quadrant to its direction approximately 7 wave cycles earlier. That is to say, the orientation of the trajectory at time 12T is in the opposite quadrant to the orientation of the trajectory at time 19T; similarly, at 13T and 20T, etc. Figure 4.30 shows the trajectory of the column with the wave starting at zero time at a wave crest.

Figure 4.31 shows the trajectory of the column given a wave trough starting at zero time. A cyclic pattern emerges as in the case of fig. 4.30 but in this case the column trajectory is in the opposite quadrant to that for fig. 4.30. Clearly then, the trajectory is sensitive to starting conditions for the time simulation solution although the pattern of 7 wave cycles persists.

Both figs. 4.30 and 4.31 are for the same structure with a buoyancy chamber 27 metres diameter and 40 metres long. The trajectory for a column with a buoyancy chamber 24m diameter and 50 metres long is shown in figs. 4.32 and 4.33 for clarity. In fig. 4.32 the starting point for the wave is at a wave trough as for that shown in fig. 4.31.

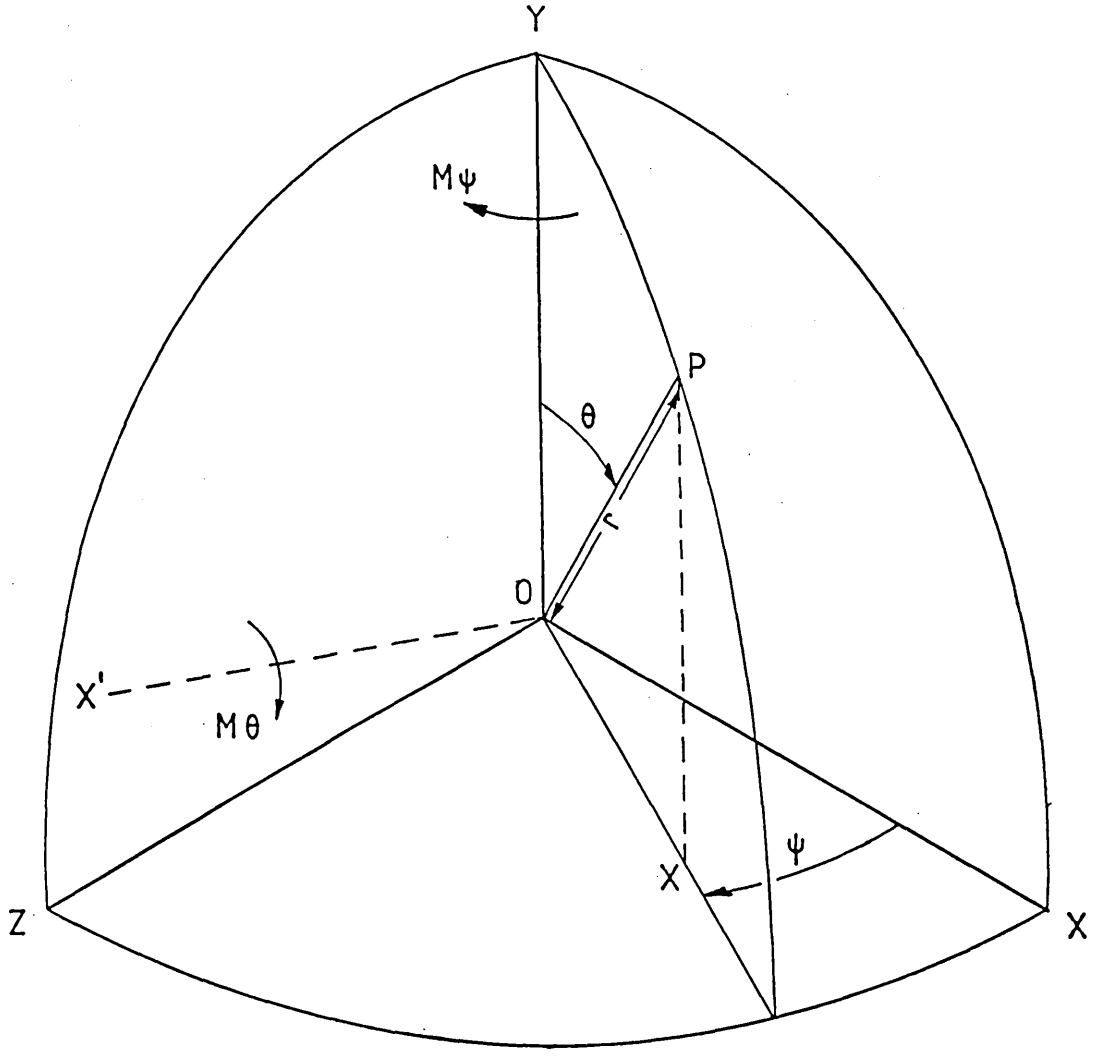

SPHERICAL CO-ORDINATE NOTATION.

FIG. 4.29

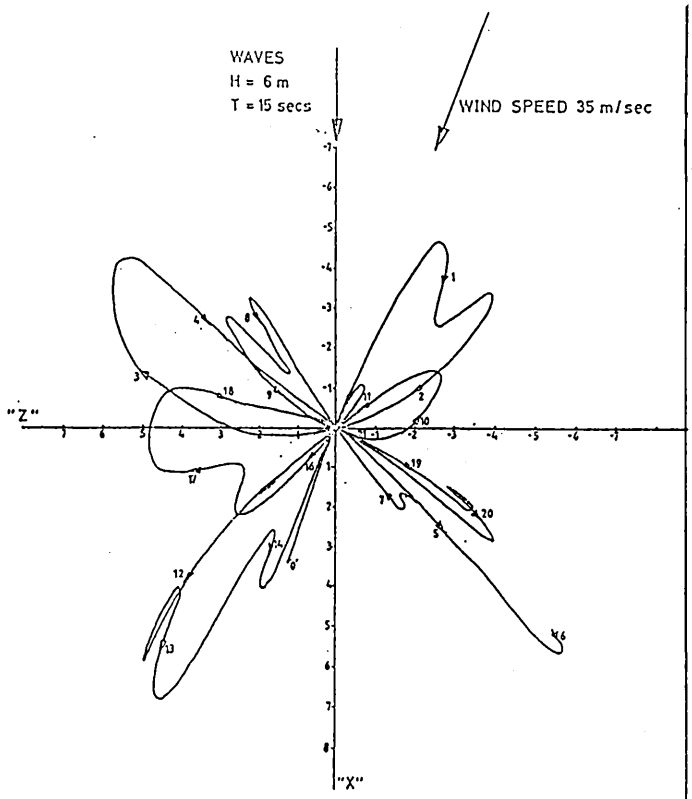

PLOT OF COLUMN TRAJECTORY STARTING AT WAVE CREST.

FIG 4.30

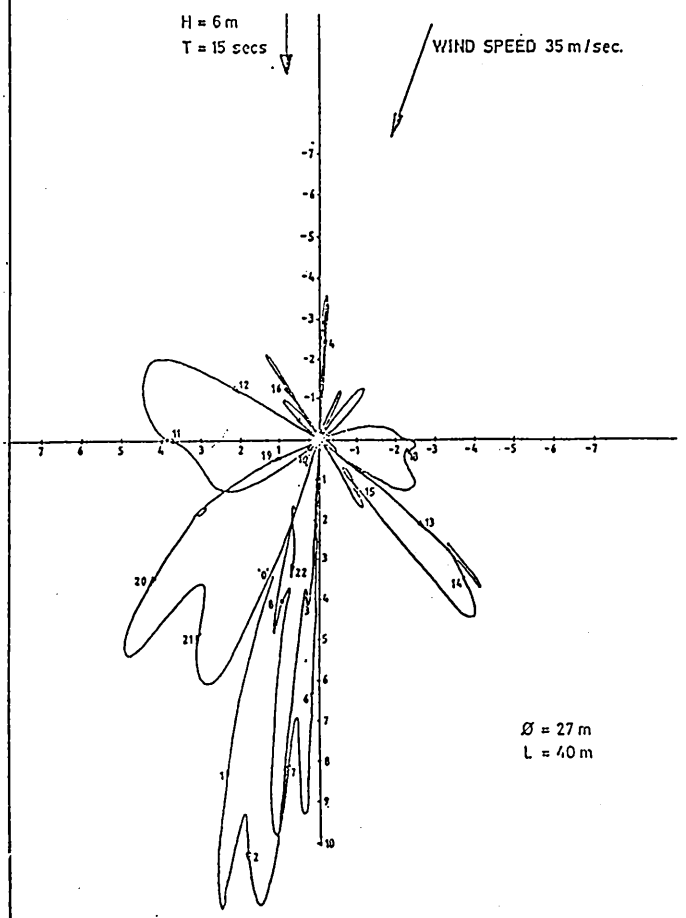

PLOT OF COLUMN TRAJECTORY STARTING AT WAVE TROUGH. FIG 4.31

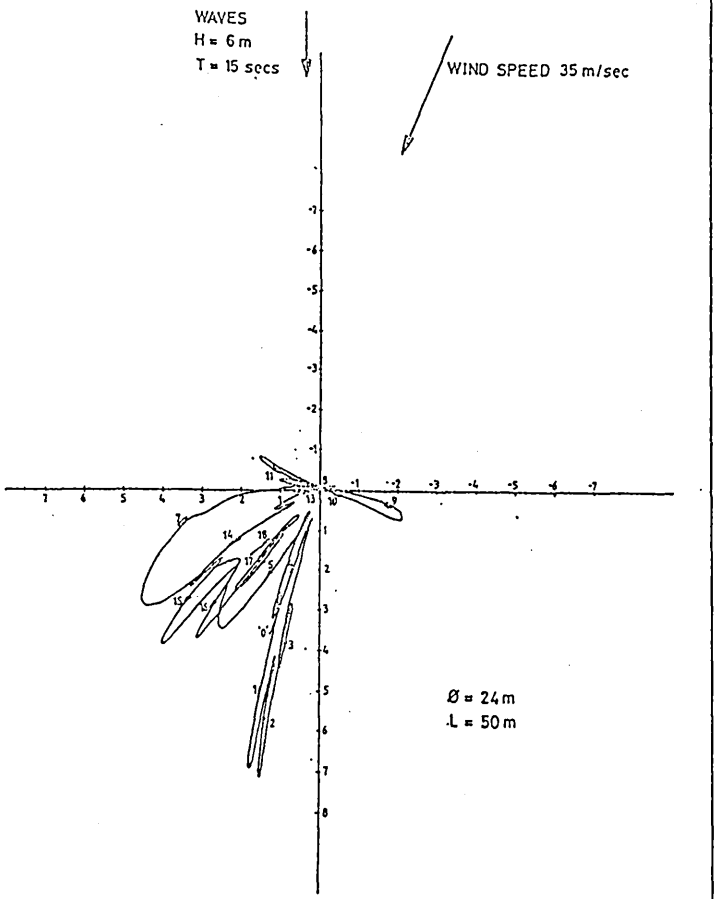

PLOT OF COLUMN TRAJECTORY
STARTING AT WAVE TROUGH.

FIG 4.32

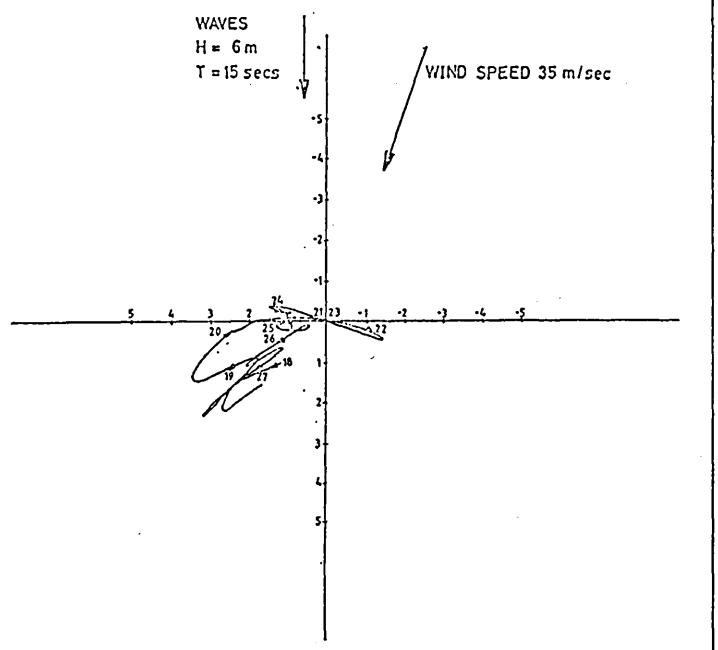

CONTINUED PLOT OF COLUMN TRAJECTORY

FIG 4.33

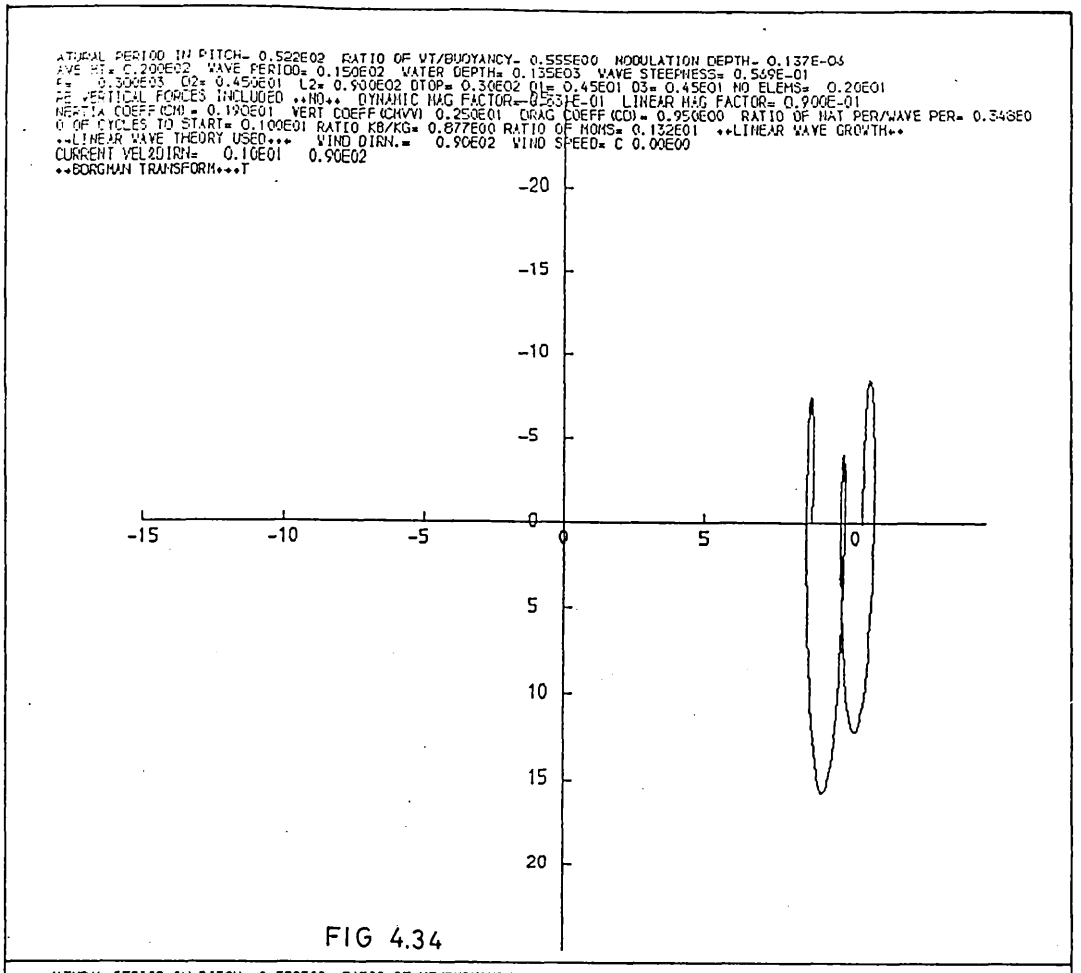

FIG 4.34

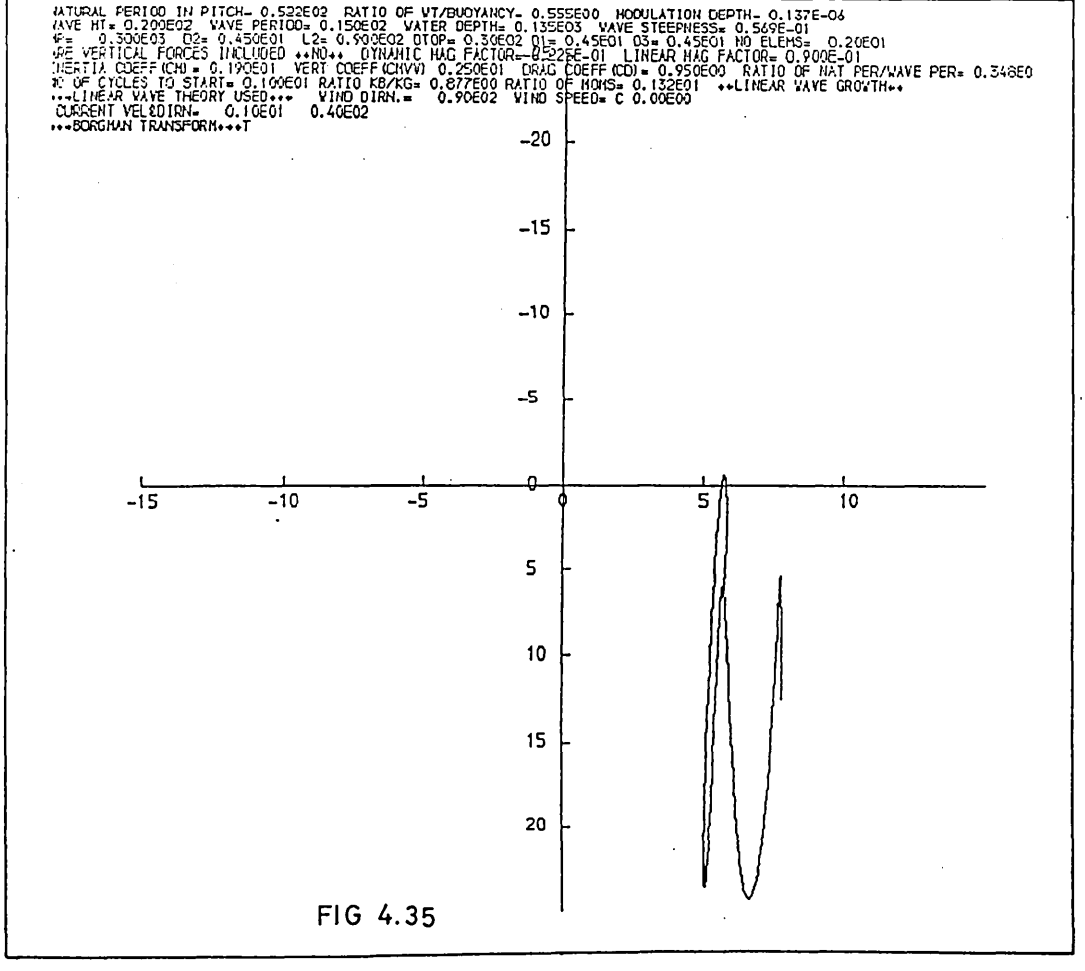

FIG 4.35

Comparison of figs. 4.32 and 4.33 illustrates a cyclic pattern emerging again but this time the most apparent pattern is repeating itself approximately every 13 wave cycles and in the same quadrant. Close inspection shows the 7 cycle pattern as in fig. 4.30 but much less pronounced. The column appears, therefore, to be performing a trajectory in a yawing sense with a natural period of approximately 105 seconds.

The sensitivity of lighter structures in shallower water to a current orthogonal to the direction of the wave travel is illustrated in fig. 4.34. A swirling trajectory is again assumed but is of a more orderly fore and aft nature, mainly as a consequence of the damping effect of the imposed current. The dominant effect of the current is illustrated again in fig. 4.35 which shows the response for the structure with a current of 1 metre per second imposed at an angle of 40^{o} to the X-axis. The effect is to bias the response in the current direction as would be expected and this concurs with the results obtained and as shown in figs. 4.24 and 4.26 for the case of uni-directional waves and currents.

4. Concluding Remarks

It has been demonstrated that a transient oscillation harmonic with the natural pitch frequency of the structure can be generated in the time simulation analysis. Experimental observations confirmed the existence of the phenomenon although no plausible correlation with any other significant wave parameter could be established. The transient greatly increases the pitch response of the structure, in some cases by 100%, and this clearly will play a very major part in the design of the structure. The most important

aspect of the increased pitch is likely to be the allowance to be made for the deck clearance above the instantaneous water surface.

The transient was also noted to be a function of the hydrodynamic viscous drag damping available and was a maximum for a value of $C_D = 0.7$ - this value is thought to represent a full scale value where Reynolds numbers are supercritical.

The non-linear transient phenomenon has been demonstrated to be a function of viscous drag forces and it is important, therefore, to adopt an analytical procedure which will deal with the relative speed squared term. Both the Wilson-θ linear acceleration method and the multi-step integration procedures are appropriate. However, the latter requires access to special routines, whereas the former is readily programmed and requires no special support routines.

Deck Mass relocation and alternative geometric shapes for the buoyancy chamber both contribute to improving the dynamic response. In particular, the conical shaped buoyancy chamber gives a marked improvement. Together these make a worthwhile contribution in reducing dynamic response.

The effects of non linear waves and currents have been shown to be important. Without currents, the non linear theory predicted greater responses than those predicted using a linear wave theory. The situation is worsened by an order of magnitude when currents are considered in combination with linear waves and mean dynamic responses were increased by 100%. Currents in combination with non linear waves increased mean dynamic responses by only 25%.

It is also noted that the mean position about which the structure oscillates, under the action of waves and currents, is not the mean which could be attributed to currents in the absence of waves. This observation, together with that on the harmonic transient motion, puts a more stringent requirement on the deck clearance to be provided.

Finally, the swirling trajectories produced by the action of multi-directional forces is to be noted. Although not of importance in a maximum response sense, they may be considered very undesirable in the context of the uncertainty associated with the direction of travel and lack of preferred direction for response. This aspect may play an even more important role from the point of view of human awareness and reaction to the motion response.

CHAPTER 5

DYNAMIC INSTABILITIES OF ARTICULATED COLUMNS

1. INTRODUCTION

In Chapter 4 it was noted that articulated columns can experience non-linear transient motions. The sensitivity of compliant structures to transient or other non-linear behaviour means that it is important to have a thorough understanding of the motion responses.

It is believed that instabilities can be experienced which will result in non-linear maximum responses, for exciting frequencies which are equal to and twice the natural pitch frequency of articulated columns.

In certain conditions the restoring stiffness of compliant structures, of which the articulated column is one particular variety, may be reduced by virtue of the wave action and thereby experience motion responses which are not sinusoidal and may even become dynamically unstable. These instabilities are commonly referred to as Mathieu instabilities in so far as the equations of motion can be shown to have solutions of the Mathieu type (63).

The natural frequency in pitch of most articulated columns is very small so that first order wave excitation at that frequency is most unlikely. However, it can be shown that wave trains which are harmonic with the pitch period of the structure can occur. It is necessary, therefore, to examine this possible mechanism as a source

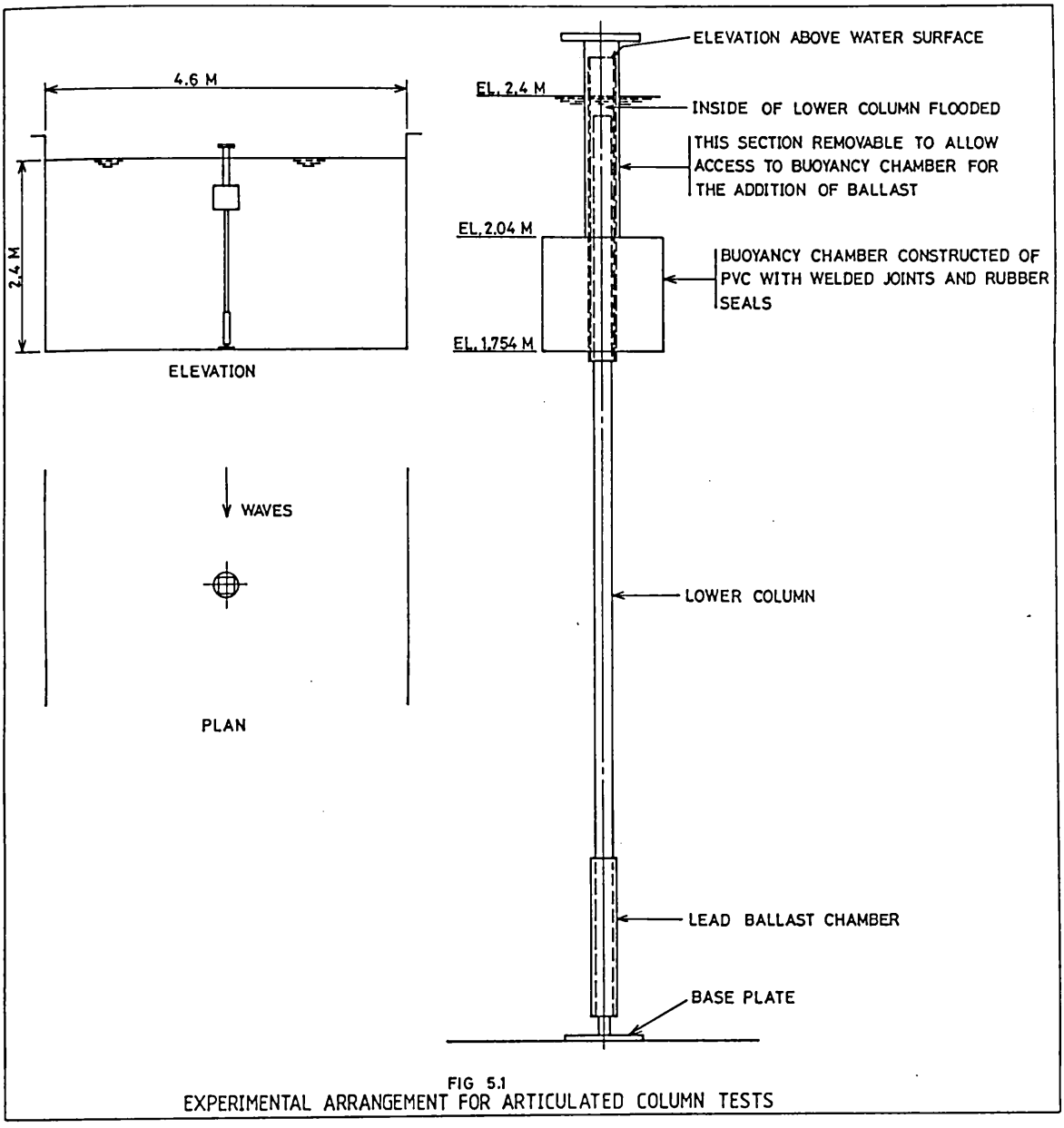

FIG 5.1
EXPERIMENTAL ARRANGEMENT FOR ARTICULATED COLUMN TESTS

of excitation and to make an assessment of the likely increased magnitude of the pitch oscillation.

This chapter first describes the development of the theory and the way in which the various stiffness components act and then goes on to examine their relative importance in the context of Mathieu instabilities.

The effects of the non linear relative velocity term in limiting the onset of the instabilities is examined as are the effects of wave growth and non linear waves. Also examined are the effects of weight to buoyancy ratios and currents. Some experimental observations are presented and these are compared with analytical results.

Finally, a description of the way in which wave groups may be generated as a consequence of the superposition of two separate regular wave trains with slightly different frequency travelling in the same direction is given. Analytical results for a structure subject to wave groups are presented.

2. MATHIEU INSTABILITIES

Essentially these instabilities are predicted when structures with time varying stiffness properties are subject to sinusoidal excitation at about twice the natural frequency in surge or pitch of the structure. It is also suggested that the range of exciting frequencies may extend to ratios of exciting frequency to natural frequency greater than 2.

Structures with natural periods in excess of 75 seconds, such as those considered in Chapter 4 may, in certain circumstances, experience these dynamic instabilities, as a consequence of the installation procedure which might be utilised. There may be periods of time during installation when the structure will have a natural frequency considerably higher than the final in situ natural frequency. Exposure to exciting forces at critical phases in the installation is obviously undesirable and it is considered, therefore, that the question of dynamic instabilities of this type be fully investigated.

Smaller structures in shallower water with pitch periods of the order of 35 to 40 secs will almost certainly be vulnerable. Indeed, the majority of existing applications for articulated columns occur in water depths of less than 140 metres. Most of these structures are used as loading platforms and mooring terminals so that for the majority of time they will have a tanker attached. This may help to suppress the onset of the instabilities since the natural surge period of the combined terminal and tanker will be very much larger than that of the terminal itself. However, problems may be encountered in the mooring phase if wave frequencies are such that there is a tendency for instabilities to develop. There are no known reports of instabilities having been observed at the full scale. However, there is one report (64) of an articulated column having become detached from its mooring although it is not known if this was directly attributable to the onset of instabilities.

The dynamic instabilities are considered to manifest themselves as a consequence of the variation in the pendulum restoring stiffness which can be considered to comprise two

components, viz:-

a. a component attributable to the variation in heave forces

b. a component attributable to the instantaneous position of the structure in the wave.

The heave force component can be considered to comprise an added mass part and a part attributable to the variation in pressure on the upper and lower faces of the buoyancy chamber as a consequence of the wave profile. Depending on the geometric configuration of the buoyuancy chamber these two parts may be in phase or not. The added mass portion will be downwards in a wave crest and upwards in a wave trough. The evaluation of the two parts is described in more detail in section 2.2.

In respect of the second component it can be shown that, when expanded, the expression for the surge force which accounts for the excursion of the structure contains a term in x which can be taken over to the left hand side of the equation of motion. This term can be considered as additional to the pendulum stiffness term and is also in phase with the added mass part of the heave force. It is the combined effect which assists the onset of dynamic instabilities. It is necessary to examine the combined effects of the three components in a realistic assessment of the possibility of dynamic instabilities.

In addition to the components mentioned above, the viscous (speed squared) damping is considered to play an important part in the limitation of the growth of the instabilities and the contribution of viscous damping increases as ω/ω_n tends to unity so that an adequate investigation must make a realistic assessment of

the contribution of non linear damping in the analysis.

Dynamic instability is a non linear phenomena and it is appropriate that the phenomena be investigated in a way which will adequately account for any non linearities involved. Accordingly this chapter sets out to examine the effects of the aforementioned components in combination with each other and in a manner which allows for the variations on an instantaneous time incremental basis.

2.1 Equations of Motion

In the first instance, neglecting for the time being the heave forces and with reference to figs. 5.1 and 5.2, consider the equation of motion,

$$I_T\ddot{\theta} + C\dot{\theta} + K_S\theta = M \qquad (5.1)$$

Neglecting potential damping and also, for the time being, neglecting viscous drag damping and the velocity forces the equation of motion can be written:-

$$I_T\ddot{\theta} + K_S\theta = \bar{X}.r.\sin\omega t \qquad (5.2)$$

where $\bar{X}.r$ is the maximum pitching moment perpendicular to the structure axis and

I_T = (Mass + Added Mass) moment of inertia

K_S = Pendulum stiffness

r = radius from articulation to the centre of force

It is noted that r is a function of the exciting frequency ω and of the elevation of the buoyancy chamber. Equation 5.2 accounts for the forces on the structure assuming it to be stationary in the waves.

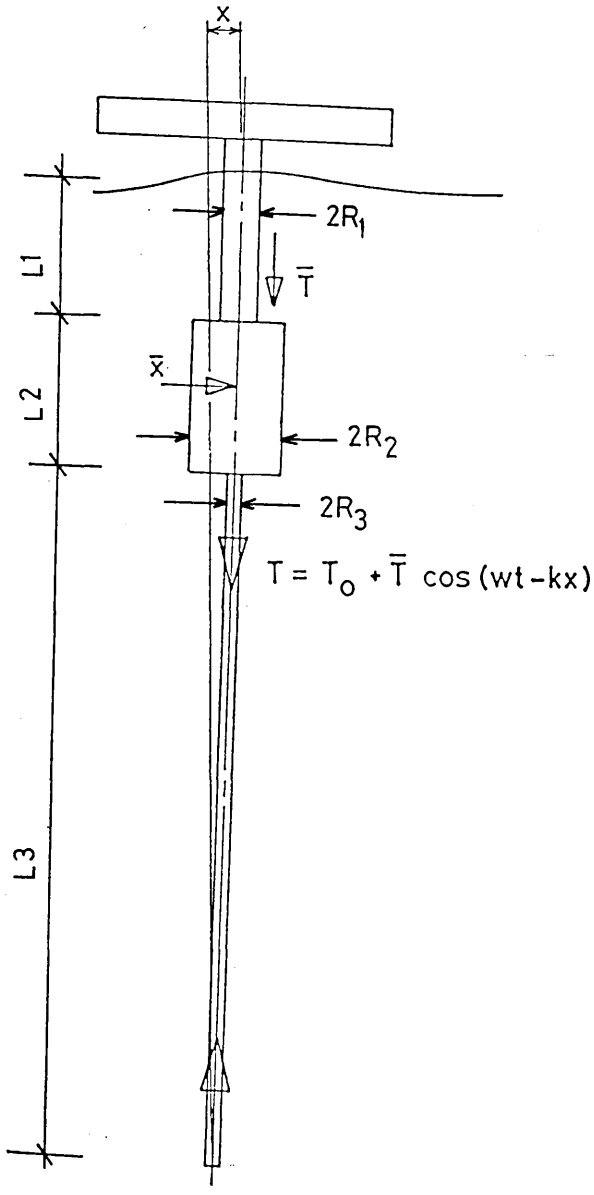

PERPENDICULAR AND AXIAL FORCES ON ARTICULATED COLUMN.

FIG. 5.2

In order that the instantaneous position of the structure relative to the reference axis of the wave is accounted for, it is necessary to rewrite equation 5.2 to allow for the excursion of the structure in the wave thus:-

$$I_T\ddot{\theta} + K_S\theta = \bar{X}.r.\sin(kx - \omega t) \qquad (5.3)$$

where k is the wave number = $2\pi/L$ and x is the excursion of the structure in the wave.

Expanding equation 5.3 by assuming that for $kx \ll 1$ that sinkx = kx and coskx = 1 then:-

$$I_T\ddot{\theta} + K_S\theta + kx.\bar{X}.\cos\omega t.r. = \bar{X}.r.\sin\omega t \qquad (5.4)$$

Now $K_S = B_F.RKB - W.RKG$

where B_F = Buoyancy force

W = Weight of structure

RKB = Distance from pivot to centre of Buoyancy

RKG = Distance from pivot to centre of Gravity

and $\theta = x/r.$

For the purposes of illustration, accepting that the buoyancy chamber is the element which attracts the major portion of wave forces, then r = RKB. (The computer program calculates forces on elemental lengths of the structure and the correct force and buoyancy distribution is thereby assured.)

Then the equation of motion can be written:-

$$I_T\ddot{\theta} + [(B_F.RKB - W.RKG)/RKB + k.\bar{X}.\cos\omega t.RKB]x = \bar{X}.RKB.\sin\omega t \qquad (5.5)$$

Consider the stiffness term:-

$$[(B_F.RKB - W.RKG)/RKB + k.\bar{X}.\cos\omega t.RKB]x \qquad (5.6)$$

The second and additional term will render the total stiffness to be sinusoidal in nature. The right hand side of the equation of motion now expresses the forces on the structure assuming that it remains stationary relative to the frame of reference of the wave.

It is also noted that in the physical sense this extra term, strictly speaking, is not a stiffness component in that it does not contribute to a variation in the tension in the lower column but that it is merely a force term in x and as such can be included in the stiffness term which is also expressed in x. In respect of the calculation of the wave exciting forces, it is noted that exactly the same result is obtained for the response when the right hand side expression for force is of the type $\bar{X}\sin(kx - \omega t)$ as is obtained when this expression is expanded and the right hand side of the equation is of the form $\bar{X}\sin\omega t$, the rest of the expression having been transferred to the left hand side of the equation and included in the stiffness term.

2.2 Time Varying Stiffness

The foregoing analysis assumes that the tension in the lower member remains constant, as it is clearly unaffected by forces perpendicular to the axis of the structure.

2.2.1 Calculation of Heave Forces

A rigorous analysis of the heaving forces on a floating structure would necessarily require the determination of the pressure and inertia components which are both functions of the wave profile with respect to the body. Under a wave crest the pressure forces may, depending on the geometry of the buoyancy chamber, act downwards and the inertia forces, as a consequence of the wave particle accelerations, will act downwards. Conversely, in a wave trough the opposite situation will prevail.

2.2.2 Pressure Forces

The Froude-Krylov pressure change on the top and lower faces of the buoyancy chamber as a consequence of the wave profile, can be written:-

$$\text{Pressure Force} = [-\rho g a_o e^{-kL_1}(\pi R_2^2 - \pi R_1^2) + \rho g a_o e^{-k(L_1 + L_2)}(\pi R_2^2 - \pi R_3^2)]\cos(kx - \omega t) \quad (5.7)$$

The first term inside the bracket is the pressure force on the top face of the buoyancy chamber and the second term is the pressure force on the bottom face.

This expression reduces to:-

$$\text{Pressure Force} = -\pi\rho g a_o e^{-kL_1}\{R_2^2 - R_1^2 - e^{-kL_2}(R_2 - R_3)\}\cos(kx - \omega t) \quad (5.8)$$

The pressure forces can be cancelled out for any particular wave frequency by setting the term inside the square bracket equal to zero, ie ratios of R_2/R_1 can be chosen such that cancellation occurs for a given wave frequency, ie

$$R_2^2(1 - e^{-kL_2}) = R_1^2 - R_3^2 e^{-kL_2} \tag{5.9}$$

2.2.3 Inertia Forces

In the case of a submerged buoyancy chamber with concentric cylinders protruding from the upper and lower faces the calculation of the inertia forces will require the determination of the added virtual mass coefficients for the upper and lower faces. This can be calculated on the basis of a strip theory and will be a function of the aspect ratios of the buoyancy chamber, the upper support column and the lower column.

The inertia force can then be written:-

$$\text{Inertia Force} = \{-\tfrac{2}{3}\rho\pi J(CVR_2R_2^3 - CVR_1R_1^3)kga_o e^{-kL_1}\cos(kx - \omega t) - \tfrac{2}{3}\rho\pi J(CVR_2R_2^3 - CVR_3R_3^2)kga_o e^{-k(L_1 + L_2)}\cos(kx - \omega t)\} \tag{5.10}$$

This reduces to:-

$$\text{Inertia Force} = -\tfrac{2}{3}\rho\pi Jkga_o e^{-kL_1}\{CVR_2R_2^3(1 + e^{-kL_2}) - CVR_1R_1^3 - e^{-kL_2}\,CVR_2R_3^3\}\cos(kx - \omega t) \tag{5.11}$$

The total force can be written thus:-

Total Heave Force = Pressure Term + Inertia Term

$$= \rho\pi g a_o e^{-kL_1} \{R_2^2(1 - e^{-kL_1}) - R_1^2 + e^{-kL_2} R_3^2$$

$$+ \frac{2}{3} Jk \left[CVR_2 R_2^3(1 + e^{-kL_2}) - CVR_1 R_1^3 - e^{-kL_2} CVR_3 R_3^3\right]\} \cos(kx - \omega t) \qquad (5.12)$$

It is not possible to cancel the inertia component of heave forces for a particular wave frequency, as is the case for pressure forces. However, zero heave force can be achieved for the combined pressure and inertia terms by the variaion of R_2, L_2 and R_3, assuming that R_1 is fixed. Both components should be assessed separately in order to make an appropriate choice of buoyancy chamber dimensions.

The heave force as given by equation (5.12) has been computed in the form of subroutine HEA. This routine requires as input, dimensions of the buoyancy chamber together with added mass coefficients CVR_1, etc. The routine was incorporated into the time simulation program to provide both pressure and inertia components of the heave force where CVR_1 etc are the added virtual mass coefficients which are functions of the aspect ratios $\pi R_1/2L_1$, etc. $J = 0.635$ and takes account of the three dimensionality of the flow. The basis upon which the added virtual mass coefficients CVR_1, etc are calculated is outlined in Appendix 5.1 which also shows the variation of the coefficients with the aspect ratio. The total force may then be calculated on the basis of the summation of individual strip components.

Consider now the inclusion of a time varying heave force on the structure. If we say that the maximum heave force along the axis of the structure is $\bar{T}_I$ then this will vary cyclically as $\bar{T}_I.\cos(kx - \omega t)$ where $\bar{T}_I$ is the inertia component of the heave force. When the geometry of the buoyancy chamber is such that the pressure component also acts downwards in a wave crest then this will also be included in $\bar{T}$. Viscous wave forces also contribute to the heave component but this is small in comparison with the predominant inertia forces.

Then, the stiffness term will become:-

$$\{(B_F.RKB-W.RKG)/RKB + k\bar{X}.\cos\omega t.RKB + \bar{T}.\cos(kx - \omega t)\}x \quad (5.13)$$

and this reduces to

$$\{(B_F.RKB-W.RKG)/RKB + (k\bar{X}.RKB + \bar{T})\cos\omega t\}x \quad (5.14)$$

The second part now contains an additional term as a consequence of the variation in the heave force and this is in phase with that term which accounts for the position of the structure in the wave.

Now the equation of motion:-

$$I_T\ddot{\theta} + \left(\frac{K_s}{r} + (k\bar{X}.r + \bar{T})\cos\omega t\right) x = \bar{X}.r.\sin\omega t \quad (5.15)$$

can be rewritten

$$\ddot{\theta} + (1 + b\cos\omega t)x = \frac{\bar{X}}{I_T}.r.\sin t \quad (5.16)$$

where $b = \dfrac{\bar{T}.r + kx.r^2}{K_s}$ and $\omega^2 = \dfrac{k_s}{I_T}$

By setting the RHS of the equation equal to zero, then:-

$$\ddot{\theta} + \omega^2(1 + b\cos\omega t)x = 0 \qquad (5.17)$$

which is Mathieu's equation and defines stability boundaries as shown in fig. 5.3.

The relative magnitude of the stiffness terms discussed is shown in fig. 5.4. These results have been computed incorporating subroutine HEA which computes the pressure and inertia heave components of force separately. The dimensions of the structure are as shown in fig. 5.1 and the aspect ratios used for CVR_1, CVR_2 and CVR_3 were 1.8, 1.65 and 2.5, respectively.

With reference to the bottom set of curves shown in fig. 5.4, ie the restoring stiffness; curve 1 is the simple pendulum stiffness of the structure. Curve 2 is the pendulum stiffness plus the pressure component of heave force. Curve 3 is the pendulum stiffness plus the pressure and inertia components of heave force and curve 4 is the total restoring stiffness, ie the pendulum stiffness plus the heave forces plus the contribution from the component which accounts for the position of the structure in the wave. For this particular stucture, the pressure component of heave force is acting in phase with the inertia component.

It would appear, therefore, that in this case the kX component makes the major contribution to the stiffness. The kX contribution is proportional to the frequency squared ($k = \omega^2/g$) and can thus increase rapidly with frequency although the effects will probably be limited by the decrease in response as ω/ω_n increases.

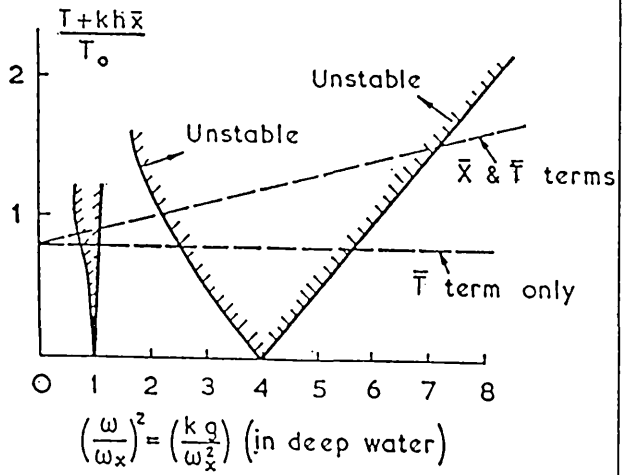

Fig. 1.1 Regions of Instability
(Reproduced from REF. 17)

FIG 5.3

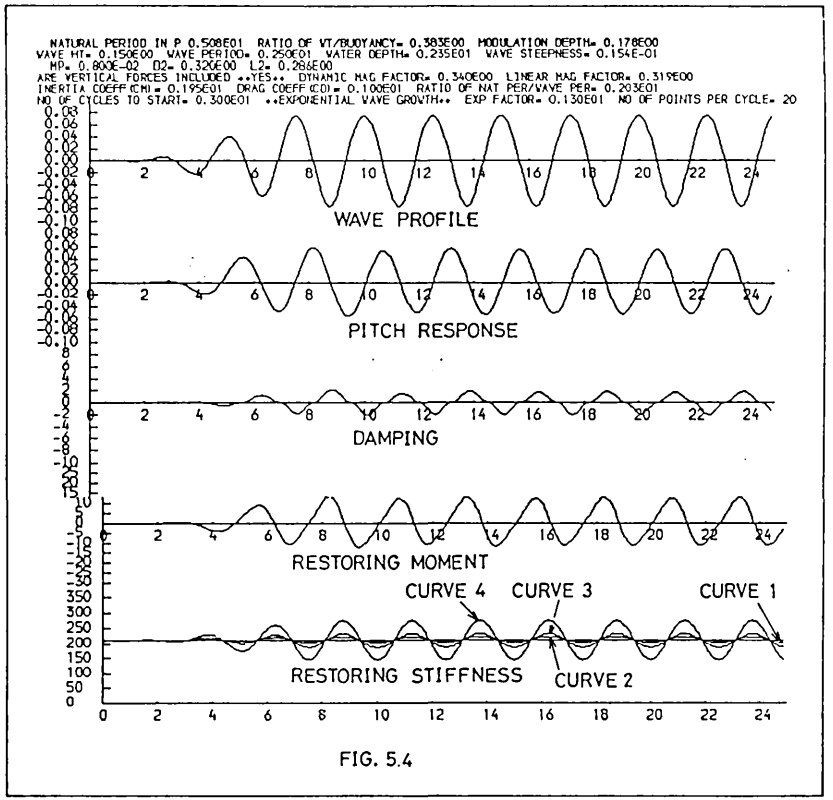

FIG. 5.4

2.3 DAMPING

Adequate representation of damping is necessary in the realistic assessment of motion response and potential damping has not been included in the above analysis. Potential damping is likely to be small for the low frequencies which are of concern in respect of possible dynamic instabilities. Material damping is only possible at the articulated joint for this SDOF model but this cannot be quantified and is assumed to be zero.

The only other available form of hydrodynamic damping available is viscous and so the relative velocity terms must be adequately accounted for and its role in limiting unstable responses assessed. The non linear viscous drag components normal to the axis of the structure have been included in this investigation and the effects on the response investigated.

As mentioned, the viscous wave forces will make a contribution to the heave component. These would be 90^{o} out of phase with the inertia forces and are much smaller in magnitude and unlikely, therfeore, to affect stability boundaries significantly.

3. ANALYTICAL RESULTS

3.1 Effects of Time Varying Stiffness

In order to investigate the dynamic instabilities the computer program described in Chapter 4 was adapted to,

a. take account of the instantaneous position of the

structure in the wave in the calculation of wave forces, and

b. take account of the variations in vertical tension as a consequence of the heave force in calculating the restoring stiffness.

The analytical results obtained show evidence of instabilities occurring for wave frequencies of twice the natural frequency in pitch and greater and these are presented.

Figures 5.4 to 5.15 relate to a model articulated column of the same dimensions as the experimental model described later and as shown in fig. 5.1. The analysis for these results is by means of the Wilson-θ-linear acceleration method. For these figures the top plot is the wave profile, the 2nd plot is the pitch response in radians, the 3rd plot is the viscous damping force, the 4th plot is the restoring moment and the bottom plot is the restoring stiffness, K_s.

The results for figs. 5.16 to 5.27 relate to full size structures and the analysis is by means of the Adams multi-step integrator. In these figures the plot of the restoring moment has been omitted.

Figure 5.5 is a plot of the pitch response versus time for a model structure with a natural period in pitch of 4.95 seconds. The wave height is 0.15 metres and period 1 second so that the ratio of natural period to exciting period is 4.7 (or $\omega/\omega_n = 4.7$). There is evidence of a slight transient which is harmonic with the natural period in pitch but otherwise the solution is stable.

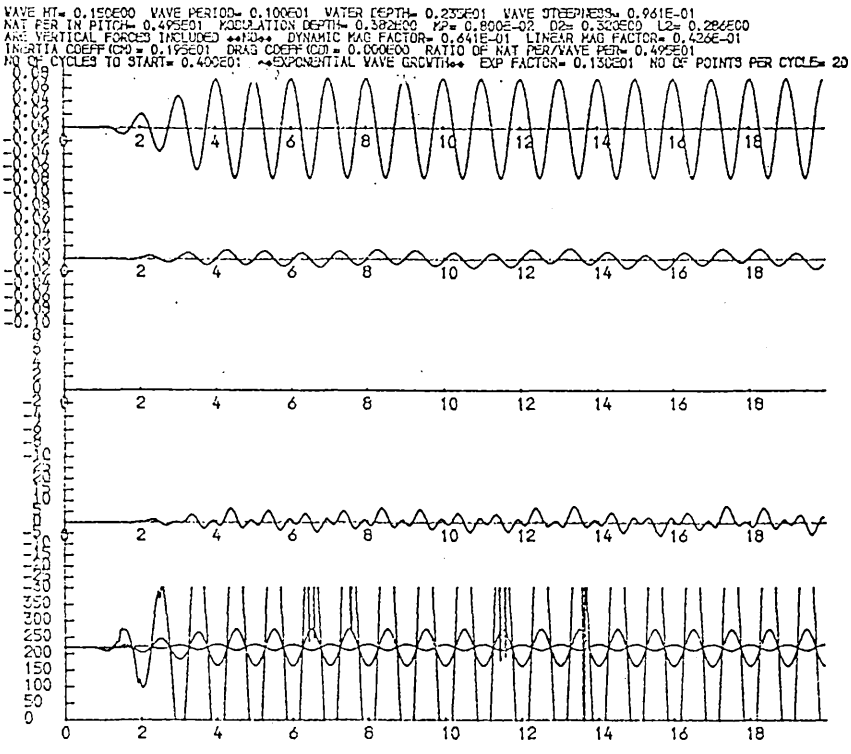
WAVE HT= 0.150E00 WAVE PERIOD= 0.100E01 WATER DEPTH= 0.235E01 WAVE STEEPNESS= 0.961E-01
NAT PER IN PITCH= 0.495E01 MODULATION DEPTH= 0.382E00 K2= 0.800E-02 D2= 0.320E00 L2= 0.286E00
ARE VERTICAL FORCES INCLUDED ↔NO↔ DYNAMIC MAG FACTOR= 0.641E-01 LINEAR MAG FACTOR= 0.426E-01
INERTIA COEFF (CM) = 0.195E01 DRAG COEFF (CD) = 0.000E00 RATIO OF NAT PER/WAVE PER= 0.495E01
NO OF CYCLES TO START= 0.400E01 ↔EXPONENTIAL WAVE GROWTH↔ EXP FACTOR= 0.130E01 NO OF POINTS PER CYCLE= 20

FIG.5.5

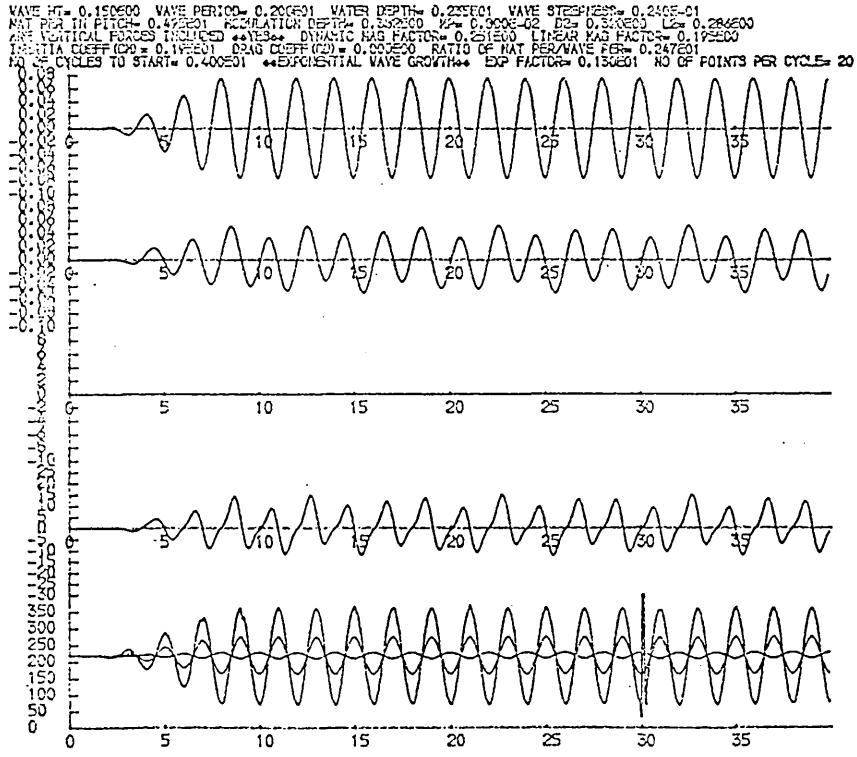
WAVE HT= 0.150E00 WAVE PERIOD= 0.200E01 WATER DEPTH= 0.235E01 WAVE STEEPNESS= 0.240E-01
NAT PER IN PITCH= 0.472E01 MODULATION DEPTH= 0.382E00 K2= 0.900E-02 D2= 0.320E00 L2= 0.284E00
ARE VERTICAL FORCES INCLUDED ↔YES↔ DYNAMIC MAG FACTOR= 0.251E00 LINEAR MAG FACTOR= 0.195E00
INERTIA COEFF (CM) = 0.195E01 DRAG COEFF (CD) = 0.000E00 RATIO OF NAT PER/WAVE PER= 0.247E01
NO OF CYCLES TO START= 0.400E01 ↔EXPONENTIAL WAVE GROWTH↔ EXP FACTOR= 0.130E01 NO OF POINTS PER CYCLE= 20

FIG.5.6

Figure 5.6 shows the response for the structure subject to a 0.15m wave with period 2 seconds (ω/ω_n = 2.47). Viscous drag damping is zero for this case. The wave frequency response has increased as expected and again the transient harmonic response is present, however the response is stable with no signs of instability.

The response for the structure subject to a 0.05m wave with period 2.5 seconds (ω/ω_n = 2) are given for viscous drag coefficients of zero and 0.6 in figs. 5.7 and 5.8, respectively. Vertical heaving forces are not included in the analysis. The response for zero damping is slightly greater than that for C_D = 0.6 but is otherwise stable. The harmonic transient is evident at the pitch frequency.

Figures 5.9 and 5.10 are similar but include the heaving forces in the analysis. The transient is more pronounced and in the case for zero damping (fig. 5.10) the transient is increasing in magnitude. So that even at this very low level of excitation (wave steepness = 0.005 or 3.6% of maximum) the instability is present.

Figures 5.11 and 5.12 are similar plots for 0.15m wave (15 metres full scale) and including vertical forces. The transient for the case of zero damping, ie fig. 5.12, is more pronounced than that in fig. 5.11 and appears to be increasing in magnitude. The large increase in the magnitude of the response when ω/ω_n = 2 (fig. 5.11) compared to that for ω/ω_n = 2.47 (fig. 5.6) is apparent from inspection of these two plots. The increase is 35% and is calculated on the basis of the maximum response in each case, ie the transient response.

Figure 5.13 shows the response for the same wave but

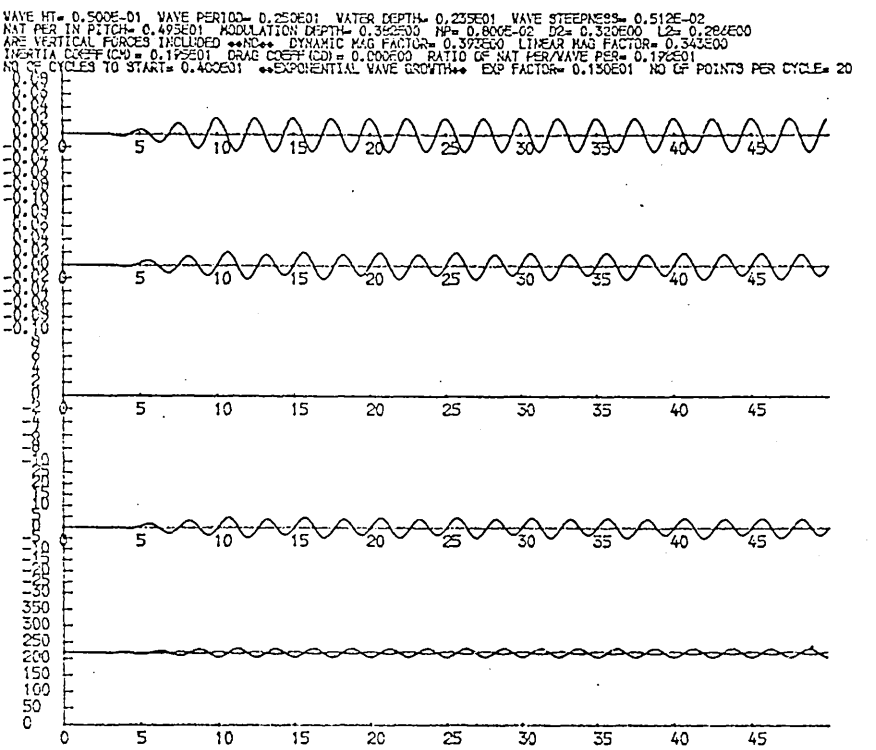
WAVE HT= 0.500E-01 WAVE PERIOD= 0.250E01 WATER DEPTH= 0.235E01 WAVE STEEPNESS= 0.512E-02
NAT PER IN PITCH= 0.493E01 MODULATION DEPTH= 0.362E00 KP= 0.800E-02 D2= 0.320E00 L2= 0.284E00
ARE VERTICAL FORCES INCLUDED ++NO++ DYNAMIC MAG FACTOR= 0.392E00 LINEAR MAG FACTOR= 0.343E00
INERTIA COEFF (CM) = 0.195E01 DRAG COEFF (CD) = 0.600E00 RATIO OF NAT PER/WAVE PER= 0.195E01
NO OF CYCLES TO START= 0.400E01 ++EXPONENTIAL WAVE GROWTH++ EXP FACTOR= 0.130E01 NO OF POINTS PER CYCLE= 20

FIG. 5.7

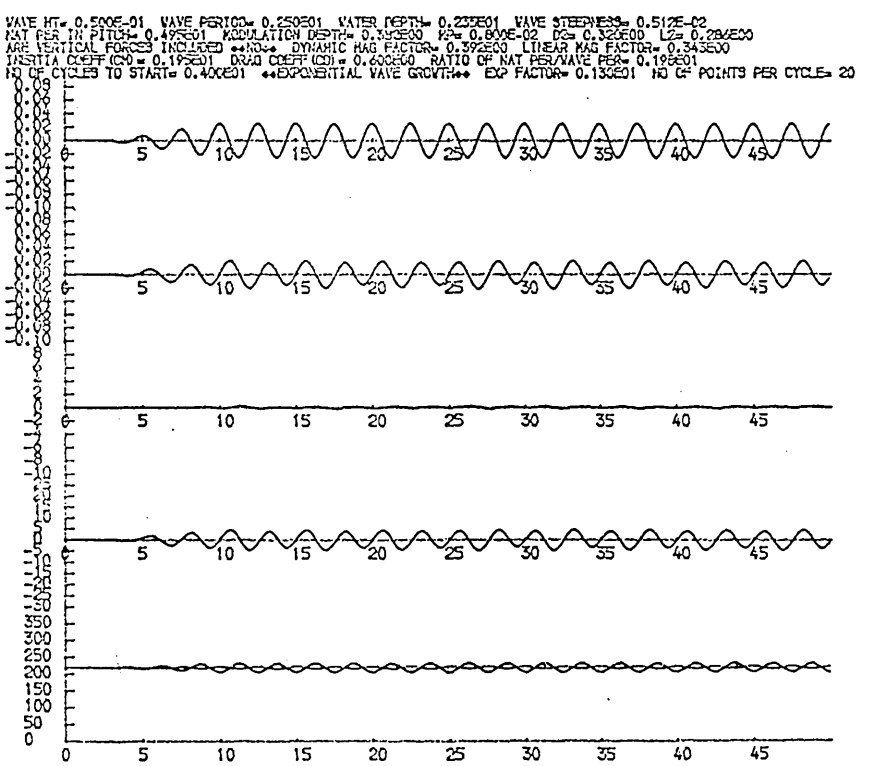
WAVE HT= 0.500E-01 WAVE PERIOD= 0.250E01 WATER DEPTH= 0.235E01 WAVE STEEPNESS= 0.512E-02
NAT PER IN PITCH= 0.493E01 MODULATION DEPTH= 0.362E00 KP= 0.800E-02 D2= 0.320E00 L2= 0.284E00
ARE VERTICAL FORCES INCLUDED ++NO++ DYNAMIC MAG FACTOR= 0.392E00 LINEAR MAG FACTOR= 0.343E00
INERTIA COEFF (CM) = 0.195E01 DRAG COEFF (CD) = 0.600E00 RATIO OF NAT PER/WAVE PER= 0.195E01
NO OF CYCLES TO START= 0.400E01 ++EXPONENTIAL WAVE GROWTH++ EXP FACTOR= 0.130E01 NO OF POINTS PER CYCLE= 20

FIG. 5.8

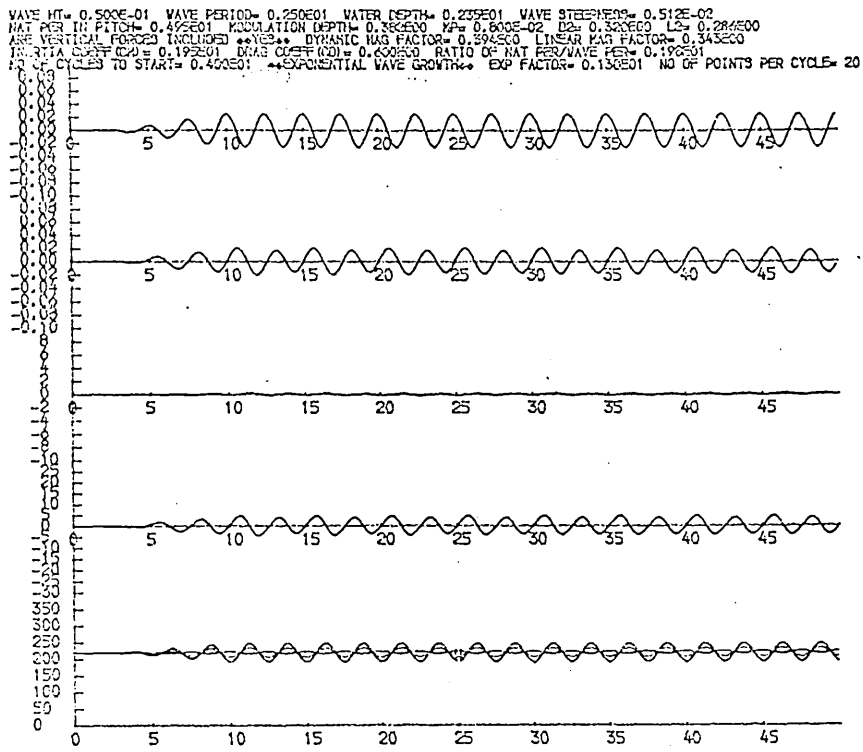

FIG. 5.9

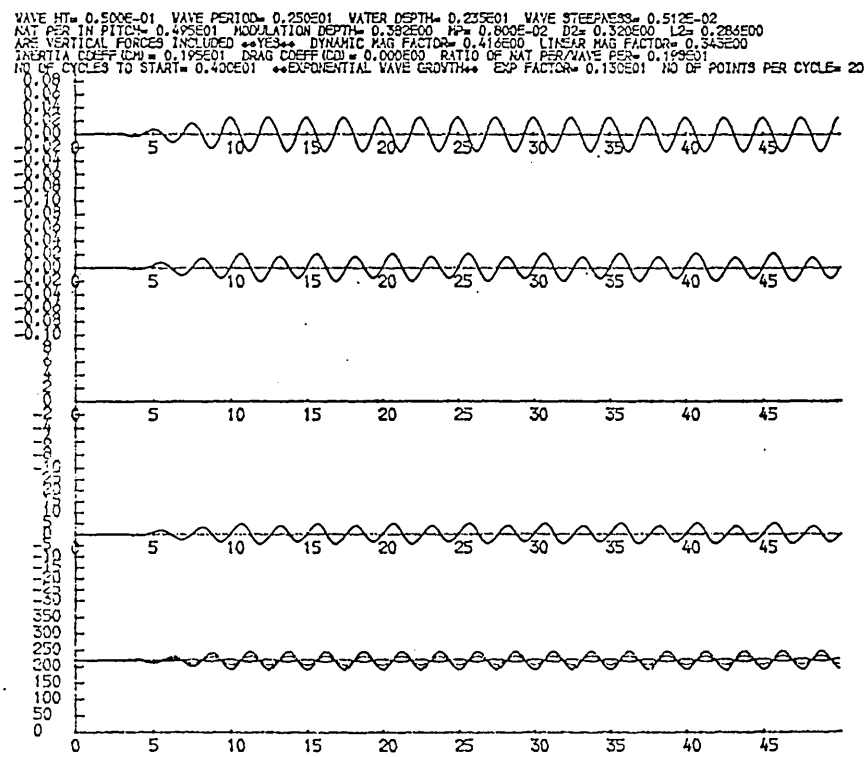

FIG. 5.10

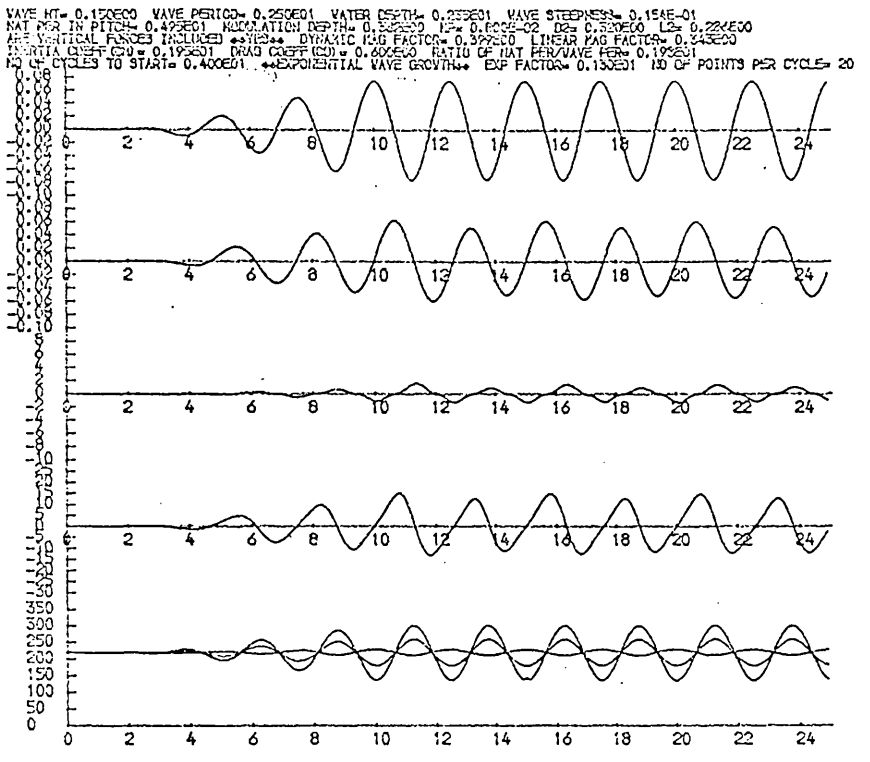

FIG. 5.11

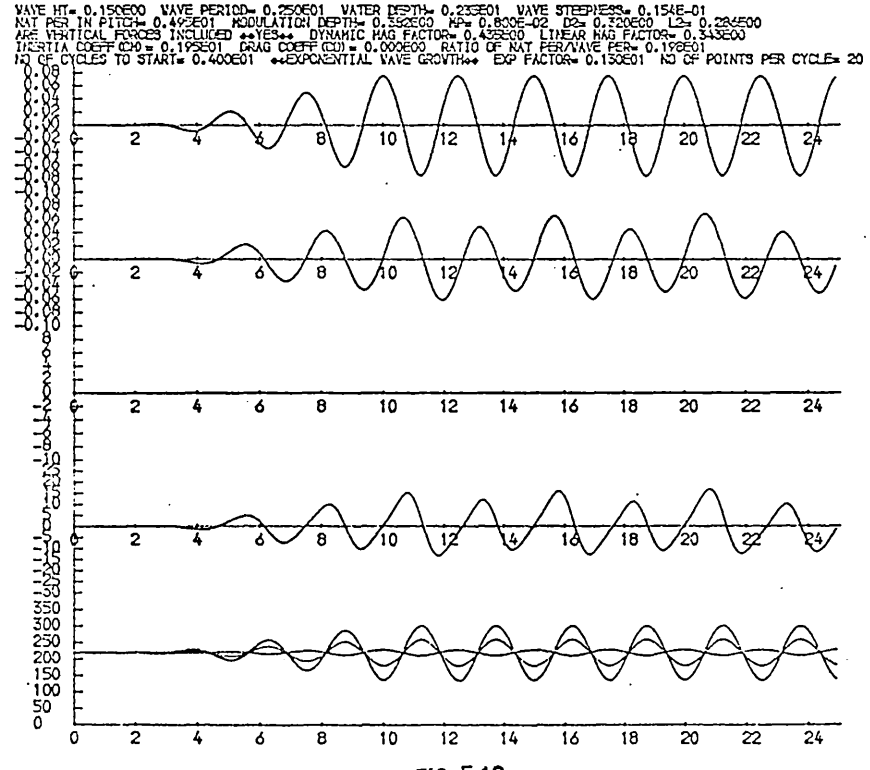

FIG. 5.12

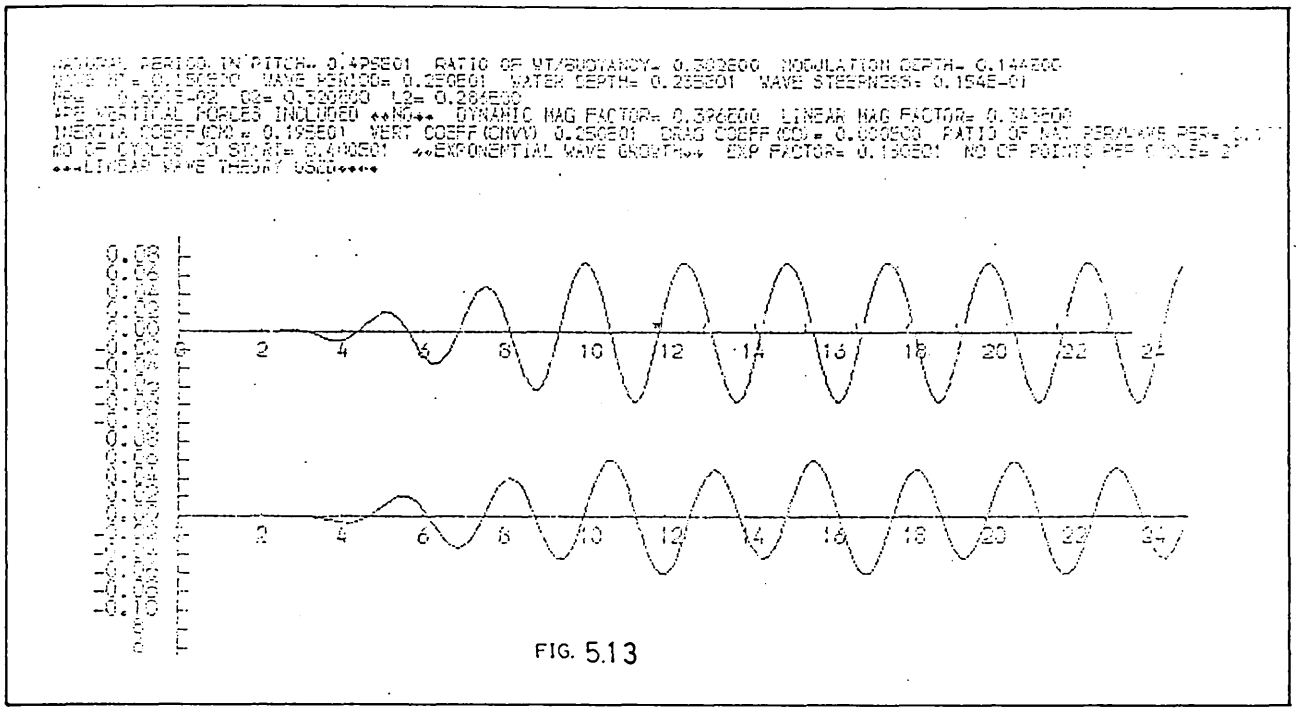
NATURAL PERIOD IN PITCH= 0.14PSE01 RATIO OF WT/BUOYANCY= 0.303E00 MODULATION DEPTH= 0.144E00
WAVE HT = 0.15E00 WAVE PERIOD= 0.2E0E01 WATER DEPTH= 0.2E5E01 WAVE STEEPNESS= 0.154E-01
2 4 6 8 10 12 14 16 18 20 22 24
2 4 6 8 10 12 14 16 18 20 22 24

FIG. 5.13

excluding heave forces in the analysis and with zero viscous drag. The response is similar to that of fig. 5.11 (heave forces included $C_D = 0.6$).

3.2. Effect of wave growth

The results obtained and shown in figs. 5.4 to 5.13 are those allowing for an exponential wave growth starting from zero and growing to full height over the first 4 wave cycles. Observations of wave growth in the experimental tank suggest an exponential growth. Real waves almost certainly assume a gradual growth to their full height although the precise nature, whether linear or exponential is uncertain.

It is necessary to assess the effects of the nature and rate at which waves grow to their full height on dynamic instabilities. Accordingly, the following results have been obtained for varying rates and type of wave growth.

Figures 5.14 and 5.15 show the response for waves at twice the natural frequency neglecting viscous damping and with heave forces excluded and included, respectively. The wave growth is imposed exponentially over 2 wave cycles. The transient is very pronounced in fig. 5.14 but the response is limited and stable.

The response in fig. 5.15, which includes vertical heave forces, shows an increasing instability and is much more pronounced than that of fig. 5.12 (4 cycles wave growth).

Figures 5. 16 and 5.17 show responses obtained for linear

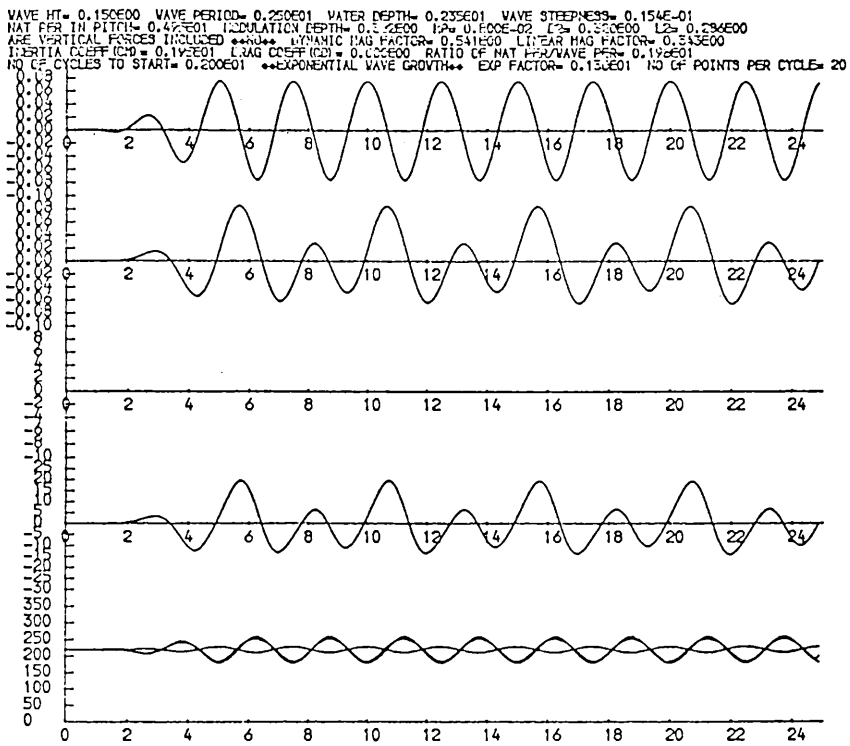

FIG. 5.14

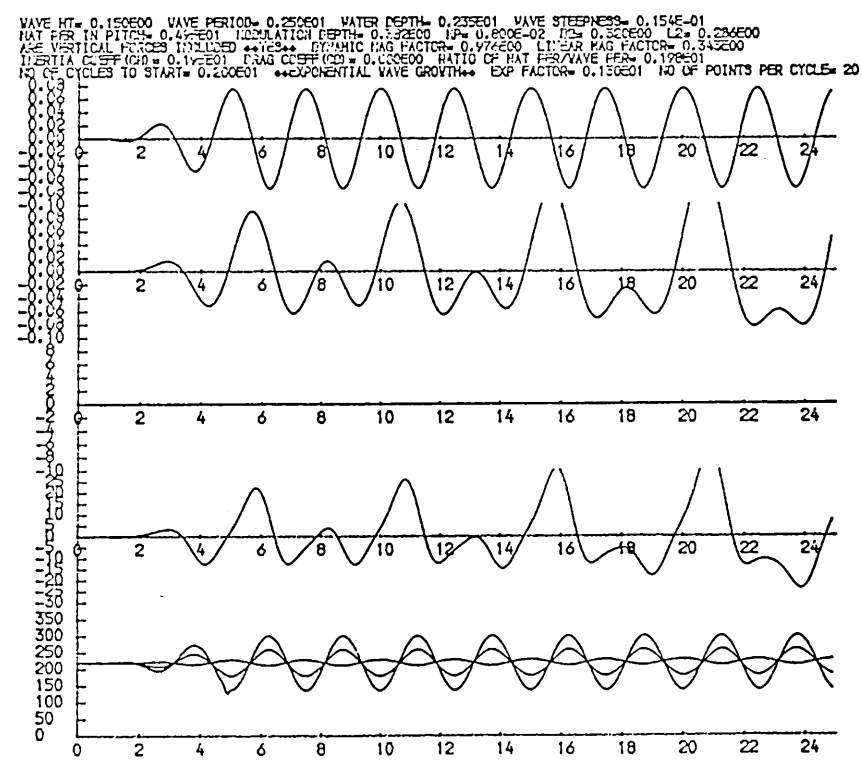

FIG. 5.15

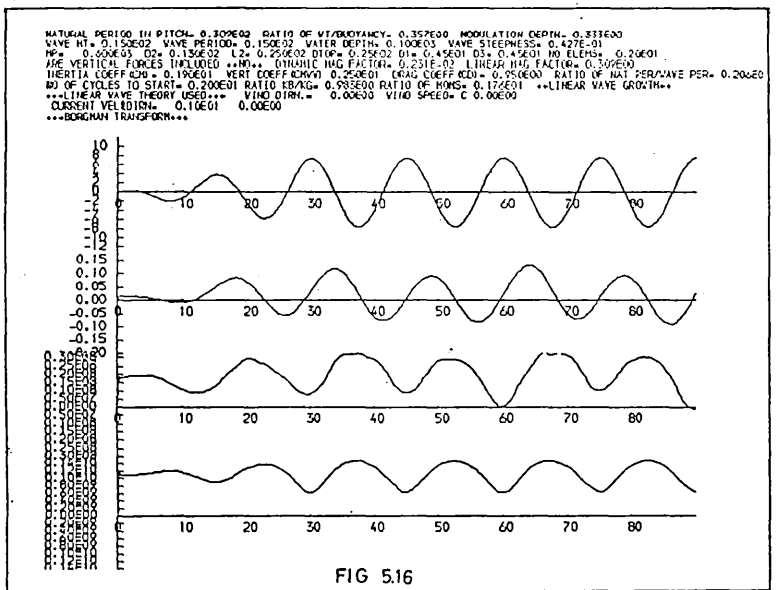

FIG 5.16

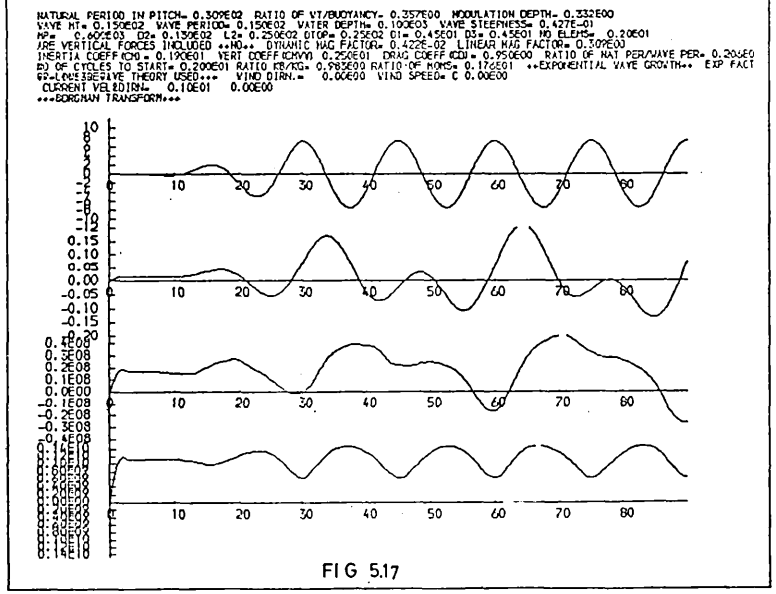

FIG 5.17

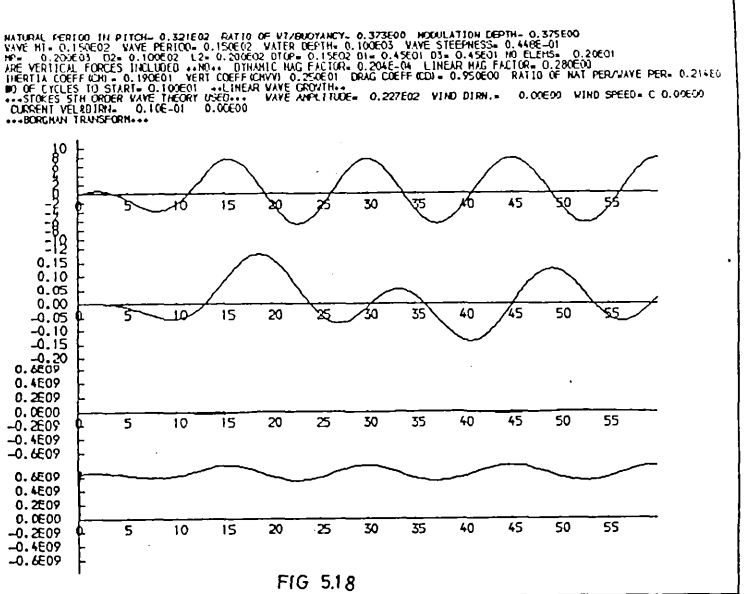

FIG 5.18

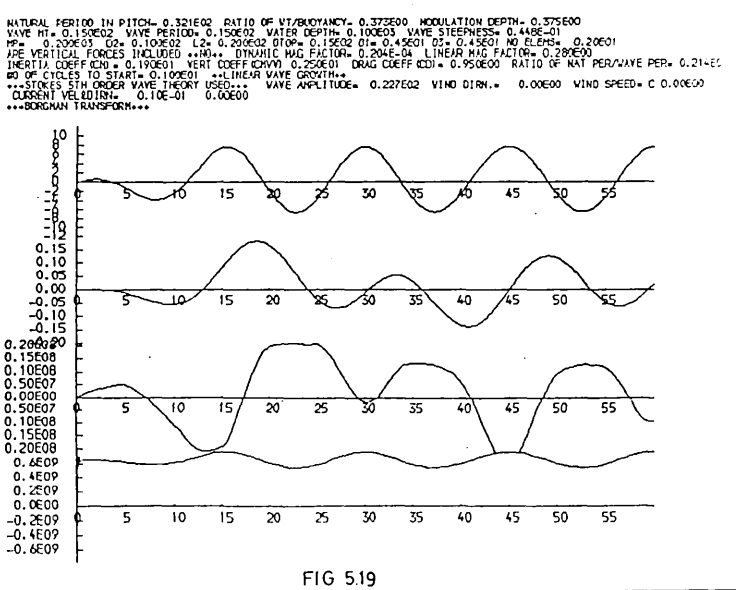

FIG 5.19

wave growth and exponential wave growth, respectively. The response for the linear wave growth is limited in magnitude whereas that for exponential growth is unstable. For the case of the exponential growth it is noted that the response does not become negative in the first cycle, whereas that for the linear growth displays a slightly negative response in the first cycle.

3.3. Effect of Linear Theory and Stokes Fifth Order Theory

A comparison of the effects of the use of linear theory and Stokes fifth order wave theory in the calculation of particle kinematics was made in Chapter 4 and some of the results indicated substantial differences in the response obtained.

In examining the dynamic instabilities of larger structures with small pitch frequencies the offending waves will themselves have fairly small frequencies so that a linear wave description is adequate. However, smaller structures in shallower water will have much greater pitch frequencies and the associated waves at twice the frequency may be steeper and assume a more non linear profile. It is pertinent therefore to examine the effects of non linear waves on the dynamic instabilities.

A measure of the magnitude of the damping force is obtained by observation of figs. 5.18 and 5.19. The damping force in fig. 5.18 is drawn to the same scale as the restoring force whereas the damping force in fig. 5.19 is drawn to a much reduced scale for clarity.

Figures 5.20 and 5.21 show the responses obtained using linear wave theory and Stokes fifth order theory, respectively. The

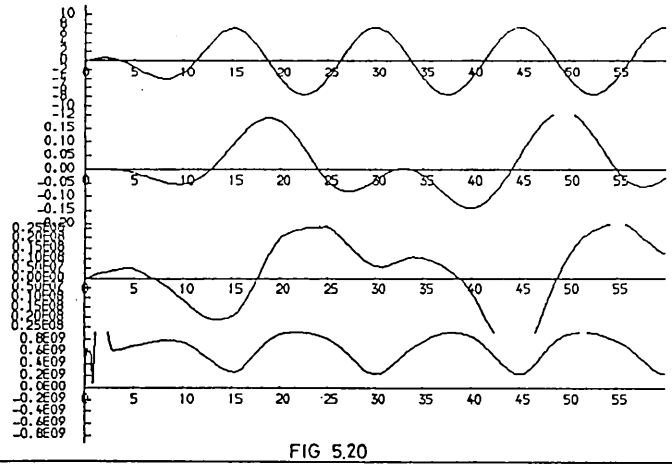

FIG 5.20

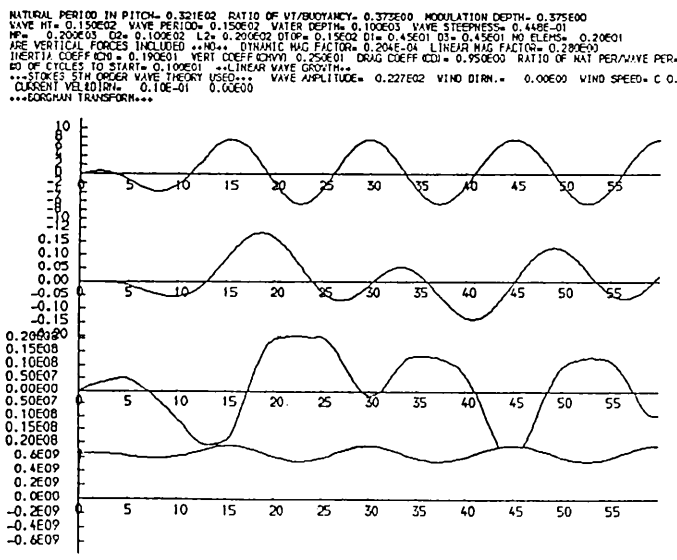

FIG 5.21

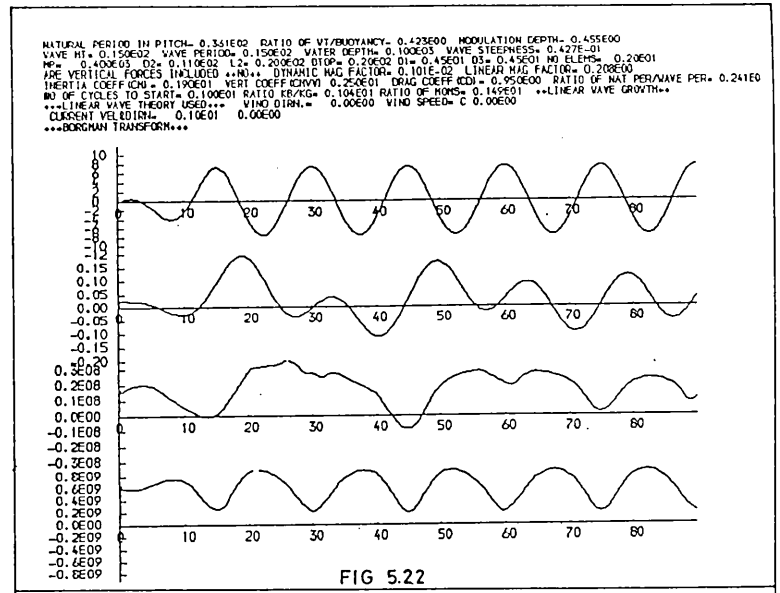

FIG 5.22

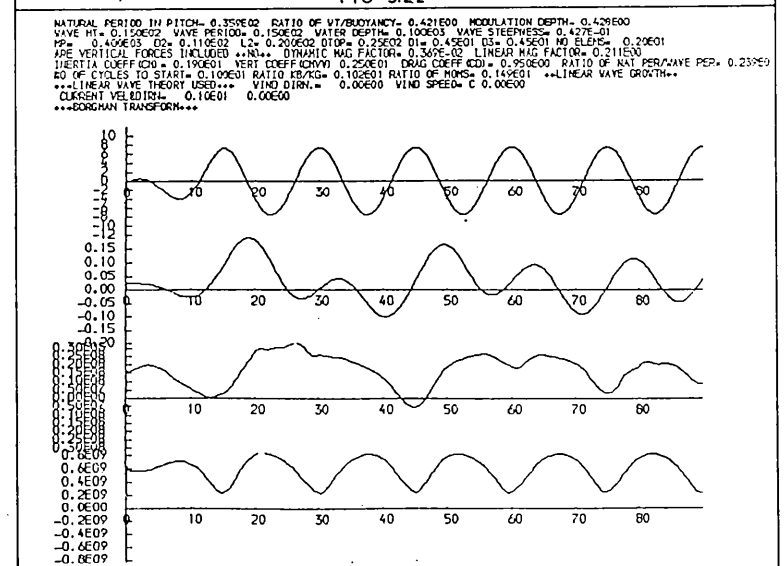

FIG 5.23

response in fig. 5.20 is unstable whereas that in fig. 5.21 is limited in magnitude, although the transient oscillation persists. It is noted that vertical forces have not been included in the analysis.

The damping forces in each case are of the same order of magnitude for the first 1.5 cycles so that it is not obvious that the damping in the Stokes fifth order solution is preventing the onset of the instability. For the wave considered, the linear theory is probably predicting inertia and drag components of force greater than those predicted by the Stokes theory (see Chapter 4, section 2.4). It is worth noting that in both those cases the wave is growing linearly in magnitude over one cycle.

3.4. Effects of Elevation of Buoyancy Chamber and Weight to Buoyancy Ratio

It is instructive to compare responses for varying elevations of buoyancy chamber and weight to buoyancy ratios. Figures 5.22 and 5.23 show the responses for a full size structure with depths of submergence of the buoyancy chamber of 20 and 25 metres below the SWL, respectively. Vertical forces have not been included and it is apparent that differences in response are minimal. Similar plots which include heave forces in the analysis are shown in figs. 5.24 and 5.25 and it is observed that the motion is marginally more stable for the structure with the greatest depth of submergence.

The effects of variation in the ratio of weight to buoyancy are shown in figs. 5.26 and 5.27 for ratios of 0.375 and 0.333, respectively. The transient oscillation persists even for those relatively small ratios of weight to buoyancy and it is apparent that the decreased ratio does not contribute to limiting the response of

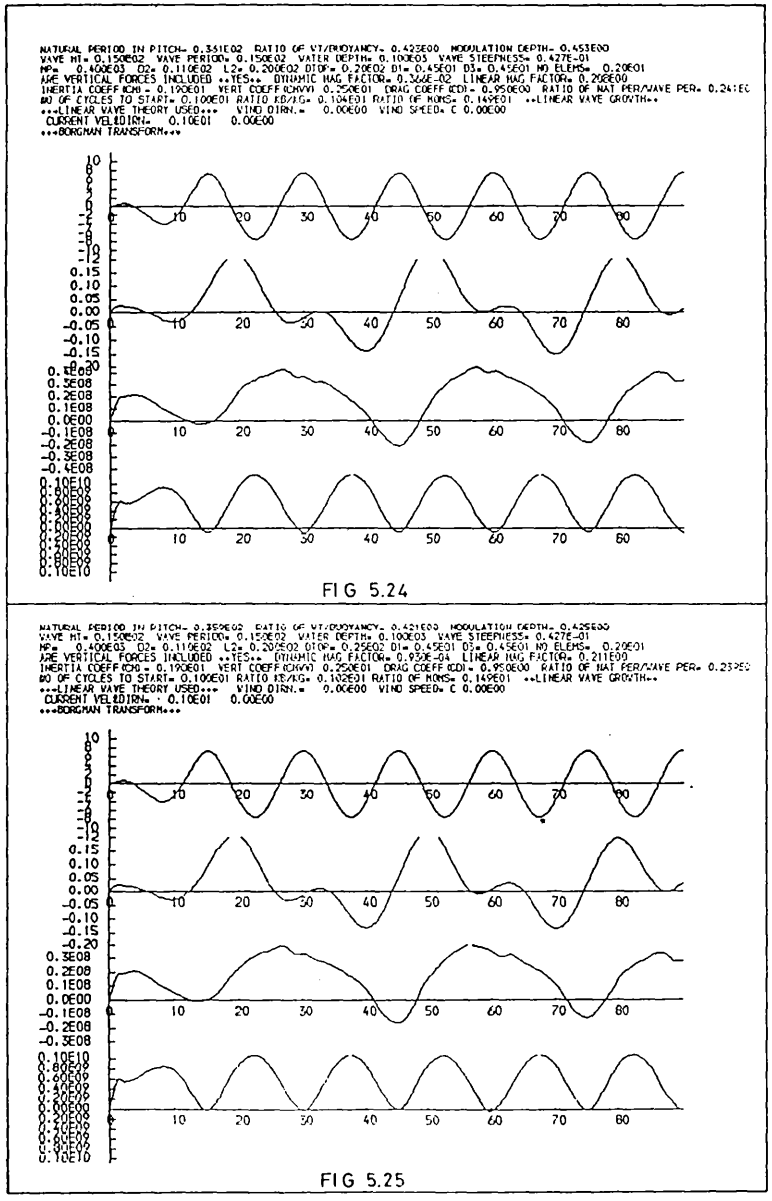

FIG 5.24

FIG 5.25

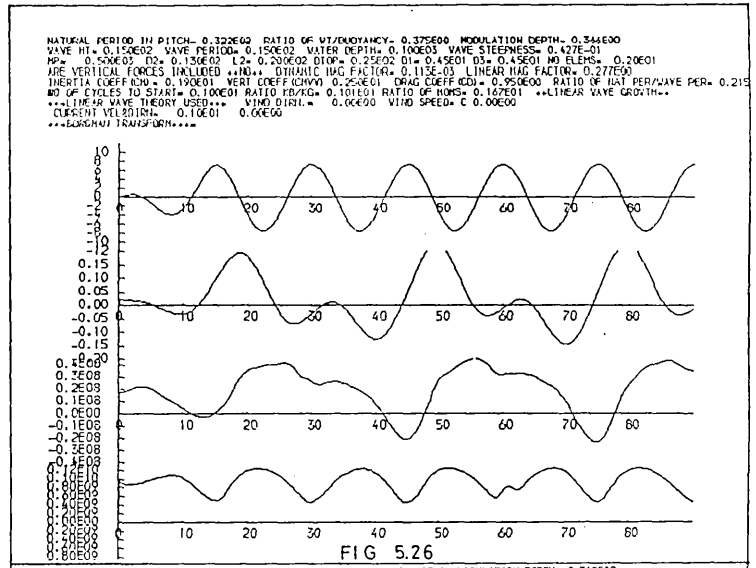

FIG 5.26

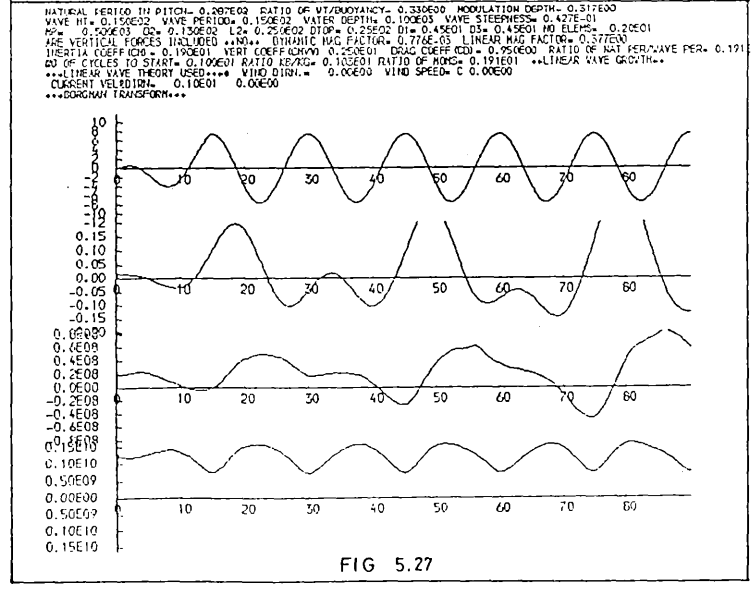

FIG 5.27

the structure. However, it is noted that for both of these figures that the wave forces are increased to the maximum value in the first wave cycle.

3.5 Effect of Current Orthogonal to Waves

The effects of non co-linear exciting forces was investigated and discussed in Chapter 4, section 3, and complex swirling trajectories were observed.

The phase lag of the response of the structure subject to non colinear exciting forces will be much the same as for the structure subject to colinear exciting forces. However, the effects of the heaving forces acting together with the out of plane movement of the structure requires consideration in the context of dynamic instabilities. Accordingly, some analytical results have been obtained and are presented.

Figures 5.28 and 5.29 show the effect of a 1 metre per second current orthogonal to the direction of wave travel for the structure excluding and including heave forces in the analysis, respectively. The transient oscillation is evident in both cases but appears to be somewhat more pronounced than that which was obtained for the single degree of freedom structure.

The maximum response for the case including heaving forces is some 20% greater than that obtained excluding heave forces. The trajectory orthogonal to the direction of wave travel is also greater when the heave forces are included in the analysis.

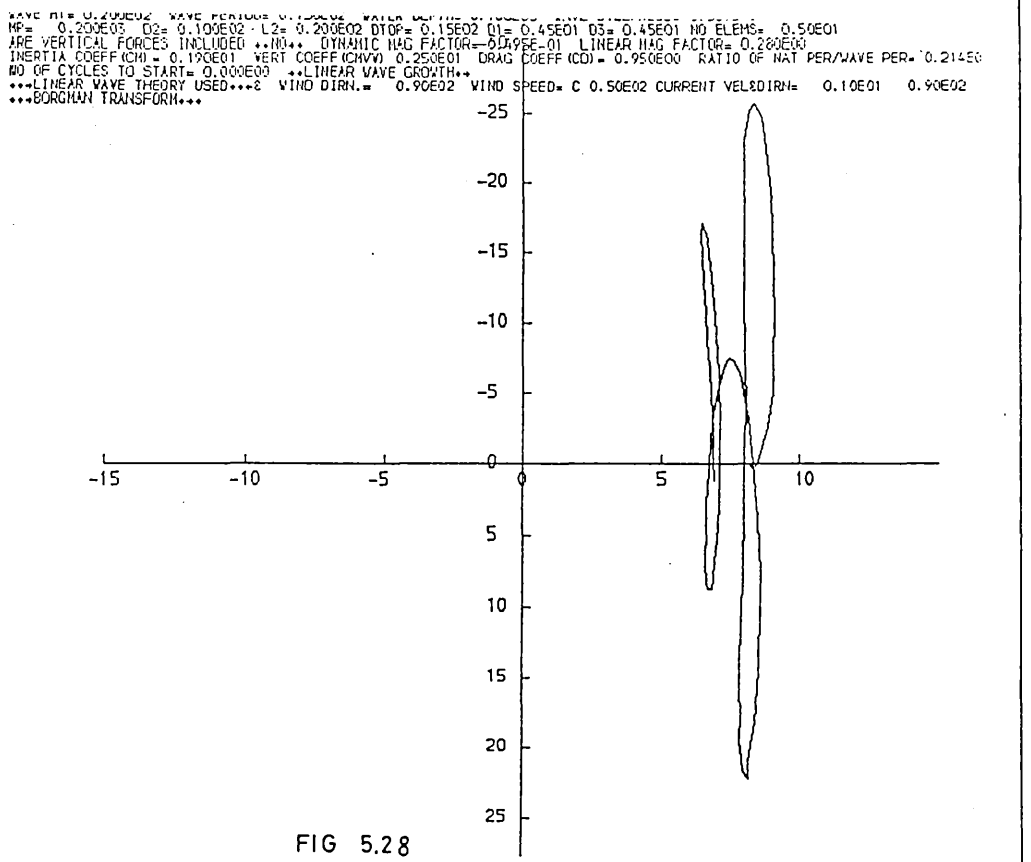

FIG 5.28

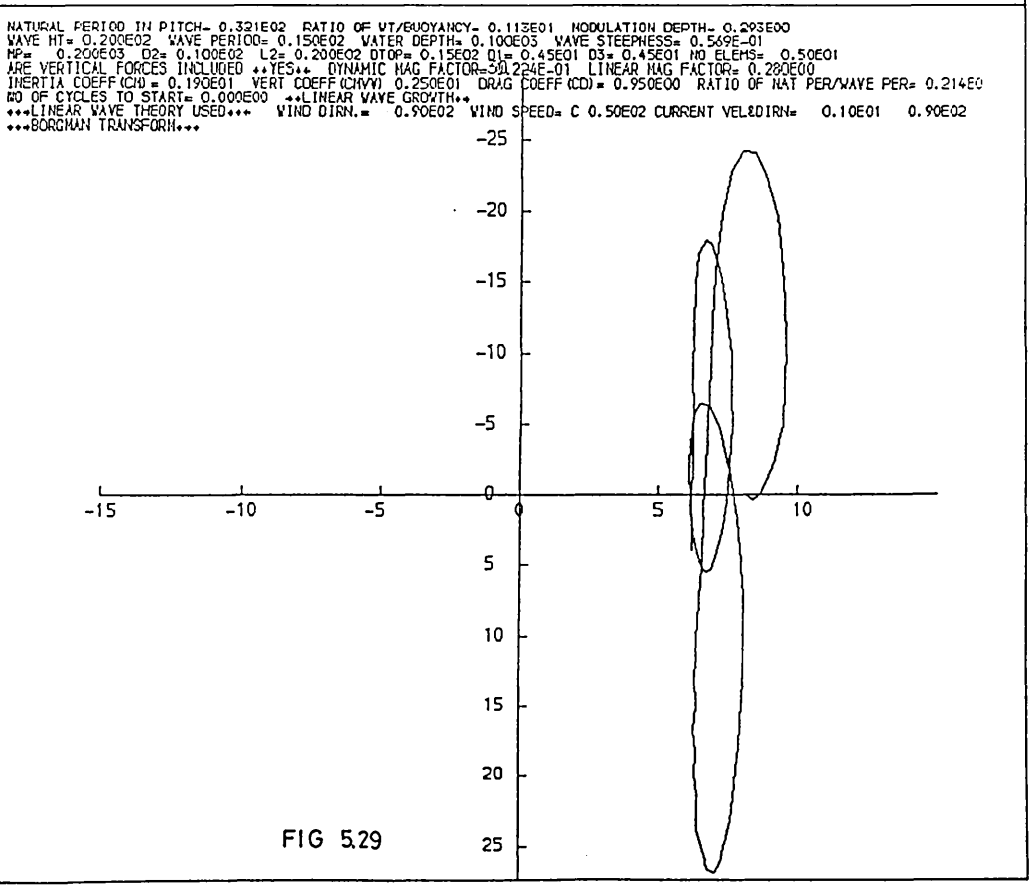

FIG 5.29

4. EXPERIMENTAL OBSERVATIONS

Analytical techniques are an economic way of obtaining information on motion response characteristics. However, in order to validate certain analytical results it is necessary to undertake physical model tests. The scaling problems have to be borne in mind in assessing the validity of the results when it is intended to extropolate these to the full scale situation.

A 1/100 scale model was adapted so that it was large enough to permit the variation of ballast mass inside the buoyancy chamber. The experimental model is as shown in fig. 5.1.

The logarithmic decrement of damping ($\delta = 2\pi\beta$) for the experimental model subjected to an initial displacement and allowed to oscillate freely, indicated approximately 2% to 6% of critical damping ($\beta = 0.02$ to 0.06) and this is shown in fig. 5.34. It is considered that the nature of the hinge connection will impose little or no damping, so that most of this is attributable to hydrodynamic damping. Furthermore potential damping is likely to be minimal for this relatively low frequency of oscillation so that the majority of the damping is likely to be viscous in origin.

Some experimental observations of the response of the model articulated column were obtained for exciting frequencies of the order of about twice the natural frequency of the model and these are presented.

Three operating conditions were simulated, viz:-

1. Basic model with no additional mass on the deck or in the

buoyancy chamber.

Natural period in pitch = 4.0 seconds.
Ratio of weight to buoyancy = 0.34

2. Basic model with 2Kg mass added to the deck.

Natural period in pitch = 5.0 seconds.
Ratio of weight to buoyancy = 0.43

3. Basic model with 4Kg mass added to the inside of the buoyancy chamber and zero deck mass.

Natural period in pitch = 5.2 seconds.
Ratio of weight to buoyancy = 0.52

Conditions 2 and 3 enable a comparison to be made of responses for structures having the same natural frequency but with different ratios of weight to buoyancy. A measure of the importance of this can then be made.

Condition 1 - fig. 5.30 shows the response in pitch for the model subject to a wave at twice the frequency of the structure. It is noted that the response is not sinusoidal with the frequency but that there is a transient oscillation at the natural frequency of the structure.

Figure 5.31 shows the response in pitch for the model subject to a wave of equal height to that of fig. 5.30 but at 2.8 times the natural frequency of the structure. The transient has disappeared and the response is approximately 50% of that in fig. 5.30.

Conditions 2 and 3 - figs. 5.32 and 5.33 show the response of the model for conditions 2 and 3 respectively and for the same wave at twice the frequency of the structure.

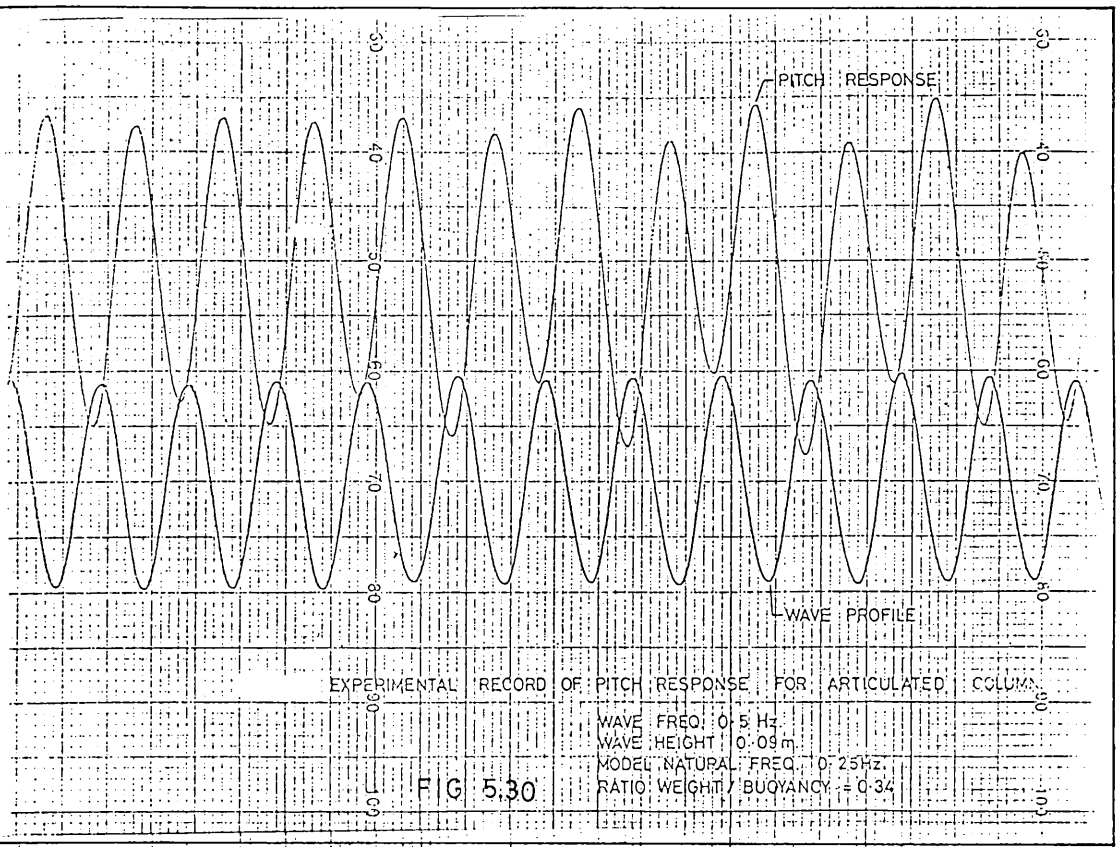

FIG 5.30

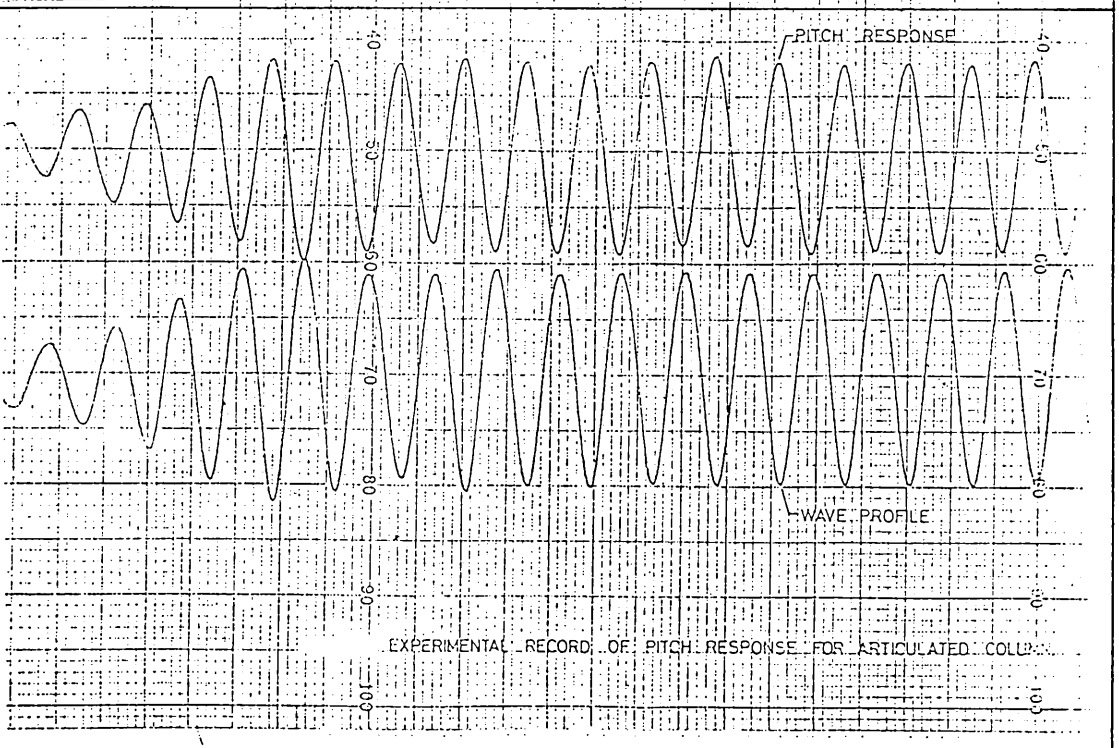

WAVE FREQ. 0·7 Hz.
WAVE HEIGHT. 0·09 m.
MODEL NATURAL FREQ. 0·25 Hz.
RATIO OF WEIGHT / BUOYANCY = 0·34

FIG 5.31

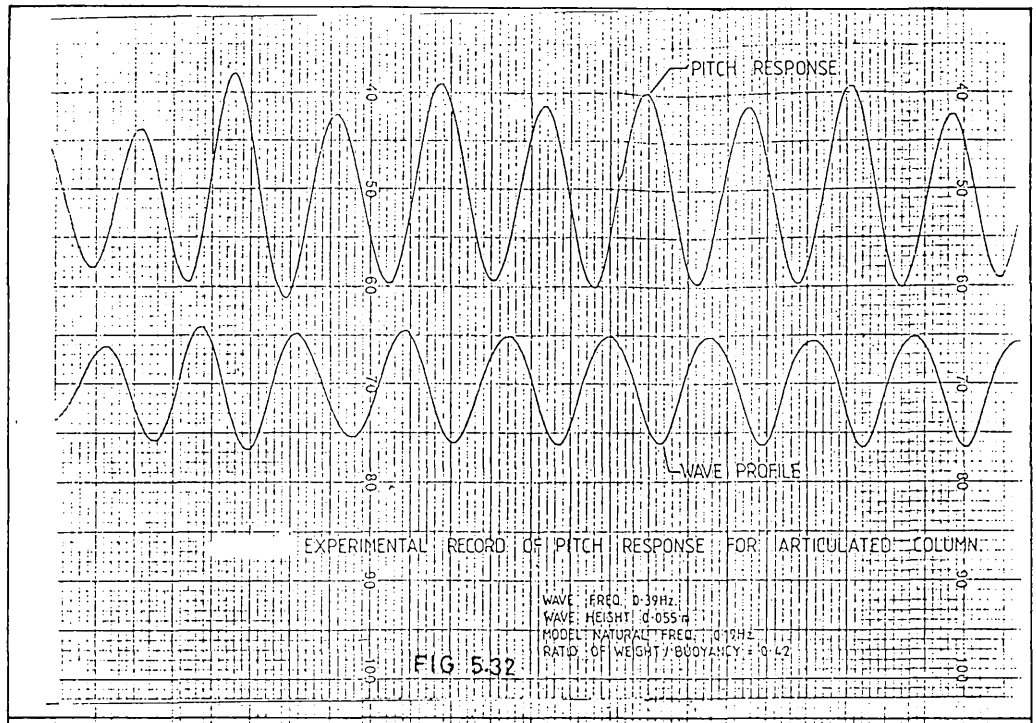

FIG 5.32

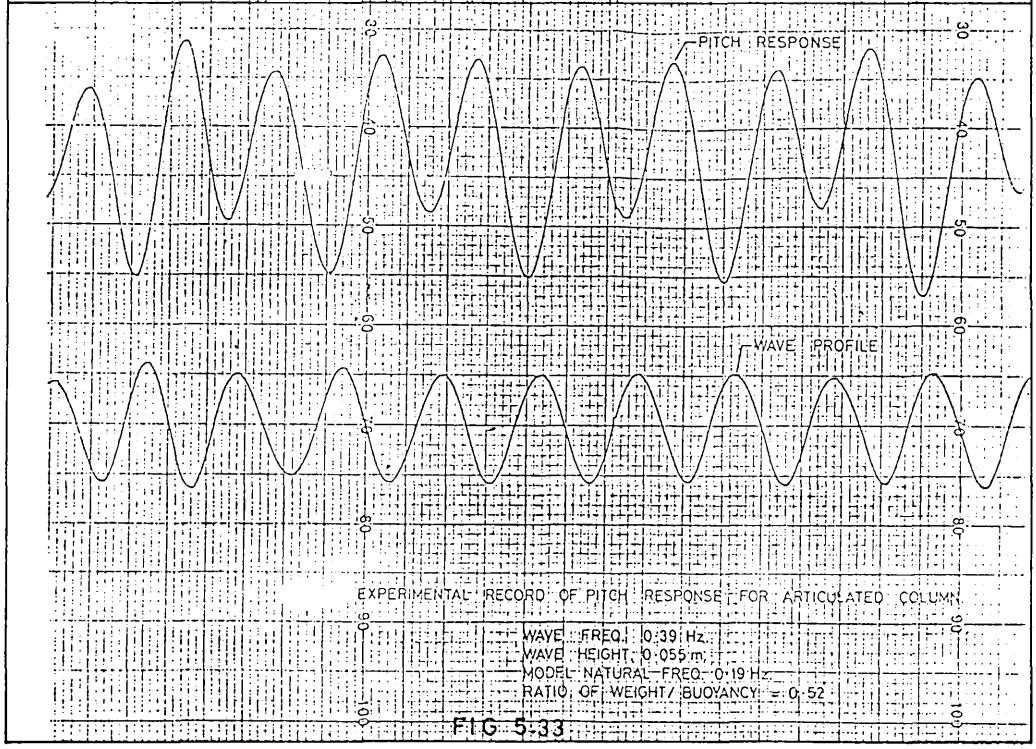

FIG 5.33

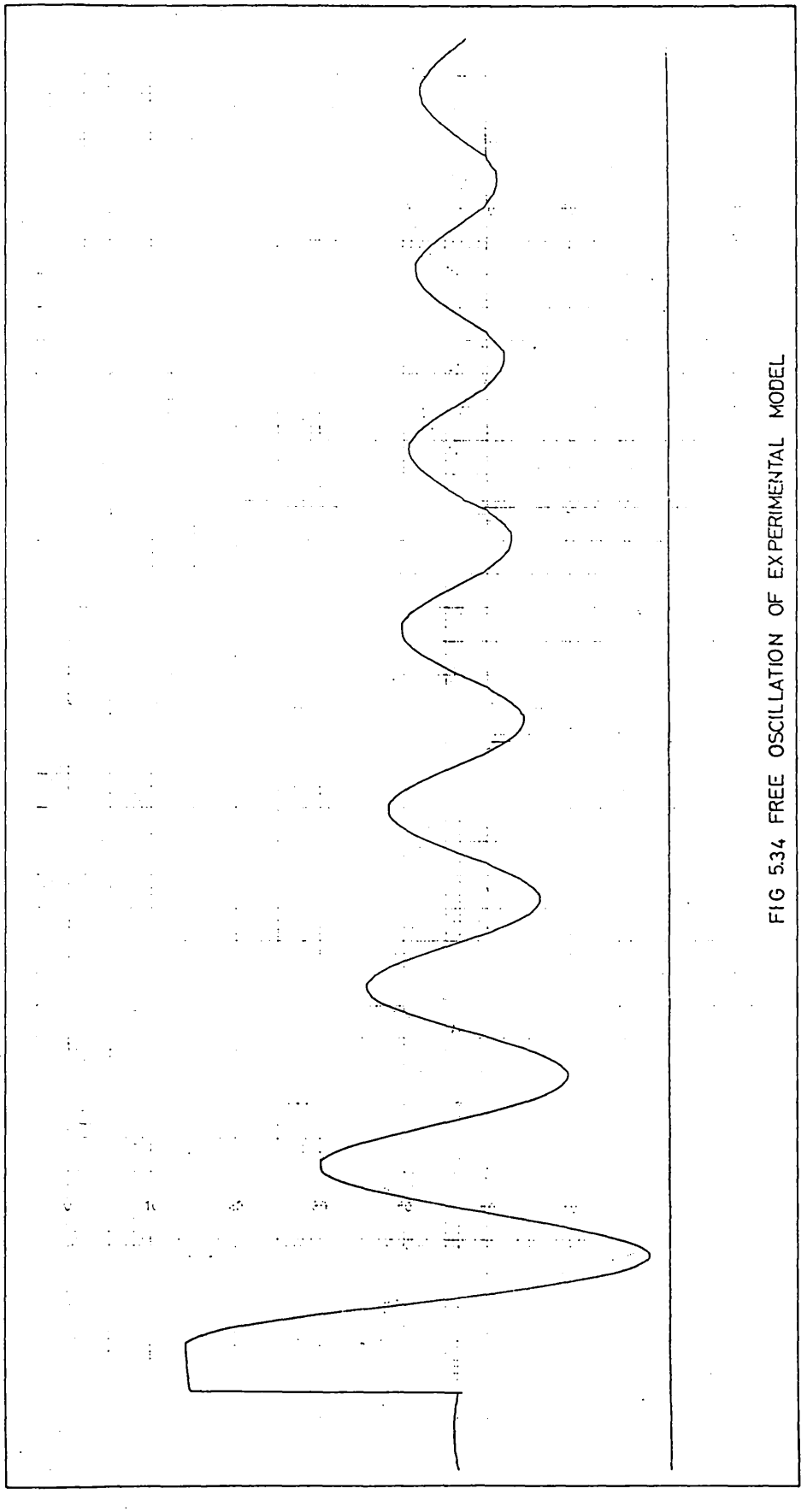

FIG 5.34 FREE OSCILLATION OF EXPERIMENTAL MODEL

The transient is much more pronounced in fig. 5.33 (condition 3) and the maximum response is approximately 15% greater than for fig. 5.32 (condition 2). Evidently the increased weight to buoyancy ratio has a significant effect on the response as would be expected.

The experimental result of fig. 5.32 (condition 2) bears direct comparison with fig. 5.5 which is the analytical prediction of the same structure subject to the same wave. The maximum pitch response recorded experimentally was + 53mm and the minimum recorded was - 40mm. The maximum pitch response apparent from fig. 5.5 is + 0.02 radians = + 50mm (-6% difference) and the minimum was 0.0175 radians = 43.7mm (9% difference).

The important observations to be made from the experimental results are:-

a. the increased response, and

b. the transient oscillation.

In fig. 5.33 the magnitude of the minimum oscillation is about 50% that of the maximum frequency response oscillation, whereas in fig. 5.32 the minimum response was approximately 85% of the maximum frequency response oscillation. Therefore, the increased weight to buoyancy ratio has the effect of increasing the maximum response while, at the same time, decreasing the magnitude of the minimum response.

It is interesting to note that the transient is qualitatively similar to the transient which the analysis predicts and is also in agreement with the transient as predicted by others (25). There is also reasonable quantitative agreement between the experimental

response and the analytical response for the part prior to the onset of the instability.

5. RESONANT RESPONSES

5.1 Wave Groups

In the absence of non linearities the response of a structure will be harmonic with the exciting wave frequency and symmetric about the axis of oscillation. When the motion of the structure is accounted for, second order forces which have the effect of imposing a nett force in the direction of the wave travel can be generated. Some of the consequences have been examined in Chapter 4 and in the preceding section of this chapter. The steady drift phenomenon has been comprehensively investigated (45) and a survey is presented in Reference (65).

Although the magnitude of the second order forces may be small in relation to the wave forces it may have a frequency component resonant with the natural pitch frequency of the structure and large motions may ensue as a consequence.

It is considered that one such way in which the resonant mechanism may be generated is as a consequence of wave groups harmonic with the natural frequency in pitch of the structure. Wave groups may be generated when two regular wave trains of slightly different frequency are travelling in the same direction. A second order 'set-down' wave may be generated as shown in fig. 5.35 and this induces an inertia force contribution, albeit small, at the set-down wave frequency.

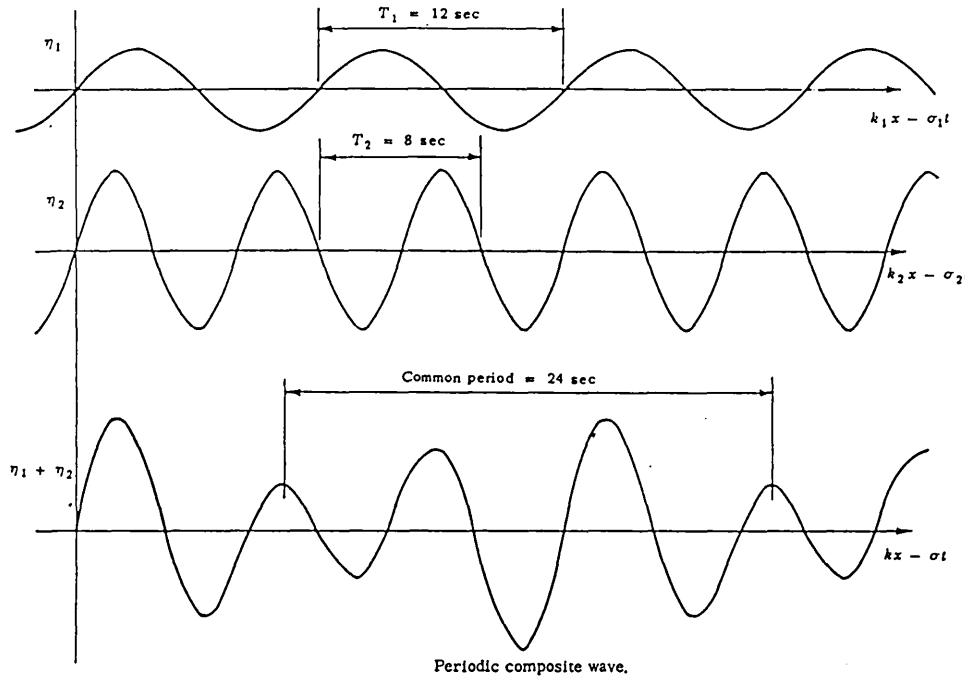

Periodic composite wave.

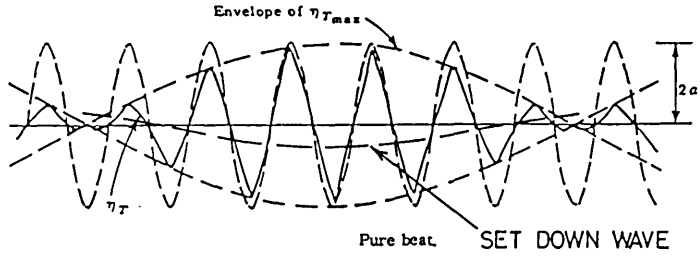

FIG 5.35 COMPOSITE WAVE TRAIN COMPRISING TWO SEPARATE WAVE TRAINS

With reference to fig. 5.35; consider two waves of equal height $2a_1$ and $2a_2$ of frequency ω_1 and ω_2 travelling in the same direction and in phase with each other. The pure beat phenomenon will ensue as shown and the resultant maximum amplitude of the wave envelope will be equal to twice the wave amplitude, ie $2a_1$.

The amplitude of the composite wave is then written:-

$$\eta_t = a_1\cos(k_1x - \omega_1t) + a_2\cos(k_2x - \omega_2t) \qquad (5.20)$$

The resultant wave group will have a period equal to $2\pi/(\omega_2 - \omega_1)$ seconds. The composite wave will have a frequency ω_a equal to $\frac{1}{2}(\omega_2 + \omega_1)$.

The amplitude of the wave envelope can be written:-

$$A_a = 2a_1\cos(\frac{\omega_2 - \omega_1}{2})t \qquad (5.21)$$

The composite wave has been modelled computationally on the basis of a regular wave with frequency ω_a having an amplitude varying with time in accordance with equation 5.21. The wave surface at any instant in time is taken as the value computed in accordance with equation 5.20. No attempt has been made to model any 'set-down' wave or any second order inertial contribution to the exciting force.

The results for the response of a structure with a natural period in pitch of 67 seconds are shown in fig. 5.36. The wave periods used were 10.2 seconds and 12 seconds. This produces a wave 'beat' or group with a frequency = $2\pi/(\omega_2 - \omega_1)$ = 0.0938 radians per second or period = 67 seconds. The height of both waves was 5 metres. The resonant response at the natural pitch frequency is very evident and displays some attenuation with time. However, the 'steady state'

NATURAL PERIOD IN PITCH= 0.670E02 RATIO OF VT/BUOYANCY= 0.512E00 MODULATION DEPTH= 0.237E00
WAVE HT= 0.100E02 WAVE PERIOD= 0.150E02 WATER DEPTH= 0.270E03 WAVE STEEPNESS= 0.285E-01
MP= 0.100E05 D2= 0.280E02 L2= 0.350E02 DTOP= 0.30E02 D1= 0.10E02 D3= 0.60E01 NO ELEMS= 0.20E01
ARE VERTICAL FORCES INCLUDED ++NO++ DYNAMIC MAG FACTOR= 0.000E00 LINEAR MAG FACTOR= 0.278E-01
INERTIA COEFF(CM) = 0.190E01 DRAG COEFF(CD) = 0.600E00 RATIO OF NAT PER/WAVE PER= 0.608E01
NO OF CYCLES TO START= 0.100E01 RATIO KB/KG= 0.975E00 RATIO OF MOMS= 0.145E01 ++LINEAR WAVE GROWTH++
+++LINEAR WAVE THEORY USED+++M WIND DIRN.= 0.00E00 WIND SPEED= C 0.00E00
CURRENT VEL&DIRN= 0.10E-01 0.00E00
+++BORGMAN TRANSFORM+++S WAVE PERIODS= 0.102E02 SECS AND 0.120E02 SECS

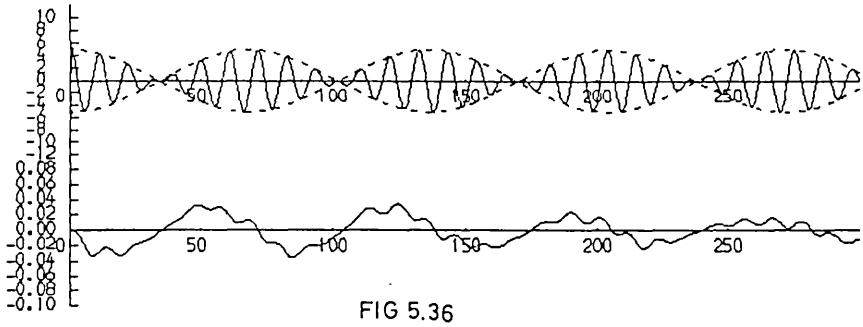

FIG 5.36

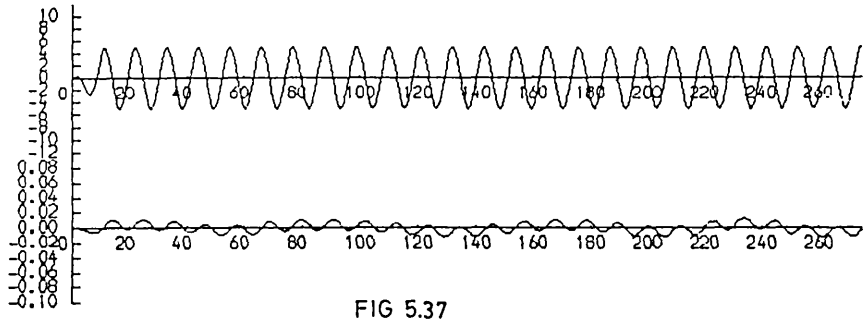

FIG 5.37

NATURAL PERIOD IN PITCH= 0.670E02 RATIO OF VT/BUOYANCY= 0.512E00 MODULATION DEPTH= 0.248E00
WAVE HT= 0.100E02 WAVE PERIOD= 0.150E02 WATER DEPTH= 0.270E03 WAVE STEEPNESS= 0.285E-01
MP= 0.100E05 D2= 0.280E02 L2= 0.350E02 DTOP= 0.30E02 D1= 0.10E02 D3= 0.60E01 NO ELEMS=S 0.20E01
ARE VERTICAL FORCES INCLUDED ++NO++ DYNAMIC MAG FACTOR= 0.000E00 LINEAR MAG FACTOR= 0.323E-01
INERTIA COEFF(CM) = 0.190E01 DRAG COEFF(CD) = 0.600E00 RATIO OF NAT PER/WAVE PER= 0.565E01
NO OF CYCLES TO START= 0.100E01 RATIO KB/KG= 0.975E00 RATIO OF MOMS= 0.145E01 ++LINEAR WAVE GROWTH++
+++LINEAR WAVE THEORY USED+++ WIND DIRN.= 0.00E00 WIND SPEED= C 0.00E00
CURRENT VEL&DIRN= 0.10E-01 0.00E00
+++BORGMAN TRANSFORMWAVEPERIODS= 0.109E02 SECS AND 0.130E02 SECS

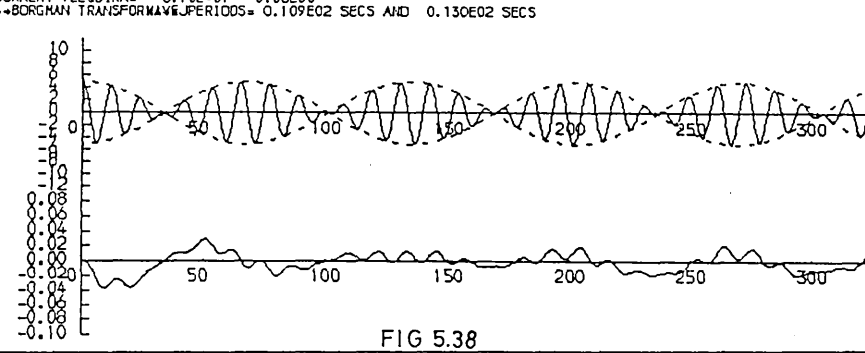

FIG 5.38

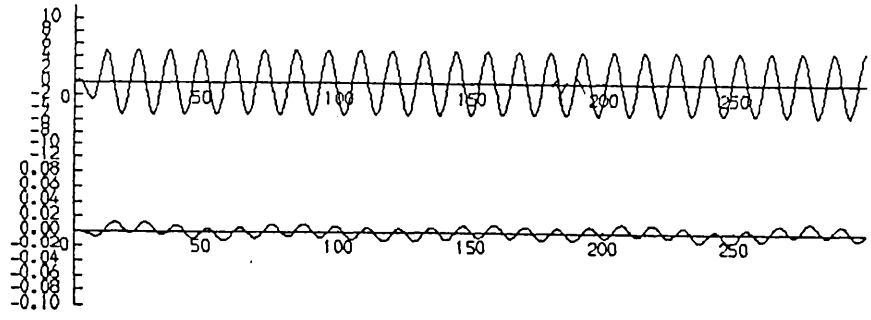

FIG 5.39

harmonic response is still some 100% greater than that obtained when the structure is subject to regular waves with a period equal to the average of both waves, ie 11 seconds and height 10 metres - this result is shown in fig. 5.37 for comparison.

Figure 5.38 is the result for waves with periods of 10.9 seconds and 13 seconds each of height 5 metres. The harmonic resonant response is somewhat better defined than that of fig. 5.36. Again for comparison, fig. 5.39 shows the results for a single wave train with waves of period 12 seconds and height 10 metres.

Figure 5.40 is the result for waves with periods of 12.3 seconds and 15 seconds, each of height 5 metres. The harmonic resonant response is considerably increased and very much better defined than for the previous cases. The magnitude of the harmonic resonant response is some 200% greater than that obtained for a single wave train with waves of period 13.6 seconds and height 10 metres. Again, for comparison, fig. 5.41 shows the response for regular waves with period equal to the average of the two separate wave trains.

A general observation from the wave group responses is that the wave frequency response lags the maximum wave frequency forces by 180^{o}, whereas the harmonic resonant response is almost in phase with the node of the low frequency 'set-down' wave. This observation is depicted in fig. 5.42 and concurs with the theoretical result for a structure excited by a wave at the natural frequency, where in general the response would lag the maximum forces by 90^{o}.

Comparison of figs. 5.38 and 5.40 also show that there is a

NATURAL PERIOD IN PITCH= 0.670E02 RATIO OF WT/BUOYANCY= 0.512E00 MODULATION DEPTH= 0.254E00
WAVE HT= 0.100E02 WAVE PERIOD= 0.150E02 WATER DEPTH= 0.270E03 WAVE STEEPNESS= 0.285E-01
MP= 0.100E05 D2= 0.280E02 L2= 0.350E02 DTOP= 0.30E02 D1= 0.10E02 D3= 0.60E01 NO ELEMS= 0.20E01
ARE VERTICAL FORCES INCLUDED ++NO++ DYNAMIC MAG FACTOR= 0.000E00 LINEAR MAG FACTOR= 0.422E-01
INERTIA COEFF(CM) = 0.190E01 DRAG COEFF(CD) = 0.600E00 RATIO OF NAT PER/WAVE PER= 0.497E01
NO OF CYCLES TO START= 0.100E01 RATIO KB/KG= 0.975E00 RATIO OF MOMS= 0.145E01 ++LINEAR WAVE GROWTH++
+++LINEAR WAVE THEORY USED+++ WIND DIRN.= 0.00E00 WIND SPEED= C 0.00E00
CURRENT VEL&DIRN= 0.10E-01 0.00E00
+++BORGMAN TRANSFORM+++ WAVE PERIODS= 0.123E02 SECS AND 0.150E02 SECS

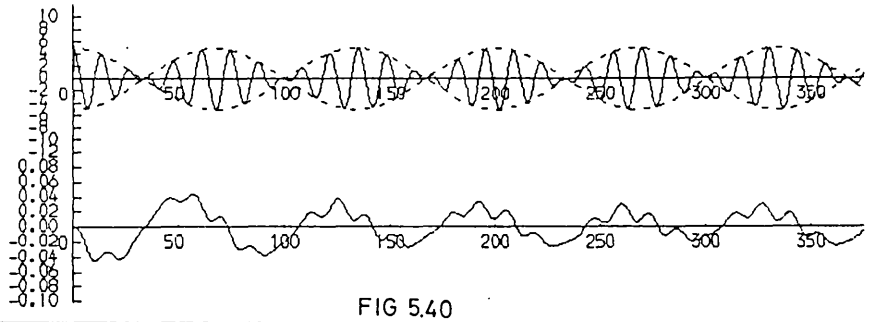

FIG 5.40

NATURAL PERIOD IN PITCH= 0.670E02 RATIO OF WT/BUOYANCY= 0.512E00 MODULATION DEPTH= 0.260E00
WAVE HT= 0.100E02 WAVE PERIOD= 0.136E02 WATER DEPTH= 0.270E03 WAVE STEEPNESS= 0.344E-01
MP= 0.100E05 D2= 0.280E02 L2= 0.350E02 DTOP= 0.30E02 D1= 0.10E02 D3= 0.60E01 NO ELEMS= 0.20E01
ARE VERTICAL FORCES INCLUDED ++NO++ DYNAMIC MAG FACTOR= 0.564E-06 LINEAR MAG FACTOR= 0.433E-01
INERTIA COEFF(CM) = 0.190E01 DRAG COEFF(CD) = 0.600E00 RATIO OF NAT PER/WAVE PER= 0.491E01
NO OF CYCLES TO START= 0.100E01 RATIO KB/KG= 0.975E00 RATIO OF MOMS= 0.145E01 ++LINEAR WAVE GROWTH++
+++LINEAR WAVE THEORY USED+++ WIND DIRN.= 0.00E00 WIND SPEED= C 0.00E00
CURRENT VEL&DIRN= 0.10E-01 0.00E00
+++BORGMAN TRANSFORM+++

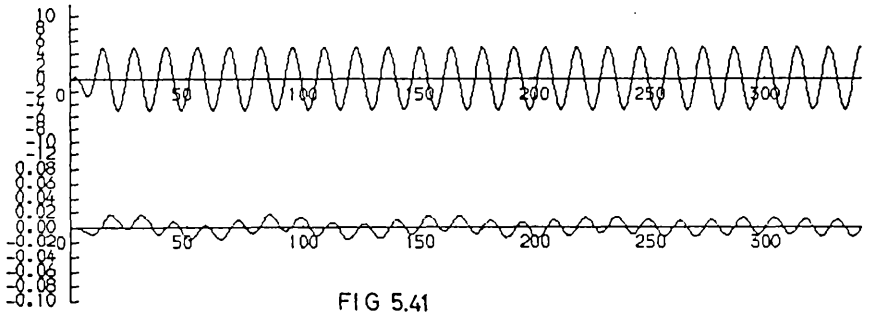

FIG 5.41

NATURAL PERIOD IN PITCH= 0.670E02 RATIO OF WT/BUOYANCY= 0.512E00 MODULATION DEPTH= 0.306E00
WAVE HT= 0.100E02 WAVE PERIOD= 0.150E02 WATER DEPTH= 0.270E03 WAVE STEEPNESS= 0.285E-01
MP= 0.100E05 D2= 0.280E02 L2= 0.350E02 DTOP= 0.30E02 D1= 0.10E02 D3= 0.60E01 NO ELEMS= 0.20E01
ARE VERTICAL FORCES INCLUDED ++NO++ DYNAMIC MAG FACTOR= 0.000E00 LINEAR MAG FACTOR= 0.422E-01
INERTIA COEFF(CM) = 0.190E01 DRAG COEFF(CD) = 0.600E00 RATIO OF NAT PER/WAVE PER= 0.497E01
NO OF CYCLES TO START= 0.100E01 RATIO KB/KG= 0.975E00 RATIO OF MOMS= 0.145E01 ++LINEAR WAVE GROWTH++
+++LINEAR WAVE THEORY USED+++ WIND DIRN.= 0.00E00 WIND SPEED= C 0.00E00
CURRENT VEL&DIRN= 0.10E-01 0.00E00
+++BORGMAN TRANSFORM+++ WAVE PERIODS= 0.123E02 SECS AND 0.150E02 SECS

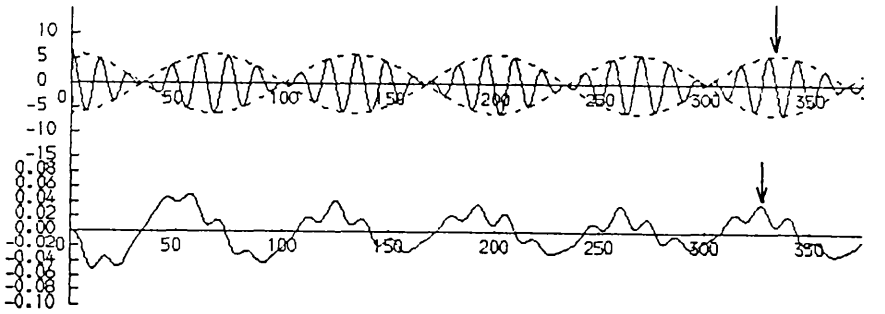

FIG 5.42

trend for resonant responses to increase fairly rapidly for relatively small increases in the wave periods, the combined maximum wave height of 10 metres remaining the same.

Figure 5.42 shows the response for waves each of a height 12 metres, ie 20% higher than for fig. 5.40, the response is increased by almost 35%. It is also observed that the wave frequency oscillatory response is greatly attenuated in the region of small group amplitude and this is be expected.

6. CONCLUDING REMARKS

Dynamic instabilities have been observed both experimentally and analytically and show reasonable quantitative agreement. Qualitatively, the agreement is very good. The transient instability is very pronounced for the increased weight to buoyancy ratio in the experimental observation and this occurs in spite of the higher damping which is probably present at the model scale and which may not be present at the full scale.

The analytical observations would suggest that heave forces, instantaneous position of the structure in calculating the wave forces, viscous drag damping and starting conditions in respect of wave growth for the time simulation analysis are all important parameters.

While the omission of heave forces in the analysis may result in an under prediction of the transient instability the nature and rate of the wave growth clearly has an important part to play in the motion response of the structure.

The inclusion of viscous damping clearly has a moderating effect in limiting the growth of the unstable motion. Potential damping has not been included in this analysis and certain structures subject to the shorter waves may generate some damping of this form. Real structures operating at post critical Reynolds numbers may be unable to generate the viscous damping necessary to moderate an instability and may, therefore, be vulnerable to dynamic instabilities.

Non linear waves suppress the onset of the instabilities and it is noted that this result is in accord with certain results obtained in the Chapter 4, where it was noted that the non linear wave suppressed a transient oscillation which was predicted using linear wave theory. It was also noted that the non linear wave predicted a transient oscillation when the value of C_D was reduced to 0.6. This suggests that there is more viscous damping available in the non linear wave and is also an indication of the importance of damping in limiting the onset of instabilities.

One possible way of generating viscous damping would be to fix 'damping' fins to the lower column. These need not be continuous along the whole length and would be sufficiently distanced from the surface not to attract very large wave exciting force. A disadvantage may be the consequential increase in static pitch in steady currents. However, current velocity profiles are seldom uniform with depth and in general the higher velocities will be associated with the near surface regions.

The experimental results confirm that a reduction in the ratio of the weight to buoyancy reduces the magnitude of the

transient and this is to be expected. However, the analytical results did not predict any reduction in the transient for reduced ratios of weight to buoyancy.

The design of compliant structures should make allowance for the possibility of dynamic instability. Production platforms in 250 metres of water and greater are likely to have natural periods in pitch of the order of 70-80 seconds. These are unlikely to suffer Mathieu instabilities from first order wave excitation.

However, there may be periods of time during the installation when the structure will have substantially greater fundamental pitch frequencies than the final operational frequency. In such situations, Mathieu instabilities may be generated by first order wave excitation. Therefore, installation procedures must make allowance in this respect.

It has been demonstrated that wave groups which are generated by two separate wave trains with slightly different frequencies can give cause for concern. The analysis predicted large increases in the resonant harmonic response when the period of the combined wave group coincided with the natural period in pitch of the structure. The precise nature of real wave groups may differ to those generated in the analysis. Nevertheless, the ability of the analytical method to predict instabilities is demonstrated.

Lighter structures in shallow water are likely to have natural periods of the order of 30-40 seconds. In such circumstances, the possibility of first order wave excitation Mathieu instability must be fully assessed.

Finally, all possible sources of excitation at the critical frequencies must be appraised and apart from the parameters investigated already, special attention should be paid to the possbility of encountering wave group frequencies in random seas, wind gusting frequencies and long swell frequencies.

CHAPTER 6

FREE VIBRATION AND FINITE ELEMENT FORMULATION

1. INTRODUCTION

The slenderness of articulated columns may render them vulnerable to dynamic excitation and it is pertinent, therefore, to perform a rigorous vibration analysis in order to assess the importance of vibration, its implications, and the constraints which may have to be imposed on any particular design concept.

Vibration frequencies will have some proportionality with $\pi^2 n^2 \sqrt{EI/m\ell^4}$ where n is the vibration mode. The first three modes are illustrated in fig. 6.1. The first is the fundamental pitch mode and a column is unlikely to experience wave excitation at that frequency. The second and third modes will have frequencies much higher than the fundamental mode and may well fall within the range of wave excitation. The second and third modes are the first and second flexural response modes respectively.

The buoyancy chamber section will have a much greater flexural rigidity than the upper and lower columns and will have some effect on the mode shapes, in that the deflected shape over the length of the buoyancy chamber will be much less pronounced than that for the lower column. However, the mode shapes are unlikely to differ greatly qualitatively from those shown in fig. 6.1.

An understanding of the dynamic response in these modes is

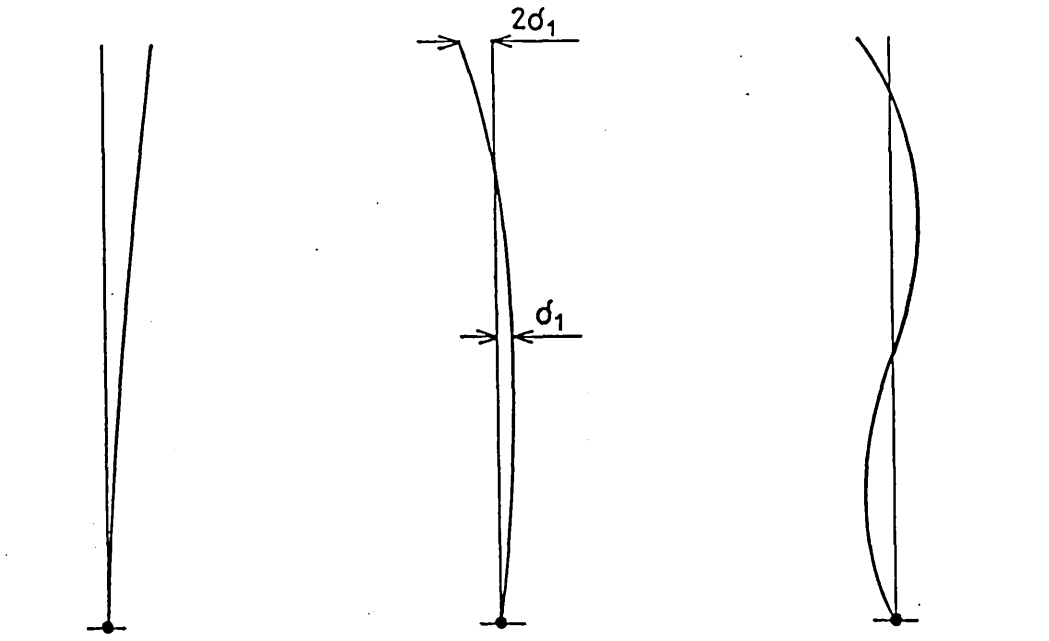

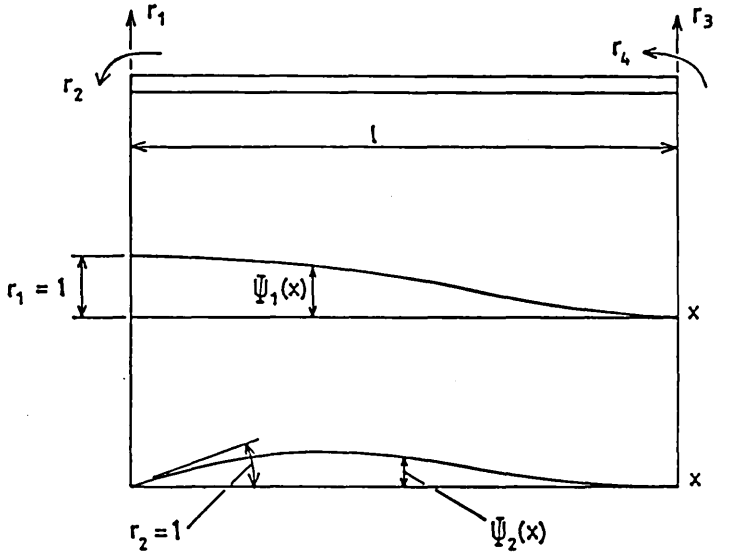

DEFLECTION POLYNOMIALS

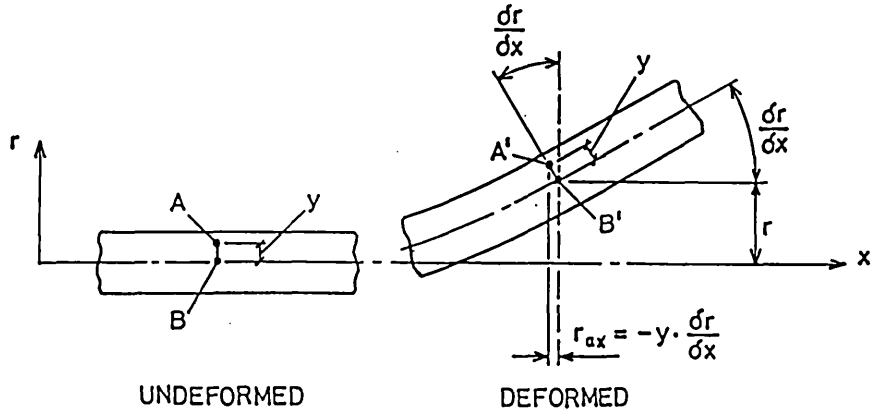

DEFORMATION OF ELEMENT

FIG 6.1

necessary not only in assessing primary structural requirements but equally the operational requirements of ancillary production and drilling equipment which will be contained in the lower column.

The structural analysis necessary in order to estimate the vibration frequencies has been carried out by means of the finite element method and the method is described and presented in this chapter.

The analytical procedure thus developed has been applied to typical structures and a number of parameter studies have been completed to determine relationships with vibration frequencies. These include the effects of water depth, plating thickness of lower column, deck mass relocation and configuration, riser mass, axial loads, buoyancy chamber dimensions and the effects of ballast placed at the bottom of the lower column. Although not an exhaustive parameter study, it is, nevertheless, comprehensive in examining those parameters thought likely to have the greatest influence on the vibration characteristics of the structures and hence on the design appraisal of any particular concept.

The practical implications of the existence of the second mode vibration are assessed in terms of structural requirements and water depth limitations. Typical nett structural weights as a function of water depth and deck mass are also presented and this gives a preliminary guide to the structural steelwork weight requirements likely for a particular application.

Finally, a column with a full fixity encastre connection at the base is analysed in terms of first, second and third resonant

flexural modes. Operational water depth ranges are suggested to avoid resonant excitation of first and second flexural modes.

2. DETERMINATION OF FREQUENCY MODES

2.1 Undamped Free Vibration

The equations of motion for free undamped vibration can be obtained by omitting the damping and forcing terms and is written thus:-

$$[M]\ddot{x} + [K]x = 0 \tag{6.1}$$

where $[M]$ and $[K]$ are mass and stiffness matrices for beam elements assembled as described in section 3.

By analogy, with the behaviour of SDOF freedoms it is assumed that the motion is simple harmonic and can be expressed for a multi degree of freedom system (MDOF system) as:-

$$x(t) = \{q\}\exp(j\omega t) \tag{6.2}$$

where $\{q\}$ is a vector of the relative amplitudes of displacement. Substituting equation (6.2) into equation (6.1) gives:-

$$(K - \omega^2 M)\{q\} = 0 \tag{6.3}$$

In order that finite amplitude oscillations are possible and to obtain a non-trivial solution to equation (6.3), the determinant, $\|K - \omega^2 M\|$ must equal zero, ie,

$$\|K - \omega^2 M\| = 0 \tag{6.4}$$

Equation (6.4) is called the frequency equation. The solution of the determinant will give an algebraic equation for the Nth degree

in the frequency parameter ω^2 for a system with N degrees of freedom. The N roots of the equation represent the frequencies of the N possible vibration modes of the system.

For real, symmetric, positive, definite stiffness and mass matrices K and M which pertain to stable structural systems all roots of the frequency equation are real and positive.

The solution of the frequency equation is discussed in more detail in section 4.3 of this chapter.

3. FINITE ELEMENT IDEALISATION AND STRUCTURE ASSEMBLAGE

The finite element method (66,67) is an established and accredited method for idealising structural assemblages in discrete elements.

The extent of the usage in this study has been confined to beam column elements and this type of element idealisation is considered satisfactory in the analysis of tubular truss structures and for structures with cylindrical (circular or other) member sections such as those anticipated for use with articulated columns. More sophisticated structural idealisations are available for the analysis of shell and plate structures and are essentially derived in terms of an appropriate polynomial which is used to express deflected shapes and boundary conditions.

Essentially, the finite element method implies that the structure can be idealised by a system of discrete elements which are connected by a finite number of nodal points. The properties of the

complete structure are then found from the evaluation of the individual element properties and then combining these as necessary to reflect the complete structural behaviour. This idealisation reduces the problem of modelling a total structural stiffness to that of evaluating the stiffness of individual elements.

Stiffness matrices may be formed from the classical beam slope deflection theory or by energy methods. However, in dynamic problems a mass matrix will be required and this should be formulated in an energy consistent manner. Accordingly, for completeness the energy consistent method for the formulation of stiffness and mass matrices is outlined in the following sections.

3.1 Shape Functions and Stiffness Matrices

Consider the beam element shown in fig. 6.1. If only tranverse deflections are assumed then the element will have two degrees of freedom at each node, ie one translational and one rotational.

The deflected shapes which are obtained for a unit displacement of each type ie, translational and rotational, are also shown. These deflected shapes are generally assumed to be those developed in a uniform beam given these displacements and are cubic hermitian polynomials which can be expressed as:-

$$\psi_1(x) = 1 - 3(x/\ell)^2 + 2(x/\ell)^3 \tag{6.5}$$

$$\psi_2(x) = x(1 - x/\ell)^2 \tag{6.6}$$

the shape functions for unit displacements at the right end are:-

$$\psi_3(x) = 3(x/\ell)^2 - 2(x/\ell)^3 \tag{6.7}$$

$$\psi_4(x) = x^2/\ell(x/\ell - 1)^3 \qquad (6.8)$$

Using these interpolation functions the deflected shape of the element can then be expressed in terms of its nodal displacements.

$$r^*(x) = \psi_1(x)r_1 + \psi_2(x)r_2 + \psi_3(x)r_3 + \psi_4(x)r_4 \qquad (6.9)$$

where the degrees of freedom are shown in fig. 6.1, or generally:-

$$r^* = [A]\{r_d\} \qquad (6.10)$$

Now strain ε is the spatial rate of change of displacement and we can relate the internal strains ε^* at a point to the nodal displacements thus:-

$$\varepsilon^* = [B]\{r_d\} \qquad (6.11)$$

where [B] is formed from the appropriate differentiation of [A] in equation (6.10).

Equating the external work done by external forces W_E to internal work done on internal forces ie, the strain energy U_S.

$$\text{Now } \Delta W_E = \int \delta r^{*T}.Z.d(\text{Vol}) + \int \delta r^{*T}.S.d(\text{area}) + \delta r^T F \qquad (6.12)$$

where (Z) the body force vector.

(S) the surface force vector.

(F) the nodal force vector and $\delta r^* = A\,\delta r$

$$\text{Now } \Delta U_S = \int \delta \varepsilon^{*T}.\sigma.d(\text{Vol}) \qquad (6.13)$$

where σ is the internal stress vector.

Now $\sigma = [D]\{\varepsilon\}$ where [D] is formed from terms containing Youngs modulus and Poissons ratio for the material used.

By the principle of minimum potential energy:-

$$U_S - W_E = 0 \tag{6.14}$$

So that:-

$$\int \delta\varepsilon^T . \sigma . d(Vol) - \int \delta r^{*T} . Z . d(Vol) - \int \delta r^{*T} . S . d(area) - \delta r^{*T} F = 0 \tag{6.15}$$

Substituting for $\delta\varepsilon$, δr^*, it can be shown that:-

$$\int B^T . D . B . d(Vol)\ r_d = \{F\} + \int A^T . Z . d(Vol) + \int A^T . S . d(area) \tag{6.16}$$

which can be written symbolically as:-

$$[K]\{r_d\} = \{F\} + \{F_{eq}\} \tag{6.17}$$

where $[K] = \iiint B^T . D . B . d(Vol)$ (6.18)

which is the stiffness matrix for the element. $\{F_{eq}\}$ are the concentrated nodal forces equivalent to the distributed forces on the element based on these doing the same work as the distributed loading under virtual displacements.

By way of illustration of the process involved, the first term of the stiffness matrix for a beam element is derived as follows.

Consider the deformation of the element according to simple beam theory and as shown in fig. 6.1. Assuming that plane sections remain plane then the axial displacement r_{ax} due to the transverse displacement y is given by $r_{ax} = - y.\delta r/\delta x$ where y is the distance from the neutral axis.

The axial strain $\varepsilon_x = \delta r_{ax}/\delta x = - y.\delta^2 r^*/\delta x^2$

The term $\delta^2 r^*/\delta x^2$ is the second derivative of the shape

functions given by equations (6.5) to (6.8).

Hence, $[B] = -\frac{y}{\ell^3}(12x - 6\ell), \ell(6x - 4\ell), -(12x - 6\ell), \ell(6x - 2\ell))$

Recalling equation (6.18):-

$$[K] = \iiint B^T.D.B.d(Vol) \tag{6.19}$$

or writing $[K] = E\int_0^{\ell} dx \iint_{Area} B^T.B.d(Area)$ (6.19a)

since D = scalar E

Now, for the first element $[K] = E\int_0^{\ell} dx \iint_{Area} -\left[\frac{y}{\ell^3}(12x - 6\ell)\right]^2 d(Area)$

Where $\iint y^2 dA$ = Moment of Inertia (I)

Then $[K] = EI \int_0^{\ell} \frac{1}{\ell^6}(12x - 6\ell)^2.dx$ (6.19b)

Integrating and substituting for ℓ gives the first term as $12EI/\ell^3$ and so on for the remaining terms.

The complete integration of equation (6.18) yields the stiffness matrix for a beam element, ie:-

$$[K] = \frac{EI}{\ell^3}\begin{bmatrix} 12 & 6\ell & -12 & 6\ell \\ & 4\ell^2 & -6\ell & 2\ell^2 \\ \text{Symm} & & 12 & -6\ell \\ & & & 4\ell^2 \end{bmatrix} \tag{6.20}$$

Thus, we have the means to develop stiffness matrices depending on the degree of sophistication required and the physical form of the elements and this is reflected in the choice of the shape functions.

The literature contains comprehensive information in this respect (68). If axial deformations were to be included, these would be uncoupled from the flexural deformations and would result in an additional $A\ell^2/I$ term in the stiffness matrix at locations pertaining to the axial translational degrees of freedom. The resulting stiffness matrix would take the following form:-

$$[K] = \frac{EI}{\ell^3}\begin{bmatrix} A\ell^2/I & 0 & 0 & -A\ell^2/I & 0 & 0 \\ & 12 & 6\ell & 0 & -12 & 6\ell \\ \text{SYMM} & & 4\ell^2 & -0 & -6\ell & 2\ell^2 \\ & & & A\ell^2/I & 0 & 0 \\ & & & & 12 & 6\ell \\ & & & & & 4\ell^2 \end{bmatrix} \qquad (6.21)$$

However, this form requires extra computation and some early analysis which compared the results obtained by using the forms of (6.21) and (6.20) showed that the translation and rotational deformations obtained were identical. This is as expected in consideration of the uncoupled degrees of freedom. The extra computation time required for the form of (6.21) was not justified and, consequently, the form of (6.20) has been adopted and is adequate. Furthermore, it can be augmented in consideration of axial forces by an additional geometric stiffness matrix which is discussed later.

The stiffness matrix is symmetric about the leading diagonal and this is attributed to Betti's law which states that the work done by one set of loads on the deflection due to a second set of loads is equal to the work of the second set of loads acting on the deflections due to the first set of loads. Compliance determines that $K = K^T$, ie symmetry.

3.2 Mass Matrices

3.2.1 Lumped Mass Matrix

The simplest procedure for defining the mass properties of an assemblage of finite elements is to assume that the mass contribution from each element is distributed to the corresponding nodal connection points relating to the translational degrees of freedom only. Figure 6.2 illustrates the way in which this is achieved.

This assumes that only translational degrees of freedom are relevant and results in a mass matrix with only diagonal terms - the off diagonal terms being zero.

The form of the lumped mass matrix is then:-

$$\begin{bmatrix} M_1 & & & 0 \\ & M_2 & & \\ & & M_3 & \\ & & & \ddots \\ 0 & & & M_n \end{bmatrix}$$

for a system with n translational degrees of freedom.

If rotational degrees of freedom are to be included then the matrix diagonal element corresponding to that degree of freedom will be zero. This condition must be satisfied since it is assumed that the mass is 'lumped' at points which have no rotational inertia.

The lumped mass matrix, although attractive in computational terms, does present problems when rotational degrees of freedom are included and when the stiffness matrix has been assembled in an energy consistent manner. That is to say, the stiffness matrix would require

the rotational degrees of freedom to be deleted in order that the diagonal mass matrix can be used in formulating the equation of motion.

The unwanted rotational degrees of freedom in the stiffness matrix can be eliminated by a process known as 'static condensation'. A procedure for this technique is described in detail in Reference (49). As an alternative to static condensation it may be possible to apply some form of mass couple to each nodal point so that rotational degrees of freedom can be accounted for. Neither approach has been used in this study. Instead the consistent energy approach has been used in the formulation of stiffness and mass matrices and load vectors.

3.2.2 Consistent Mass Matrix

The mass matrix may also be derived in a manner similar to that which was used in the derivation of the stiffness matrix. This results in the consistent mass matrix of the following form:-

$$M = \frac{\rho A_s \ell}{420} \begin{bmatrix} 156 & 22\ell & 54 & -13\ell \\ & 4\ell^2 & 13\ell & -3\ell^2 \\ \text{SYMM} & & 156 & -22\ell \\ & & & 4\ell^2 \end{bmatrix} \qquad (6.22)$$

The off diagonal terms will require more computational effort. However, this is considered justified in the dynamic analysis of compliant structures. All structural and hydrodynamic masses can be allowed for in assembling the mass matrix and this is described in greater detail in section 4.2.

3.3 Geometric Stiffness Matrice

3.3.1 Linear Approximation

If we assume that axial deformations are uncoupled from flexural and translational degrees of freedom then the simple linear shape functions will define the axial geometric stiffness and the $A\ell^2/I$ term in the 6 x 6 matrix of 6.21 will describe axial forces and displacements.

3.3.2 Consistent Geometric Stiffness

A higher order approximation to the geometric stiffness can be obtained by assuming that coupling exists but that the axial deformations are sufficiently small and can be neglected. It is assumed that the axial load P is constant over the length of the element.

This results in an additional 'geometric stiffness matrix' K_G, ie

$$K_G = \pm P \begin{bmatrix} 6/5\ell & 1/10 & -6/5\ell & 1/10 \\ & 2\ell/15 & -1/10 & -\ell/30 \\ \text{SYMM} & & 6/5\ell & -1/10 \\ & & & 2\ell/15 \end{bmatrix} \qquad (6.23)$$

where P = axial force

The total stiffness matrix will then become equal to:-

$$K = K + K_G \qquad (6.24)$$

Adequate description of axial loads must be allowed for and the additional geometric stiffness term will facilitate this requirement.

4. COMPUTER IMPLEMENTATION

4.1 Assembling Stiffness and Mass Matrices

The total structural assemblage is accomplished by the assembly of the stiffness matrices pertaining to each individual element. Nodal displacements will then be compatible at the common nodal points and net external loads will be equivalent to the algebraic sum of the resolved components of each elemental nodal force vector. The description of the development of the equivalent nodal force vectors is relevant to Chapter 7 and is described there.

By way of illustration of the assembly procedure fig. 6.2 shows how the elemental stiffnesses are added into the total assemblage. It is necessary to refer elemental matrices to a 'global co-ordinate system' for the total structure. This is done by means of a transformation matrix $[\gamma]$ so that:-

$$\{r\}_{\ell} = [\gamma]\{r\}_{g} \tag{6.25}$$

where $[\gamma] = \begin{bmatrix} \gamma_1 & 0 \\ 0 & \gamma_1 \end{bmatrix}$ (6.26)

$$[\gamma_1] = \begin{bmatrix} \cos\alpha & \sin\alpha & 0 \\ 0 & 0 & 1 \end{bmatrix}$$

so that

$$[\gamma] = \begin{bmatrix} \cos\alpha & \sin\alpha & 0 & 0 & 0 & 0 \\ 0 & 0 & 1 & 0 & 0 & 0 \\ 0 & 0 & 0 & \cos\alpha & \sin\alpha & 0 \\ 0 & 0 & 0 & 0 & 0 & 1 \end{bmatrix} \tag{6.27}$$

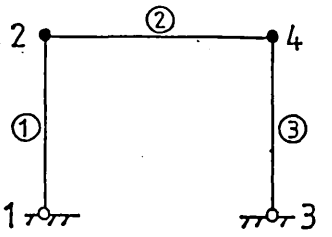

STIFFNESS FOR ELEMENT ①, $K^{①} = \left[\begin{array}{c|c} K_{11}^{①} & K_{12}^{①} \\ \hline K_{21}^{①} & K_{22}^{①} \end{array}\right]$

$K^{②} = \left[\begin{array}{c|c} K_{22}^{②} & K_{24}^{②} \\ \hline K_{42}^{②} & K_{44}^{②} \end{array}\right]$

ELEMENT STIFFNESS MATRICES

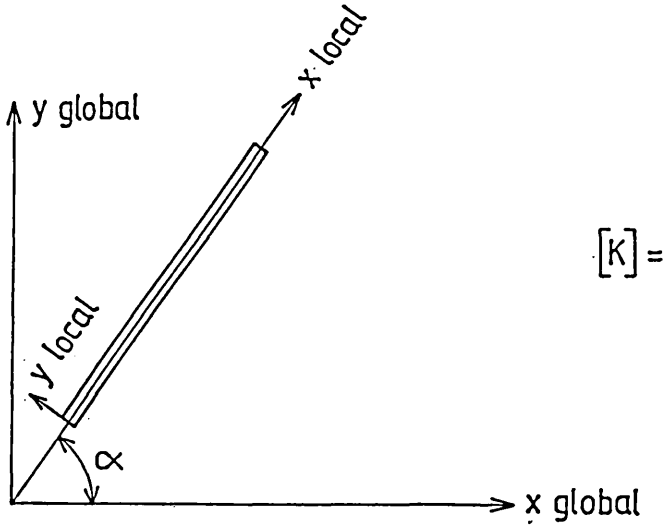

LOCAL AND GLOBAL COORDINATES

$$[K] = \left[\begin{array}{c|c|c|c} K_{11}^{①} & K_{12}^{①} & 0 & 0 \\ \hline K_{21}^{①} & K_{22}^{①}+K_{22}^{②} & 0 & K_{24}^{②} \\ \hline 0 & 0 & K_{33}^{③} & K_{34}^{③} \\ \hline 0 & K_{42}^{②} & K_{43}^{③} & K_{44}^{②}+K_{44}^{③} \end{array}\right]$$

ASSEMBLED MATRICE

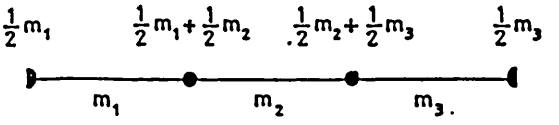

LUMPED MASS NOTATION FIG 6.2

For a virtual displacement:-

$$\{\delta r\}_{\ell} = [\gamma]\{\delta r\}_{g} \tag{6.28}$$

but the work done must be equal so that

$$\delta r_{\ell}^{T}.F_{\ell} = \delta r_{g}^{T}.F_{g} \tag{6.29}$$

It follows that $F_{g} = [\gamma]^{T}.F_{\ell}$ (6.30)

Now $F_{g} = [K]_{g}\, r_{g}$ (6.31)

and $F_{\ell} = [K]_{\ell}\, r \quad = [\gamma^{T}]^{-1}.F_{g}$ (6.32)

so that $F_{g} = [\gamma]^{T}[K]_{\ell}\ \{r\}_{\ell}$

$$= [\gamma]^{T}[K]_{\ell} \quad \{r\}_{\ell} \tag{6.33}$$

The global element stiffness matrix is:-

$$\underset{6x6}{[K]_{g}} = \underset{6x4}{[\gamma]^{T}}\ \underset{4x4}{[K]_{\ell}}\ \underset{4x6}{[\gamma]} \tag{6.34}$$

Equivalent nodal forces due to distributed loading must also be transformed to a common global datum, ie

$$\{F_{eq}\} = [\gamma]^{T}\,[A]^{T}.S.d(Vol) \tag{6.35}$$

4.2 Structural Configuration

The form of structures investigated has been limited to those comprising circular cylindrical sections. This form of construction has considerable advantages over truss type structures from the fabrication and inspection points of view. However, it is likely that there will be limitations in respect of the stiffness properties and an assessment of these limitations has been attempted.

Figure 6.3 shows the general arrangement of the typical

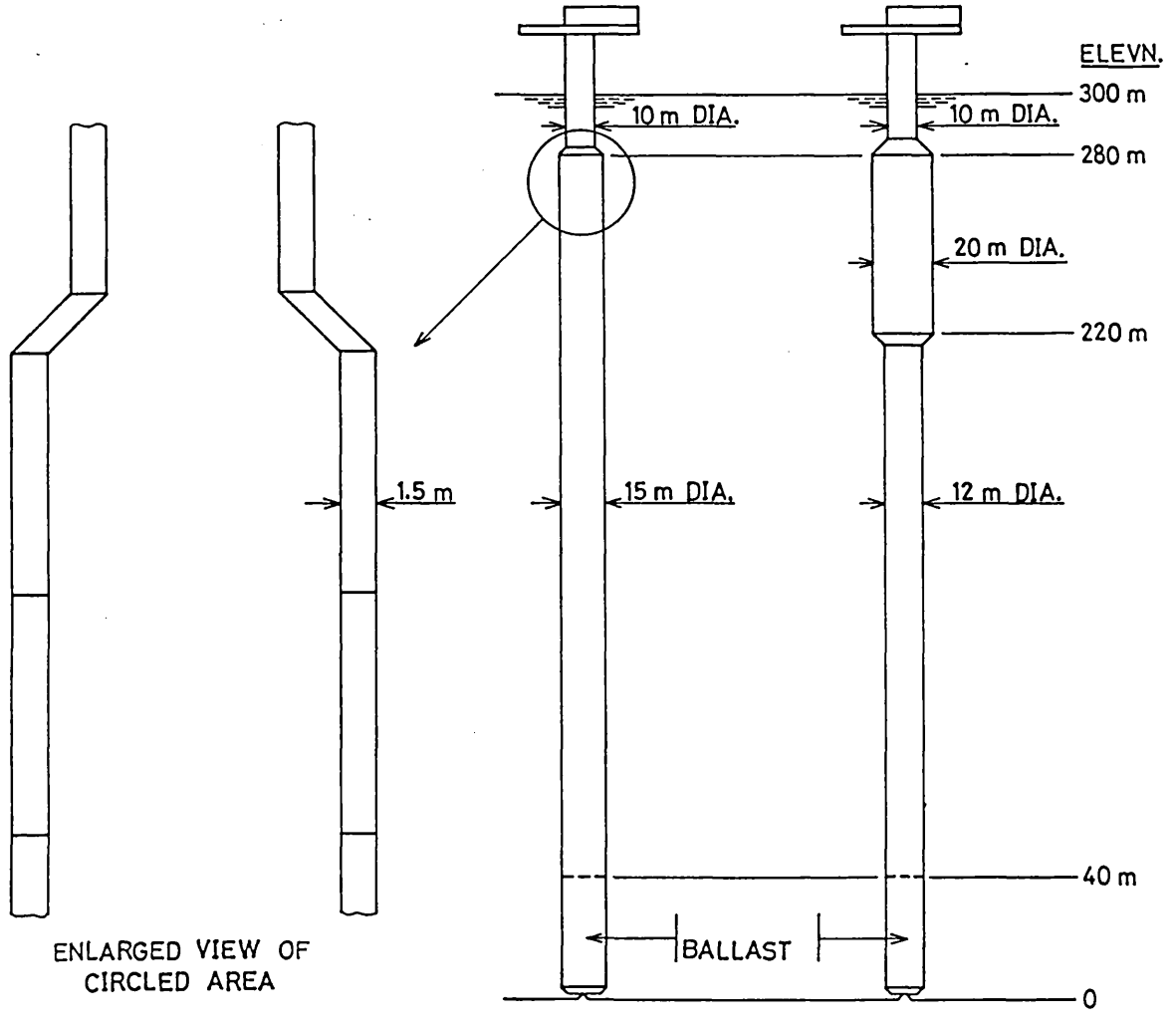

FIG 6.3

POSSIBLE ARRANGEMENTS FOR ARTICULATED COLUMNS

configuration of the structures investigated. The amount of ballast at the lower end of the lower column is calculated on the basis that there will be an uplift or tensile force at the articulation of about 10% of the net buoyant force. The diameter of the ballast may be specified at any dimension but for convenience it has been assumed to be the same as the diameter of the lower column. The stiffness of elements relevant to the ballast is calculated on the same basis as for other structural elements and it may be prudent in a design to allow for an increase in stiffness where ballast is located.

Twenty finite beam column elements have been used and this is considered to provide a realistic idealisation of the structure in finite elements.

The consistent mass matrix allows for the inclusion of all relevant structural masses for elements and any additional masses such as those for risers and other ancillary equipment located inside the lower column. Also included in the consistent mass matrix is the added virtual mass component for each element.

The consistent mass matrix, once assembled for the whole structure, will also allow for the inclusion of any additional 'lumped' masses which are simply added in to the appropriate location within the matrix. The deck mass can be allowed for in this manner and the way in which this is achieved computationally is further investigated in section 5.3.

Inclusion of a flooded lower column is allowed for as an option in the assembly of the mass matrix.

4.3 Solution of the Eigenvalue Problem

The analytical solution of equation (6.4) is cumbersome and not readily amenable to computerisation. One way to solve equation (6.4) is to reduce it to a standard eigenvalue problem of the form

$$(A - \lambda I)q = 0 \tag{6.36}$$

This can be done by multiplying equation (6.3) by M^{-1}

So that:-

$$(M^{-1}K - \lambda I)q = 0 \tag{6.37}$$

where $[M]^{-1}[K] = [A]$ and $[I]$ = identity matrix = $[M]^{-1}[M]$

and $\lambda = \omega^2$

Alternatively, multiplying equation (6.4) by $[K]^{-1}$

then $[A] = [K]^{-1}[M]$

and $\lambda = 1/\omega^2$ = Eigenvalue; q = Eigenvector

There are a number of ways of solving equation (6.37) on an iterative basis, ie Givens, Householder and Jacobi methods (67).

The method utilised in this study was the Householder method which is available as a standard NAG (62) routine F02AEF, and the use of this in the solution of the eigenvalue problem is described in the next section.

4.4 Computer Programs

A computer program comprising a number of subroutines was developed to solve the eigenvalue problem and the development and functions of the various subroutines are as follows. A flowchart for the program is shown in fig. 6.3A.

Subroutine INCON - This routine reads the input data in terms of the number of elements being used and the numbering system used for nodal connections. Global nodal co-ordinates are calculated and read into arrays and connectivity arrays are formed. This determines common nodal connections for all of the elements. INCON calls subroutines VAPROP and BOUND.

Subroutine VAPROP - This routine computes the properties for each element and reads these into arrays. The properties computed are the cross sectional area, the second moment of area, the displacement volume and the diameter. VAPROP requires nodal co-ordinates and connectivities as input together with data describing the geometry. The data computed by VAPROP is stored in array PROP and is later used in the assembly of the stiffness and mass matrices.

Subroutine BOUND - Applies the boundary conditions in terms of translation and rotation at the articulation. The full size N x N arrays are used in the solution of the eigenvalue problem and subroutine BOUND deletes degrees of freedom which are not relevant to the solution. There are two options ie, restrained or free for each boundary degree of freedom.

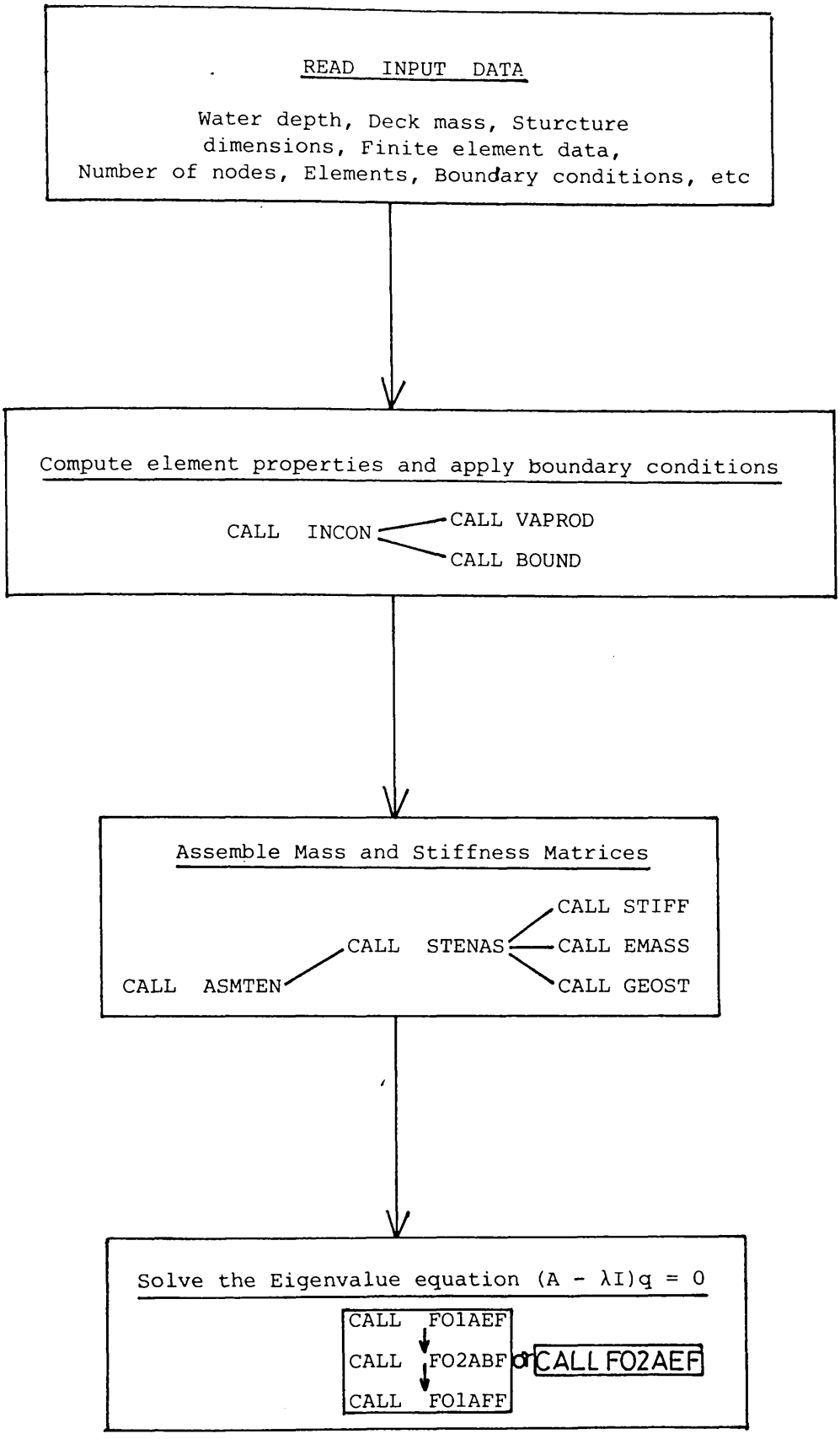

Fig.6.3A Flow Diagram for Solution of Eignevalue Equation

Subroutine AXLOAD - This routine computes the distribution of axial load at each nodal point and takes into account the hydrostatic pressures acting on exposed horizontal plan areas, such as those at cross-sectional changes, ie at the top and bottom of the buoyancy chamber etc, in the calculation. All relevant structural masses are included in the calculation. Input data required is connectivity arrays and property arrays PROP.

Subroutine ASTEN - This routine assembles the mass and stiffness arrays for each element into the total arrays for the whole structure. ASTEN loops on each element in turn and calls STENAS which adds successive array elements into the total global arrays.

Subroutine STIFF - Computes each elemental stiffness matrice in accordance with the form of (6.20) and requires array PROP as input.

Subroutine EMASS - Computes the consistent mass matrice for each element in accordance with the form of (6.22) and requires array PROP as input.

Subroutine GEOST - Computes the consistent geometric stiffness matrice for each element in accordance with the form of (6.23).

Subroutine F02AEF reduces the equations of motion, as assembled into stiffness and mass matrices in the form of equation (6.37), to the standard eigenvalue form of $Ax = \lambda Ix$ and solves for all of the eigenvalues and their corresponding eigenvectors.

A detailed description of the use of the program is outlined in Appendix 6.1 and this also contains the results of a program written by a third party which was used as a basis for comparison of results and confirmation that the routines were operating satisfactorily.

5. ANALYTICAL RESULTS

The structural configuration investigated in Chapters 4 and 5 in rigid body motion form comprised a very slender lower column. Some initial vibration analysis suggested second mode vibration periods of the order of 20 seconds and third mode vibration periods of the order of 5 seconds. These, obviously, would produce unacceptable deformations and stresses in respect of the wave spectrum the structure might be expected to encounter.

Accordingly, the structures investigated further all have a lower column of minimum diameter 9 metres and, from the vibration point of view, this is the minimum value which can be tolerated for structures of this type and size in water depths exceeding about 200 metres. Typical general arrangements are shown in fig. 6.3.

An alternative to the concept of providing a lower member in possession of flexural stiffness is to provide a lower member without flexural stiffness. Tethers or chains are the obvious choice and these eliminate the flexural response problem. This approach is tending towards the tension leg platform concept with an accompanying range of other engineering considerations, not least of which would be the question of resonant heave and pitch responses which will tend to have natural periods in approximate proportionality with water depth.

The computer program described was adapted so that the various parameters believed to be most relevant could be examined and their relationship with vibration periods established. All of the computations were made on the main frame ICL 2988 computer at the University of Glasgow.

5.1 Variation in Vibration Mode Frequency with Thickness of Lower Column

The slenderness of the lower column must be thoroughly investigated and the variation in vibration mode periods as a function of diameter and equivalent thickness is thought meaningful in this context. Accordingly the computed results are presented.

Figure 6.5 shows the variation in mode period with equivalent thickness of the lower column for a structure in 270 metres of water having a deck mass of 150,000 KN and other data as shown. In this plot the lower column has been assumed to be flooded.

It is evident that very considerable reductions in the second mode vibration periods can be achieved by increasing the equivalent thickness values up to approximately 60-70 mm. Thereafter, the reduction in period begins to flatten out with very little improvement for increasing thickness. The problem of achieving acceptably high second and third mode frequencies is apparent.

There is a great deal of energy in the North Sea at wave periods of the order of 6-10 seconds so that, in reality, we must be aiming to achieve an upper limit to a second mode period of the order of, say, 5 to 6 seconds and less, depending on stress levels reached.

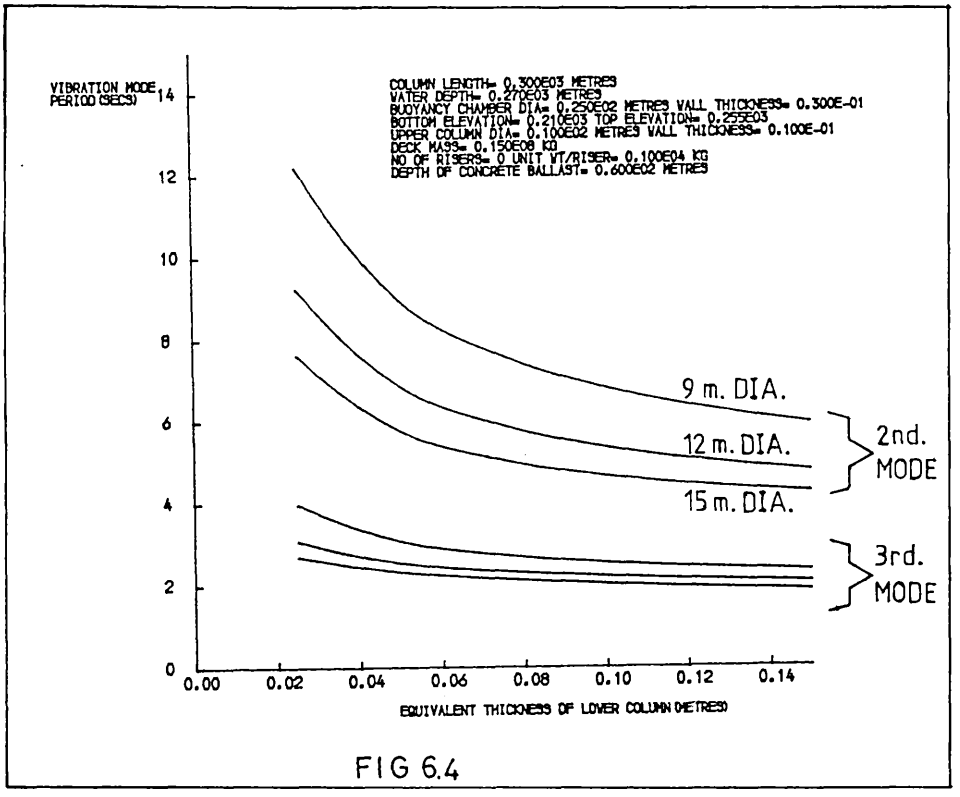
VIBRATION MODE PERIOD (SECS)
COLUMN LENGTH= 0.300E03 METRES
WATER DEPTH= 0.270E03 METRES
BUOYANCY CHAMBER DIA= 0.250E02 METRES WALL THICKNESS= 0.300E-01
BOTTOM ELEVATION= 0.210E03 TOP ELEVATION= 0.255E03
UPPER COLUMN DIA= 0.100E02 METRES WALL THICKNESS= 0.100E-01
DECK MASS= 0.150E08 KG
NO OF RISERS= 0 UNIT WT/RISER= 0.100E04 KG
DEPTH OF CONCRETE BALLAST= 0.600E02 METRES
9 m. DIA.
12 m. DIA.
15 m. DIA.
2nd. MODE
3rd. MODE
0
2
4
6
8
10
12
14
0.00
0.02
0.04
0.06
0.08
0.10
0.12
0.14
EQUIVALENT THICKNESS OF LOWER COLUMN (METRES)

FIG 6.4

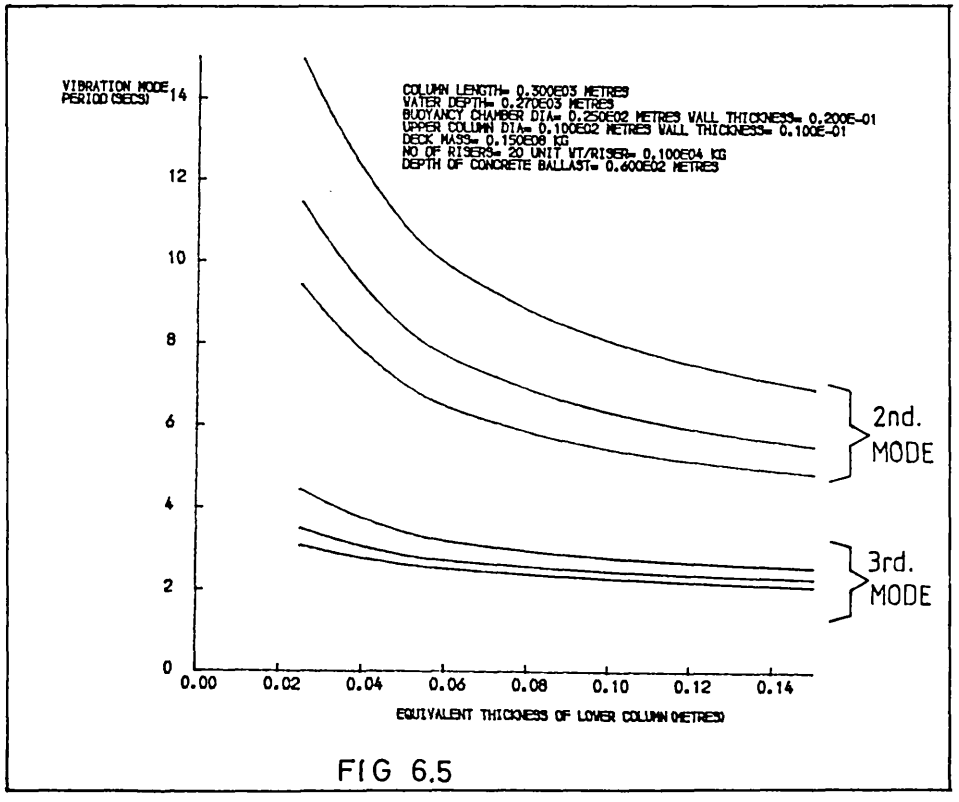
VIBRATION MODE PERIOD (SECS)
COLUMN LENGTH= 0.300E03 METRES
WATER DEPTH= 0.270E03 METRES
BUOYANCY CHAMBER DIA= 0.250E02 METRES WALL THICKNESS= 0.200E-01
UPPER COLUMN DIA= 0.100E02 METRES WALL THICKNESS= 0.100E-01
DECK MASS= 0.150E08 KG
NO OF RISERS= 20 UNIT WT/RISER= 0.100E04 KG
DEPTH OF CONCRETE BALLAST= 0.600E02 METRES
2nd. MODE
3rd. MODE
0
2
4
6
8
10
12
14
0.00
0.02
0.04
0.06
0.08
0.10
0.12
0.14
EQUIVALENT THICKNESS OF LOWER COLUMN (METRES)

FIG 6.5

For a structure with a payload of 150,000KN, in 270 metres of water, a minimum lower column diameter of 12 metres with an equivalent thickness of about 110 mm, is necessary in order to ensure a second mode period of approximately 6 seconds.

An annular type of lower column construction, such as that shown in fig. 6.3, is anticipated and this would probably be augmented by some stringer stiffener arrangement for the length of the column. The steel thickness necessary to satisfy flexural rigidity requirements, in fact, does provide an unexpected bonus in that it is very likely that the lower column can be designed to withstand the water pressures at 300 metres depth.

Accordingly, it is instructive to investigate the improvements expected in reduction of mode periods if it is assumed that the lower column is watertight and dry. Figure 6.4 shows the results for the same structure as in fig. 6.5 but with the lower column dry. The second mode period for a 12 metre diameter lower column, with an equivalent thickness of 80 mm, is 6 seconds which is to be compared with 7 seconds for the flooded structure, ie a reduction of 14%.

The ability to design the lower column to be watertight will also reduce the buoyancy requirements of the buoyancy chamber. The reduction in displaced volume near to the water surface will reduce wave loading and this, in turn, will improve dynamic performance characteristics. The main advantages will be that the lower column will be easily accessible for its entire length. This has very great attractions in respect of riser and ancillary equipment maintenance.

5.2 Variation in Vibration Mode Frequency with Water Depth

Vibration periods will have a proportionality with $\sqrt{m\ell^4/EI}$ so that large increases in vibration periods would be expected as the water depth is increased.

The variation in second and third mode periods as a function of water depth is shown in figs. 6.6 and 6.7 for the lower column flooded and lower column dry, respectively. Here again, the very considerable improvement in the case of the dry column is apparent. Again, the problem of limiting mode periods to an acceptable level in water depths greater than 300 metres is apparent.

5.3 Effects of Deck Mass Relocation and Configuration

Deck masses are likely to play a major role in the vibration characteristics of articulated columns, by virtue of their distance from the articulation. Accordingly, it is necessary to examine the effects of the magnitude of the deck mass on the vibration modes. By association it follows that the physical configuration of the deck mass will also play an important part. This is examined both in the context of relocating a percentage of the deck mass to the buoyancy chamber and in the lateral distribution of the deck mass at the deck level.

In Chapter 4 the advantages of relocating deck masses in the buoyancy chamber was investigated in respect of dynamic response and considered to be of merit. These advantages are further complemented in respect of vibration frequencies, as is apparent from fig. 6.8 which shows the variation in mode period as a function of percentage

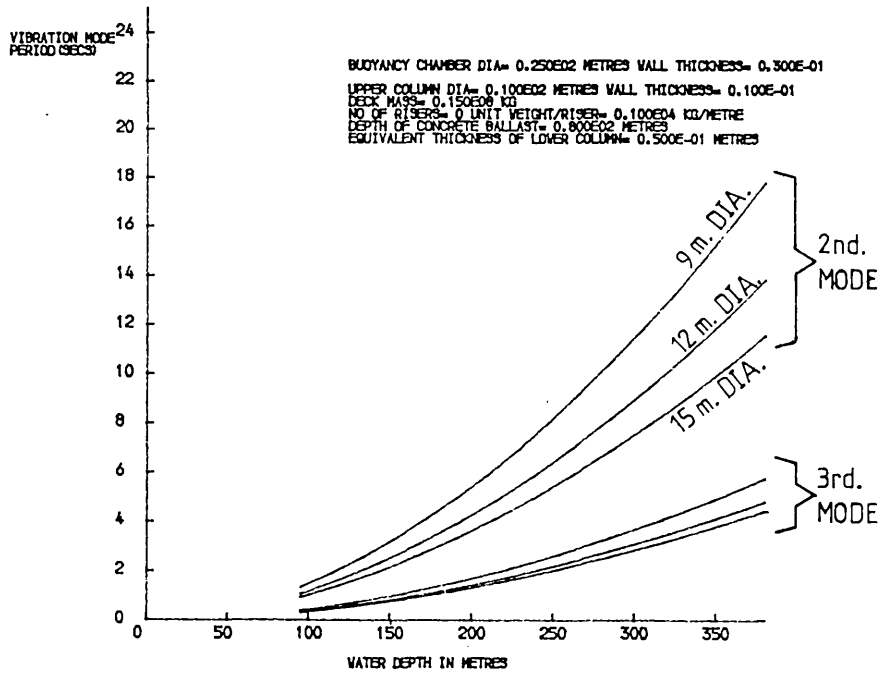
VIBRATION MODE PERIOD (SECS)
BUOYANCY CHAMBER DIA= 0.250E02 METRES WALL THICKNESS= 0.300E-01
UPPER COLUMN DIA= 0.100E02 METRES WALL THICKNESS= 0.100E-01
DECK MASS= 0.150E08 KG
NO OF RISERS= 0 UNIT WEIGHT/RISER= 0.100E04 KG/METRE
DEPTH OF CONCRETE BALLAST= 0.800E02 METRES
EQUIVALENT THICKNESS OF LOWER COLUMN= 0.500E-01 METRES
9 m. DIA.
12 m. DIA.
15 m. DIA.
2nd. MODE
3rd. MODE
WATER DEPTH IN METRES

FIG 6.6

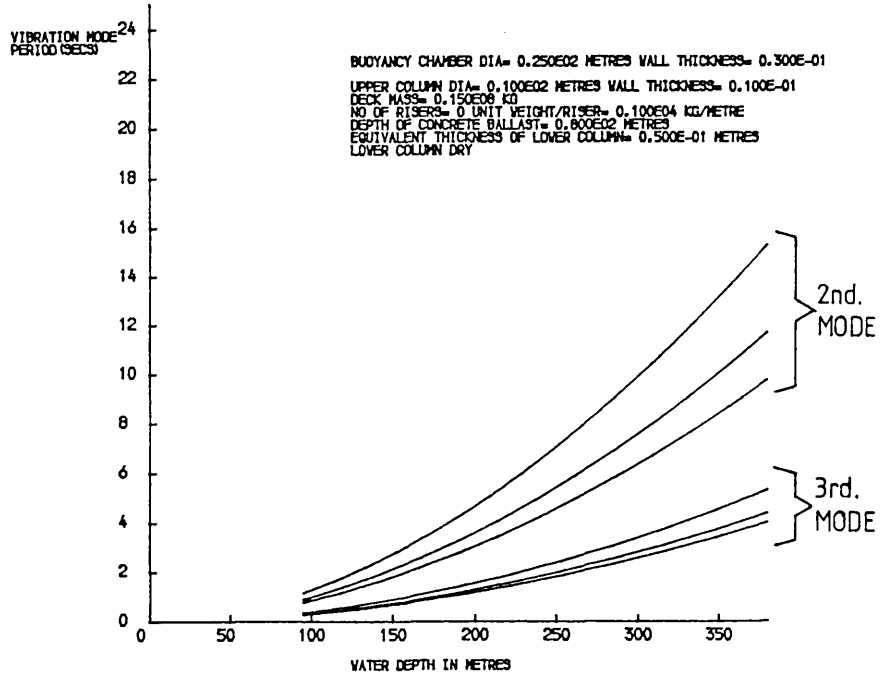
VIBRATION MODE PERIOD (SECS)
BUOYANCY CHAMBER DIA= 0.250E02 METRES WALL THICKNESS= 0.300E-01
UPPER COLUMN DIA= 0.100E02 METRES WALL THICKNESS= 0.100E-01
DECK MASS= 0.150E08 KG
NO OF RISERS= 0 UNIT WEIGHT/RISER= 0.100E04 KG/METRE
DEPTH OF CONCRETE BALLAST= 0.800E02 METRES
EQUIVALENT THICKNESS OF LOWER COLUMN= 0.500E-01 METRES
LOWER COLUMN DRY
2nd. MODE
3rd. MODE
WATER DEPTH IN METRES

FIG 6.7

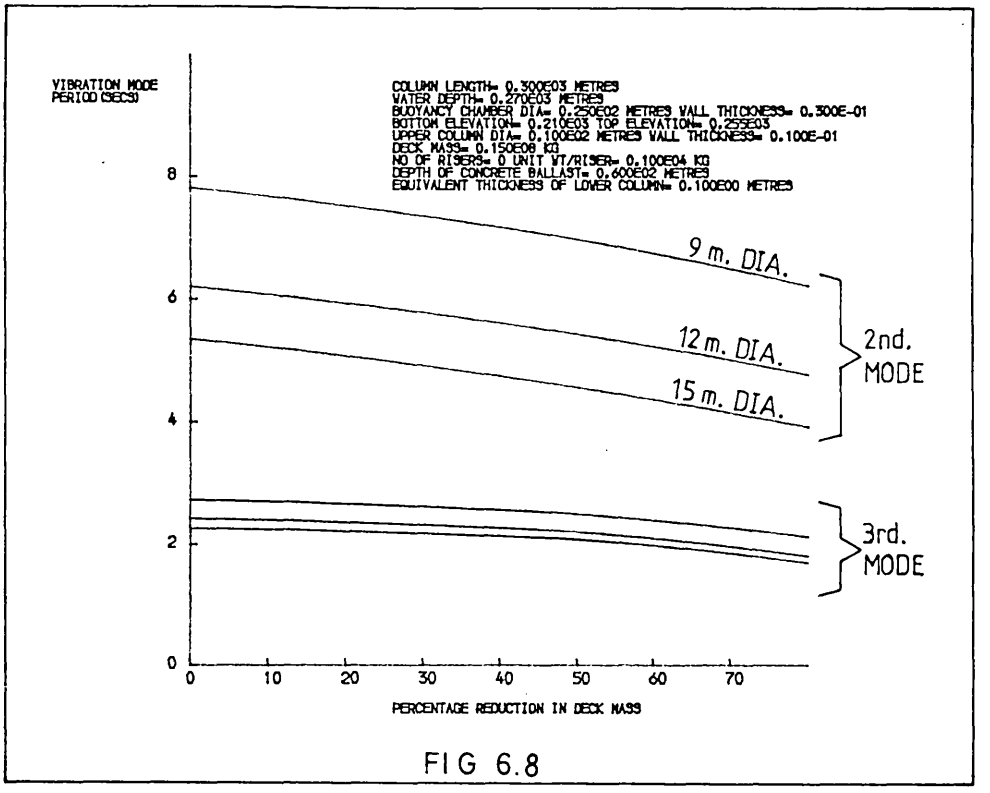
VIBRATION MODE
PERIOD (SECS)
COLUMN LENGTH= 0.300E03 METRES
WATER DEPTH= 0.270E03 METRES
BUOYANCY CHAMBER DIA= 0.250E02 METRES WALL THICKNESS= 0.300E-01
BOTTOM ELEVATION= 0.210E03 TOP ELEVATION= 0.255E03
UPPER COLUMN DIA= 0.100E02 METRES WALL THICKNESS= 0.100E-01
DECK MASS= 0.150E08 KG
NO OF RISERS= 0 UNIT WT/RISER= 0.100E04 KG
DEPTH OF CONCRETE BALLAST= 0.600E02 METRES
EQUIVALENT THICKNESS OF LOWER COLUMN= 0.100E00 METRES
9 m. DIA.
12 m. DIA.
15 m. DIA.
2nd. MODE
3rd. MODE
8
6
4
2
0
0
10
20
30
40
50
60
70
PERCENTAGE REDUCTION IN DECK MASS

FIG 6.8

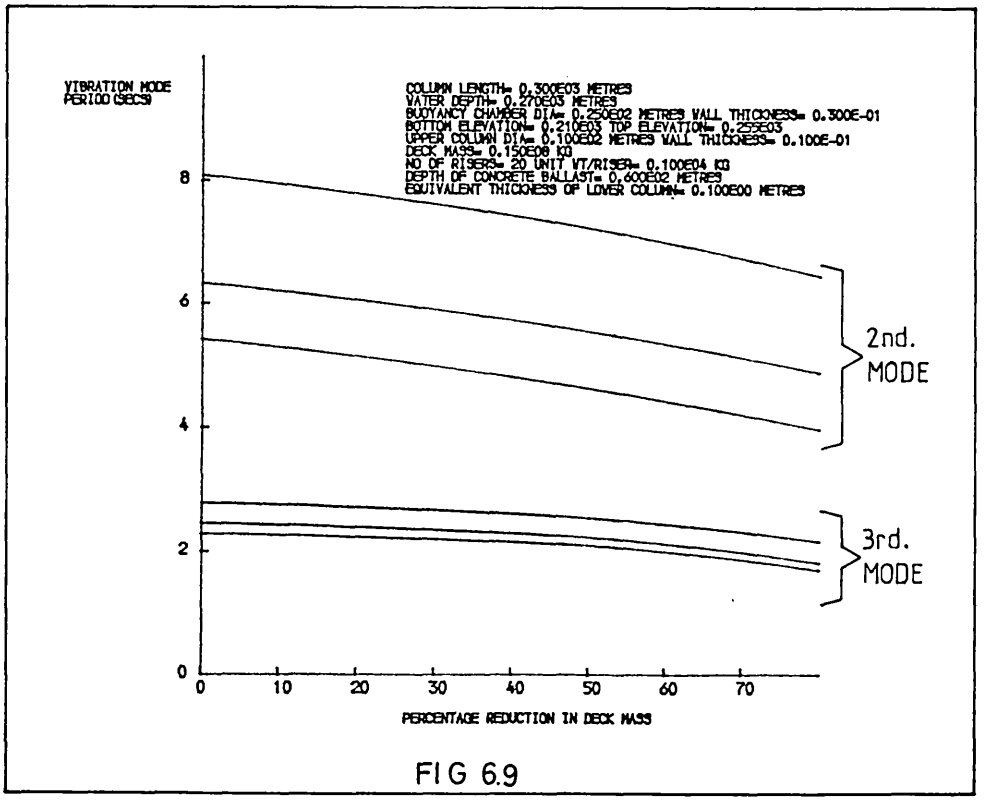
VIBRATION MODE
PERIOD (SECS)
COLUMN LENGTH= 0.300E03 METRES
WATER DEPTH= 0.270E03 METRES
BUOYANCY CHAMBER DIA= 0.250E02 METRES WALL THICKNESS= 0.300E-01
BOTTOM ELEVATION= 0.210E03 TOP ELEVATION= 0.255E03
UPPER COLUMN DIA= 0.100E02 METRES WALL THICKNESS= 0.100E-01
DECK MASS= 0.150E08 KG
NO OF RISERS= 20 UNIT WT/RISER= 0.100E04 KG
DEPTH OF CONCRETE BALLAST= 0.600E02 METRES
EQUIVALENT THICKNESS OF LOWER COLUMN= 0.100E00 METRES
2nd. MODE
3rd. MODE
8
6
4
2
0
0
10
20
30
40
50
60
70
PERCENTAGE REDUCTION IN DECK MASS

FIG 6.9

reduction in deck mass. 100% reduction is most unlikely. However, 40-50% is conceivable and this results in a 15% reduction in the second mode period for columns of 9, 12 and 15 metres diameter. Figure 6.9 is for a structure containing twenty risers, whereas fig. 6.8 is for a structure without risers. In both cases the lower column is flooded.

Similar plots for a structure with a deck mass of 100,000 KN are shown in figs. 6.10 and 6.11. The reductions achieved are somewhat less than for the 150,000 KN structure as would be expected. Figures 6.4 to 6.11 were obtained on the computational basis that the total deck mass could be accommodated as an additional lumped mass. This is then added to the consistent mass element relating to the transverse degree of freedom at the end of the last element of the structural idealisation, see fig. 6.12.

The mass of the deck superstructure, a priori, will be a function of the lateral distribution of the deck payload. The weight sensitivity of articulated columns will demand a rigorous design appraisal of deck payload configurations in order to minimise superstructure weights. The spreading of the deck payload laterally can be likened to a mass damping in respect of vibrations. Some assessment of the variation of vibration frequencies with lateral distribution of deck payload is necessary in order to put the preceeding design argument in context.

The lateral distribution of deck mass has been modelled computationally on the basis that the mass can be approximated as two discrete 'lumped' masses located at a distance $\ell a/2$ from the centre line of the structure, see fig. 6.12. This mass couple is added to the

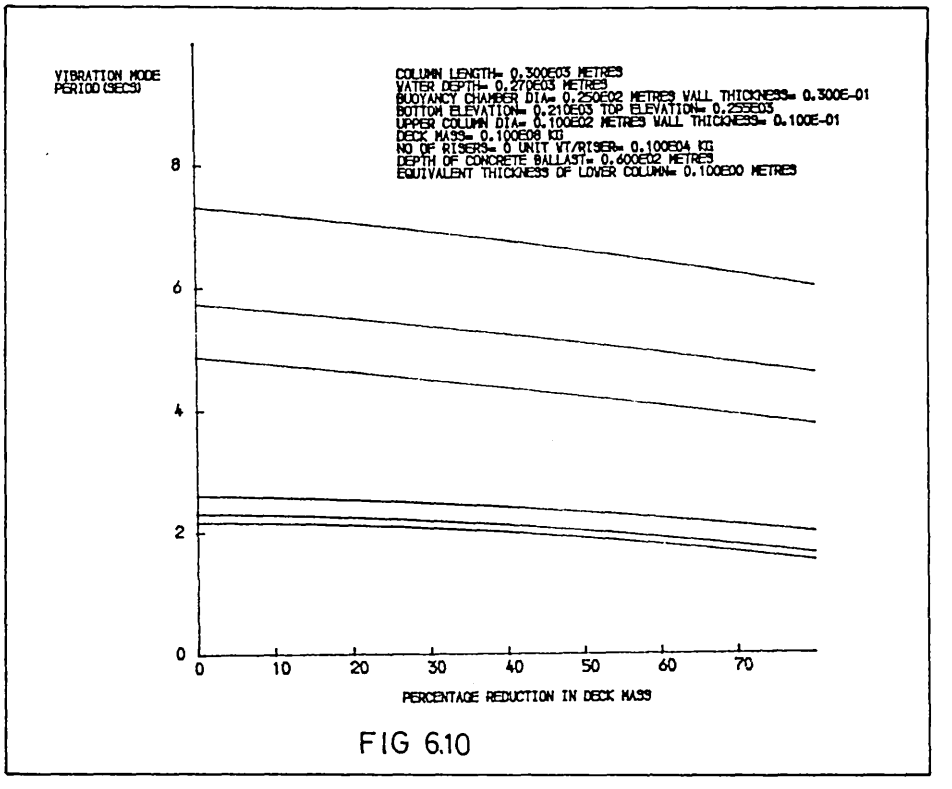

FIG 6.10

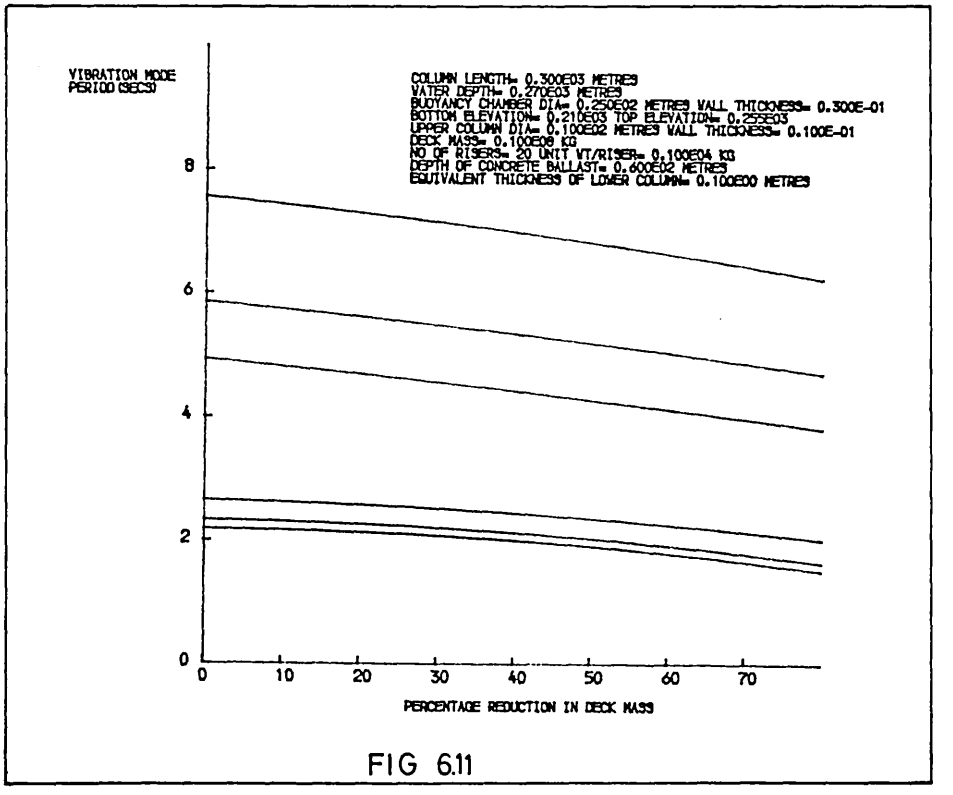

FIG 6.11

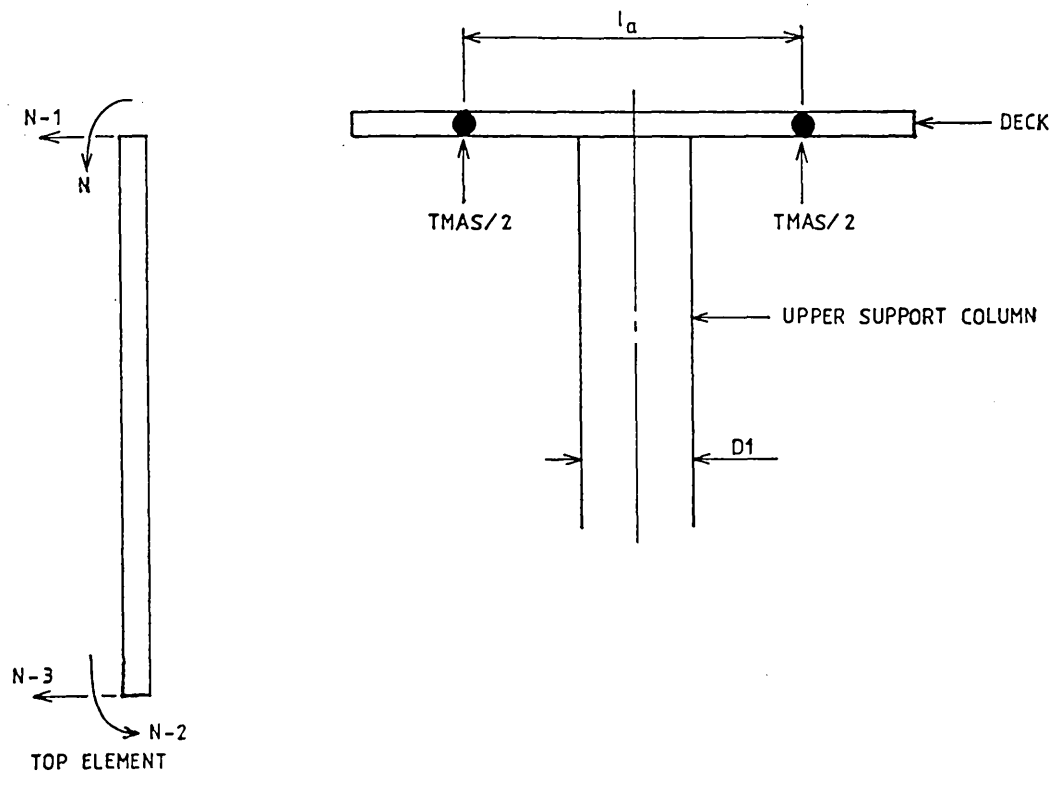

EQUIVALENT LATERAL DISTRIBUTION OF DECK LOADS

FIG 6.12

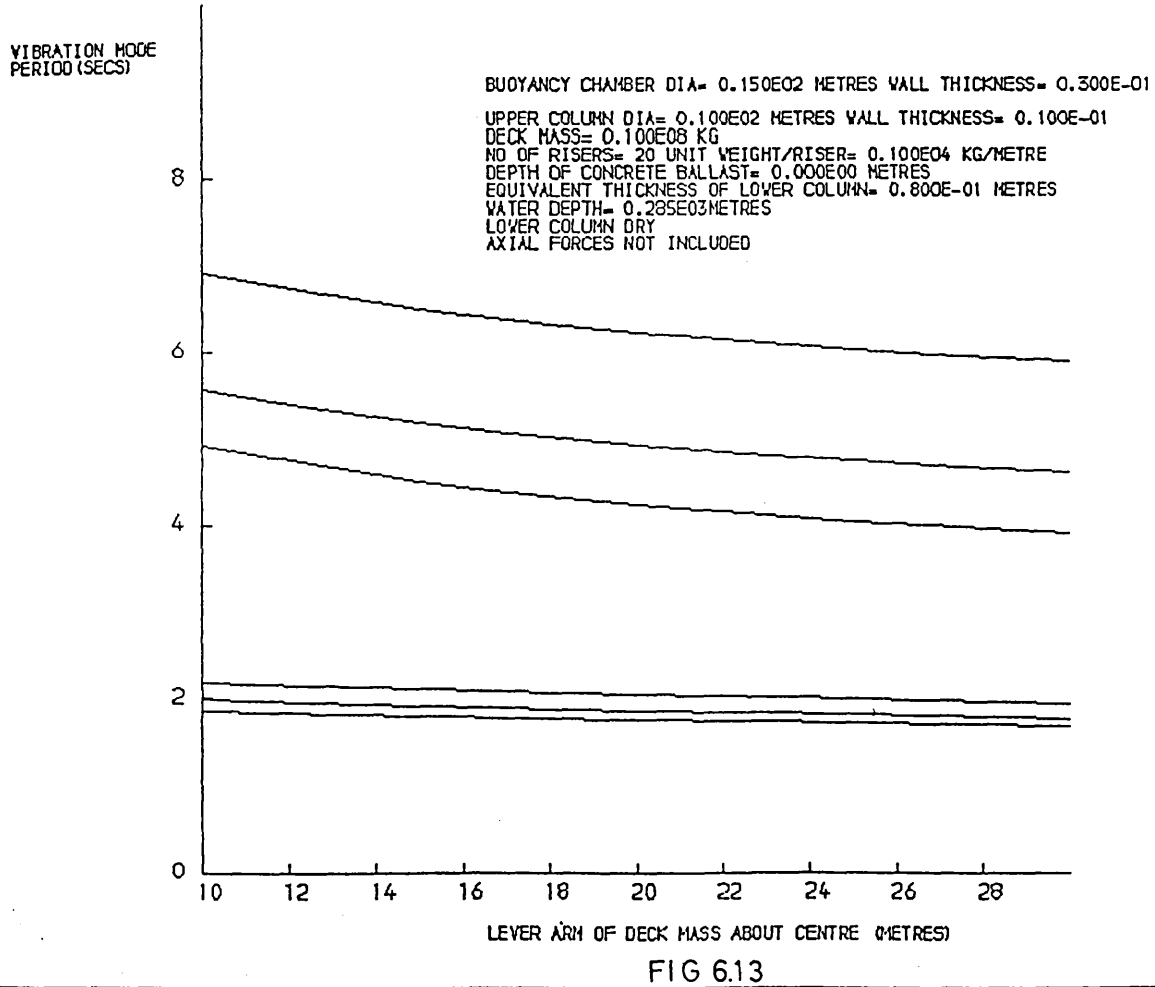

FIG 6.13

consistent mass matrix term corresponding to the rotational degree of freedom at the end of the last element. A proportion of the deck mass is attributed to the transverse degree of freedom.

Figure 6.13 shows the variation in vibration periods as a function of the lever arm of the deck mass about the centre line. Very significant gains in period reductions are achieved by increasing the lever arm up to about 20 metres, which is equivalent to a 40 metre wide deck, and thereafter the gains are only nominal. It is likely that a minimum tolerable deck width, in respect of operational requirements, will be of the order of 30-40 metres so that the results obtained must be assessed in the light of minimum deck width required. Nevertheless, there is scope for optimising and the contribution of deck mass distribution to reducing vibration periods is noted.

5.4 Variation in Vibration Mode Frequency with Riser Mass

The variation in mode period with riser mass is shown in figs. 6.14 and 6.15, for structures having payloads of 100,000KN and 150,000KN, respectively. In both cases the lower column is flooded. The plots assume twenty risers per structure and a unit weight of 10KN per metre length of riser. The effect of the mass of risers is only nominal and this is to be expected as the total riser mass is of the order of 20% of the total mass per unit length of the lower column when this is flooded. The mass of risers will have a more significant effect on vibration periods when the lower column is watertight.

5.5 Variation in Vibration Mode Frequency with Axial Loads and Buoyancy Chamber Dimensions

The effect of axial loads is demonstrated by considering the

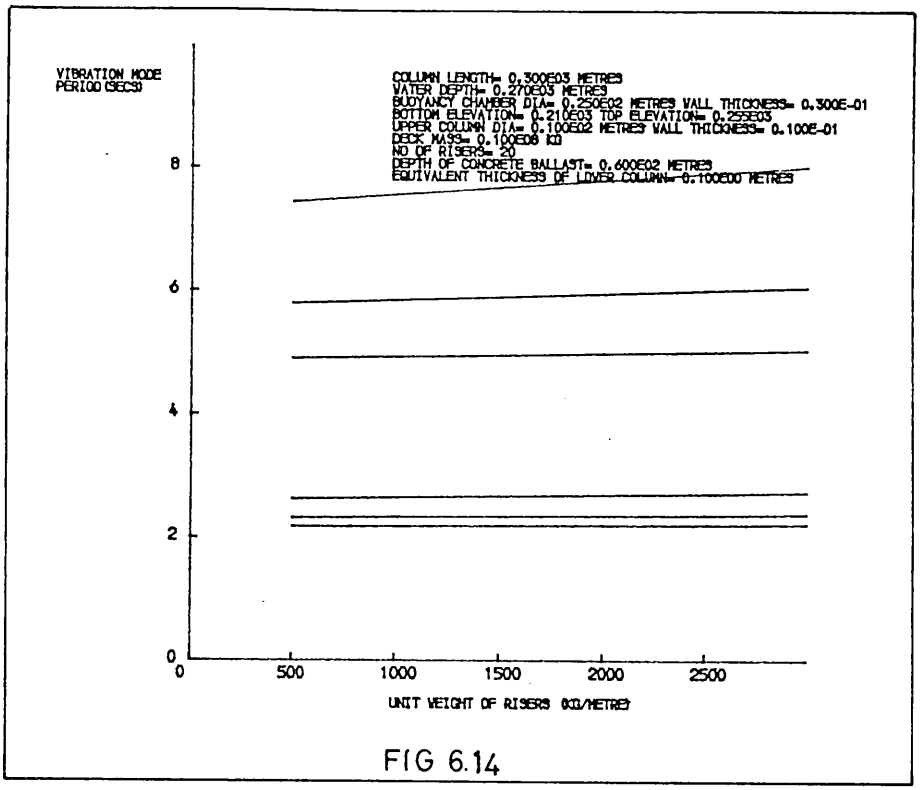

FIG 6.14

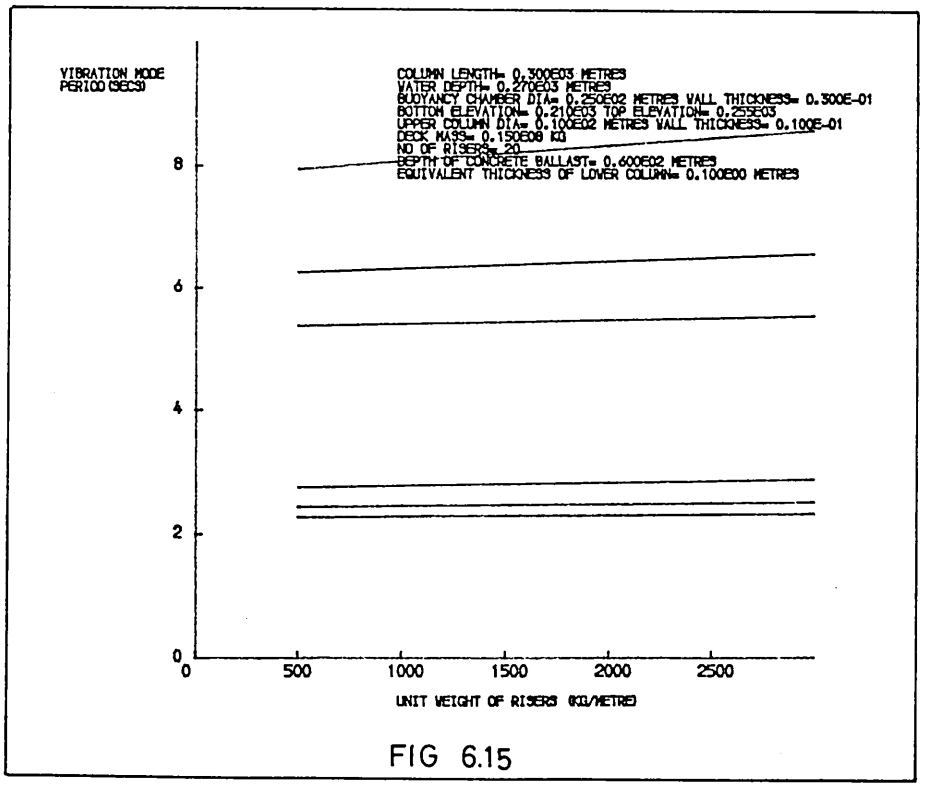

FIG 6.15

equation of motion for a simply supported beam subject to lateral vibrations (68), ie:

$$EI\delta^4 y/\delta x^4 - P.\delta^2 y/\delta x^2 = -\rho.A.\delta^2 y/\delta t^2 \qquad (6.38)$$

The term on the right hand side is the inertia force of the mass of the vibrating beam.

Assuming a solution to equation (6.38) of the form:-

$$y = X(A_o \cos\omega t + B_o \sin\omega t) \qquad (6.39)$$

Substituting equation (6.39) in (6.38) gives:-

$$EI\frac{\delta^4 X}{\delta x^4} - P.\frac{\delta^2 X}{\delta x^2} = \rho.A.\omega^2 X \qquad (6.40)$$

For a simply supported beam:-

$$X_i = \sin\frac{i\pi x}{\ell} \qquad (i = 1, 2, 3.....\infty) \qquad (6.41)$$

Substituting this expression into equation (6.40), gives the corresponding angular frequency of vibration:-

$$\omega_i = \frac{i^2\pi^2 a}{\ell^2}\sqrt{1 \pm \frac{P\ell^2}{i^2 EI\pi^2}}$$

where $a = \sqrt{EI/\rho A}$

The term $P\ell^2/i^2\pi^2 EI$ is the ratio of the axial load to the Euler critical buckling load and, for a tensile load, the term is additive and the frequencies will increase, whereas for a compression load the term is subtractive and the frequencies will decrease.

The effect of axial forces is readily allowed for in the analysis by the inclusion of the geometric stiffness matrix in the

equation of motion. In the case of undamped free vibrations, it can be included in the equation of motion as follows:-

$$M\ddot{x} + (K + K_G)\, x = 0 \qquad (6.43)$$

As discussed previously, the geometric stiffness matrix is derived and multiplied by the axial load, assuming that this is constant over the length of the element. In the case of articulated columns, where the axial load distribution is not constant along the whole length of the structure, it is necessary to ensure that the axial load at any particular node is referred to the degrees of freedom pertaining to that node.

By way of illustration of the effect of axial loads on a fairly slender structure, it is observed from fig. 6.16 that the mode periods are reduced for increasing axial tensions. The third mode curves are of particular interest in that they show maxima for the 10,000KN and 20,000KN tensile loads for a column with a diameter of approximately 1.5 metres.

It is expected that the effects of axial loads will be much less pronounced for larger diameter structures, such as those being investigated, and this is apparent from fig. 6.17 which shows the variation in mode period as a function of axial tension.

Conversely, as axial tensions increase frequencies, axial compressive loads will reduce frequencies. The effects of excluding and including the axial distribution of load for the structures considered are shown in figs. 6.18 and 6.19, respectively. Second mode vibration periods are increased on average by 15% for a 9 metre column and by 6% for a 15 metre diameter column in 250 metres of water.

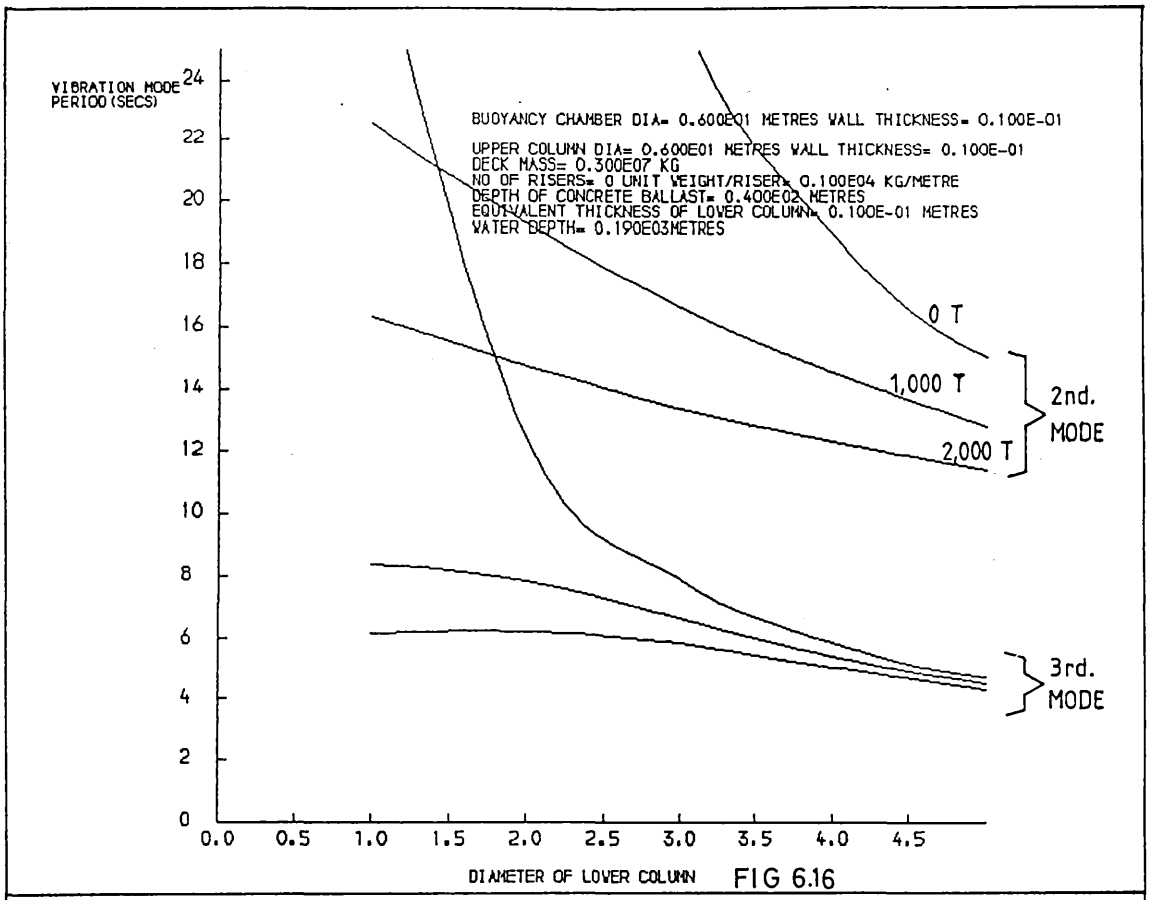

FIG 6.16

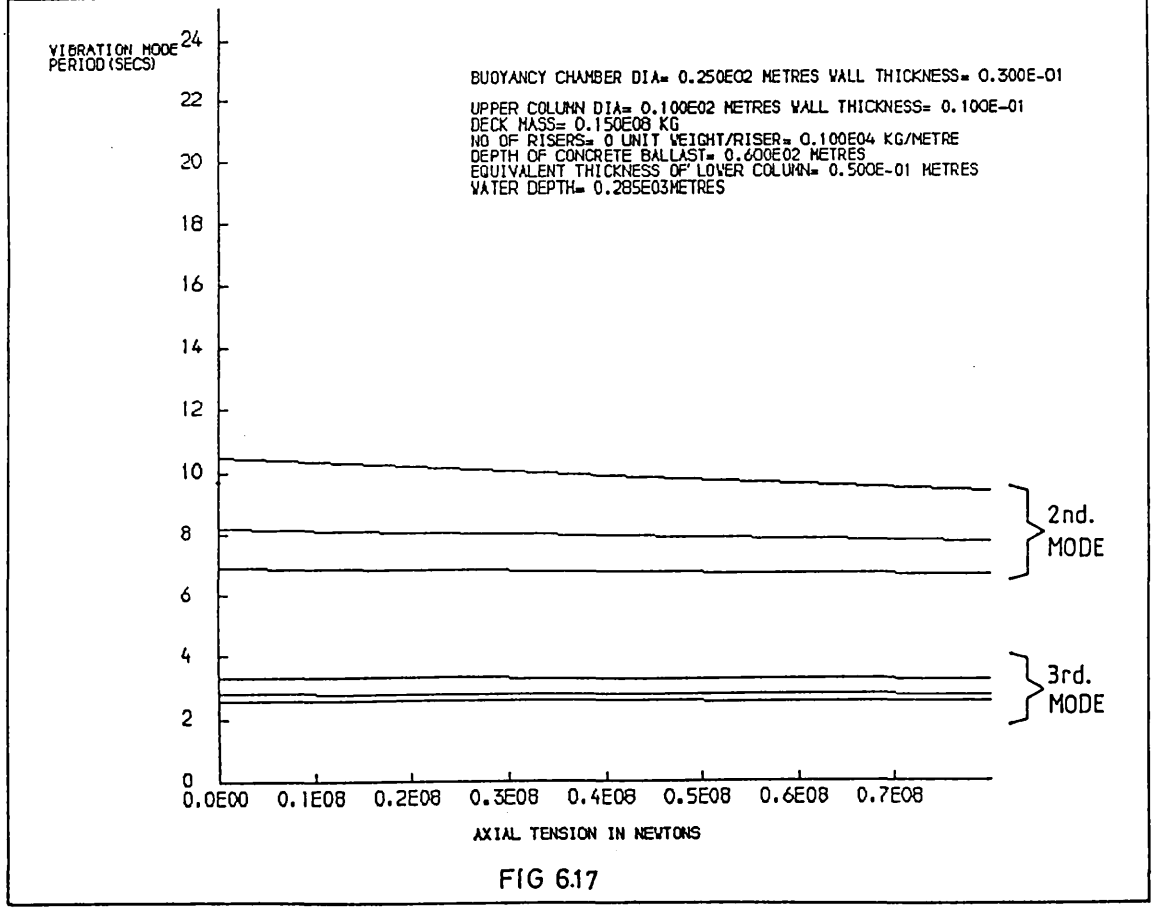

FIG 6.17

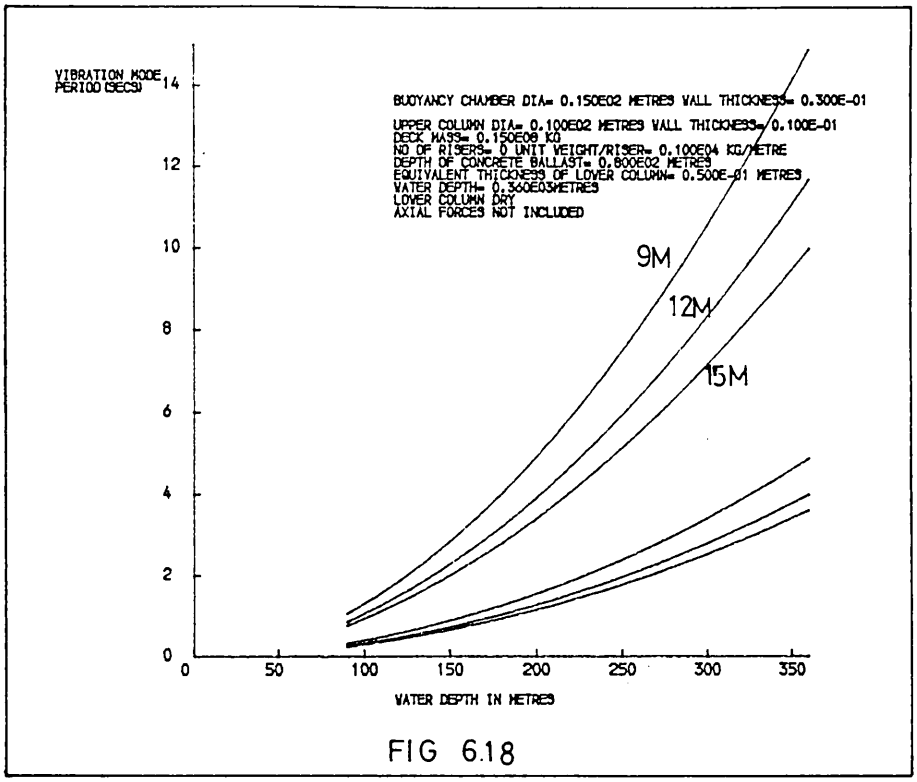

FIG 6.18

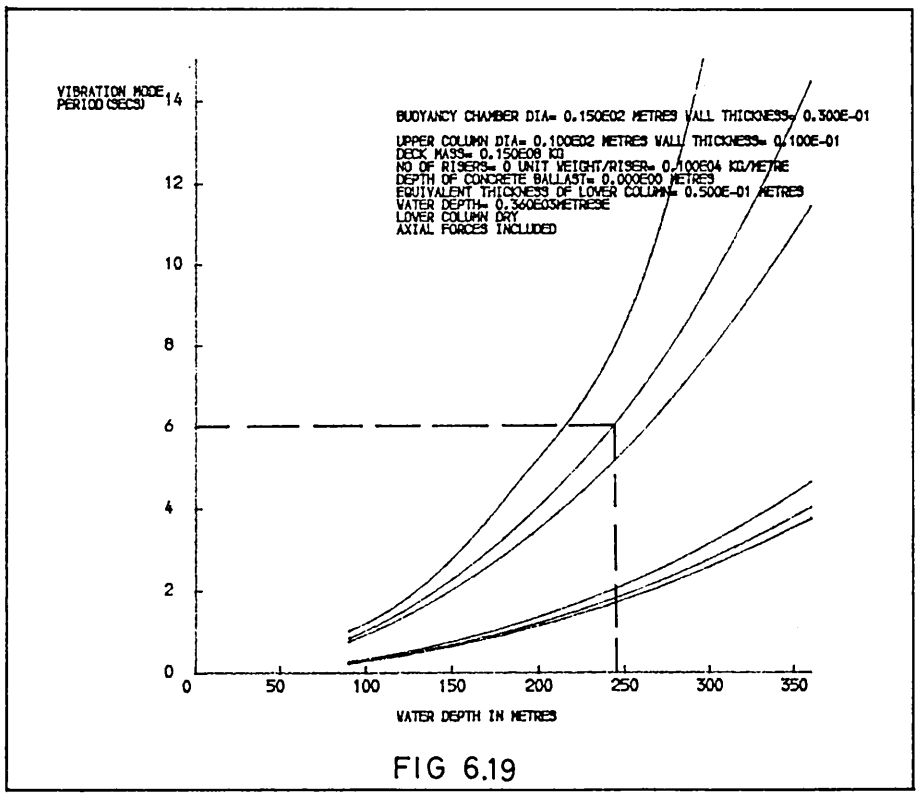

FIG 6.19

Axial loads in the column are also a function of the dimensions of the buoyancy chamber, as exposed horizontal plan areas will be subject to vertical hydrostatic pressures. Figure 7.12 shows the axial distribution of load in a structure with a lower column diameter of 12 metres and a buoyancy chamber 20 metres in diameter. The bottom of the buoyancy chamber is at an elevation of approximately 200 metres and the effect of the uplift on reducing the axial compressive loads in the lower column is apparent. The increased compressive loads near the bottom of the column are attributed to the high density drilling mud ballast located there.

As the buoyancy chamber is located fairly near to the top of the structure, the effects of the flexural rigidity of the chamber would not be expected to greatly affect the second mode vibration. However, the added mass contribution will increase with the diameter of the chamber. Therefore, it is instructive to examine the effects of increasing the buoyancy chamber diameter on the vibration, from the point of view of axial load distribution, increased flexural rigidity and added mass contribution.

Figure 6.20 shows the variation in vibration mode period as a function of buoyancy chamber diameter for a structure with a lower column 12 metres in diameter and 100 mm equivalent thickness. The top curve is that obtained when the axial load distribution is included in the analysis and the lower curve is that obtained excluding axial loads. The general trend is for vibration periods to decrease with increasing buoyancy chamber diameter. The reduction is approximately 15% when axial loads are included and 7% when they are excluded.

The lower curve gives a good indication of the effects of flexural rigidity and added mass contribution, since the axial loads are excluded. In this case, the vibration mode is decreasing with increasing buoyancy chamber diameter. The improvement is most marked for the smaller values of diameter and becomes only nominal as the diameter increases. The increased flexural rigidity for the larger diameter and its tendency to reduce vibration periods is countered by the increased added mass contribution, which will tend to increase periods, in approximate equal measure.

The top curve gives a good measure of the effects of the axial load reduction as a consequence of uplift on the lower face of the buoyancy chamber as the diameter is increased. This accounts for the extra 8% reduction over that achieved when the axial loads are not included.

5.6 Variation in Vibration Mode Frequency with Length of Ballast.

Some form of ballast will be necessary as previously discussed and accordingly it is necessary to make some assessment of the effects of the ballast material on vibration characteristics.

If mud were to be used as a ballast material then this would make no contribution to the flexural rigidity of the relevant section and, accordingly, this would mean that an increased flexural rigidity may need to be provided over that section of the lower column. The flexural rigidity for the ballast sections is calculated on the same basis as for other structural elements.

Figure 6.21 shows the plot of vibration mode period in seconds

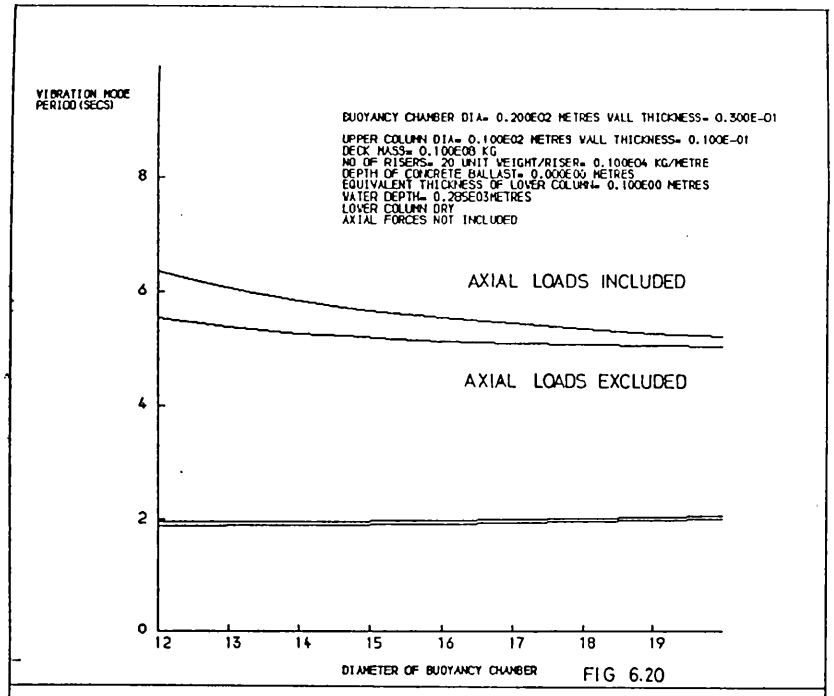

FIG 6.20

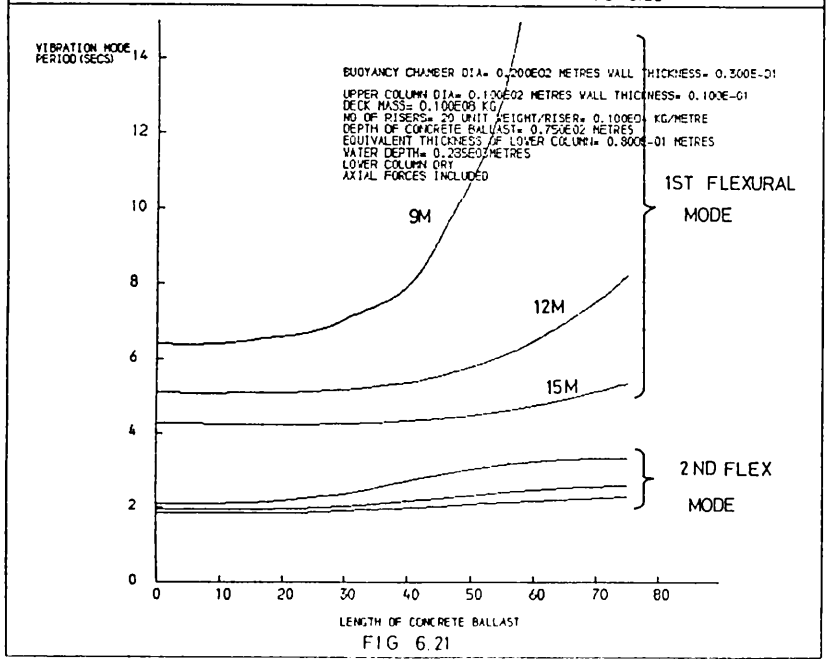

FIG 6.21

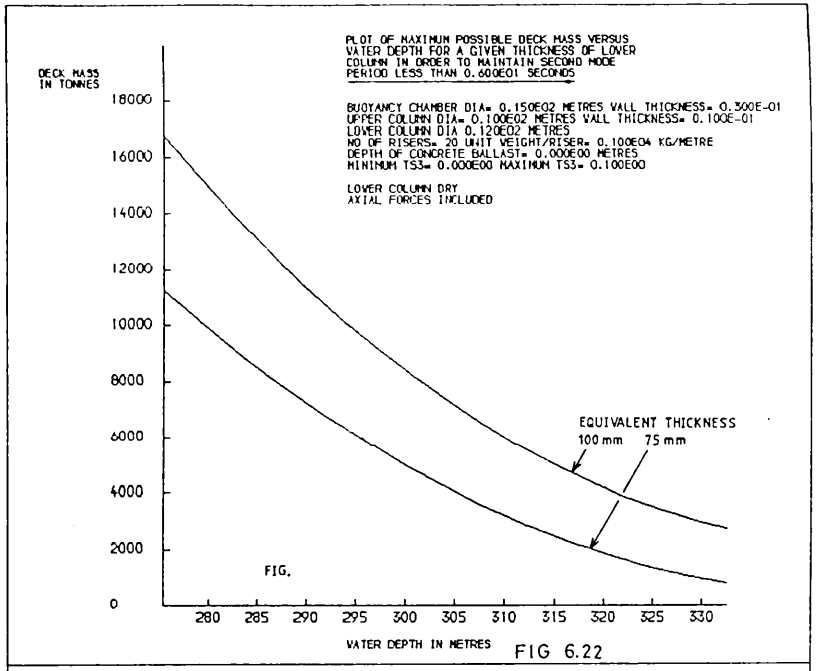

FIG 6.22

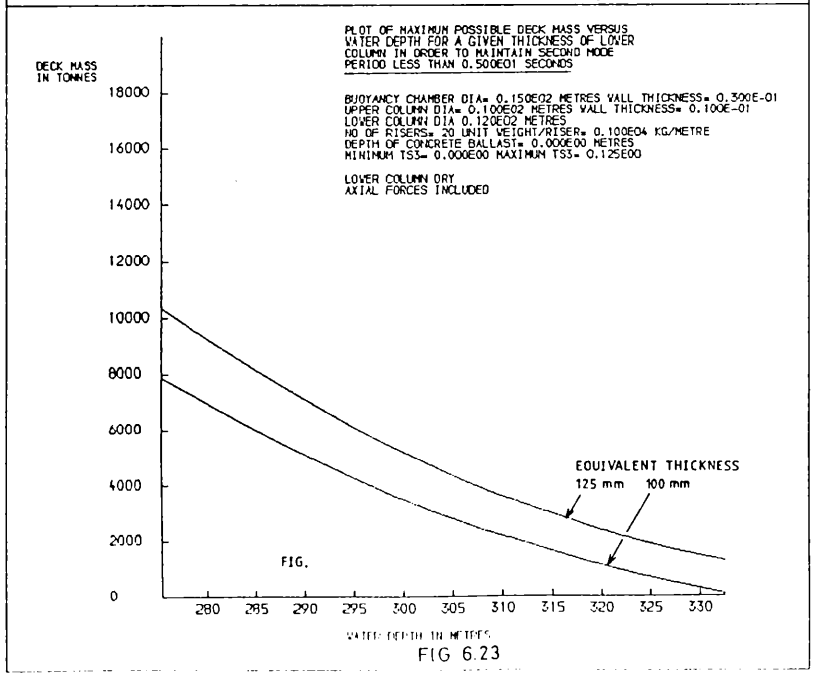

FIG 6.23

as a function of the length of ballast material as measured from the bottom of the structure. The very rapid increase in the second mode period for the 9 metre diameter column reflects the very slender nature of the column. The increase in the third mode period for the 9 metre diameter column is also noted. The rates of increase in the second mode periods reduces with increasing diameter as would be expected. Axial forces are included in the analysis so that the correct axial force distribution and its effect on the vibration will be accounted for in the solution of the Eigenvalue problem.

5.7 Practical Implications

The parameter studies described give a very good illustration of their relative importance and their relationship to vibration periods. For a given water depth and lower column structure, the deck mass is the variable which has the greatest effect on vibration periods.

Figure 6.19 indicates the maximum water depth tolerable in order to maintain second mode vibration periods for a given structure. For a maximum second mode period of 6 seconds, a structure with a deck mass of 150,000 KN and a lower column 15 metres diameter and 50mm thick is limited to a maximum water depth of approximately 250 metres.

It is instructive to compute the maximum deck mass allowable against water depth, assuming a fixed dimension for the lower column, in order to achieve a specified second mode vibration period. The calculation requires that an iterative procedure is employed to optimise the deck mass and this is done by means of a bisection method, which effectively halves the error in each iteration. The

results obtained, as shown in figs. 6.22 and 6.23, allow a maximum error of ± 0.5% on the second mode vibration period of 6 seconds and 5 seconds, respectively.

Trends for production equipment are towards much lighter components and fig. 6.24, which is reproduced from reference (29), shows typical deck load requirements for a floating production system in the North Sea. Typical requirements to produce 60,000 BPD oil and 30 MMSCFD gas are shown to be approximately 40670 KN. Assuming that a total deck mass, including the structural steelwork, of 50,000 KN is feasible, the limitations on water depth for a structure of this size are shown in figs. 6.25 and 6.26, for equivalent thicknesses of 80 mm and 50 mm respectively.

Figure 6.26 bears direct comparison with fig. 6.19. Both are for structures with identical lower column dimensions but with deck masses of 50,000 KN and 150,000 KN respectively. Figure 6.19 indicates a maximum water depth of 245 metres for the 12 metre diameter column to maintain the second mode period at 6 seconds. The maximum water depth for this period as shown in fig. 6.26 is 280 metres - a 15% increase.

It is important to be able to make some assessment of the total structural weight requirements for a structure, given the payload and the operating depth. Accordingly, figs. 6.27 to 6.28 have been produced. The iterative procedure used was the same as that for figs. 6.22 and 6.23, ie the maximum error in the second mode period is ± 0.5%.

Figures 6.27 and 6.28 show the maximum deck mass as a function

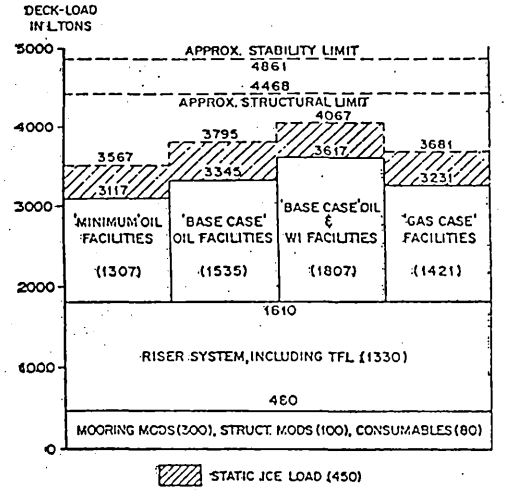

DECK LOAD BUILD-UP — MULTIBORE RISER FPS

FIG 6.24 (REF 29)

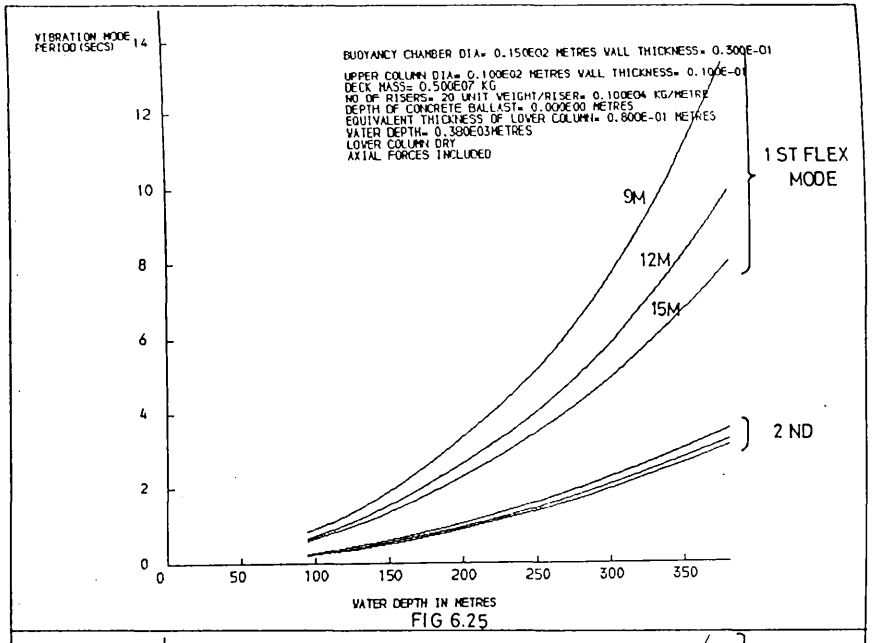

FIG 6.25

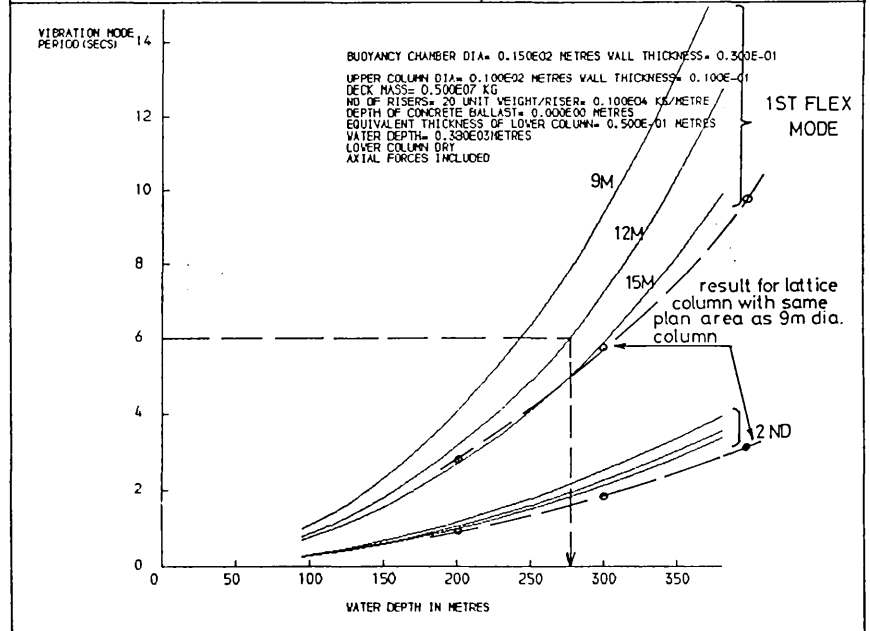

FIG 6.26

of the nett weight of the structure necessary to maintain the second mode period equal to 5 seconds, for various water depths. Figure 6.28 is basically an extension of fig. 6.27 in order to take the maximum deck mass to 90,000 KN.

Referring to figs. 6.27 and 6.28; the curve for 285 metres of water shows approximate proportionality in deck mass and nett structural weight up to the maximum deck mass of 90,000 KN. The curve for 308 metres of water shows that the ratio of nett structural weight to deck mass is of the order of 2.0, up to a value of the deck mass of approximately 80,000 KN. Thereafter, the nett structural weight required increases very rapidly with deck mass. The curve for 322 metres of water shows very large increases in nett structural weight for small increases in deck mass.

Similarly, figs. 6.29 and 6.30 are those obtained for a second mode period of 6 seconds. The limit of weight and deck mass proportionality for the second mode period occurs for a water depth of approximately 308 metres, an 8% increase in depth over that for the second mode period of 5 seconds.

It is noted that the nett structural weight is calculated assuming fixed masses for the buoyancy chamber and the upper support column. Also, the equivalent thickness of the lower column, makes no allowance for internal stiffeners. This is not thought to contribute to significant errors in the estimation of the structural weights, as the equivalent thicknesses are such that if stiffeners are to be used then the thickness may be reduced, ie the reduction in equivalent thickness will be offset by the increased weight of the stiffeners - the overall flexural stiffness remaining approximately constant.

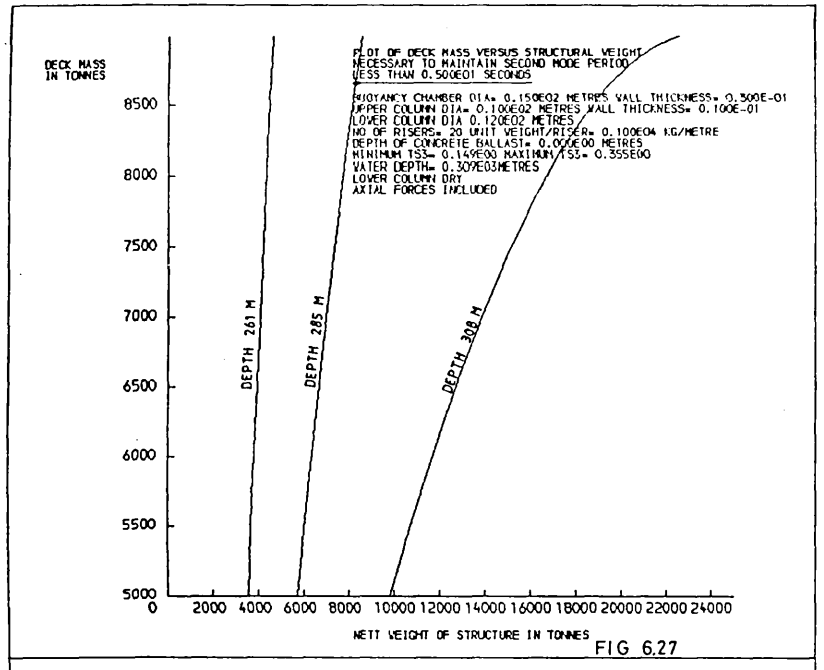

FIG 6.27

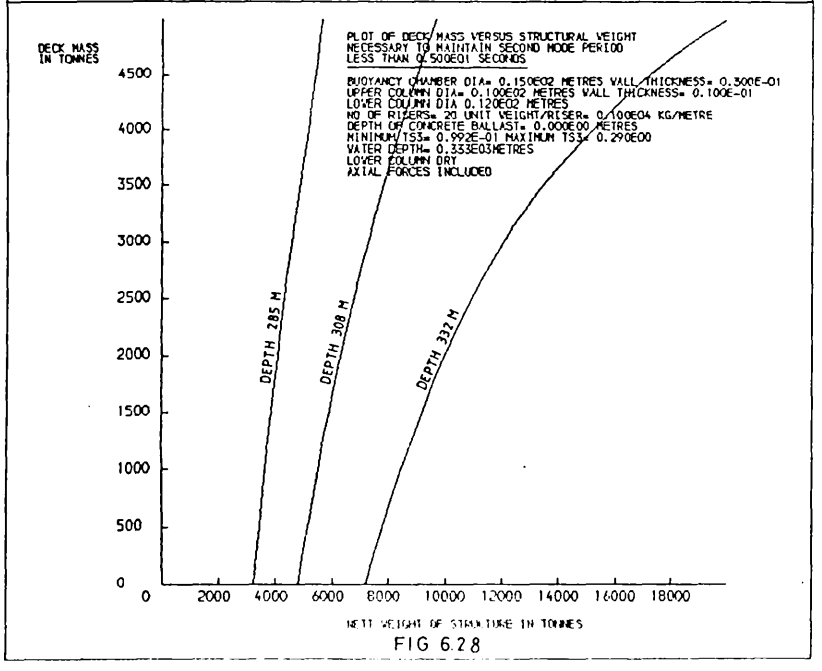

FIG 6.28

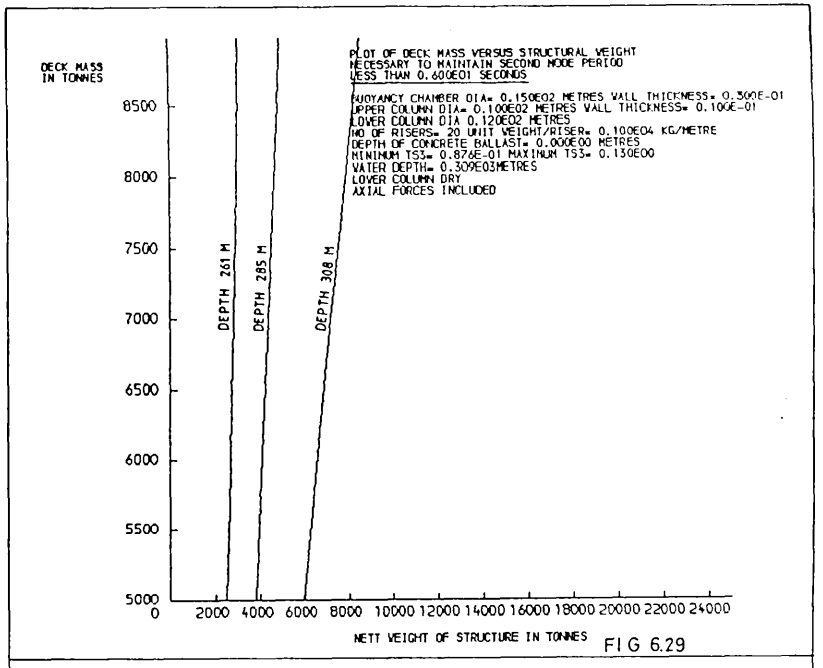

FIG 6.29

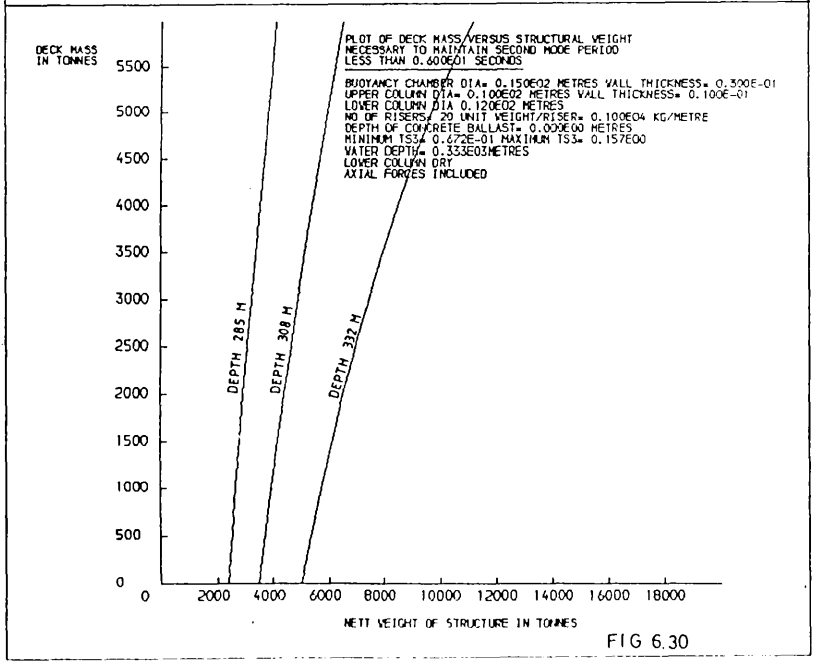

FIG 6.30

Figures 6.22 to 6.30 make no allowance for relocation of deck masses in the buoyancy chamber and this, as has already been demonstrated, will improve the structures vibration characteristics and increase operating water depths by a small amount.

The proportionality of deck mass with structural weight is noted in figs. 6.27 to 6.30 up to limiting water depths. It is accepted practice to express the payload of compliant structures as a percentage of the displacement. For most semi-submersibles, for example (71), this ratio is of the order of 0.2 to 0.3. For those articulated columns just discussed, and for a maximum water depth of 308 metres, the ratio of payload to structural steelwork weight is approximately 1.0 and this increases as depth decreases. This is a significant improvement over that for semi-submersibles and other compliant systems.

5.8 Full Fixity Encastre Column

An alternative to the articulated joint at the bottom of the lower column is to provide a connection with full fixity, such that no rotation about the connection is permitted. Such a connection is proposed for use with a new deep water loading/mooring system (69,70), see fig. 6.31.

The encastre connection means that the section at the base will have to resist the total moment generated as a consequence of zero rotation. The first three vibration mode shapes for the column with full fixity are shown in fig. 6.31. The first mode is analogous to the rigid body mode of the articulated column except that there is no rotation at the connection.

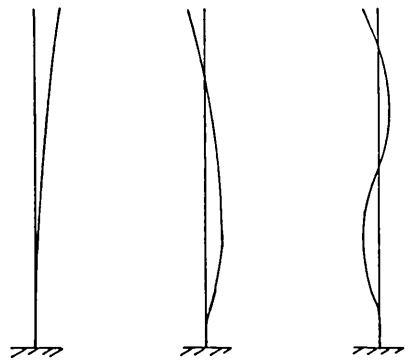

FIRST THREE VIBRATION MODE SHAPES FOR ENCASTRE

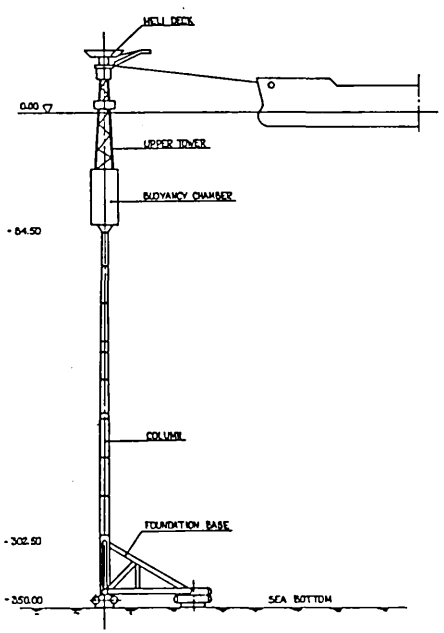

COLUMN WITH FULL FIXITY AT BASE
FIG 6.31

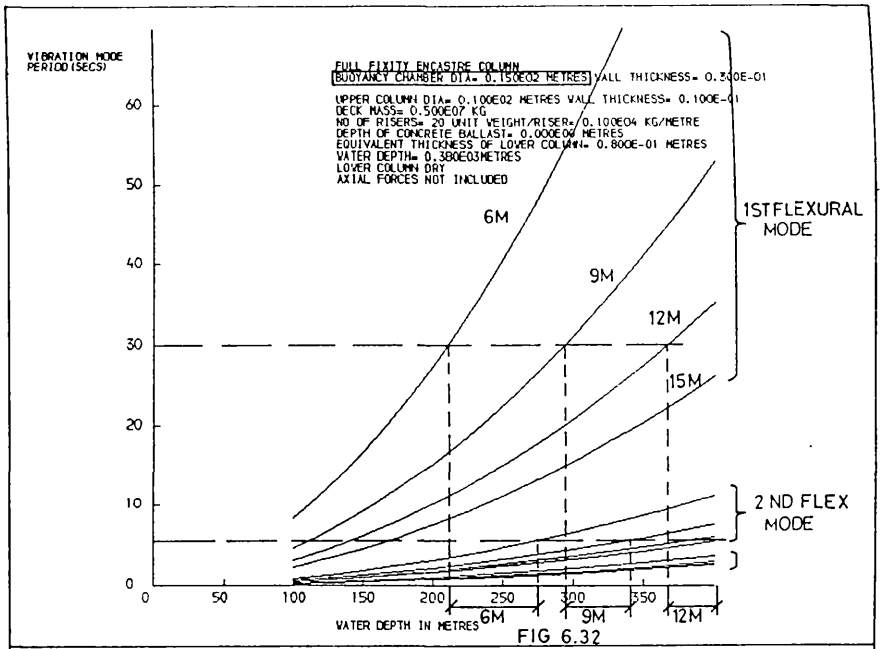

FIG 6.32

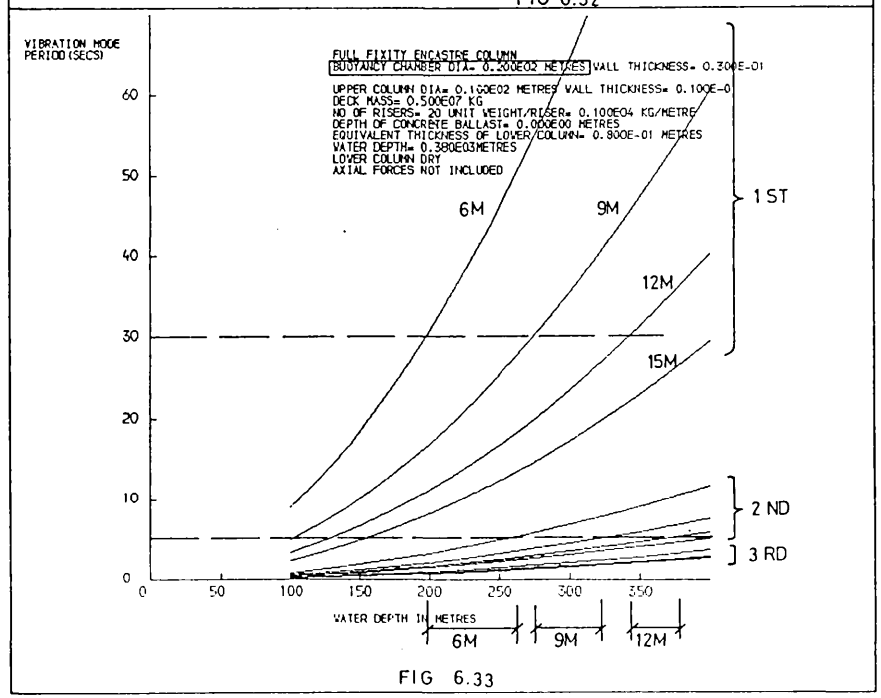

FIG 6.33

The program described in section 4.4 was amended to include the additional boundary condition to restrict rotation at the base connection. Figure 6.32 shows the results of the program in the form of a plot of the vibration mode period as a function of water depth. The structure is the same as that for fig. 6.25. The first mode period is that which displays the greatest increase for increasing water depth. Qualitatively, the trends are very similar to those obtained for the articulated column (see fig. 6.25).

The curves indicate that it is possible to design the structure such that the first and second mode periods are greater than and less than, respectively, likely wave spectra. This is analogous to the articulated column for the rigid body mode and the first flexural response mode. With the articulated column, the rigid body mode was of little consequence in terms of bending stress, whereas for the column with full fixity, the first mode period should be much greater than expected wave spectra to avoid resonant excitation.

In terms of design criteria for first and second mode vibration periods, it will be necessary to stipulate minimum and maximum values, respectively. This puts upper and lower limits on water depth for any particular column design, whereas in the case of the articulated column, an upper limit was imposed.

Imposing 'minimum' and 'maximum' values of 30 seconds and 5 seconds for the first and second mode periods, respectively, the water depth ranges for various diameters of lower column are shown in fig. 6.32. The trend is for the water depth range to decrease in magnitude as column diameters increase. This indicates that the fixed

connection column is more effective as water depth is reduced.

The effects of increasing the diameter of the buoyancy chamber and, therefore, the added mass is displayed in fig. 6.33 which shows the same curves but for a structure with a 20 metre diameter buoyancy chamber.

5.9 Lower Column of Lattice Construction

The limitations in depth for the circular cylindrical structural section have been established on the basis of second mode vibration constraints. The circular cylindrical section offers benefits in terms of riser accommodation, maintenance, etc, as discussed. It is also a relatively straightforward structure to fabricate and it possesses its own buoyancy which will aid installation. The major drawback is the very large added virtual mass of the section and this plays an important part in the vibration.

Structures which comprise a lower column of lattice construction have been proposed. This is less attractive than the circular cylindrical structure on many counts. However, it will have advantages in that the added virtual mass of the structural assemblage will be much less than that of the cylindrical section. This will affect the vibration characteristics and, for this reason, it was felt necessary to make an assessment of the vibration frequencies for such a structure.

The structural modelling of a lattice arrangement of members is the same as that described in this chapter. However, the computational task is greatly increased as a consequence of the

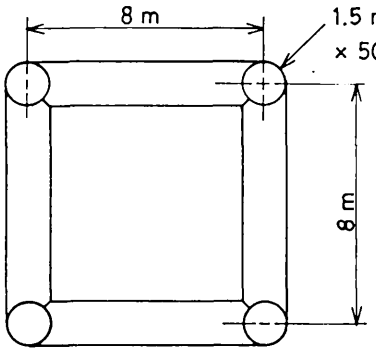

PLAN

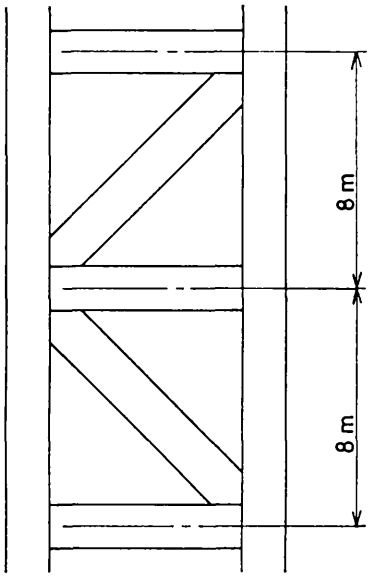

ELEVN.

MASS AND STRUCTURAL DATA

	LATTICE COLUMN	CYLINDRICAL COLUMN
AREA OF STEEL	1.0 m^2	1.4 m^2
SECOND MOMENT OF AREA	16.7 m^4	14.3 m^4
ADDED VIRTUAL MASS OF SECTION	24 TONNES PER METRE LENGTH	63.6 TONNES PER METRE LENGTH

LATTICE CONSTRUCTION FOR LOWER COLUMN

FIG. 6.34

increased number of members. For example, one bay of the assemblage as shown in fig. 6.34, comprises 5 members, each with 4 degrees of freedom, ie a total of 20 degrees of freedom. The cylindrical structure analysed comprised 20 elements with a total of 42 degrees of freedom. On the basis that 20 bays will provide an adequate lattice structural assemblage, the total number of degrees of freedom will be 20 x 20 = 400. The computer programs described can be amended to compute the associated structural matrices but limitations in time prevented a full analysis of such a structure.

However, an alternative mathematical model is legitimate in making a preliminary assessment of the vibration behaviour. This method is on the basis of applying the value for the flexural rigidity of the lattice structure to that of a beam column element with 4 degrees of freedom. The mass matrix can be generated in a similar manner.

On the basis that the plan area of the lower column remained the same as that for a 9 metre diameter column, it corresponds to a square with 8 metre sides (see fig. 6.34). Four vertical columns, one in each corner, each 1.5 metres in diameter and 50mm wall thickness, have been modelled. Horizontal and diagonal bracing are as shown in fig. 6.34 and these are modelled on the basis that they do not contribute to the second moment of area but are included in the calculation for an equivalent added virtual mass for the assembly. The equivalent area and mass data are shown in fig. 6.34, compared to that for a 9 metre diameter column, 50mm thick.

The results of the vibration analysis for this assemblage are plotted in fig. 6.26 in order that the curves obtained for the second

and third mode vibration periods can be compared with those for the 9 metre diameter column. The very significant reduction in the vibration periods is noted. These are approximately 30% less at 200 metres water depth to approximately 40% less at 400 metres.

6. CONCLUDING REMARKS

The free undamped vibration analysis by means of the finite element method provides a useful insight into the vibration behaviour of the structural assembly.

The dominant effect of the lower column properties, compared to those of the buoyancy chamber, is noted in determining the vibration frequencies in that the moment of inertia of the buoyancy chamber has been shown to have little influence on the vibration.

The relationship between the vibration frequencies and the equivalent thickness of the lower column is noted and the optimum equivalent thickness for the three diameters considered appears to be in the region of 50-85mm. Thereafter the improvement in vibration frequencies is only nominal. It is also noted that trends for the third mode vibration frequencies are similar to those for the second mode frequencies and are more pronounced at the lower values of frequency.

The fairly rapid increase in vibration periods with water depth is to be expected, nevertheless the advantages to be gained in respect of the dry lower column are noted and, for example, the curves for the 12 metre diameter dry and the 15 metre diameter wet columns are almost identical as is observed from figs. 6.6 and 6.7.

Relocation of deck masses has a significant effect on reducing the vibration periods whereas the gains in respect of riser mass are only nominal.

The effects of axial tensile loads is noted particularly in the case of very slender structures as is to be expected, and is less pronounced for the types of structure considered. The distribution of axial loads plays an important role in the vibration periods and this is observed in the similarity of the curves for the 12 metre diameter dry and the 15 metre diameter columns as shown in figs. 6.18 and 6.19. The tendancy for the increased diameter of the buoyancy chamber, as a consequence of both the increased flexural rigidity and the reduced compressive axial loads, to reduce 2nd mode periods is also noted.

The effects of the ballast material are significant for the 9 metre and 12 metre diameter lower columns and is nominal for the 15 metre diameter column. Improvements are possible in this area if the diameter of the ballast is made greater than the lower column diameter so that the length of the ballast is reduced.

The single most important parameter in respect of the reduction of vibration periods is the deck mass and this is as expected. However, the contributions from other parameters ie, diameter of lower column and thickness, diameter of buoyancy chamber, length of ballast and lateral distribution of deck mass are noted and, on a cumulative basis, would constitute a significant contribution in reducing vibration periods.

The practical implications of the above work for proposed structures is that water depths cannot greatly exceed 300 metres and

the major parameter in this respect is the total deck mass. However, very favourable nett structural weight characteristics are possible within this range and these are greatly improved for small reductions in the water depth.

The advantages of the full encastre connection will manifest themselves in reduced first mode motions and negate the requirement for an articulated connection at the base. However, in respect of the encastre connection considerable bending moments will have to be accommodated at the base and the foundation will have to be designed to withstand the large cyclic moments transmitted to the base. This aspect is further discussed in Chapter 7, section 7.

The advantages in adapting a lattice construction for the lower column has been demonstrated and reductions in second mode periods of the order of 35% were achieved. This is a very significant reduction and it is noted that the area of steel for the lattice column was some 30% less than for the circular cylindrical column. It is considered that very substantial gains are to be made in adopting a lattice construction for the lower column. However, the disadvantages in terms of riser, accommodation, etc, have to be weighed against improved vibration characteristics.

In conclusion it is believed that a careful optimisation of the parameters considered would result in a structure with a sufficiently high second mode vibration frequency. Third mode vibration frequencies are unlikely to be a cause for concern.

CHAPTER 7

FORCED VIBRATION OF ARTICULATED COLUMNS

1. INTRODUCTION

The undamped free vibration as presented in Chapter 6 provides a necessary insight into the dynamic behaviour of articulated columns and would be an essential part of any design feasibility study. The free vibration analysis is also a prerequisite to the dynamic analysis in the time domain in that accurate values of vibration frequencies are required for application in the time domain.

Having established that vibration mode periods for typical structures considered are likely to be in the range of probable wave energy spectra to be encountered, it is necessary to examine the forced vibration response.

There are, essentially, two ways of investigating the forced dynamic response of structures ie, by a frequency domain analysis or by a direct integration method in the time domain.

This chapter first describes the analysis in the frequency domain and then goes on to describe the development of the various techniques which combine to give the full forced vibration analysis in the time domain. The program development and solution method thus described is applied to typical structures subject to regular waves at frequencies equal to and less than the second mode vibration frequency. The relative importance of certain parameters is then examined.

The responses obtained will be those for waves of the order of 5-7 seconds period acting on structures with typical dimensions as shown in fig. 6.3. The ratio of diameter to wave length (D/L) is, thus, approaching the limiting value of approximately 0.2 where diffracted and radiated potentials become significant and beyond which the validity of the Morison approach may be in question. The upper support column for the structures considered is likely to be 10-12 metres diameter. A 6 second wave is 56 metres long and the D/L ratio for the upper column will be in the region of 0.18 to 0.21. The errors in the calculation of wave forces on the upper column using the Morison approach are, therefore, thought to be small.

The top of the buoyancy chamber is likely to be located some 20-30 metres beneath the still water level (SWL). The maximum wave steepness limits a 6 second wave to a height of approximately 8-9 metres. Bearing in mind that the wave forces decrease exponentially with depth, the upper support column will be responsible for the major proportion of the forces on the upper support column and the buoyancy chamber combined. Therefore, it is thought that the errors in respect of the wave forces on the buoyancy chamber will be very small. It is believed that despite possible small overestimations in loading the approach is valid and valuable in the examination of certain aspects of response pertaining to the second mode excitation.

The monopile structure which was analysed in Chapter 6 is examined in the full time domain vibration analysis and certain non-linear behaviour is assessed.

Finally, some experimental data which have been obtained for a model articulated column with a length scale of 1/100 and which has a

very flexible lower column is presented. The experimental results obtained are compared with the results of an analysis of the model configuration and the effects of non linear waves is examined.

Eatock Taylor (28) has obtained added mass and damping coefficients from the radiated and diffracted potentials for articulated columns and the conclusions were that the Morison approach tended to overestimate responses for the shorter waves.

A comprehensive loading mechanism which would include the time variation of the diffracted and the radiated potentials could be incorporated into the vibration analysis routines which have been developed. Such an approach, albeit time consuming computationally, would be valuable in order to calibrate and compare results obtained by the Morison approach to wave loading.

2. MATRIX ASSEMBLY

The mass and stiffness matrices are assembled in the same way as described in chapter 6. However, in chapter 6 the full size matrices were used to aid the solution of the eigenvalue problem.

Stiffness and mass matrices for most structural systems are well ordered in that they are usually 'symmetrical' about the diagonal. In addition, they are generally 'banded' about either side of the leading diagonal. Other off diagonal elements are zero. The symmetry and bandedness, if taken advantage of, greatly reduces computer storage requirements and the computational task, as it is no longer necessary to perform computations on array elements which are not relevant to the solution of the problem.

Figure 7.1 shows the way in which the reduced size matrix is achieved. For clarity the array elements in the original full size matrix (OLD) are shown in their new locations in the new reduced size matrix (NEW). The symmetry of the matrices means that computations are only performed on one half of the full size matrix. The original full size N x N matrix reduces in size to an N x MS matrix where MS is the semi band width. The relationship between the full band width MF and the semi band width MS is MF = 2*MS-1.

3. RAYLEIGH DAMPING

Rayleigh showed that a damping matrix of the form $C = \gamma M + \mu K$ will satisfy the orthogonality conditions necessary in order to permit uncoupling of the equations of motion (49). The coefficients γ and μ are arbitrary proportionality factors which can be evaluated on the basis that the amount of critical damping in any particular mode is known.

When the damping matrix is mass proportional, ie $C = \gamma M$ then the damping ratio will be inversely proportional to the frequency of vibration and the higher modes will be very lightly damped. Conversely when the damping is stiffness proportional, ie $C = \mu K$, then the damping ratio is proportional to the frequency and the higher modes will be heavily damped.

4. MODAL SUPERPOSITION

The dynamic response of structures which possess linear characteristics is readily investigated by modal co-ordinate

superposition methods. This requires the evaluation of the relevant eigenvalues and the corresponding eigenvectors as shown in chapter 6.

Using the eigenvalues and eigenvectors thus obtained it can be shown that the equations of motion can be reduced to a set of uncoupled equations of motion by the following transformation process.

On the assumption that the total displacement of the structure can be obtained as the sum of the individual modal components then:-

$$X = \phi_1 Y_1 + \phi_2 Y_2 + \phi_3 Y_3 \ldots\ldots\ldots \phi_n Y_n$$

or in matrix notation $X = \phi\, Y$ (7.1)

where ϕ = mode shape matrix

Y = generalised coordinates

so that the transformation from generalised coordinates Y, to geometric coordinates X is by means of the mode shape matrix ϕ.

The evaluation of any normal coordinate Y_n is obtained by multiplying equation (7.1) by the product of the transpose of the corresponding modal vector ϕ^T and the mass matrix M, thus:-

$$\phi_n^T M\, x = \phi_n^T M\, \phi_n Y \qquad (7.2)$$

since $\dot{x} = \phi\dot{Y}$

and $\ddot{x} = \phi\ddot{Y}$

since the mode shapes do not change with time.

So that the equation of motion:-

$$M\ddot{x} + C\dot{x} + Kx = F(t) \tag{7.3}$$

can be written

$$\phi_n^T M \phi_n \ddot{Y}_n + \phi_n^T C \phi_n \dot{Y}_n + \phi_n^T K \phi_n Y_n = \phi_n^T F(t) \tag{7.4}$$

where M_n = generalised or modal mass matrix = $\phi_n^T M \phi_n$

K_n = generalised or modal stiffness matrix = $\phi_n^T K \phi_n$

$F(t)$ = generalised or modal force vector = $\phi_n^T F(t)$

The equation of motion can then be written:-

$$\ddot{Y}_n + 2\beta_n \omega_n \dot{Y}_n + \omega_n^2 Y_n = \frac{\phi_n^T F(t)}{M_n} \tag{7.5}$$

and this is the equation of motion for a SDOF system.

The normal coordinates Y_n have thus been used to reduce the N coupled equations of motion to a set of N uncoupled SDOF equations which can be solved in the usual way for a SDOF system. The total response is then obtained by superposing the response for each degree of freedom into the aggregate.

For linear systems the advantages of the modal superposition method lies in the fact that only the first few modes, over and above that mode being investigated, need to be included as providing a significant contribution to the response. This greatly reduces the computation task to that of working on the first few modes generally.

An example of the frequency response spectra thus obtained for a typical structure is shown in figs. 7.2 and 7.3, excluding and including the geometric stiffness, respectively. The second mode response spectrum for the analysis including geometric stiffness is some 10% greater than that excluding the geometric stiffness.

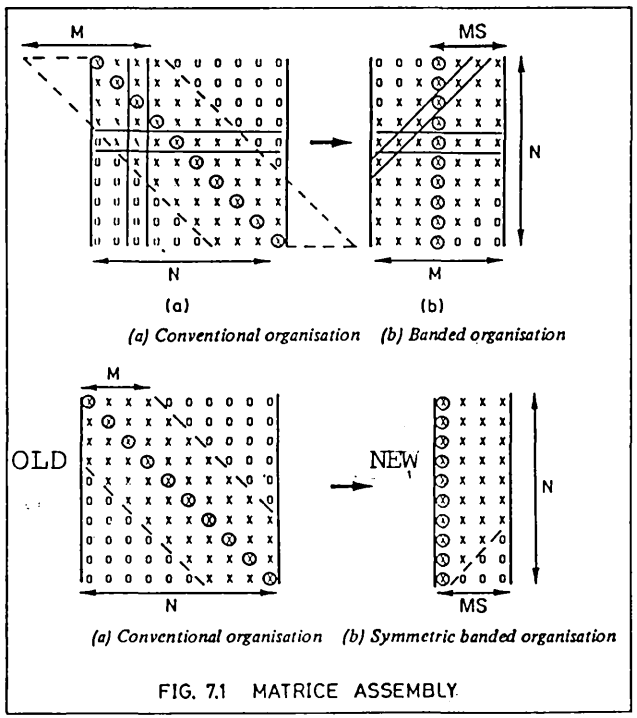

FIG. 7.1 MATRICE ASSEMBLY

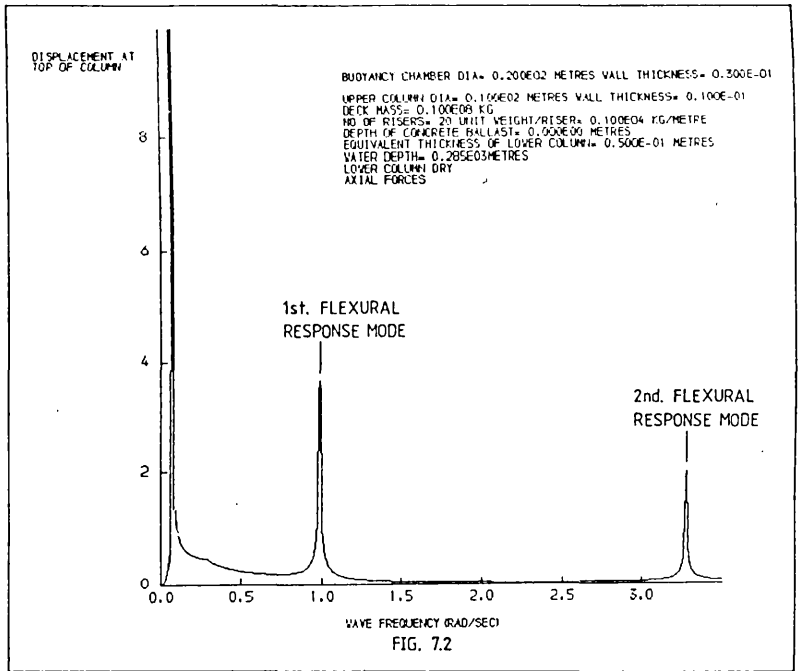

FIG. 7.2

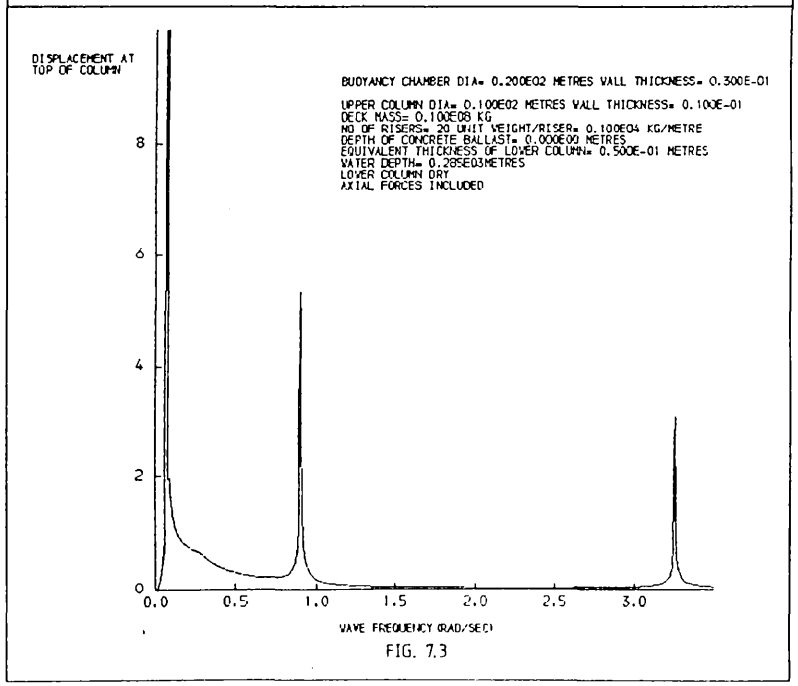

FIG. 7.3

FREQUENCY RESPONSE SPECTRA FOR ARTICULATED COLUMN

The first 10 modes of a possible 41 were included in the analysis for figs. 7.2 and 7.3. The inclusion of a greater number of modes did not have any significant effect on the solution obtained and this is confirmation that only the first few modes need to be included.

The disadvantages in using the modal superposition method in a time incremental solution, as applied to articulated columns in particular or compliant structures in general, lies in the difficulty in treating the relative velocity term on the RHS of the equation of motion. It is then necessary to employ an equivalent linearisation of the velocity squared term. The solution then proceeds on the basis of making an assumption as to the magnitude of the structural velocity and iterating until the solution converges to an acceptable level of accuracy.

In the structural analysis of compliant structures, where there is significant interaction of structural motions with wave and current motions, it is desirable to employ a step by step direct integration procedure which will allow for the quantification of any non-linearities with time.

5. DIRECT INTEGRATION PROCEDURES

Articulated columns can display certain non linear response behaviour and this was demonstrated in Chapters 4 and 5 of this thesis. The direct integration approach to the solution of the equations of motion was demonstrated to be of value in predicting the

non linear behaviour for the rigid body single degree of freedom system.

When physical properties change with time it is desirable to take account of the changes as they may significantly affect responses. The importance of accounting for the relative motion of the structure with waves and current has been demonstrated in chapters 4 and 5. Other examples of physical properties which may change are stiffness influence coefficients which will change as a consequence of time varying geometric stiffness such as those which would ensue in consideration of heave forces. Non linear material damping and plastic analysis are also examples where quantification in time would be necessary to truly reflect structural behaviour.

Essentially direct integration procedures are based on the response being calculated for each increment of time for a linear system having the properties as defined at the beginning of a specified time interval. The properties are modified at the end of the time interval to conform with the state of stress and deformation at that time. Therefore, the non linear analysis is approximated as a sequence of the analyses of successively changing linear systems.

The implementation of a direct integration procedure basically involves reducing the simultaneous differential equations of motion to a set of simultaneous algebraic equations, by means of the introduction of a simple relationship between displacement, velocity and acceleration.

The most popular and widely used direct integration schemes appear to be:-

a. The central difference method.

b. Newmark-Wilson method.

c. Crank-Nicholson method.

d. Houbolt method.

The central difference method is an explicit integration scheme in that values to be computed at the next time step are based on values obtained for the previous time step. The other methods are implicit schemes, where some assumption about the nature of the variation in motion over the time step is implied.

The implicit integration schemes pose the problem of solving non linear equations at the beginning and end of each time step, ie at t and at $t + \Delta t$ so that the solution can proceed. Newton Raphson iterative procedures are sometimes used to do this. Alternatively, it is possible to transfer the non linear terms to the right-hand side of the equation of motion and treat them as additional loads to the right-hand side load vector. A Taylor's series expansion is then utilised to express the new loads as functions of the previous time step. This procedure reduces the problem to a set of simultaneous algebraic equations.

The central difference method suffers the main disadvantage that it is only conditionally stable. In order for the solution to produce finite results, the time step Δt must be less than T_n/π where T_n is the lowest vibration mode period in the structure being analysed.

Newmark-Wilson Method

This method is a most flexible integration procedure and is

based on the following expressions for velocity and displacement at the end of each time step.

$$\dot{U}_{t+\Delta t} = \dot{U}_t + \Delta t(1-\delta)\ddot{U}_t + \Delta t.\delta.\ddot{U}_{t+\Delta t} \tag{7.6}$$

$$U_{t+\Delta t} = U_t + \Delta t\dot{U}_t + \Delta t^2(\tfrac{1}{2}-\alpha)\ddot{U}_t + \Delta t^2\,\ddot{U}_{t+\Delta t} \tag{7.7}$$

The coefficients α and δ are chosen for the accuracy of the solution required. With values of $\alpha = 1/2$ and $\delta = 1/6$ the procedure reduces to the linear acceleration method which is a conditionally stable method. This method was utilised in the dynamic analysis presented in chapters 4 and 5 of this thesis and the recurrence relations are derived in Appendix 4.1. An unconditionally stable method is the Wilson-θ method with $\theta \geq 1.4$ (72).

The solution method finally adopted for use in the time simulation vibration analysis presented in this chapter is that with values of $\alpha = 1/2$ and $\delta = 1/4$. This is known as the constant average acceleration method and is an unconditionally stable method without numerical damping.

The relative merits of some solution procedures are discussed in references (73 to 75).

5.1 Consistent Nodal Loads

Distributed loads acting on discrete elements can be represented as equivalent nodal loads. The formulation of consistent nodal loads has the same basis as that for the formulation of the consistent mass and stiffness matrices as derived in chapter 6 and is by means of the integration of the shape functions [A].

Hence the equivalent nodal loads are given by:-

$$\{F_{eq}\} = \int_0^{\ell} [A]^T . S . ds \tag{7.8}$$

where S is the intensity of load.

Recalling the shape functions as given by equations (6.5) to (6.8) in Chapter 6, we can write the shape function for the beam element shown in fig. 7.4 as:-

$$[A] = \left[1-3\left(\frac{s}{\ell}\right)^2 + 2\left(\frac{s}{\ell}\right)^3, \ell\left(\frac{s}{\ell} - 2\left(\frac{s}{\ell}\right)^2 + \left(\frac{s}{\ell}\right)^3\right), 3\left(\frac{s}{\ell}\right)^2 - 2\left(\frac{s}{\ell}\right)^3, \ell\left(-\left(\frac{s}{\ell}\right)^2 + \left(\frac{s}{\ell}\right)^3\right)\right] \tag{7.9}$$

For the case of a beam element subject to a uniformly distributed load 'S' per unit length, the equivalent nodal loads will be given by integration of equation (7.2), ie

$$\{F_{eq}\} = S\int_0^{\ell} [A]^T ds$$

$$\{F_{eq}\} = S \begin{Bmatrix} \ell/2 \\ \ell^2/12 \\ \ell/2 \\ -\ell^2/12 \end{Bmatrix} \tag{7.10}$$

and these are usually referred to as the fixed end loads relating to the degrees of freedom as shown in fig. 7.4.

When the intensity of loading is not uniform along the length of the element the explicit evaluation of the integral of equation (7.8) becomes a very lengthy process. In such cases it is prudent to employ some quadrature formulae to integrate the load on the element.

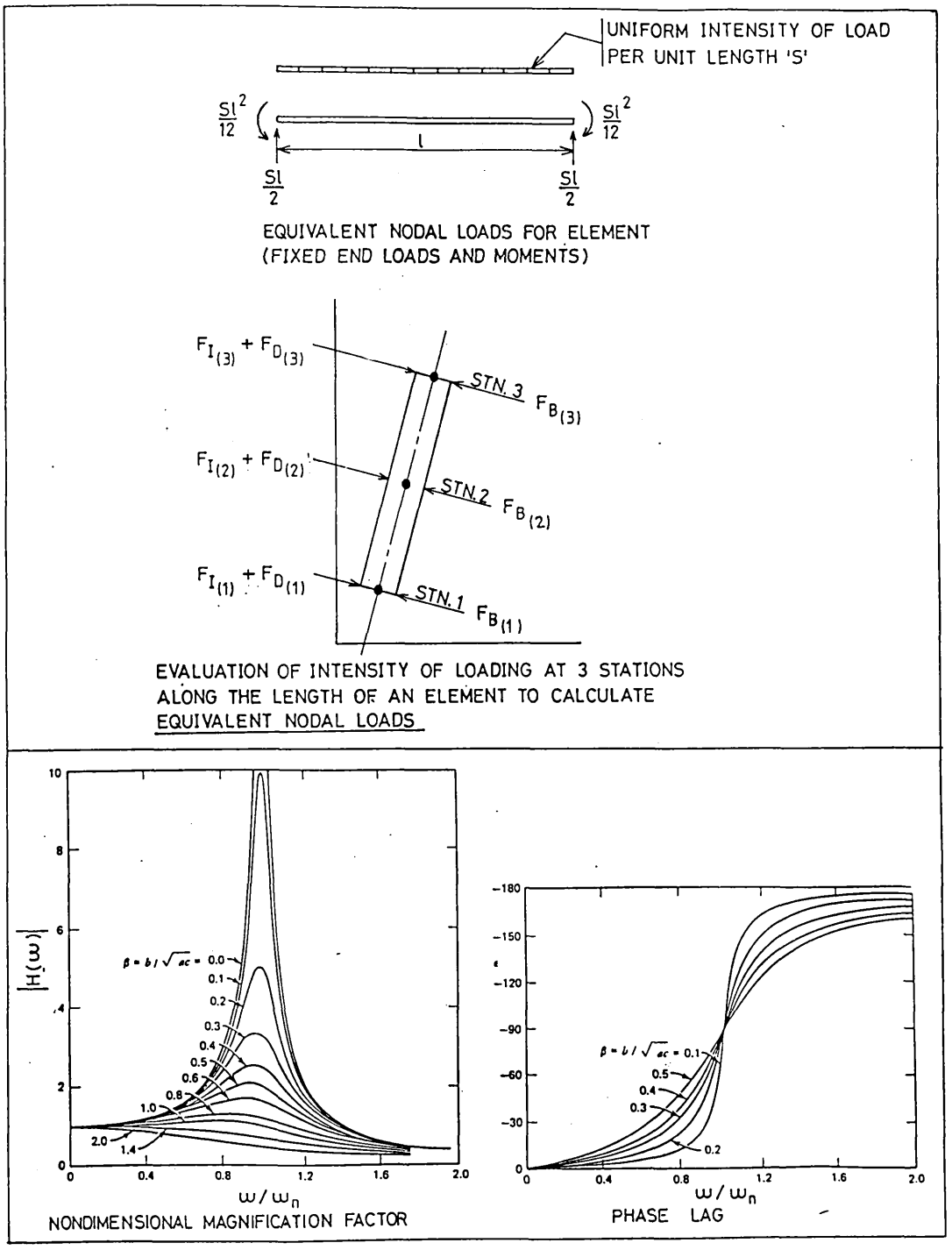
UNIFORM INTENSITY OF LOAD
PER UNIT LENGTH 'S'
Sl²/12
l
Sl/2
EQUIVALENT NODAL LOADS FOR ELEMENT
(FIXED END LOADS AND MOMENTS)
F_I(3) + F_D(3)
STN. 3
F_B(3)
F_I(2) + F_D(2)
STN. 2
F_B(2)
F_I(1) + F_D(1)
STN. 1
F_B(1)
EVALUATION OF INTENSITY OF LOADING AT 3 STATIONS
ALONG THE LENGTH OF AN ELEMENT TO CALCULATE
EQUIVALENT NODAL LOADS
|H(ω)|
β = b/√ac = 0.0
0.1
0.2
0.3
0.4
0.5
0.6
0.8
1.0
1.4
2.0
ω/ωn
NONDIMENSIONAL MAGNIFICATION FACTOR
β = b/√ac = 0.1
0.5
0.4
0.3
0.2
ω/ωn
PHASE LAG

FIG. 7.4

The Gaussian quadrature formulae have been used to integrate the loading and evaluate the equivalent nodal loads.

The Gaussian quadrature formulae integrates a function between specific limits by taking the sum of the value of the function f(x), multiplied by a weighting function w_j, for n number of stations at which the function has been evaluated, ie

$$\int_{-1}^{+1} f(x)dx = \sum_{j=1}^{n} w_j f(x_j) \qquad (7.11)$$

By evaluating the loading intensity at 3 stations on each element, ie at each end of the element and at the mid point, then:-

$$\begin{aligned} x_1 &= -0.77445967 & w_1 &= 0.55556 \\ x_2 &= 0.0 & w_2 &= 0.88889 \\ x_3 &= 0.77455967 & w_3 &= 0.5555 \end{aligned} \qquad (7.12)$$

For compatability with the form of equation (7.11) it is necessary to adjust the limits and the integration variable 'ds' in equation (7.8).

This can be done by setting $x = (\frac{2s}{\ell} - 1)$ (7.13)

so that, $ds = \frac{\ell}{2}.dx$

the limits are then changed to -1 to +1

so that,

$$F_{eq} = \int_{-1}^{+1} [A(x)]^T S.dx$$

$$= \sum_{j=1}^{n} w_j A(x_j) Sx_j \qquad (7.14)$$

Recalling equation (7.13), ie $x_j = \frac{2s}{\ell} - 1$

this can be re-written $\frac{s}{\ell} = \frac{x_j + 1}{2}$ for j = 1 to 3.

The evaluation of the shape functions for each station is then performed on the basis that,

$$(\frac{s}{\ell})_j = \frac{1 + x_j}{2} \text{ for } j = 1 \text{ to } 3$$

so that $(\frac{s}{\ell})_1 = (1 - 0.77445967)/2$

$$(\frac{s}{\ell})_2 = \tfrac{1}{2} \qquad (7.15)$$

$$(\frac{s}{\ell})_3 = (1 + 0.7744596)/2$$

For a particular element the process is to evaluate the four shape functions for each station and multiply these by the weighting function w_j and the intensity of loading for that station. This is done for each degree of freedom and the sumnation of terms is taken.

This process has been programmed in the form of three subroutines, namely SHAPFN, FEQUIV and FEQTOT and these are described in section 5.3.

5.2 Intensity of Loading

With reference to fig.7.4; the actions of the various forces on an elemental length of the structure are as shown. The non conservative forces acting on an elemental length comprise:-

a. Wave loads, ie drag and inertia components F_D and F_I.

b. Buoyancy force F_B.

The intensity of force per unit length attributable to a) is evaluated in the same way as those forces described in Chapter 4. The assumption that the buoyancy force F_B acts as a distributed load along the length of each element is in contradiction to the laws of hydrostatics which strictly, speaking, state that buoyancy forces can only act on exposed end faces such as those at the top and bottom of the buoyancy chamber and at the bottom of the lower column, see fig. 7.4. Applying the buoyancy forces in this manner gives rise to numerical instabilities in the numerical integration procedure and so the buoyancy forces have been assumed to act in a distributed manner as shown. This is not considered to give rise to significant errors in the solution.

5.3 Computer Program Implementation and Solution of the Equations of Motion

The mass and stiffness matrices are assembled as described in section 2 using subroutine ASMCON.

Subroutine LINWAV calculates wave particle kinematics according to linear wave theory.

Subroutine STOKE calculates wave particle kinematics according to Stokes' fifth order wave theory.

Additional subroutines to compute equivalent nodal loads in accordance with section 5.1 are:-

Subroutine SHAPFN evaluates the shape function for each station as given in equations (7.9) and (7.15).

Subroutine FEQUIV evaluates the equivalent nodal load for each element. The input required for FEQUIV are the values of the shape functions from SHAPFN, the weighting functions w_j and the intensity of loading for each station.

Subroutine FEQTOT evaluates the sum of the equivalent nodal loads for each nodal point along the length of the structure and requires, as input, the equivalent nodal loads for each element as evaluated in FEQUIV.

Subroutines ADSUB and MULBAV are routines to add matrices and multiply condensed matrices by vectors, respectively.

The equations of motion:-

$$M\ddot{x} + C\dot{x} + Kx = F(t)$$

are solved as outlined in fig. 7.5 and it is noted that, in order to avoid the accumulation of numerical errors, initial accelerations are calculated prior to the calculation for displacements (step B2). These accelerations are then used in the calculation for the effective load vector ie, step B1. It is considered that this procedure eliminates the possibility of errors accumulating were the recurrence relations in step B3 only used to calculate the accelerations.

The Gauss elimination procedure is used to solve for accelerations and displacements and this has been programmed in the form of subroutine SLBVI which takes account of the symmetry and bandedness of the matrix in the solution of the standard form $Ax = B$.

6. ANALYTICAL RESULTS

6.1 Effects of Concentrated and Distributed Loads

Initial versions of the program developed to solve the forced vibration in the time domain attempted to utilise the linear acceleration method, which had been successfully used for the dynamic analysis presented in chapters 4 and 5 of this work. The solutions obtained were unstable and it was necessary, therefore, to investigate the stability of alternative procedures. In the event the Newmark-Wilson method with $\alpha = 1/2$ and $\delta = 1/4$ ie, the constant average acceleration method proved to provide stable solutions and was used in all subsequent time simulation analysis of the forced vibration.

Program development was in stages so that initially a program was developed to investigate the response of a cantilever beam subject to static loads and sinusoidally varying loads, either concentrated or evenly distributed along the length of the beam. It is instructive to compare the responses for the cantilever beam subjected to sinusoidal excitation at the same frequency as the second mode vibration frequency. Figures 7.6 and 7.7 show the responses obtained for the beam subject to a point load and a distributed load, respectively. The first of the four plots is the magnitude of the exciting force. The second and third plots are the displacements of the mid nodal joint and end nodal joint, respectively, and the fourth plot is the displacement of the beam along its length at a time when the displacement at the end of the beam is maximum.

The intensity of the distributed load is such that it would produce the same static bending moment as the point load which is

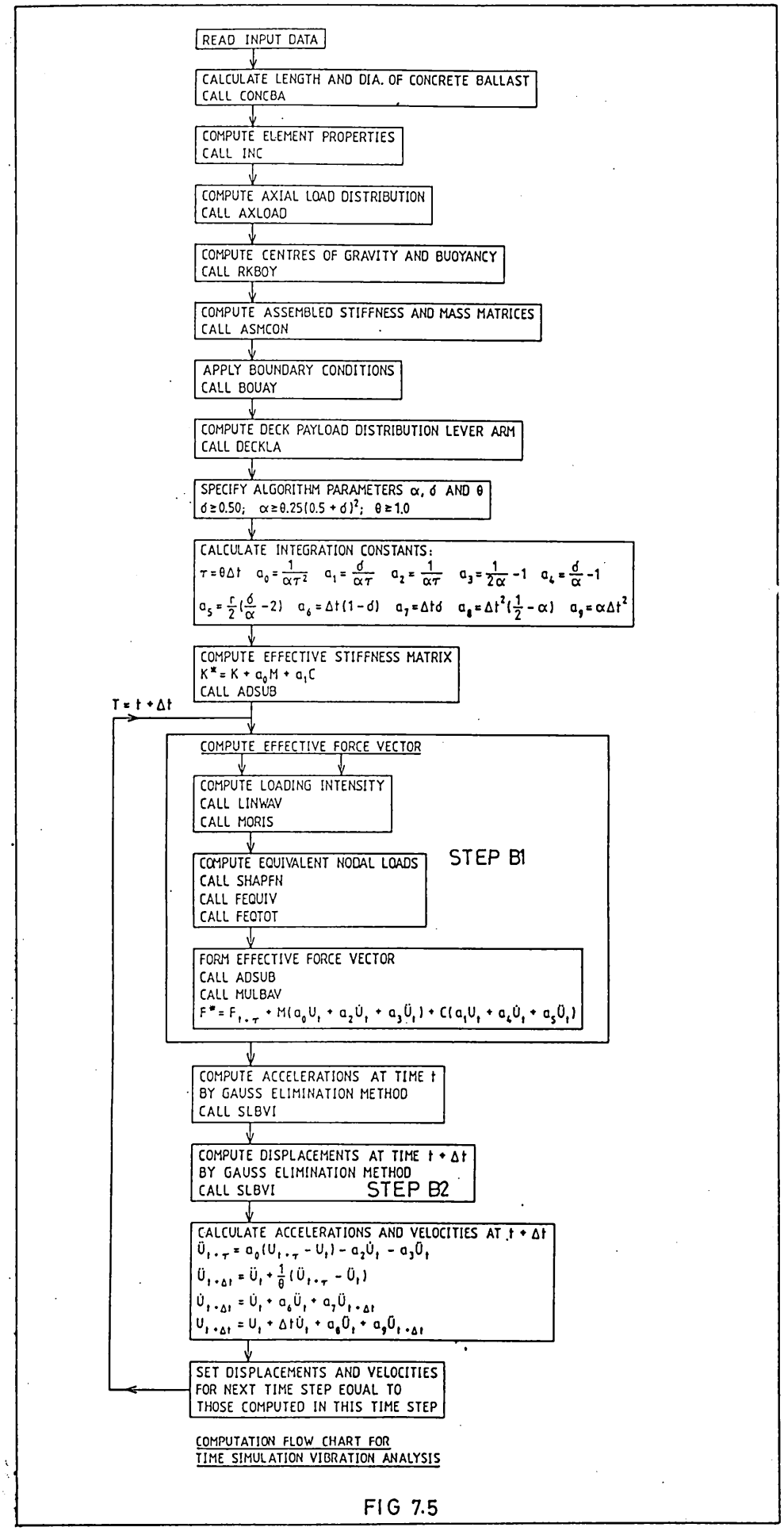

COMPUTATION FLOW CHART FOR
TIME SIMULATION VIBRATION ANALYSIS

FIG 7.5

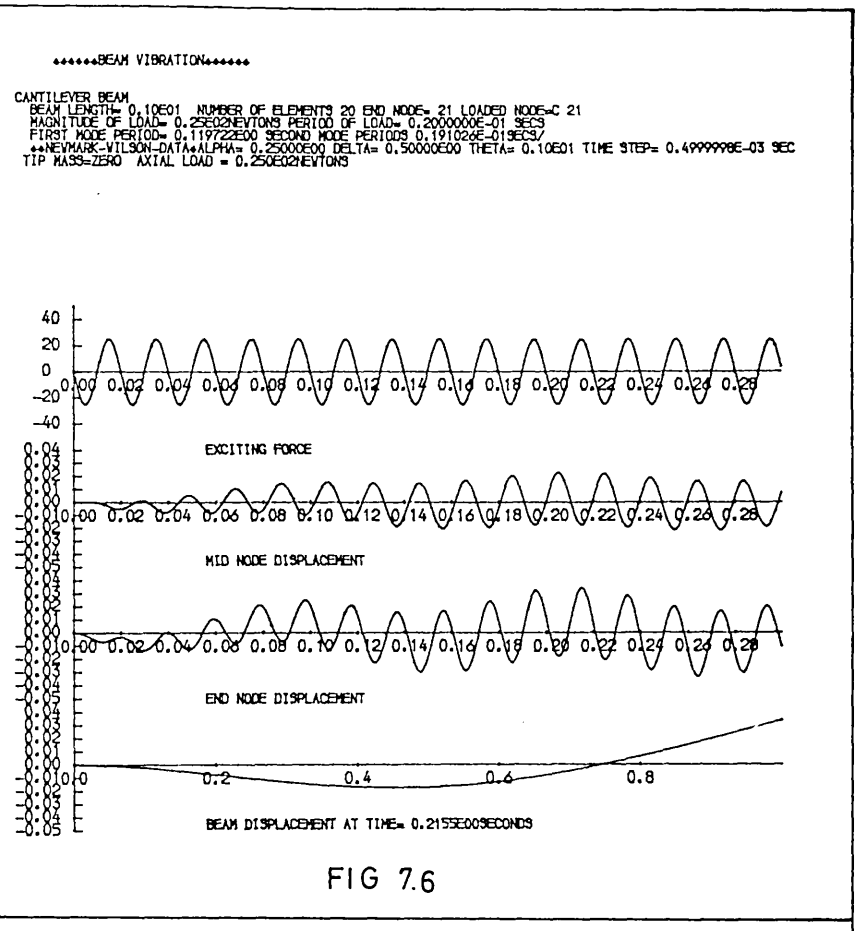
******BEAM VIBRATION******
CANTILEVER BEAM
BEAM LENGTH= 0.10E01 NUMBER OF ELEMENTS 20 END NODE= 21 LOADED NODE=C 21
MAGNITUDE OF LOAD= 0.25E02NEWTONS PERIOD OF LOAD= 0.2000000E-01 SECS
FIRST MODE PERIOD= 0.119722E00 SECOND MODE PERIODS 0.191026E-01SECS/
**NEWMARK-WILSON-DATA*ALPHA= 0.25000E00 DELTA= 0.50000E00 THETA= 0.10E01 TIME STEP= 0.4999998E-03 SEC
TIP MASS=ZERO AXIAL LOAD = 0.250E02NEWTONS
EXCITING FORCE
MID NODE DISPLACEMENT
END NODE DISPLACEMENT
BEAM DISPLACEMENT AT TIME= 0.2155E00SECONDS

FIG 7.6

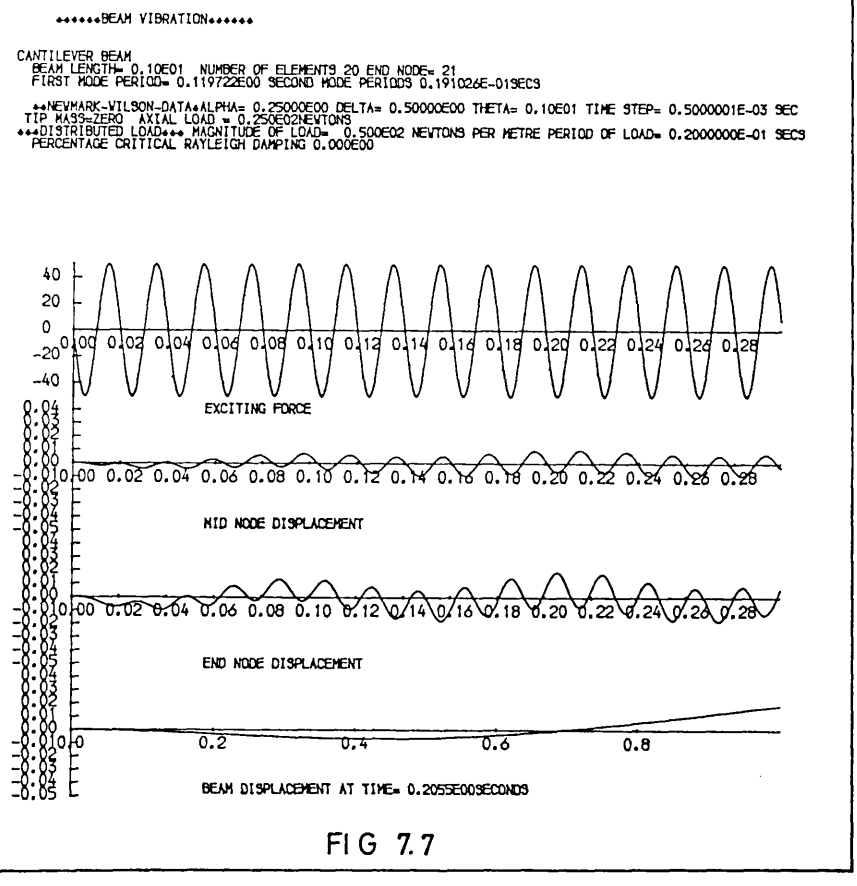
******BEAM VIBRATION******
CANTILEVER BEAM
BEAM LENGTH= 0.10E01 NUMBER OF ELEMENTS 20 END NODE= 21
FIRST MODE PERIOD= 0.119722E00 SECOND MODE PERIODS 0.191026E-01SECS
**NEWMARK-WILSON-DATA*ALPHA= 0.25000E00 DELTA= 0.50000E00 THETA= 0.10E01 TIME STEP= 0.5000001E-03 SEC
TIP MASS=ZERO AXIAL LOAD = 0.250E02NEWTONS
DISTRIBUTED LOAD MAGNITUDE OF LOAD= 0.500E02 NEWTONS PER METRE PERIOD OF LOAD= 0.2000000E-01 SECS
PERCENTAGE CRITICAL RAYLEIGH DAMPING 0.000E00
EXCITING FORCE
MID NODE DISPLACEMENT
END NODE DISPLACEMENT
BEAM DISPLACEMENT AT TIME= 0.2055E00SECONDS

FIG 7.7

applied to the end of the cantilever. The effect of the distributed loading is to attenuate the vibratory response as is observed from fig. 7.7. The response for the distributed load is about 60% of that for the point load.

6.2 Effects of Rayleigh Damping

When frequency domain analysis is used it is necessary to evaluate damping matrix coefficients γ and μ, as discussed in section 3. Time domain analysis reduces this problem to one of selecting an appropriate value for the amount of critical damping β present, for inclusion in the damping term $C\dot{x}$, where $C = 2\beta\omega_n M$.

The effects of zero percent critical Rayleigh damping and 0.5% critical Rayleigh damping on the response of the forced vibration are shown in figs. 7.8 and 7.9, respectively. It is apparent that even this moderate amount of 0.5% damping attenuates the vibratory response significantly.

6.3 Response of Structures to Waves

A computer program based on the flowchart in fig. 7.5 was developed to account for the wave forces, as described, and specify the boundary conditions necessary to ensure rotation about but no translation at the articulated joint. The effects of certain parameters on the forced vibration were then assessed and are presented as follows.

6.3.1 Effects of Geometric Stiffness Matrix

It was noted in the free vibration analysis presented in

chapter 6 that the inclusion of the axial distribution of loading, as reflected in the geometric stiffness matrix, significantly altered the second mode vibration period. Accordingly some analytical results have been obtained to make some assessment of the relative importance of this parameter on the forced vibration in the time domain.

Figure 7.11 shows the response for a structure excited by a wave at the same frequency as the second mode vibration frequency and excluding the geometric stiffness in the analysis. In this case the second mode period is 6.18 seconds. Figure 7.10 shows the response for the same structure but including the geometric stiffness term in the analysis. Accordingly, the second mode period is 6.67 seconds.

The nature of the response is very different in the latter case and it eventually becomes unstable. Clearly then the inclusion of the geometric stiffness in this particular case is very important and to neglect it would be in error.

The structure appropriate to figs. 7.10 and 7.11 has a lower column 12 metres diameter and 50 mm equivalent thickness. The critical Euler buckling load for this section, assuming pinned end conditions, is $\pi^2 EI/L^2$ which equals 771,470KN. The average axial load is 240,000KN. Figure 7.12 shows the distribution of axial loads for this structure. The net compressive loading is apparent and explains the increased vibration period.

Figures 7.13 and 7.14 show the responses from an analysis which imposed average axial loads of 125,000KN and 100,000KN, respectively, on the structure. The response is stable for the latter, whilst that for the former is unstable, indicating a maximum allowable

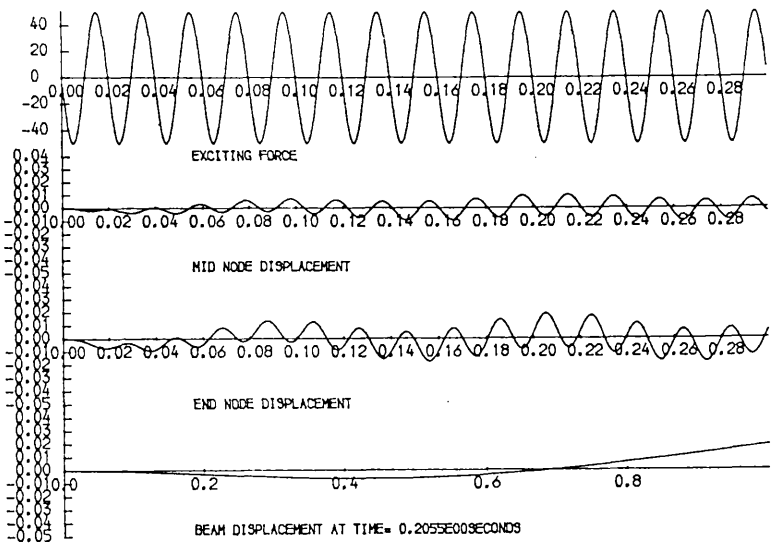
******BEAM VIBRATION******
CANTILEVER BEAM
BEAM LENGTH= 0.10E01 NUMBER OF ELEMENTS 20 END NODE= 21
FIRST MODE PERIOD= 0.119722E00 SECOND MODE PERIODS 0.191026E-019ECS
**NEWMARK-WILSON-DATA*ALPHA= 0.25000E00 DELTA= 0.50000E00 THETA= 0.10E01 TIME STEP= 0.5000001E-03 SEC
TIP MASS=ZERO AXIAL LOAD = 0.250E02NEWTONS
DISTRIBUTED LOAD MAGNITUDE OF LOAD= 0.500E02 NEWTONS PER METRE PERIOD OF LOAD= 0.2000000E-01 SECS
PERCENTAGE CRITICAL RAYLEIGH DAMPING 0.000E00
EXCITING FORCE
MID NODE DISPLACEMENT
END NODE DISPLACEMENT
BEAM DISPLACEMENT AT TIME= 0.2055E00SECONDS

FIG 7.8

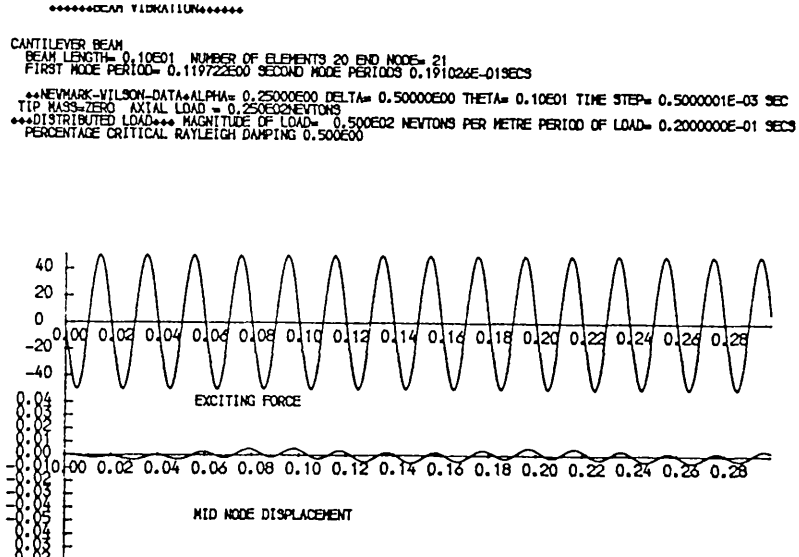
******BEAM VIBRATION******
CANTILEVER BEAM
BEAM LENGTH= 0.10E01 NUMBER OF ELEMENTS 20 END NODE= 21
FIRST MODE PERIOD= 0.119722E00 SECOND MODE PERIODS 0.191026E-019ECS
**NEWMARK-WILSON-DATA*ALPHA= 0.25000E00 DELTA= 0.50000E00 THETA= 0.10E01 TIME STEP= 0.5000001E-03 SEC
TIP MASS=ZERO AXIAL LOAD = 0.250E02NEWTONS
DISTRIBUTED LOAD MAGNITUDE OF LOAD= 0.500E02 NEWTONS PER METRE PERIOD OF LOAD= 0.2000000E-01 SECS
PERCENTAGE CRITICAL RAYLEIGH DAMPING 0.500E00
EXCITING FORCE
MID NODE DISPLACEMENT
END NODE DISPLACEMENT
BEAM DISPLACEMENT AT TIME= 0.2070E00SECONDS

FIG 7.9

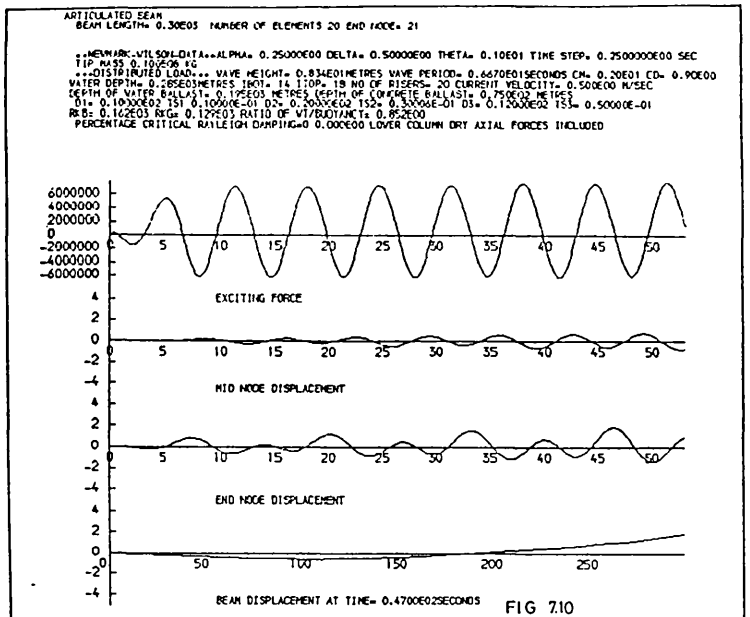

FIG 7.10

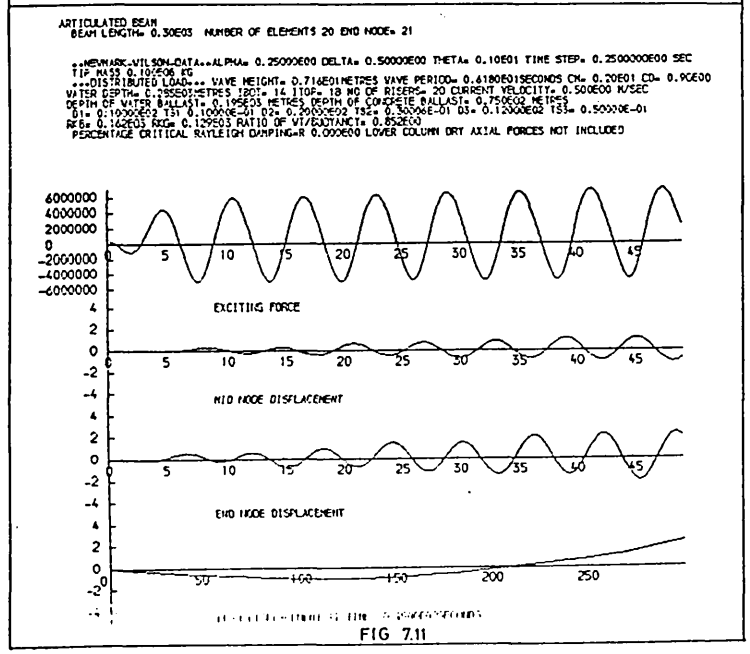

FIG 7.11

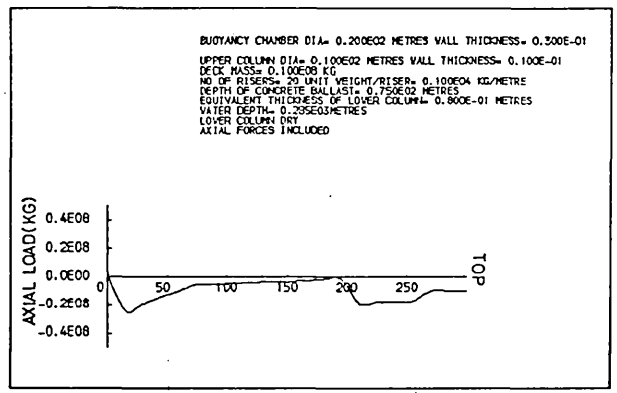

AXIAL DISTRIBUTION OF LOAD ON COLUMN

FIG 7.12

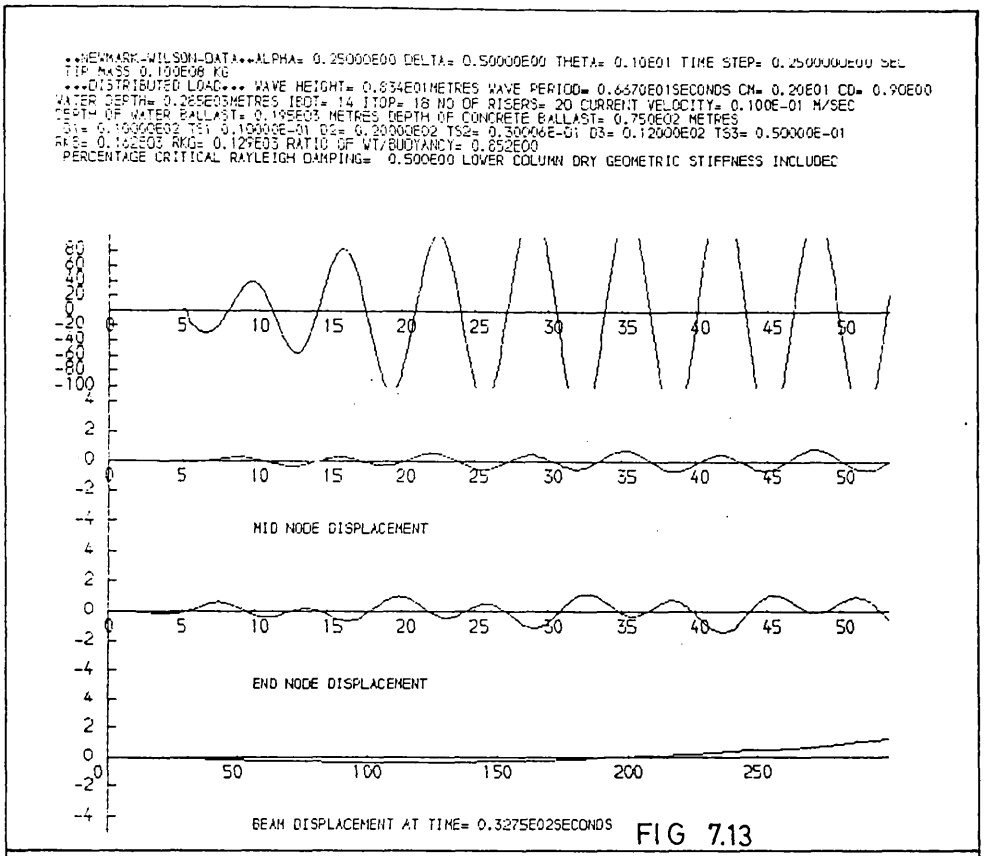

FIG 7.13

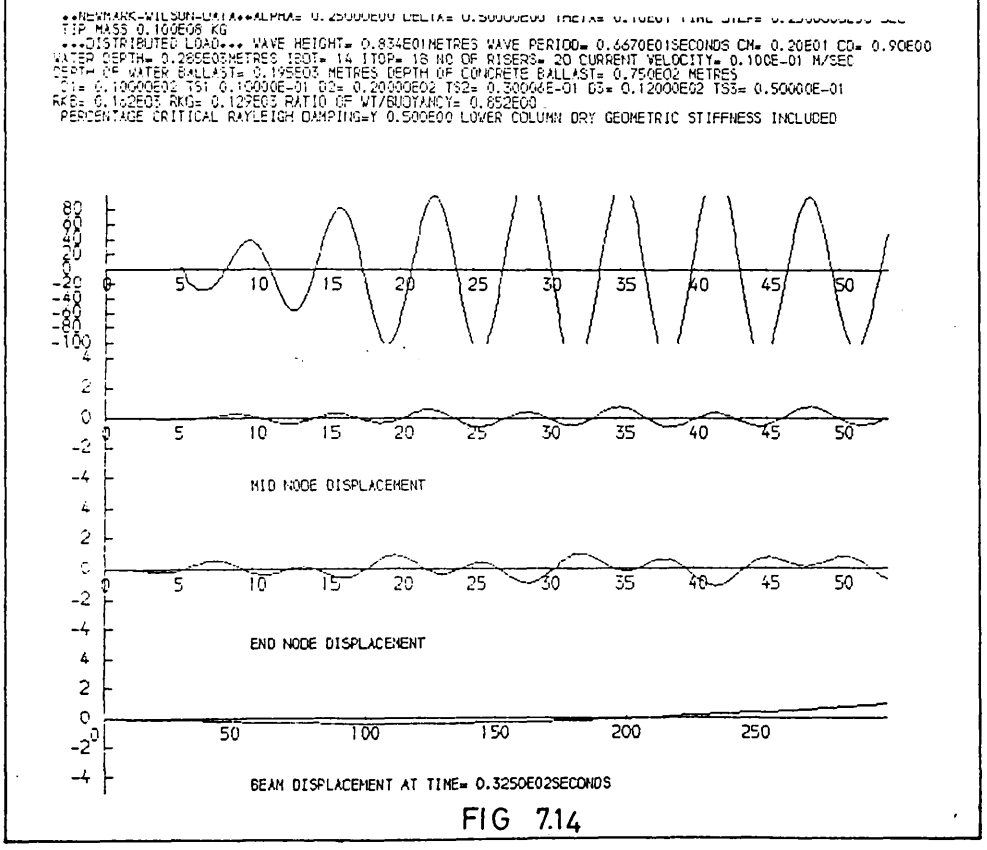

FIG 7.14

axial load of 100,000KN. This load corresponds to an effective length of the structure of 2.77L.

Figures 7.15 and 7.16 show the responses for a structure with a lower column 12 metres diameter and equivalent thickness 65 mm, excluding and including the geometric stiffness in the analysis, respectively. The transient response persists for the latter case but the solution is stable.

This instability, in part, may be attributable to the numerical integration procedure used, although this is thought to be unlikely since the procedure is unconditionally stable. The stability bounds may narrow as vibration frequencies increase for the same length of integration step Δt but this would infer that the solution would become less stable for the structure with the increased flexural rigidity.

The top plot for both these figures is the bending stress at the mid nodal connection as calculated from the nodal rotations which are generated in the analysis. The stress levels are significant. It should be noted, however, that the wave steepness used in the analysis is 0.12 or 80% of the maximum wave steepness.

Figures 7.17 and 7.18 show the responses obtained for a structure with an equivalent thickness of 80mm, excluding and including the geometric stiffness in the analysis, respectively. The transient in the latter is considerably reduced in magnitude but is nevertheless present. Responses are generally about 50% greater than those obtained excluding the geometric stiffness.

++NEWMARK-WILSON-DATA++ALPHA= 0.25000E00 DELTA= 0.50000E00 THETA= 0.10E01 TIME STEP= 0.2500000E00 SEC
TIP MASS 0.100E08 KG
+++DISTRIBUTED LOAD+++ WAVE HEIGHT= 0.637E01METRES WAVE PERIOD= 0.5830E01SECONDS CM= 0.20E01 CD= 0.90E00
WATER DEPTH= 0.285E03METRES IBOT= 14 ITOP= 18 NO OF RISERS= 20 CURRENT VELOCITY= 0.100E-01 M/SEC
DEPTH OF WATER BALLAST= 0.195E03 METRES DEPTH OF CONCRETE BALLAST= 0.750E02 METRES
D1= 0.10000E02 TS1 0.10000E-01 D2= 0.20000E02 TS2= 0.30006E-01 D3= 0.12000E02 TS3= 0.65000E-01
RKB= 0.162E03 RKG= 0.129E03 RATIO OF WT/BUOYANCY= 0.664E00
PERCENTAGE CRITICAL RAYLEIGH DAMPING= 0.500E00 LOWER COLUMN DRY GEOMETRIC STIFFNESS NOT INCLUDED

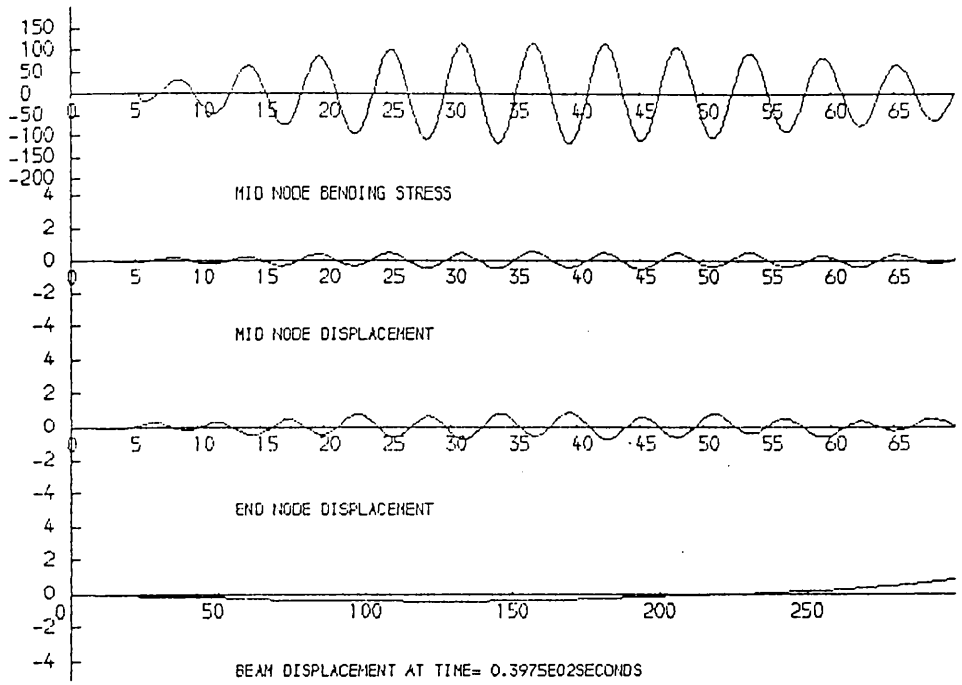

FIG 7.15

++NEWMARK-WILSON-DATA++ALPHA= 0.25000E00 DELTA= 0.50000E00 THETA= 0.10E01 TIME STEP= 0.2500000E00 SEC
TIP MASS 0.100E08 KG
+++DISTRIBUTED LOAD+++ WAVE HEIGHT= 0.720E01METRES WAVE PERIOD= 0.6200E01SECONDS CM= 0.20E01 CD= 0.90E00
WATER DEPTH= 0.285E03METRES IBOT= 14 ITOP= 18 NO OF RISERS= 20 CURRENT VELOCITY= 0.100E-01 M/SEC
DEPTH OF WATER BALLAST= 0.195E03 METRES DEPTH OF CONCRETE BALLAST= 0.750E02 METRES
D1= 0.10000E02 TS1 0.10000E-01 D2= 0.20000E02 TS2= 0.30006E-01 D3= 0.12000E02 TS3= 0.65000E-01
RKB= 0.162E03 RKG= 0.129E03 RATIO OF WT/BUOYANCY= 0.664E00
PERCENTAGE CRITICAL RAYLEIGH DAMPING= 0.500E00 LOWER COLUMN DRY GEOMETRIC STIFFNESS INCLUDED

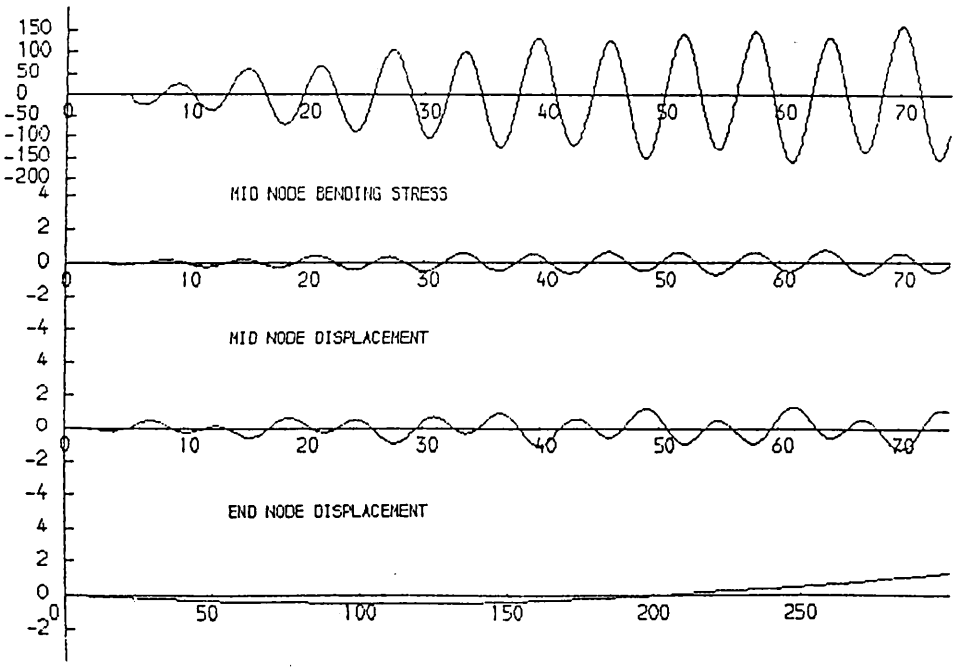

FIG 7.16

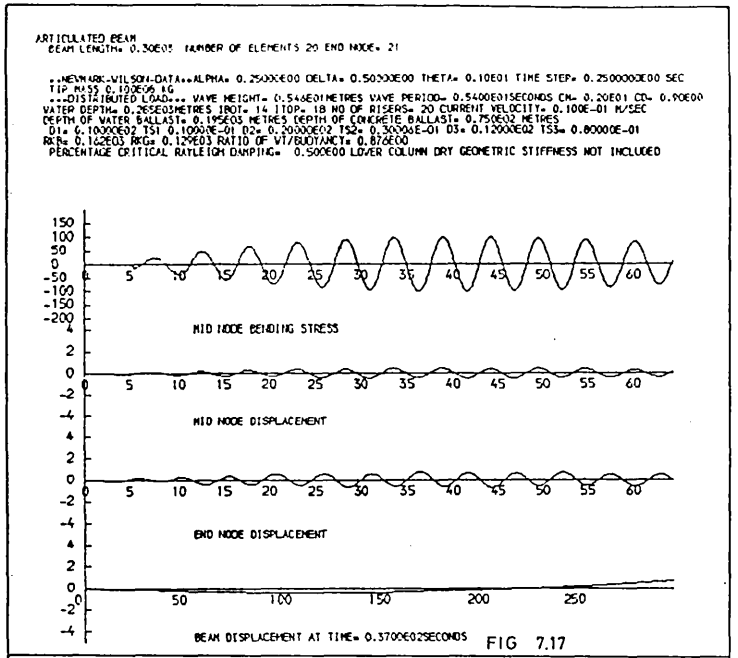

FIG 7.17

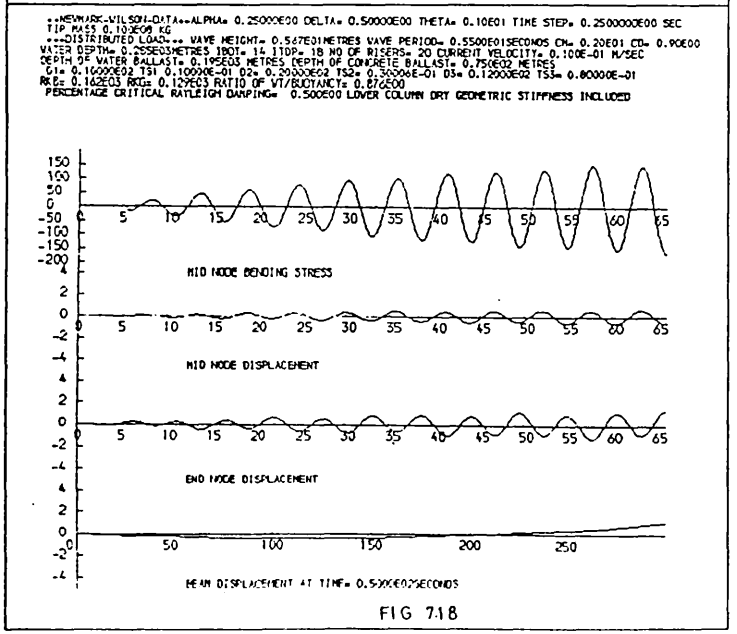

FIG 7.18

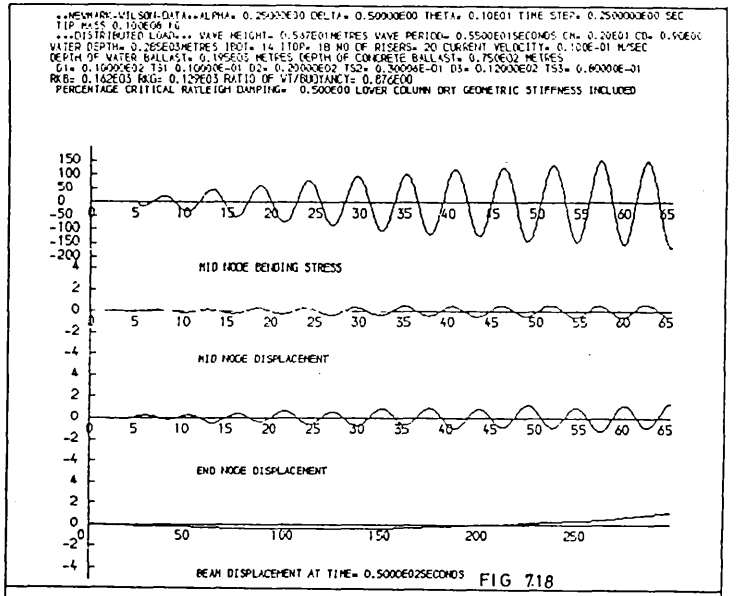

FIG 7.18

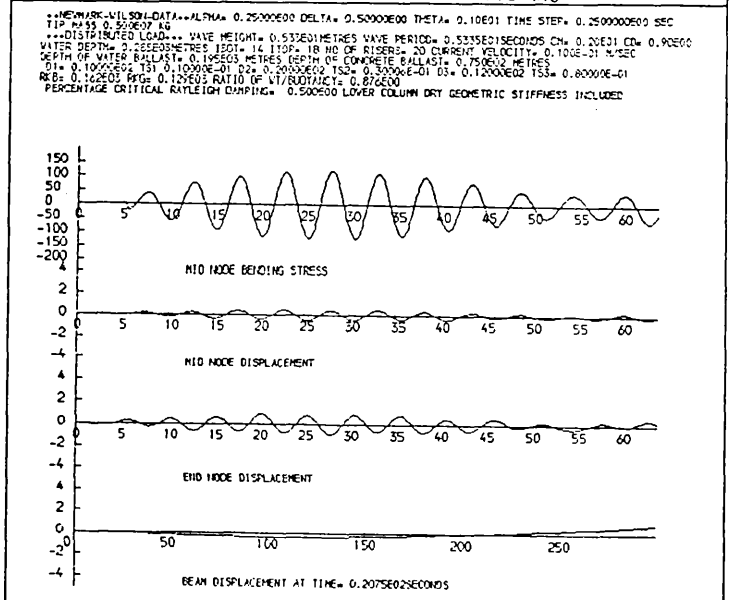

FIG 7.19

6.3.2 Deck Mass Relocation and Configuration

In Chapter 4 it was noted that the dynamic response characteristics of structures were somewhat improved as a consequence of relocating deck masses in the buoyancy chamber. In Chapter 6 it was noted that this would also increase the second mode vibration frequency. The effects of different lateral distributions of deck mass waves was also noted. Accordingly, it is desirable to examine the response in the time domain as a consequence of the partial relocation of deck masses and in terms of varying lateral distribution.

Figure 7.19 shows the response of the structure with 50% of the deck mass relocated in the buoyancy chamber. The second mode vibration period has been reduced to 5.335 seconds. The response is similar to that for the structure with no deck masses relocated (again shown above fig. 7.18 for comparison) for the first seven cycles and is then considerably reduced. There are indications that the response increases thereafter. It is also noted that the maximum stress levels are approximately 75% of the stress levels for the structure with no relocation of the deck mass (fig. 7.18).

In Chapter 6 the lateral distribution of the deck mass was shown to decrease vibration modes as the effective lever arm of the deck mass about the centre line of the deck was increased. Responses have been obtained for two different values of lever arm and are shown in figs.7.20 and 7.21. The first of these is for an effective lever arm of 15 metres, ie an equivalent deck width of 30 metres, and the latter is for an effective lever arm of 30 metres, ie an equivalent deck width of 60 metres. Second mode vibration periods for these two

cases are 5.02 seconds and 4.49 seconds, respectively. The results shown are for waves with these periods. The stress levels at the mid nodal point for the structure with the increased lever arm are approximately 10% greater than those for the other structure.

The width of the deck is a parameter for optimisation together with certain other interdependent parameters, as discussed in Chapter 2, and it is likely that the trend will be towards reductions in the width rather than increases so that the increased stress levels may not be realised. However, the trend is to be noted and will play a part in any optimisation procedures which are undertaken in respect of deck widths, upper support column dimensions, etc.

6.3.3 Effects of C_D on Response

The relatively high frequency of the second mode vibration means that the inertia forces will dominate the response. In the absence of currents, the drag contribution would not normally be expected to play a major part in the response. However it is instructive to obtain a measure of the effects of different levels of hydrodynamic viscous damping and accordingly the results as shown in figs. 7.22 and 7.23 are presented.

These show the response for the structure subject to the same wave and for values of drag coefficient $C_D = 0.9$ and $C_D = 0.6$, respectively. There is no appreciable difference in response for these two values of drag coefficient.

In order to fully assess the effects of the viscous term on the response, it is pertinent to compare responses in the absence of

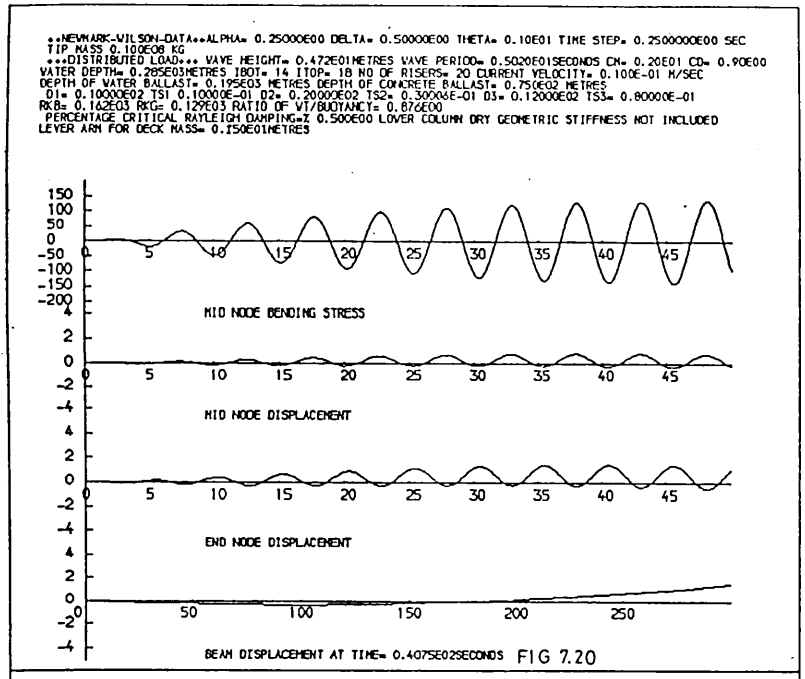

FIG 7.20

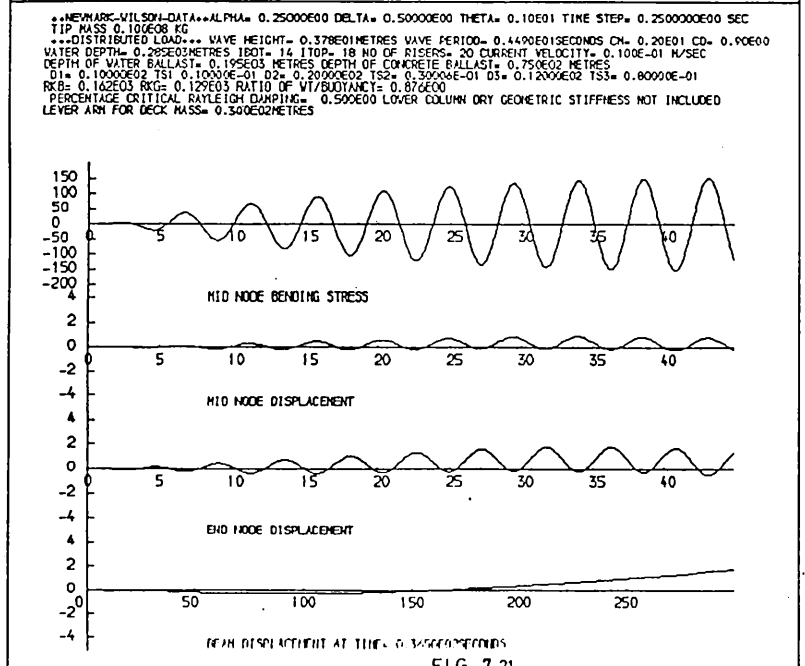

FIG 7.21

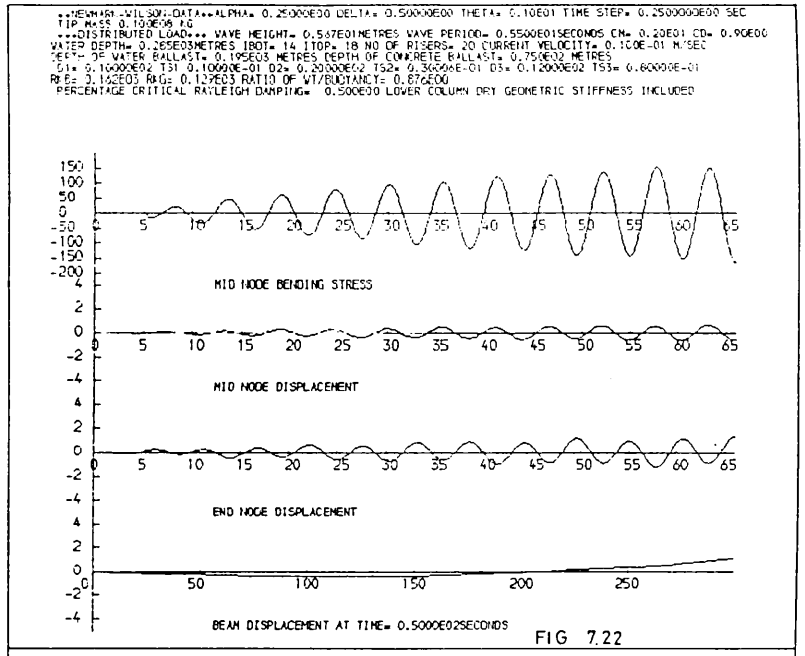

FIG 7.22

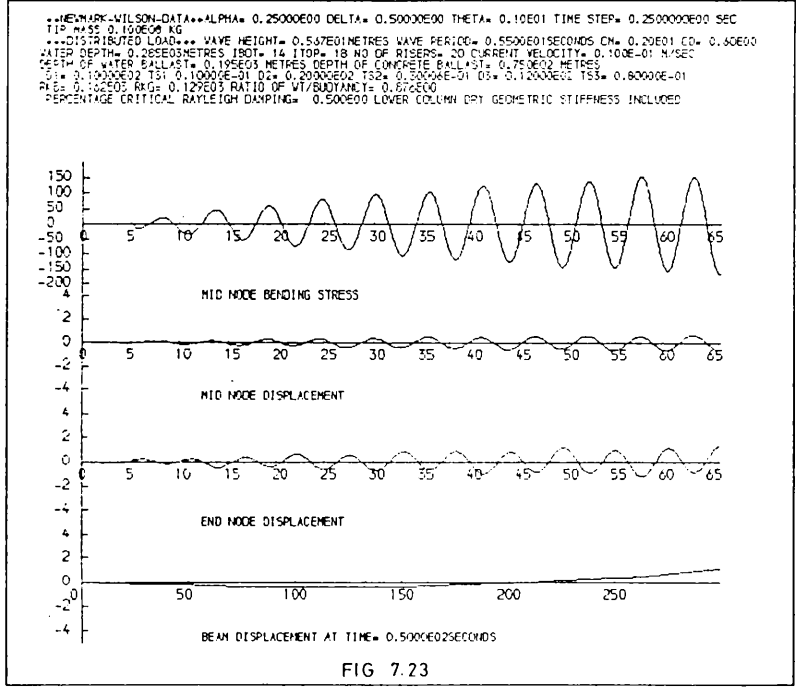

FIG 7.23

any viscous contribution to the forcing functions. Accordingly, figs. 7.24 and 7.25 have been obtained for drag coefficients of $C_D = 0.9$ and C_D = zero, respectively. For both these plots the excursion of the structure in the wave is ignored, in order to make a direct assessment of the contribution of the drag term.

The linearity of the response in fig. 7.25 is apparent and is as would be expected since the forcing function is linear and consists only of the inertia term in the Morison equation. There is no transient response as in fig. 7.24 and, therefore, it is reasonable to attribute the transient response in fig. 7.24., in the main, to the viscous drag contribution to the forcing function.

The transient is also noted to comprise a steady drift component, since the response is not sinusoidal about the vertical axis. Further experimental observations, relevant to this observation, are made in section 7 of this chapter. The transient is responsible for mean increased responses. However, the magnitude of the relative response of the top and middle of the column is reduced as are bending stresses as shown in fig. 7.24 ie, including the relative speed squared term. Maximum bending stresses in fig. 7.25 are approximately $300N/mm^2$ whereas in fig. 7.24 the maximum stresses are approximately $230N/mm^2$

6.3.4 Effects of Current on Response

The previous section highlights the importance of the viscous term in damping the responses and stress levels. Steady currents, in combination with waves, could therefore be expected to have some damping effect and this can be expected to increase as current

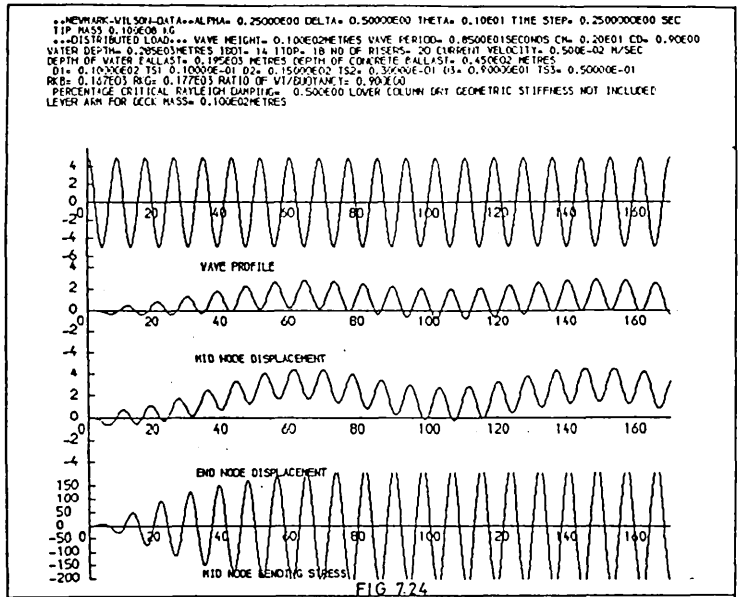

FIG 7.24

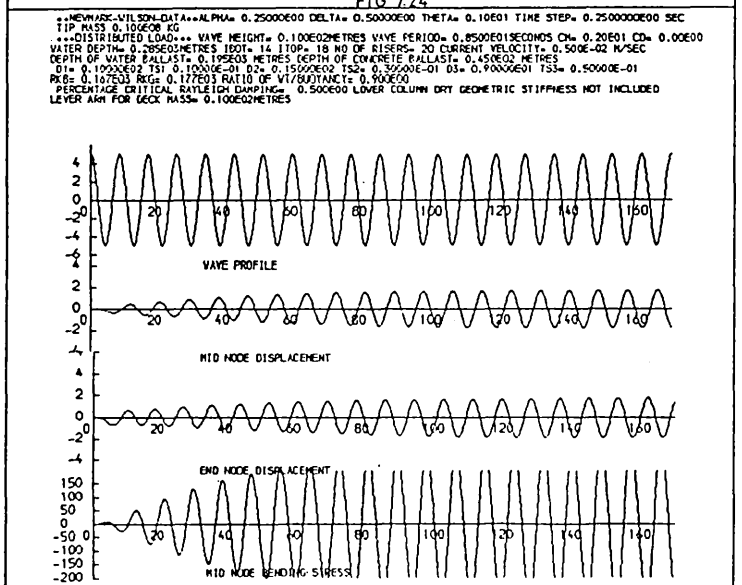

FIG 7.25

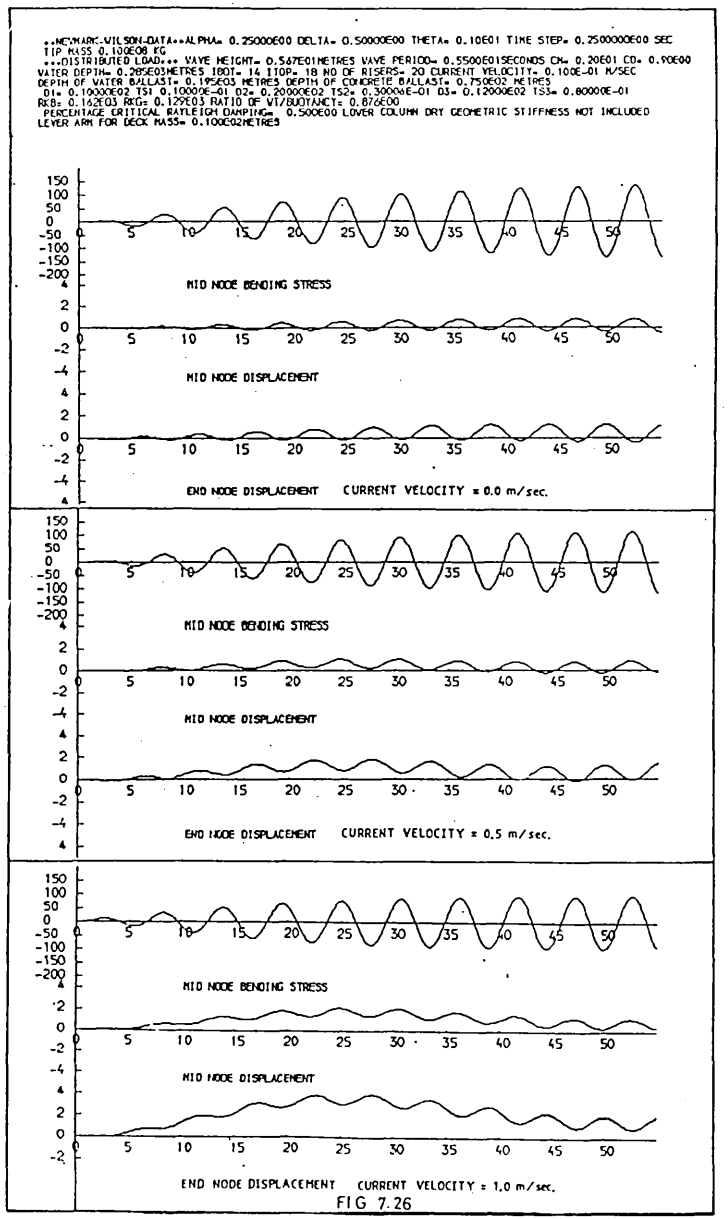

FIG 7.26

velocities increase. The results obtained for zero current, 0.5 m/sec and 1 m/sec acting co-linearly with the waves are presented in fig. 7.26.

The mean response of the end nodal point is increased and this is to be expected. The attenuation in the mid nodal point bending stress for the increased current is apparent and is a measure of the damping influence of the imposed current on the response.

6.3.5 Response to Waves with Frequency less than the second Mode Vibration Frequency

The level of excitation possible at the second mode vibration frequency has been observed. However, it is also instructive to observe responses of the structure when subject to waves of frequencies less than the second mode vibration frequency.

Figures 7.27 and 7.28 show responses for waves of period 6 seconds and 7 seconds, respectively. The response is attenuated as shown in fig. 7.28 and this is to be expected in consideration of the reduction in the dynamic magnification factor as the ratio of exciting frequency to natural frequency decreases. This is readily appreciated from fig. 7.4 which shows the dynamic magnification as a function of the ratio of exciting frequency to natural frequency.

Figures 7.29 and 7.30 are the responses obtained for an 8 second wave and a 10 second wave, respectively. The mid nodal point and the end nodal point are now in phase and the most striking feature in the latter is the very marked reduction in stress levels.

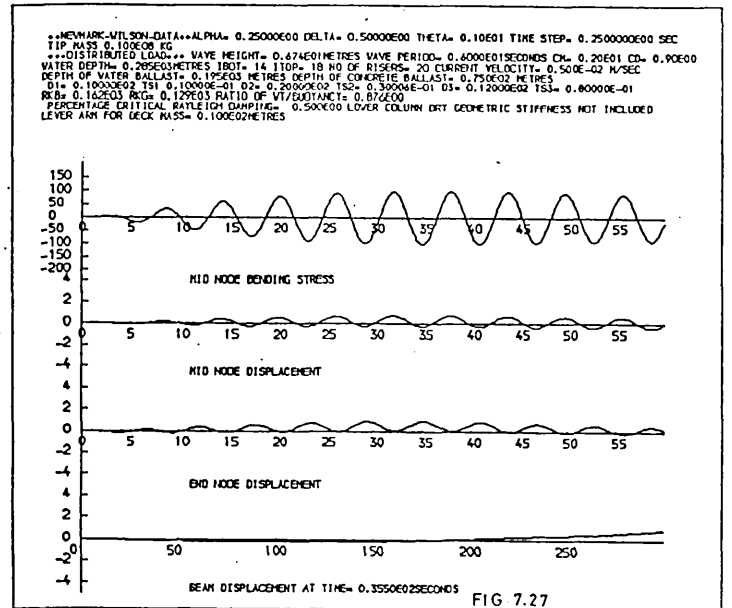

FIG 7.27

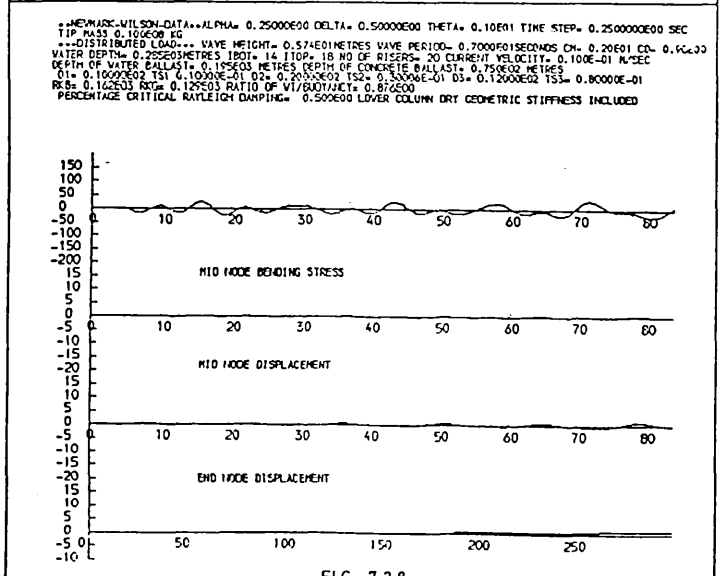

FIG 7.28

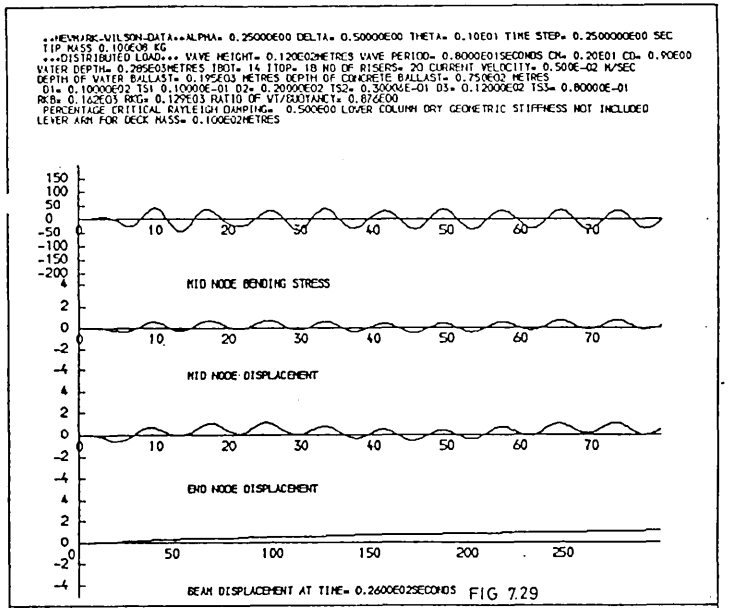

FIG 7.29

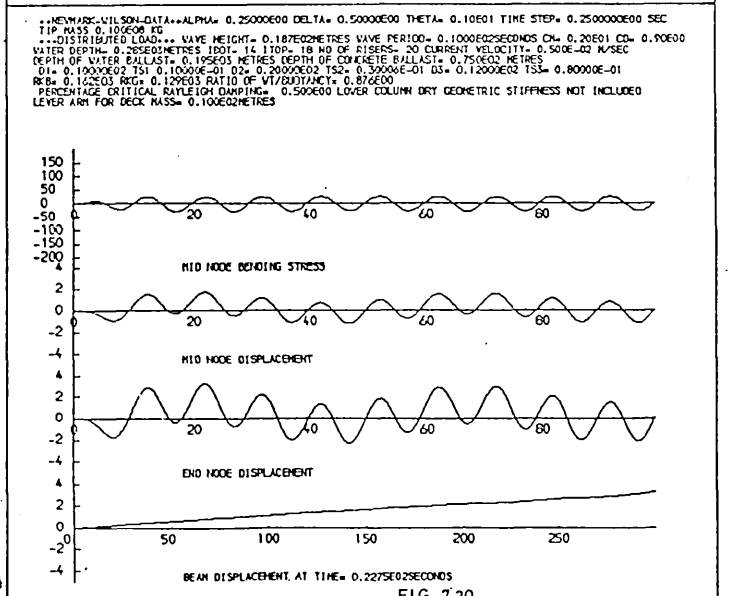

FIG 7.30

It is also interesting to observe the presence of the transient oscillation which is harmonic with the natural period in pitch of the structure and is qualitatively very similar to the transient which was predicted in the rigid body analysis presented in Chapter 4.

6.3.6 Effects of Wave Groups on Response

The rigid body dynamic analysis in chapter 5 describes the transient oscillations possible for certain wave frequencies and groups of waves. The transient was seen to increase considerably for wave groups with a frequency harmonic with the natural period in pitch of the structure.

For completeness, it is pertinent to examine the effects of wave groups on the elastic vibration responses. It is conceivable that a group of waves having the same period as the fundamental pitch period, could be generated by two waves of slightly different frequency but approximately equal to the first flexural response mode frequency.

Figure 7.31 shows the response for a structure which has a fundamental pitch period of approximately 95 seconds and a first flexural response mode period of 8.5 seconds. The wave group is generated by two separate wave trains with periods of 8.2 seconds and 8.93 seconds each with a height of 5 metres. The average wave period of 8.5 seconds is coincident with the first flexural mode period. The attenuation in the response in the region of diminished wave height is to be expected as is the transient response. Figure 7.32 has been prepared for comparison and shows the results for a regular wave with a period of 8.5 seconds and height 10 metres.

++NEWMARK-WILSON-DATA++ALPHA= 0.25000E00 DELTA= 0.50000E00 THETA= 0.10E01 TIME STEP= 0.2500000E00 SEC
TIP MASS 0.100E08 KG
+++DISTRIBUTED LOAD+++ WAVE HEIGHT= 0.575E01METRES WAVE PERIOD= 0.8500E01SECONDS CM= 0.20E01 CD= 0.90E00
WATER DEPTH= 0.285E03METRES IBOT= 14 ITOP= 18 NO OF RISERS= 20 CURRENT VELOCITY= 0.500E-02 M/SEC
DEPTH OF WATER BALLAST= 0.195E03 METRES DEPTH OF CONCRETE BALLAST= 0.450E02 METRES
D1= 0.10000E02 TS1 0.10000E-01 D2= 0.15000E02 TS2= 0.30000E-01 D3= 0.90000E01 TS3= 0.50000E-01
RKB= 0.167E03 RKG= 0.177E03 RATIO OF WT/BUOYANCY= 0.900E00
PERCENTAGE CRITICAL RAYLEIGH DAMPING= 0.500E00 LOWER COLUMN DRY GEOMETRIC STIFFNESS NOT INCLUDED
LEVER ARM FOR DECK MASS= 0.100E02METRES T1 = 8.2 secs ; T2 = 8.93 secs

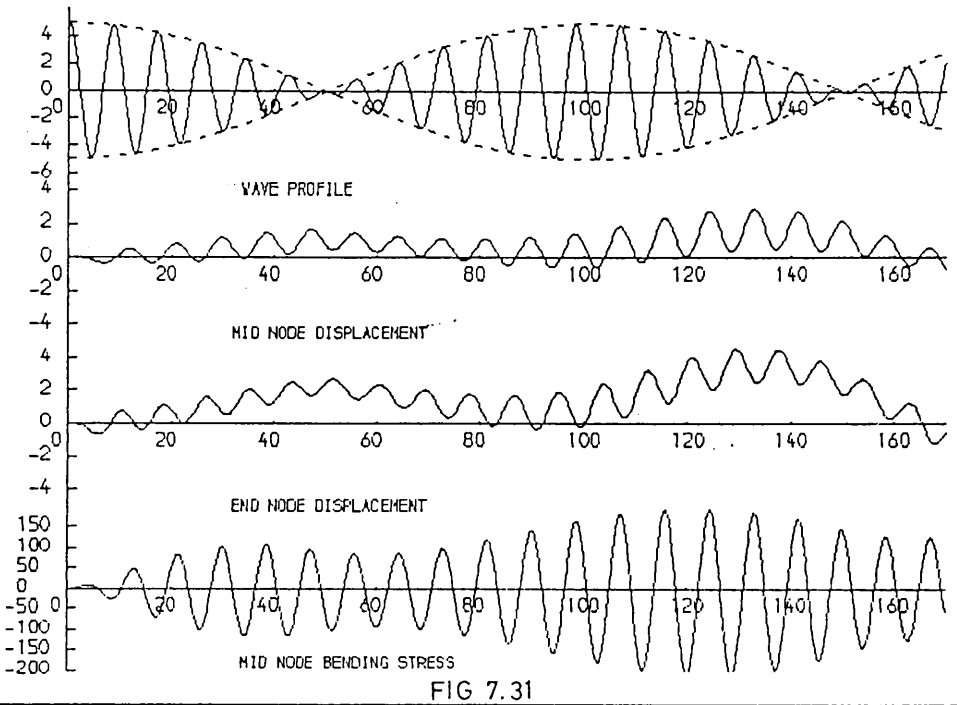

FIG 7.31

++NEWMARK-WILSON-DATA++ALPHA= 0.25000E00 DELTA= 0.50000E00 THETA= 0.10E01 TIME STEP= 0.2500000E00 SEC
TIP MASS 0.100E08 KG
+++DISTRIBUTED LOAD+++ WAVE HEIGHT= 0.100E02METRES WAVE PERIOD= 0.8500E01SECONDS CM= 0.20E01 CD= 0.90E00
WATER DEPTH= 0.285E03METRES IBOT= 14 ITOP= 18 NO OF RISERS= 20 CURRENT VELOCITY= 0.500E-02 M/SEC
DEPTH OF WATER BALLAST= 0.195E03 METRES DEPTH OF CONCRETE BALLAST= 0.450E02 METRES
D1= 0.10000E02 TS1 0.10000E-01 D2= 0.15000E02 TS2= 0.30000E-01 D3= 0.90000E01 TS3= 0.50000E-01
RKB= 0.167E03 RKG= 0.177E03 RATIO OF WT/BUOYANCY= 0.900E00
PERCENTAGE CRITICAL RAYLEIGH DAMPING= 0.500E00 LOWER COLUMN DRY GEOMETRIC STIFFNESS NOT INCLUDED
LEVER ARM FOR DECK MASS= 0.100E02METRES

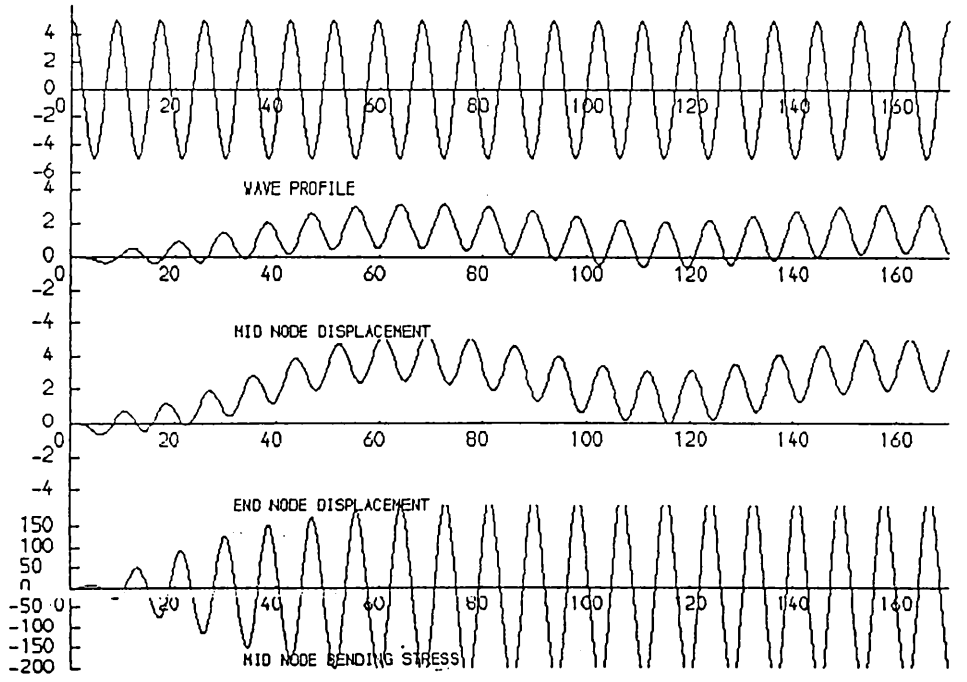

FIG 7.32

The response for the top and the middle of the column is antiphase as expected and the bending stress at the middle is of the order of $\pm 200 N/mm^2$.

Transient responses for both figures are of the same order of magnitude. However stress levels for the wave group response of fig. 7.31 are somewhat less than for the regular wave.

6.3.7 Full Fixity Encastre Column

The effects of fixity on the bottom joint was examined in Chapter 6 in terms of free vibrations. It is instructive to examine the response of a structure with full fixity at the bottom and, accordingly, fig. 7.33 has been prepared.

Plots of the bending stress at the bottom and middle of the column are given together with displacement at the top and the overturning moment on the base of the structure. The response of the top of the structure, as shown in fig. 7.33, bears direct comparison with the response for the structure shown in fig. 7.30 which is for an articulated column of the same structural dimensions. There is a modest reduction in response as shown in fig. 7.33 and the magnitude of the overturning moment on the base is reduced. The transient oscillation harmonic with the first flexural response mode is also apparent.

Figure 7.34 shows the response for a structure with a payload of 50,000KN and a lower column 6 metres in diameter. The transient oscillation is apparent. However, it is not harmonic with the first

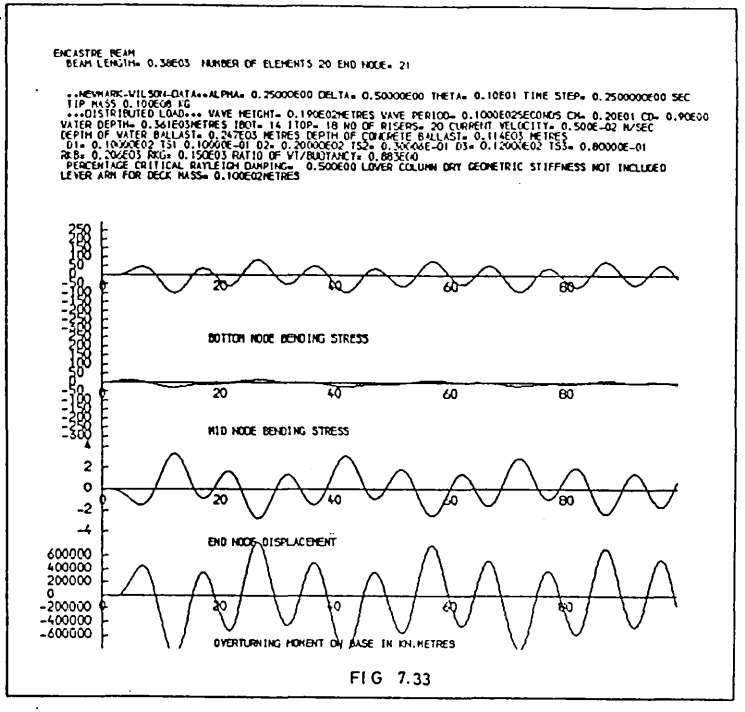

FIG 7.33

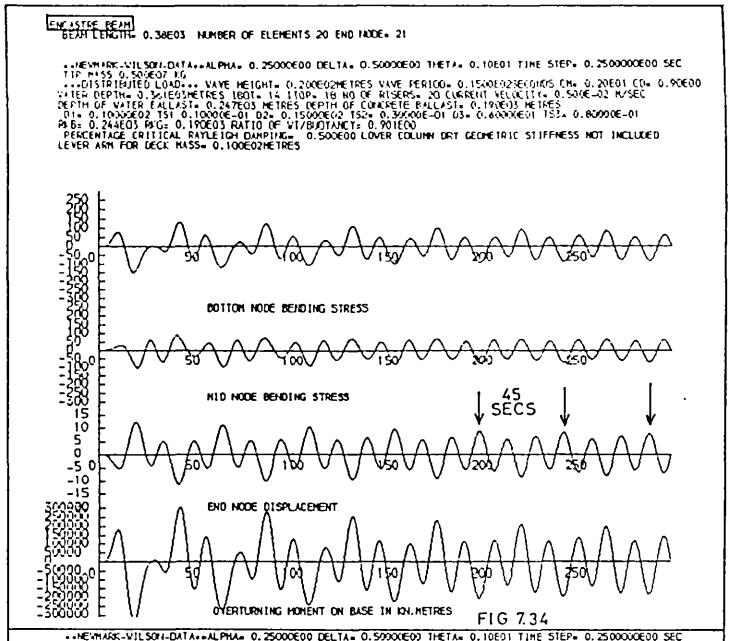

FIG 7.34

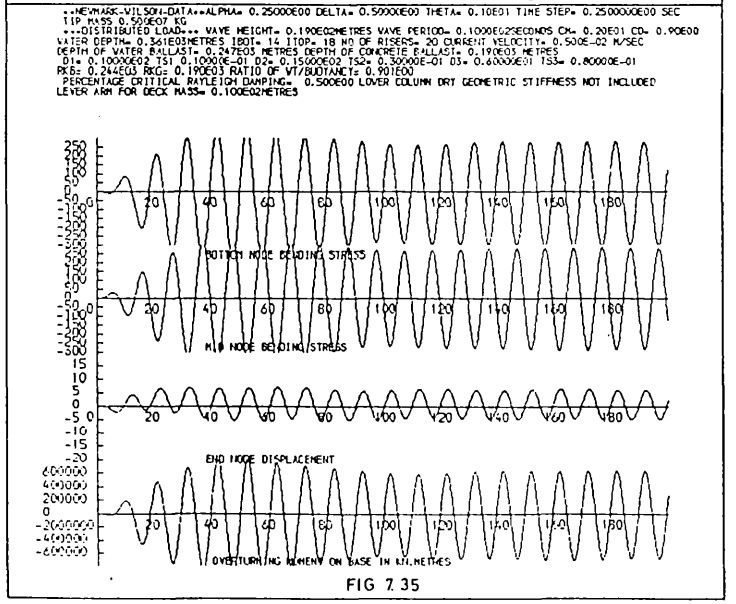

FIG 7.35

flexural response mode, which for this structure is approximately 90 seconds (see fig. 6.32), but appears to have a frequency of twice the first flexural response mode. This response is analogous to the Mathieu instability type of reponse, as was investigated in Chapter 5 of this study, and is particularly noteworthy in that the wave frequency is six times the first flexural response frequency. This is an important observation since it is not suggested by any formal theory.

By way of confirmation of the second flexural response mode, fig. 7.35 has been prepared and shows the response for a 10 second wave. The anti-phase of the top and middle displacements is noted from observation of the bending stress plots for the bottom and middle points on the structure.

7. EXPERIMENTAL OBSERVATIONS

Any analytical procedures applied to the dynamic analysis of articulated columns must be verified before the use of such procedures can proceed with confidence to their application to prototype structures. Experimental data may suffer certain limitations in respect of scaling but the underlying physical trends can be observed by this means. The value of experimental data in the case of the rigid body dynamic analysis was noted in Chapters 4 and 5 and the results obtained confirm certain response characteristics as predicted analytically.

It is very difficult to manufacture an experimental model which scales both physical and dynamic elastic vibration characteristics of a prototype articulated column. It is necessary to

reduce the flexural rigidity of the lower column by some means, so that the resulting vibration frequencies will be within the range which the wavemaker can generate. At the University of Glasgow the experiment tank, which measures 76 metres x 4.6 metres x 2.4 metres, has a wavemaker capable of generating waves with maximum frequencies of the order of 2Hz. Accordingly, the design of the model must be such that the maximum second mode frequency is of this order of magnitude.

It is only possible to achieve frequencies of the order desired by:-

a. reducing the diameter of the lower column and by using a material such as aluminium which has linear elasticity for a fairly small stiffness value, ie $6.9.10^{10} N/mm^2$ (c.f. steel $21.10^{10} N/mm^2$, and

b. by the addition of 'lumped' masses attached to the lower column.

With these considerations in mind the experimental model, as shown in fig. 7.36, was designed and constructed. The use of lead washers as 'lumped' masses allows for a range of mass distributions and, therefore, it is possible to adjust the vibration frequency in this way. Buoyancy is provided by the 112 mm diameter PVC tube which is of annular construction, the inner annulus being flooded. The experimental model thus constructed bears little resemblance to a scaled down prototype articulated column but this is not important as the intention is to validate analytical techniques and the experimental arrangement can be modelled precisely in the analysis. This aspect is described in more detail in section 7.3.

It was desired to measure the response of the top and mid

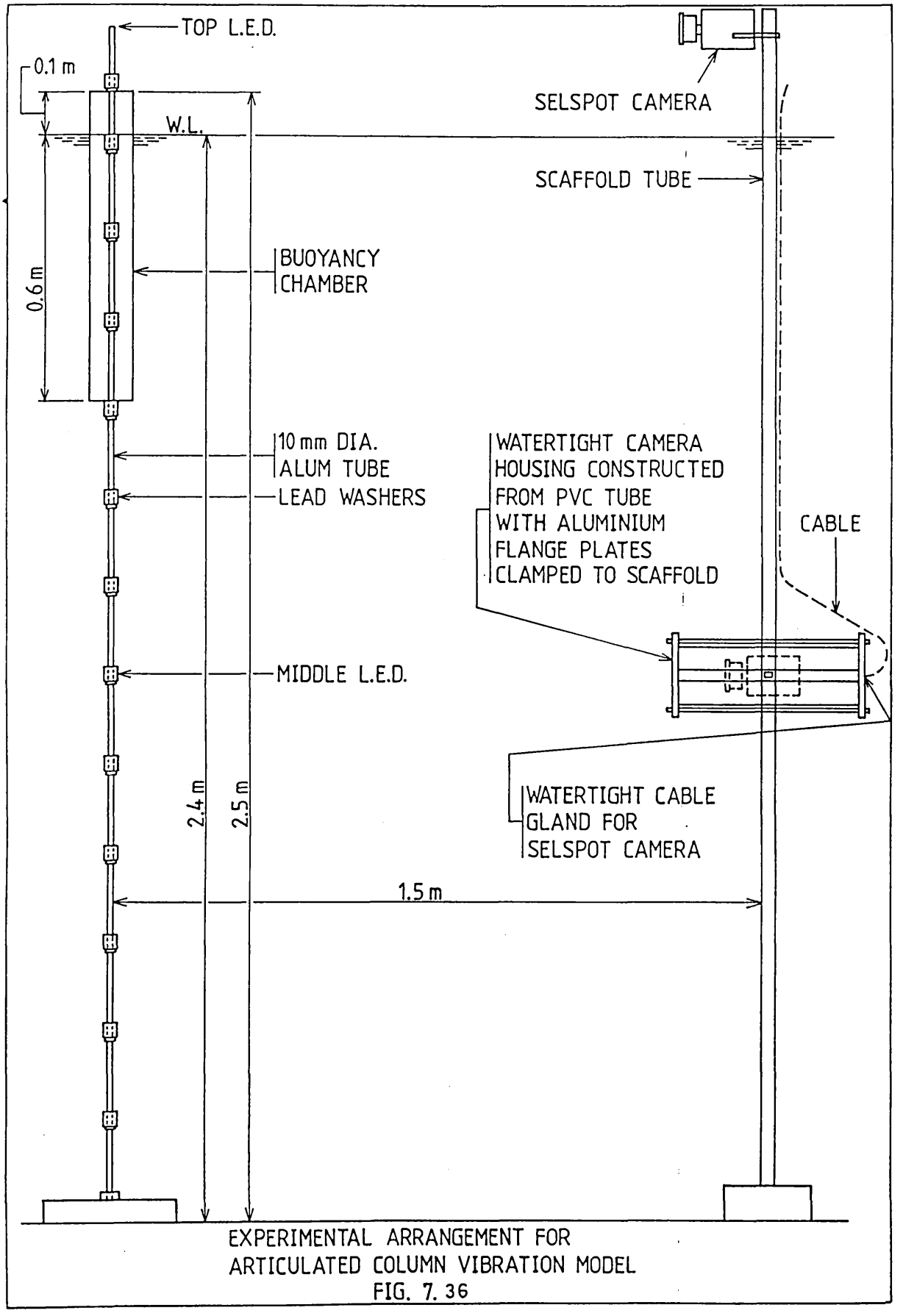

EXPERIMENTAL ARRANGEMENT FOR ARTICULATED COLUMN VIBRATION MODEL

FIG. 7.36

point of the column. Conventional LVDT's and their attachments would impart unacceptably high damping on the structure and it was decided, therefore, to use a Selspot camera with light emitting diodes attached to those locations which were to be monitored. A special waterproof camera housing was constructed and this contained the Selspot camera used to monitor the movement of the mid point of the column. The arrangement of the cameras relative to the model is shown in fig. 7.36.

In order to achieve a satisfactory quality of output signal from the submerged camera it was necessary to place it to within 1.5 metres of the model. However, the submerged depth of the camera is such that it is unlikely that the camera housing will affect the flow field significantly. The output signals from both Selspot cameras and the wave probe were recorded on paper by means of a pen recorder.

7.1 Description of Model Tests

It was primarily intended to obtain experimental data on the forced vibration at the second vibration mode frequency. The construction of the model allows for adjusting the distribution of equal lumped masses on the lower column and at the top of the column. By this means it is possible to achieve the same vibration frequency for different lumped masses on the lower column by adjusting the mass at the top of the column. This makes it possible to examine and verify the influence of deck masses on the vibration characteristics.

Five series of tests were completed for the frequencies shown in Table 7.1. For each condition, waves of heights varying between 14 mm and 95 mm were generated and the response of the top and middle

of the column observed and recorded on paper tape. The tabulated results of the tests are given in Appendix 7.1. The distribution of mass for the five conditions examined are as shown in Table 7.1.

The number of lead washers allocated to each nodal connection point along the length of the structure having been fixed, it was necessary to 'tune' the structure. By adding lead washers to the top of the structure the natural frequency is changed. By this means, the required amount of mass necessary at the top of the model could be determined by observing the magnitude of the anti-phase response of the top and middle of the structure. The amount of mass at the top was adjusted until the anti-phase response was observed to be maximum for a wave at the specified frequency.

It was not possible to achieve precisely the same frequency for all conditions, as can be seen from Table 7.1. However, conditions 2-5 are within 4% of each other. The greatest error is for condition 1 which had a frequency of some 10% greater than those for conditions 3, 4 and 5.

Test Condition	Weight per Nodal Point (Kg)	Weight at Top (Kg)	Frequency (Hz)
1	0.089	0.379	1.3
2	0.1115	0.4	1.22
3	0.1338	0.3568	1.18
4	0.156	0.2899	1.175
5	0.223	0	1.175

Table 7.1 Experimental Test Conditions

7.2 Experimental Results

Figure 7.37 shows a typical pen recording obtained for one of the conditions. Plot 1 is the wave profile. Plot 2 is the response of the top of the column and plot 3 is the response of the middle of the column. These are not phase compensated and the phase relationship is shown so that the correction must be applied in comparing the responses of the top and middle of the column. The phase difference between plots 2 and 3 is three divisions on the recording paper, ie plot 2 is three divisions in advance of plot 3. By applying this correction it is observed that the responses are anti-phase. The calibration for the two light emitting diodes (LED's) was not the same, the signal for the middle LED being greater than that for the top LED.

It can be seen from fig. 7.37 that a transient oscillation is present and is harmonic with the natural period of the structure in pitch. Figure 7.37 also shows a steady drift offset of the structure from the vertical and this is in proportion for both the top and the middle displacements as would be expected.

Figures 7.38 to 7.41 show the wave frequency oscillatory response part of the top and middle displacements as a function of wave height for each test condition. In all cases the displacement at the middle of the column is greater than that at the top. This is in agreement with the free vibration eigenvalue analysis of the model structure and is a consequence of the very slender lower column. The displacements are greatest for condition 1, ie the condition with the maximum amount of mass at the top of the column. The displacements

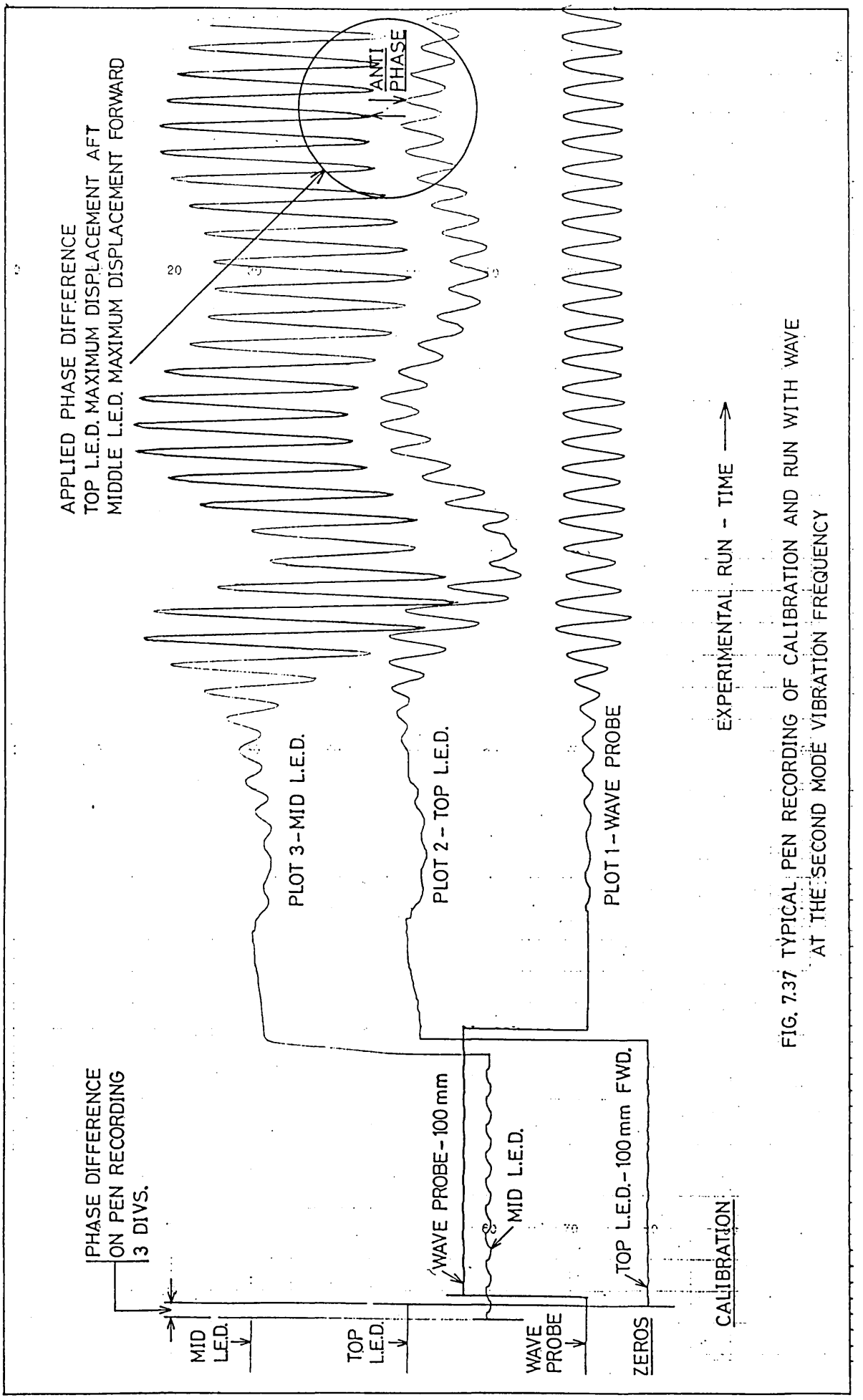

FIG. 7.37 TYPICAL PEN RECORDING OF CALIBRATION AND RUN WITH WAVE AT THE SECOND MODE VIBRATION FREQUENCY

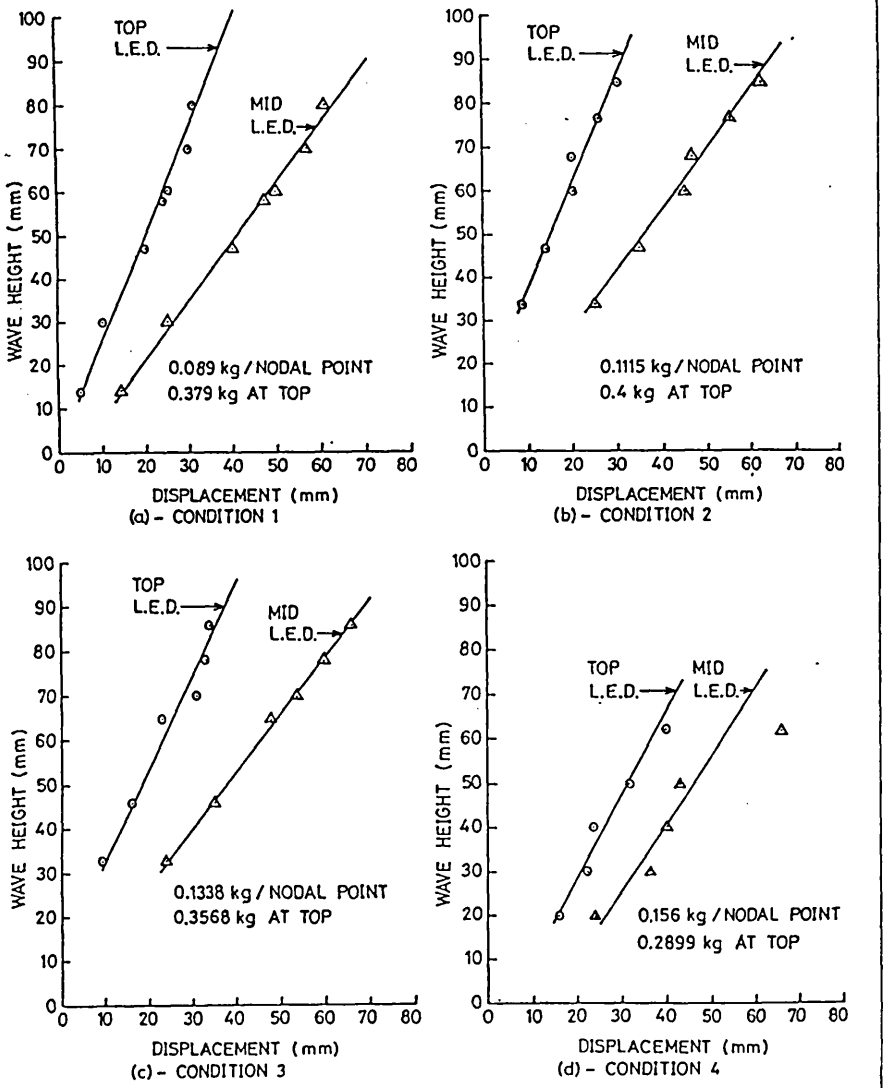

PLOTS OF EXPERIMENTAL RESULTS FOR MODEL ARTICULATED COLUMN

FIG. 7.38 — 7.41

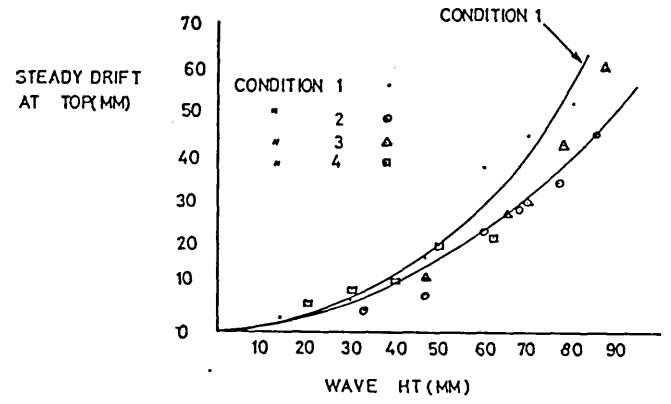

EXPERIMENTAL RESULTS FOR FLEXIBLE ARTICULATED COLUMN

FIG 7.42

decrease as the amount of mass at the top is reduced and this is to be expected.

It is also observed that in general the ratio of the middle displacement to the top displacement decreases with increasing wave height. From fig. 7.38 it is seen that the ratio of middle to top displacement is 2.66 for a wave height of 15 mm and decreases to 1.9 for a wave height of 80 mm. The decrease in the ratio is most likely to be attributed to the viscous speed squared drag force on the lower column.

The steady drift from the vertical is also seen to increase as a function of the wave height and this is to be expected since drift forces are a function of the square of the wave height.

Plots of steady drift as a function of wave height for each test condition are shown in fig. 7.42. The results for condition 1 display the most marked variation of steady drift with wave height. The results for conditions 2, 3 and 4 are quite closely grouped together. Nevertheless, the trend for steady drift to decrease, as the mass at the top decreases, is evident.

7.3 Structural Assemblage and Computer Implementation

The Computer programs described in Chapter 6 (for the eigenvalue solution) and in this chapter (for the time simulation analysis) were modified to account for the geometry and mass distribution of the model, as shown in fig. 7.36.

Analytical results for the second mode vibration frequencies

were found to be within 5% of the frequencies at which the models were found to have the greatest responses. Analytical trends in respect of the top and middle displacements are in accord qualitatively with the experimental results in that the displacements increase with increasing top mass, as does the ratio of the middle to top displacements. This good agreement is taken as confirmation of the adequacy of the program in predicting frequencies.

The buoyancy chamber on the model is fixed to the aluminium tubing by means of a screwed connection at the bottom and a close fitting locating connection at the top. There may be,therefore, some discontinuity in fixity at these locations and this might be expected to slightly affect the stiffness. However, the good agreement with the analysis and experiment confirms that any errors in this respect are likely to be minimal.

A linear elastic analysis has been performed and it has been assumed that the PVC buoyancy chamber behaves elastically and has a value for Young's modulus of elasticity of $2.75.10^{3} N/mm^{2}$. PVC is not truly linear elastic but the errors for small strains will be minimal and are not thought to contribute significantly to the analysis.

The lead washer 'lumped' masses are incorporated into the analysis by adding the amount to the relevant mass corresponding to the translational degree of freedom pertaining to the nodal connection considered.

Thirteen finite elements each 200mm in length have been used in the analysis. The bottom of the buoyancy chamber corresponds to nodal connection number 10 and the top corresponds to a mid element

point but this has been allowed for in the assembly of the mass and stiffness matrices.

7.4 Analytical Results

7.4.1 Effects of Linear Wave Theory

Figure 7.43 shows the results of the analysis for the model arrangement relating to condition number 5, ie 6 lead washers per nodal connection and 16 washers at the top. The wave generated was 73mm high with period 0.83 seconds. The wave frequency response displacements at the top and middle are 68mm and 84mm, respectively, ie the ratio of mid to top displacement = 1.24.

Corresponding experimental displacements were 45mm and 65mm, respectively, (mid to top displacement ratio = 1.45). A transient oscillation, harmonic with the natural period in pitch, is just perceptible. A steady drift from the vertical of approximately 35mm is observed and this compares with an experimental observation of steady drift equal to approximately 50mm.

Figure 7.44 shows the analytical results for a 90mm wave with period 0.83 seconds for the same structural configuration. Top and middle displacements are 84mm and 100mm, respectively, (mid to top displacement ratio = 1.19) compared to experimental displacements of 67mm and 79mm, respectively, (mid to top displacement ratio = 1.17). The steady drift component is approximately 50mm compared to an experimental value of 90mm. The results concur qualitatively with the experimental results which display a decrease in the mid to top displacement ratio for increasing wave height.

++NEWMARK-WILSON-DATA++ALPHA= 0.25000E00 DELTA= 0.50000E00 THETA= 0.10E01 TIME STEP= 0.2500000E-01 SEC
TIP MASS 0.357E00 KG
+++DISTRIBUTED LOAD+++ WAVE HEIGHT= 0.730E-01METRES WAVE PERIOD= 0.8300E00SECONDS CM= 0.19E01 CD= 0.10E01
WATER DEPTH= 0.245E01METRES IBOT= 10 ITOP= 14 NO OF RISERS= 0 CURRENT VELOCITY= 0.500E-04 M/SEC
DEPTH OF WATER BALLAST= 0.183E01 METRES DEPTH OF CONCRETE BALLAST= 0.000E00 METRES
D1= 0.11200E00 TS1 0.25000E-02 D2= 0.11200E00 TS2= 0.25000E-02 D3= 0.95000E-02 TS3= 0.15000E-02
RKB= 0.211E01 RKG= 0.216E01 RATIO OF WT/BUOYANCY= 0.490E00
PERCENTAGE CRITICAL RAYLEIGH DAMPING= 0.250E01 LOWER COLUMN FLOODED GEOMETRIC STIFFNESS NOT INCLUDED
LEVER ARM FOR DECK MASS= 0.100E02METRES

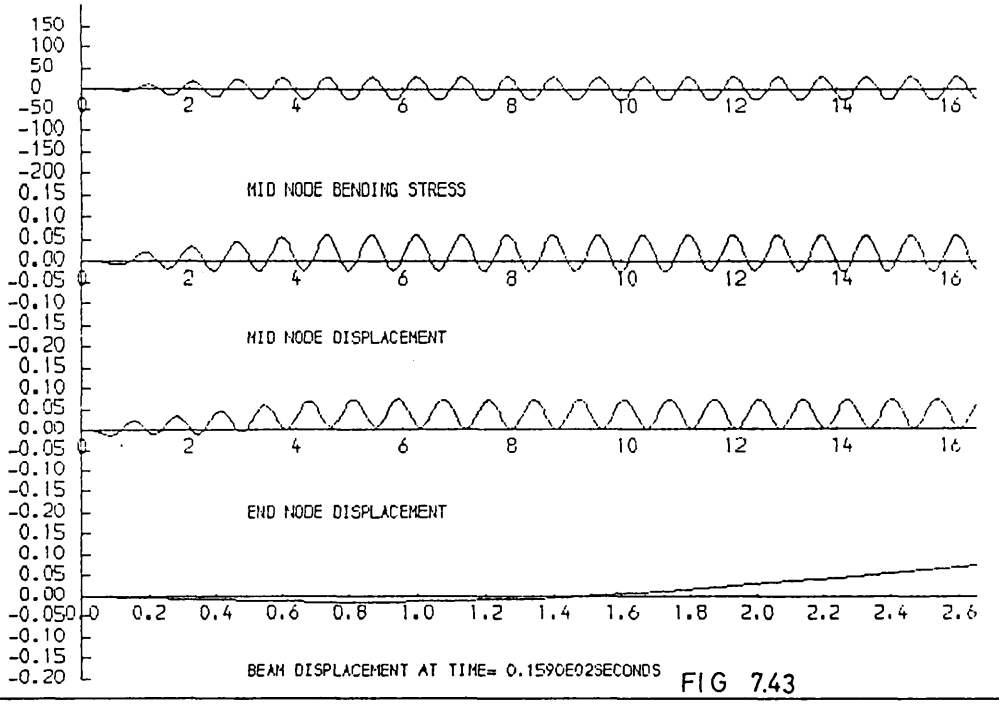

FIG 7.43

++NEWMARK-WILSON-DATA++ALPHA= 0.25000E00 DELTA= 0.50000E00 THETA= 0.10E01 TIME STEP= 0.2500000E-01 SEC
TIP MASS 0.357E00 KG
+++DISTRIBUTED LOAD+++ WAVE HEIGHT= 0.900E-01METRES WAVE PERIOD= 0.8300E00SECONDS CM= 0.19E01 CD= 0.10E01
WATER DEPTH= 0.245E01METRES IBOT= 10 ITOP= 14 NO OF RISERS= 0 CURRENT VELOCITY= 0.500E-04 M/SEC
DEPTH OF WATER BALLAST= 0.183E01 METRES DEPTH OF CONCRETE BALLAST= 0.000E00 METRES
D1= 0.11200E00 TS1 0.25000E-02 D2= 0.11200E00 TS2= 0.25000E-02 D3= 0.95000E-02 TS3= 0.15000E-02
RKB= 0.211E01 RKG= 0.216E01 RATIO OF WT/BUOYANCY= 0.490E00
PERCENTAGE CRITICAL RAYLEIGH DAMPING= 0.250E01 LOWER COLUMN FLOODED GEOMETRIC STIFFNESS NOT INCLUDED
LEVER ARM FOR DECK MASS= 0.100E02METRES

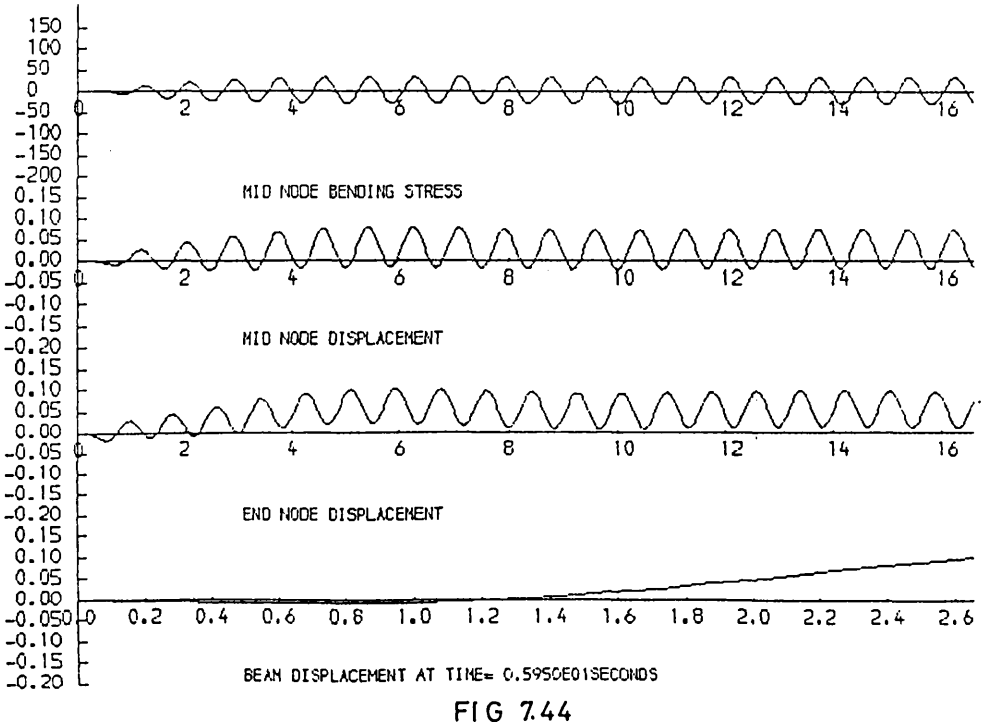

FIG 7.44

A general observation in regard to the phase of the response should be noted. The analytical model predicts that the maximum displacement at the top of the column lags the wave crest by approximately 30^{o}, ie the response lags the maximum forces by 120^{o}. The experimental observations would suggest that the response lags the maximum wave force by 90^{o} ie, the response is in phase with the wave crest. The small discrepancy in the analytical phase lag may occur if exciting frequencies are slightly different to natural frequencies and is not thought to be attributable to any other significant factor.

7.4.2 Effects of Stokes Fifth Order Waves

It is pertinent to examine the effects of Stokes' fifth order waves on the response since some of the waves considered are relatively steep, ie the 73mm wave is 50% of maximum steepness and the 95mm wave is 68% of maximum steepness. Particle velocities and accelerations for these waves are some 6-8% greater by Stokes' fifth order theory than by linear wave theory.

Figure 7.45 shows the result for the 73mm wave using Stokes's fifth order theory in the analysis. The transient oscillation is more pronounced at the start and is effectively damped out in time. The top displacement has increased to 74mm (9% greater than by the linear wave theory) and the middle displacement is the same.

Figure 7.46 shows the result for the 95mm wave using Stokes' theory. Again the transient is more pronounced to start and the steady drift has increased. Both the top and middle displacements are less than those as predicted using the linear wave theory, being 79mm and

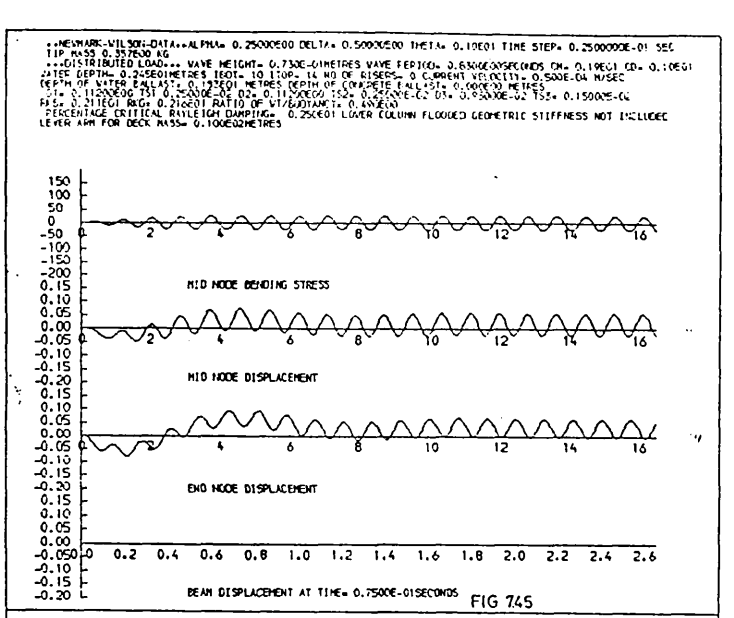

FIG 7.45

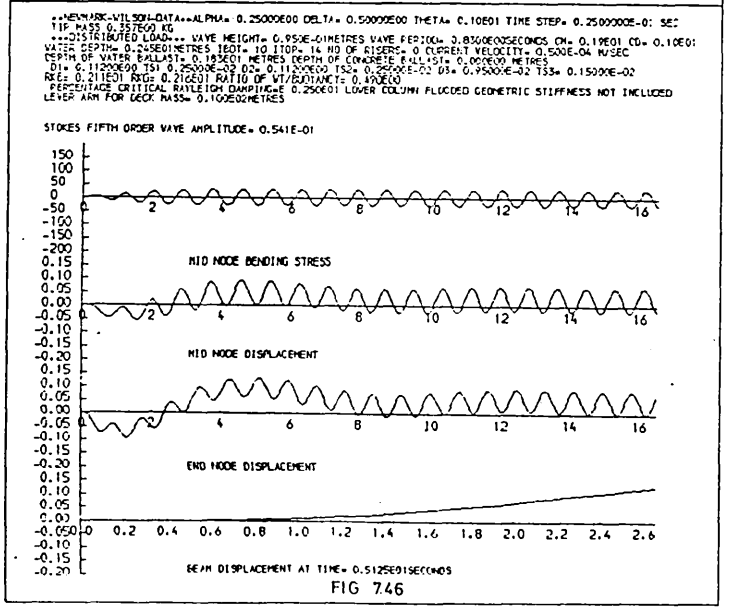

FIG 7.46

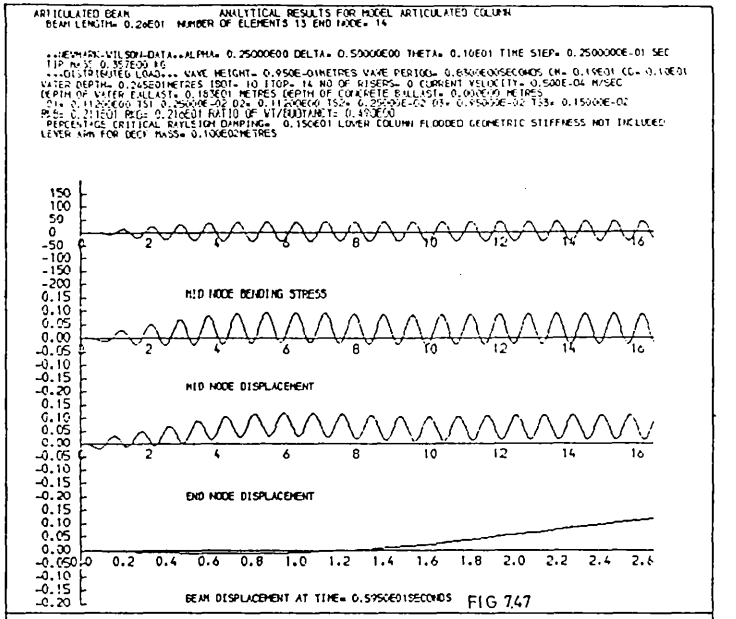

FIG 7.47

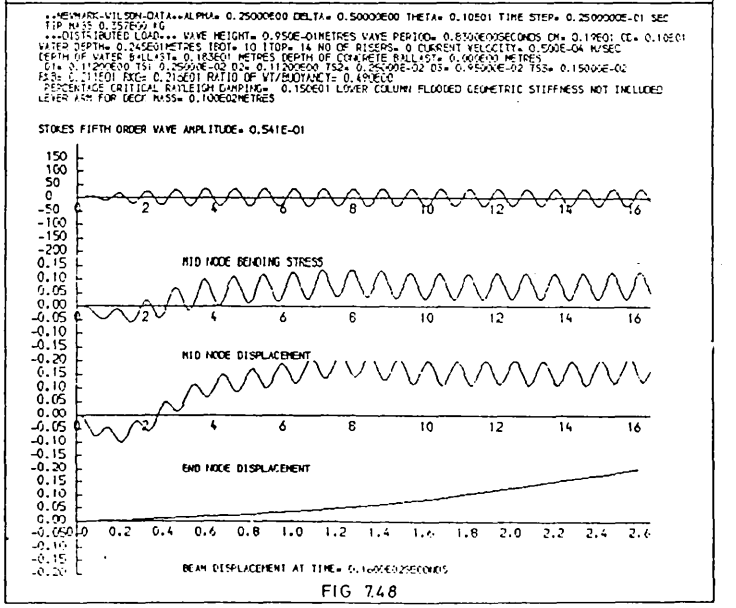

FIG 7.48

95mm, respectively. These values are greater than those obtained experimentally and are +13% for the top displacement and +26% for the middle displacement.

The effects of Rayleigh damping is illustrated by comparing fig. 7.43 which is for 2.5% of critical Rayleigh damping with fig. 7.47 which is for 1.5% critical damping. Both these results are for linear wave theory. The middle displacement has increased to 115mm, otherwise the results are very similar.

Figure 7.48 shows the result obtained for 1.5% critical damping using Stokes' fifth order wave theory. The transient is considerably increased as is the steady drift component which is now approximately 150mm. This is some 55% greater than the experimental steady drift. These results indicate that a value for critical Rayleigh damping of the order of 2% would produce analytical results similar in magnitude to the experimental value.

There is good qualitative agreement between the analytical results and those obtained experimentally in respect of top and middle displacements, transient oscillations, and steady drift components. Quantitatively, the errors decrease with increasing wave height and the best agreement is obtained using Stokes' fifth order wave theory.

The rate of increase of displacements is greater for fig. 7.38, ie condition 1, which is for the maximum mass at the top of the column. The rate of increase decreases as the mass at the top is reduced.

8. CONCLUDING REMARKS

The full finite element vibration analysis, in the time domain presented, highlights the harmonic vibration which may exist when the structure is excited with waves at the same frequency as the first resonant flexural mode frequency. The magnitude of stress levels is significant, in spite of the relatively small magnitude of the exciting forces involved.

The Newmark-Wilson integration operator with $\alpha = 1/2$ and $\delta = 1/4$ provides the most stable solution and the unsuitability of the Wilson-θ linear acceleration method for MDOF systems is noted. In appraising the results of any time incremental analysis the integration procedure used must be borne in mind. However, the results obtained are thought to be reasonable and the integration procedure used does not possess numerical damping.

Very small amounts of Rayleigh damping were shown to significantly affect the response but the uncertainties relating to the use of a realistic amount precludes the justified inclusion of larger amounts of damping.

The non-linear responses obtained as a consequence of the inclusion of the axial forces is particularly important and these indicated a 'threshold' level or a 'quasi' dynamic buckling load falling far short of the static critical Euler buckling load. This dynamic aspect of the buckling analysis clearly plays a very major role in the vibration analysis and, in part, poses the question of integration operator stability.

While different drag coefficients did not appear to influence the vibration responses noticeably, the current of 1 metre per second shifted the mean response as would be expected. The importance of including the viscous speed term is observed, particularly for the more slender structures, and the contribution of this term in producing the transient and steady drift responses is noted.

Relocation of deck masses did not have any marked effect on the forced vibratory response. Apart from increasing second and third mode frequencies, the advantages will be otherwise associated with improved statics, etc, as discussed in Chapters 2 and 4.

The attenuation in stress levels obtained for waves with frequencies less than the second mode vibration frequency are to be expected and confirms the transition from second mode vibration to fundamental mode vibration.

The monopile structure displayed modest reduction in the motion response compared to the articulated column. The resonant response at twice the frequency of the first flexural response mode is a significant observation and this resonant response can apparently be induced by waves with frequencies which have multiples greater than twice the first resonant flexural mode. This phenomenon is of particular concern as a possible source of dynamic instability.

The experimental data obtained, albeit for a structure with exaggerated mass distribution and flexural rigidity, correlates very well qualitatively with the analytical predictions. The prediction of the steady drift component in the response is noted and although different to the experimental value it is, nevertheless, an important observation.

The analysis presented calculates forces to the SWL and not to the instantaneous water surface which is assumed to be coincident with nodal connection point number 13 (see fig. 7.36). There is, therefore, no nett drag component of force entering into the calculation which might otherwise, in part, account for the steady drift. If the excursion of the structure in the wave was not accounted for the nett forces integrated over one wave cycle would be zero. This would infer that, after the initial transient had been damped out, the structure would oscillate about the vertical and not experience any second order drift effects (see fig. 7.25). However, the effect of the viscous speed squared term and its role in the transient and steady drift response was noted in section 6.3.6 and this will, in the main, explain the experimental and analytical prediction for the model. The excursion of the structure in the wave does make a contribution, albeit of a much reduced size, to that of the speed squared term.

The good qualitative agreement between experiment and theory vindicates the efficacy of the full vibration time series solution in the analysis of compliant structures in general and articulated columns in particular.

CHAPTER 8

CONCLUSIONS AND RECOMMENDATIONS

This study has addressed those aspects pertaining to the proposed use of articulated columns as production platforms, which are thought most likely to have a fundamental impact on the feasibility of the concept. At the same time, it has attempted to validate the use of time simulation methods to examine the non-linearities in response which play a major role in the design of compliant structures.

Conclusions have been given at the end of relevant chapters thoughout the work. These are of a very specific nature in relation to the contents of the chapter and, it is desirable to remark upon the main findings in a more general sense. In particular it is important to assess the inter-dependence of these and the way in which they work in combination to affect concept design feasibility.

As noted in Chapter 1, articulated columns have been used successfully for some time in a number of applications, mostly in connection with tanker moorings but for a few small oil field production platforms. In Chapter 2 the principal concepts relevant to production platforms were reviewed and it was shown that, potentially, the maximum benefit would be obtained from the use of the buoyancy chamber as accommodation for plant and machinery or as storage space. Through reduction in the height of the centre of gravity, this greatly reduces the constraints on the design of the deck and its support column. Containment of risers, etc within the lower column offers considerable advantages in respect of giving protection from wave and

impact loading as well as making inspection easier and safer. This feature is greatly enhanced when the lower column is designed to be watertight. Installation and relocation are feasible provided they are carefully planned at the design stage. The gravity type foundation reduces problems in that area and, indeed, at the removal stages upon completion of the production.

In Chapter 3 the evaluation of wave loads was assessed in the context of articulated columns. The way in which drift forces could be generated was also assessed, as was the importance of accounting for the forces up to the instantaneous water surface and in respect of structural displacements. The Morison approach to loading, incorporating the aforementioned features, is reasonable provided the ratio of D/L does not exceed about 0.2 and it provides a means by which the viscous drag relative speed squared term can be incorporated. This is of merit in the analysis of compliant structures in general and articulated columns in particular.

The rigid body dynamic analysis presented in Chapter 4 highlights the transient response which the time series analysis predicted. Experiments confirmed the phenomenon and it will have a major part to play in the design of the upper support column and the deck structure. Deck clearance requirements will obviously have to be assessed with the increased pitch in mind. It is also likely to feature as a primary consideration in respect of production and, where applicable, drilling activities. The transient phenomenon is damped out in time as expected. Two numerical procedures were used, ie direct integration and multi-step methods, and they produced essentially the same results so that confidence in the mathematical modelling was established.

The relationship between the transient and the viscous drag damping was noted, especially when waves superimposed on currents were examined. Non-linear wave theory had a marked effect on the response, and this, together with the effects of currents, exemplifies the need to account for viscous drag in the analysis. The assessment of the minimum deck clearance required must take all of these factors into account.

All possible sources of dynamic instabilities were examined and it was shown in Chapter 5 that several of these could give rise to Mathieu type and other instabilities. Again, viscous drag damping plays an important role and is an area for concern, since it will be of fairly low order at full scale Reynolds numbers. The time series analysis provides an efficient means of assessing the magnitude of the non-linear oscillations. The importance of heave forces and of the consistent time history approach in accounting for the instantaneous position of the structure in the waves was established.

As noted, fully operational production platforms are unlikely to experience Mathieu type instabilities as a consequence of first order wave excitation. However, other sources may exist and special attention has to be paid to the installation procedure to ensure that consequent pitch frequencies are sufficiently low. Harmonic resonant response instabilities brought on by specific wave groups were shown to produce large motions and clearly their possible existence in a seaway must be carefully assessed and allowed for. The versatility of the time series analysis in dealing with wave groups was demonstrated.

Having examimed the rigid body dynamic behaviour, attention

was directed towards other areas considered likely to give rise to problems. Hence, the examination of elastic vibration as presented in Chapters 6 and 7. The free vibration finite element analysis suggests that the first and second mode flexural vibration frequencies are likely to give cause for concern. The single most important parameter in this respect is the deck mass and it was shown that a substantial relocation to the buoyancy chamber greatly improved the vibration characteristics. This, albeit for different reasons, concurs with the findings in Chapter 2 where the advantages were related to static stability.

Vibration constraints mean that the thickness of the lower column is likely to be such that it can be designed to withstand the external water pressures. This is beneficial both from the point of view of access to risers, etc and in extending operational depths as well as reducing buoyancy chamber requirements. For a maximum payload of approximately 60,000KN, the circular cylindrical annular steel section investigated is feasible for maximum water depths of approximately 300 metres. At this depth the payload to structural weight ratio for the structure is of the order of 1.00 and this is competitive with alternative compliant structure concepts. The adequacy of the finite element method as a means of conducting parametric studies of the free vibration analysis of articulated columns has been demonstrated.

Although the advantages of using a circular cylindrical watertight section for the lower column are significant, there are obvious limitations as described. The alternative structural form for the lower column comprising a lattice structure of small diameter members has been shown to be very efficient in reducing the vibration

problems. This form of structure will also be lighter than the equivalent circular cylindrical section. However, the design and fabrication will be less straightforward but the lattice structure is established and should not present unsurmountable problems. Access to risers and the maintenance of these are the main disadvantages.

The existence of the non-linear behaviour as observed in the rigid body analysis, necessarily determined that a full vibration analysis in the time domain be undertaken for completeness. This analysis confirms the existence of non-linear behaviour attributable, in the main, to viscous drag. The non-linear behaviour was observed experimentally and also confirmed by the analysis and this vindicates the analytical method used, despite possible limitations in the use of the Morison approach to loading. The non-linear behaviour referred to is, again, the transient drift, which comprises a steady varying component harmonic with the fundamental pitch frequency and a steady drift component. The ability of the simplified Morison approach to predict such behaviour is attributed to the viscous drag component and a component which accounts for the instantaneous position of the structure in the wave, the latter having much less effect than the former.The full time simulation finite element analysis, highlights the non linear behaviour which must be carefully understood and demonstrates the adequacy of this approach.

The design of new concepts must be conservative and can only proceed with confidence when consideration has been given to all conceivable problem areas. The process must involve evaluation and re-evaluation to increase confidence limits in the adequacy of the work. Recommendations for future work must involve an element of hindsight; nevertheless it is consideed that attention to the

following recommendations will augment the work presented in this thesis.

The buoyancy chamber is of such central importance both from the static and dynamic points of view, that it is essential to make an assessment of possible uses. This can be achieved in a most effective manner by cultivating the interest and involvement of potential industrial operators. Also in this context it will be desirable to undertake further investigation of the optimisation procedure as suggested in Chapter 2. These together are likely to make an effective contribution, in that they will help to resolve problems in that area, thus allowing for greater concentration on other critical areas for design, such as the lower column.

Further analytical work in respect of waves, both linear and non-linear, and currents is needed in order to fully understand the viscous drag contribution. Experimental work will be of considerable merit and a means of simulating a steady current to act with waves should be sought. Some form of carriage traversing the length of the experimental tank is possible.

Resonant responses are an area of concern and more analytical work is necessary in assessing the possibility of wave groups in random seas. There are a number of ways of doing this in the time domain and this work should be complemented with experimental observations. It would also be beneficial to generate wave groups from two regular wave trains.

The circular cylindrical section as proposed for the lower column, will have advantages in respect of construction and

maintenance. However, as water depths increase beyond 280-300 metres, a more critical appraisal of the vibration will be necessary if the simple section is to be retained. It may be necessary to make a more rigorous assessment of wave loading and this may require a full diffraction and radiation analysis in the time domain. However, the importance of the visous drag term is noted and would need to be accounted for in any such analysis. More work is required in the analysis of lattice structures especially in the time domain. The nature of the construction may give rise to increased viscous drag forces and these have been shown to be important.

In respect of first flexural mode vibration response, it would be desirable to make an assessment of any non-linear inertia forces (63). These may arise as a consequence of the vertical displacement of structural elements as the column vibrates. This can readily be incorporated into the time simulation analysis. Further analysis of the role of the viscous drag term in first flexural responses is also recommended.

Finally, it is recommended that some attention be given to an alternative structure: the conventional guyed tower designs provide buoyancy support to a small percentage of the total weight of the structure, deriving most of its restoring stiffness from guy lines. It is believed that a structure with the desirable response characteristics of the guyed tower and the load bearing capacity of the articulated column is feasible. This structure would provide buoyancy support to a substantial proportion of the total weight and derive the remaining stiffness from attached guy lines. The dynamics of the guy lines would need to be incorporated but the time simulation analysis will readily accommodate this. Indeed, it would be necessary

to assess the dynamic behaviour of the guy lines to investigate resonant amplification of these.

APPENDIX 4.1

Derivation of recurrence relations for displacement, velocity and acceleration for the linear acceleration method.

Assuming that the acceleration $\ddot{\theta}$, of the column varies linearly over a series of time steps t_i, $t_i + \Delta t$, $t_i + 2\Delta t$

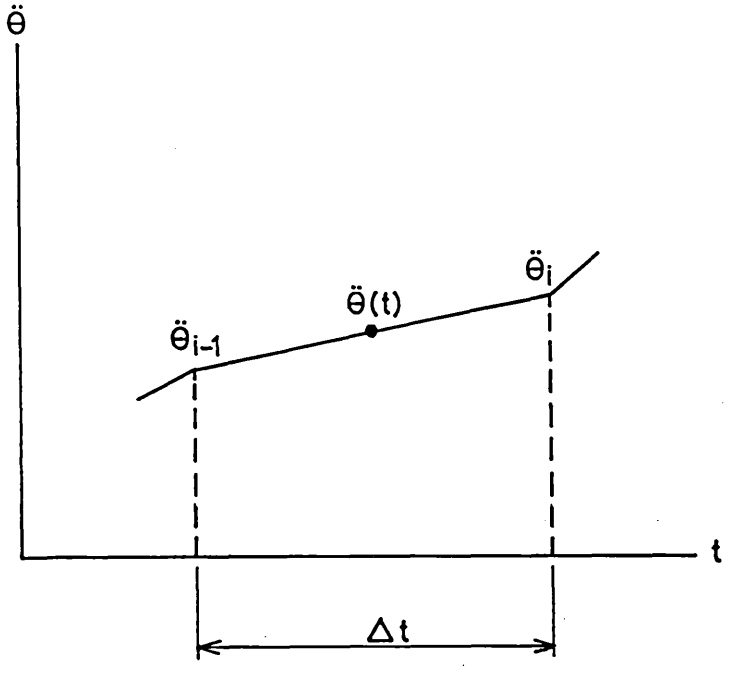

and if $\ddot{\theta}_i = \ddot{\theta}(t_i)$

then $\ddot{\theta}(t) = \ddot{\theta}_{i-1} + (\ddot{\theta}_i - \ddot{\theta}_{i-1}).\frac{t}{\Delta t}$, $t_{i-1} \leqslant t \leqslant t_i$

and integrating w.r.t. time

$$\dot{\theta}(t) = \ddot{\theta}_{i-1}.t+(\ddot{\theta}_i-\ddot{\theta}_{i-1}).\frac{t^2}{2\Delta t}+\dot{\theta}_{i-1}$$

and $$\theta(t)= \ddot{\theta}_{i-1}.\frac{t^2}{2}+(\ddot{\theta}_i-\ddot{\theta}_{i-1}).\frac{t^3}{6\Delta t}+\dot{\theta}_{i-1}.t+\theta_{i-1}$$

now let $t = \Delta t$

then

$$\dot{\theta}_i = \dot{\theta}_{i-1}+\frac{\Delta t}{2}(\ddot{\theta}_i+\ddot{\theta}_{i-1})$$

and $$\theta_i = \theta_{i-1}+\dot{\theta}_{i-1}.\Delta t+\frac{\Delta t^2}{6}(2\ddot{\theta}_{i-1}+\ddot{\theta}_i)$$

rewriting we have the expression for the acceleration

$$\ddot{\theta}_i = \frac{6}{\Delta t^2}(\theta_i-\theta_{i-1})-\frac{6}{\Delta t}.\dot{\theta}_{i-1}-2\ddot{\theta}_{i-1}$$

APPENDIX 4.2

The evaluation of wave particle kinematics by Stokes fifth order wave theory proceeds in accordance with the following definitions.

Results of Stokes Fifth Order Wave Theory.

Velocity potential, ϕ	$\frac{k\phi}{c} = \sum_{n=1}^{5} \phi'_n \cosh(nks) \sin(n\theta)$
Wave celerity, c	$\frac{c^2}{gd} = \frac{\tanh(kd)}{kd} [1 + \lambda^2 C_1 + \lambda^4 C_2]$
Surface elevation, η	$k\eta = \sum_{n=1}^{5} \eta'_n \cos(n\theta)$
Horizontal particle velocity, u	$\frac{u}{c} = \sum_{n=1}^{5} n\,\phi'_n \cosh(nks) \cos(n\theta)$
Vertical particle velocity, w	$\frac{w}{c} = \sum_{n=1}^{5} n\,\phi'_n \sinh(nks) \sin(n\theta)$
Horizontal particle acceleration, $\partial u/\partial t$	$\frac{\partial u/\partial t}{\omega c} = \sum_{n=1}^{5} n^2\,\phi'_n \cosh(nks) \sin(n\theta)$
Vertical particle acceleration, $\partial w/\partial t$	$\frac{\partial w/\partial t}{\omega c} = -\sum_{n=1}^{5} n^2\,\phi'_n \sinh(nks) \cos(n\theta)$
Temporal derivative of ϕ	$\frac{\partial\phi/\partial t}{c^2} = -\sum_{n=1}^{5} n\,\phi'_n \cosh(nks) \cos(n\theta)$
Pressure, p	$\frac{p}{\rho gd} = 1 - \frac{s}{d} - \frac{c^2}{gd}\left\{\frac{\partial\phi/\partial t}{c^2} + \frac{1}{2}\left[\left(\frac{u}{c}\right)^2 + \left(\frac{w}{c}\right)^2\right]\right\}$

where

$\phi'_1 = \lambda A_{11} + \lambda^3 A_{13} + \lambda^5 A_{15}$, $\phi'_2 = \lambda^2 A_{22} + \lambda^4 A_{24}$,
$\phi'_3 = \lambda^3 A_{33} + \lambda^5 A_{35}$, $\phi'_4 = \lambda^4 A_{44}$, $\phi'_5 = \lambda^5 A_{55}$,
$\eta'_1 = \lambda$, $\eta'_2 = \lambda^2 B_{22} + \lambda^4 B_{24}$, $\eta'_3 = \lambda^3 B_{33} + \lambda^5 B_{35}$,
$\eta'_4 = \lambda^4 B_{44}$, $\eta'_5 = \lambda^5 B_{55}$.

The coefficients A, B, C are known functions of kd only, given by Skjelbreia and Hendrickson

The equations to be solved simultaneously are:-

$$\frac{1}{kd}[\lambda + B_{33}\lambda^3 + (B_{35} + B_{55})\lambda^5] = \frac{H}{2d}$$

$$kd \tanh(kd)\,[1 + C_1\lambda^2 + C_2\lambda^4] = 4\pi^2 \frac{d}{gT^2}$$

Fifth order wave lengths usually lie somewhere between linear wave length and 1.2 times linear wave length; a suitable starting point for an iterative procedure would lie between these two limits.

Current m/s	0.25			0.5			0.75			1.00		
Cylinder Dia	R_e	f_s	T_s	R_e	f_s	T_s	R_e	f_s	T_s	R_e	f_s	T_s
4	1.10^6	0.0125	80	2.10^6	0.025	40	3.10^6	0.0375	26	4.10^6	0.05	20
6	$1.5.10^6$	0.0083	120	3.10^6	0.0167	60	$4.5.10^6$	0.025	40	6.10^6	0.033	30
8	2.10^6	0.0063	160	4.10^6	0.0125	80	6.10^6	0.018	53	8.10^6	0.025	40
10	$2.5.10^6$	0.005	200	5.10^6	0.01	100	$7.5.10^6$	0.015	67	10.10^6	0.02	50
20	$5.0.10^6$	0.0025	400	10.0^6	0.005	200	$15.0.10^6$	0.0075	133	20.10^6	0.01	100

R_e - Reynolds number f_s - vortex shedding freq (Hz) T_s - vortex shedding period (secs)

where $f_s = S_t U/D$ and S_t = Strouhal number

Table of Vortex Shedding Frequencies and Cylinder Diameter for (S_t = 0.2)

Table of vortex shedding frequencies for cylinders of varying diameter as a function of current velocity in metres per second, based on an average Strouhal number equal to 0.2.

APPENDIX 4.4

With reference to fig. 4.29; the X and Z axes are orthogonal and in the horizontal plane parallel to the sea bed. The motion of the column is considered in the θ plane YOP, which is defined by the angle θ and in the ψ plane XOZ, as shown. Rotations are, therefore, considered about the OY and OX axis, respectively.

The Lagrange equation for a system of forces can be written:-

$$\frac{\partial}{\partial t}\left(\frac{\partial L}{\partial \dot{q}}\right) - \frac{\partial L}{\partial q} = F_q$$

where $L = T - V$

and F_q = non-conservative forces

T = kinetic energy of system

V = potential energy of system (only conservative forces)

Consider an element of mass at a distance r_t from the articulation. It will have a velocity expressed in spherical co-ordinates equal to $(r_t^2.(\dot{\theta}^2 + \dot{\psi}^2 \sin^2\theta)$.

The kinetic energy of the element can be written, therefore, as:-

$$T = \tfrac{1}{2}m.r_t^2.(\dot{\theta}^2 + \dot{\psi}^2 \sin^2\theta)$$

$$= \tfrac{1}{2}.I.(\dot{\theta}^2 + \dot{\psi}^2\sin^2\theta)$$

The potential energy is given by, $V = -(1 - \cos\theta)mg$

and the Lagrangian is written as $L = T - V$

$$= \tfrac{1}{2}I(\dot{\theta}^2+\dot{\psi}^2\sin^2\theta) + mg(1 - \cos\theta)$$

applying Lagranges method by the differentiation of L with respect to θ, $\dot{\theta}$, ψ and $\dot{\psi}$ the equations of motion are derived.

$$I\ddot{\theta} - I\dot{\psi}^2 \sin\theta\cos\theta + K\sin\theta = M_\theta$$

and $$I\ddot{\psi}\sin^2\theta_t + 2I\dot{\psi}\dot{\theta}\sin\theta\cos\theta = M_\psi$$

where $K = (B_F.RKB - W.RKG)$

The $\dot{\psi}^2$ and the $\dot{\psi}\dot{\theta}$ part in the second term in each equation is attributed to a centrifugal and a coriolis component of force, respectively.

M_θ and M_ψ are the sums of moments about the OX^1 and OY axes, respectively. As for the SDOF system, the non-conservative moments are calculated using the modified form of the Morison equation to account for column motions.

Evaluation of Forces

Forces are evaluated on the basis that components normal to the axis of structure are relevant. Accordingly, the drag components are derived as follows assuming relative velocity of the structure and fluid.

Consider a current VC at an angle α to the X axis

$VC_x = VC\cos\alpha \quad VC_z = VC\sin\alpha \quad VC_y = 0$

The resultant velocity of current and wave particle velocities U_{res} is given by:-

$$U_{res} = \begin{Bmatrix} U + VC_x \\ V + VC_y \\ Z + VC_z \end{Bmatrix} \text{ where } z = 0.0$$

Components normal to the axis of the structure, U_{nx}, U_{ny} and U_{nz} are obtained by means of the transformation matrix,

$$A = \begin{bmatrix} (1 - C_x^2) & -C_xC_y & -C_xC_z \\ -C_xC_y & (1 - C_y^2) & -C_yC_z \\ -C_xC_z & -C_yC_z & (1 - C_z^2) \end{bmatrix}$$

where $C_x = \sin\theta\cos\psi$

$C_y = \cos\theta$

$C_z = \sin\theta\sin\psi$

ie $$\begin{Bmatrix} U_{nx} \\ U_{ny} \\ U_{nz} \end{Bmatrix} = A.U_{res}$$

the velocity of an element of the structure at a distance r from the articulation O is given by:-

$$\begin{Bmatrix} U_{cx} \\ U_{cy} \\ U_{cz} \end{Bmatrix} = r.B. \qquad \text{where } B = \begin{bmatrix} \cos\theta\sin\psi & \sin\psi\cos\psi \\ -\sin\theta & 0 \\ \cos\theta\cos\psi & -\sin\theta\sin\psi \end{bmatrix}$$

the relative normal velocity is then given by:-

$$U_{rx} = U_{nx} - U_{cx}$$

$$U_{ry} = U_{ny} - U_{cy}$$

$$U_{rz} = U_{nz} - U_{cz}$$

so that M_{DX}

$$M_{DY} = \tfrac{1}{2}\rho.r.D.C_D.|U_{rel}|(U_{rx},U_{ry},U_{rz})^T$$

M_{DZ}

where $U_{rel} = \sqrt{U_{rx}^2 + U_{ry}^2 + U_{rz}^2}$

The moments of inertia forces are then calculated as follows:-

$$M_{IX}, M_{IY}, M_{IZ} = \rho VC_M.A. \begin{Bmatrix} u \\ v \\ o \end{Bmatrix} .r.$$

The Fluid Added Mass moments of forces are calculated thus:-

$$M_{AX}, M_{AY}, M_{AZ} = \rho V.r.(C_M - 1) \begin{Bmatrix} a_{cx} \\ a_{cy} \\ a_{cz} \end{Bmatrix}$$

where a_{cx}, a_{cy} and a_{cz} are differentials with respect to time of the velocities of the structure as given by U_{cx}, U_{cy} and U_{cz}

ie $a_{cx} = [\ddot{\theta}\cos\theta\sin\psi + \ddot{\psi}\sin\theta\cos\psi - (\dot{\theta}^2 + \dot{\psi}^2)\sin\theta\sin\psi + 2\dot{\theta}\dot{\psi}\cos\theta\cos\psi]$

$a_{cy} = [\ddot{\theta}\sin\theta - \dot{\theta}^2\cos\theta]$

$a_{cz} = [\ddot{\theta}\cos\theta\cos\psi - \ddot{\psi}\sin\theta\sin\psi - (\dot{\theta}^2 + \dot{\psi}^2)\sin\theta\cos\psi - 2\dot{\theta}\dot{\psi}\cos\theta\sin\psi]$

the total moments of forces are then given by:-

$$M_{TX} = -M_{AX} + M_{IX} + M_{DX}$$
$$M_{TY} = -M_{AY} + M_{IY} = M_{DY}$$
$$M_{TZ} = -M_{AZ} = M_{IZ} = M_{DZ}$$

By vector analysis the moments in the θ and ψ directions are given by:-

$$M = \int_0^{di} C_y(M_{TX}\sin\psi + M_{TZ}\cos\psi) - M_{TY}\sin\theta).dr$$

and $$M = \int_0^{di} (C_Z M_{TX} - C_X M_{TZ})dr$$

these moments are substituted into the equations of motion which can then be solved incrementally.

APPENDIX 5.1

EVALUATION OF ADDED VIRTUAL MASS COEFFICIENTS IN THE CALCULATION OF HEAVE FORCES

Consider the disc as shown in fig. A5.1.

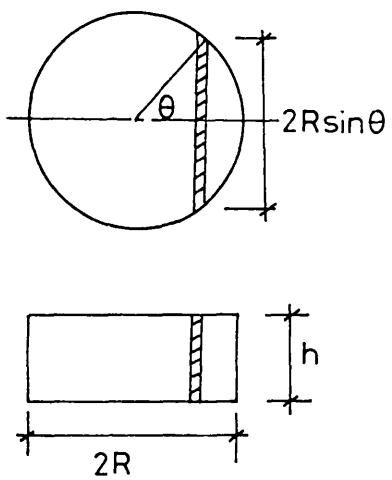

FIG A5.1

/

The added virtual mass of a strip of width δx and length $2R\sin\theta$ is equal to $\pi(R\sin\theta)^2 C_V \delta x$, where C_V is appropriate to an aspect ratio of $2R\sin\theta/h$.

By integrating, the added virtual mass for the complete disc may be written as:-

$$\text{Complete AVM} = 2\int_0^{\pi/2} \rho\pi C_V (R\sin\theta)^2 R d\theta . \sin\theta$$

C_V will be a function of θ and the evaluation of this integration can be made more staightforward by taking a mean aspect ratio for the whole disc of:-

$$\frac{\pi R^2}{2Rh} = \frac{\pi R}{2h}$$

The complete AVM is then written:-

$$AVM = 2 \int_{o}^{\pi/2} \rho\pi(R^3 \sin^3\theta) C_V . J . d\theta$$

where J = 0.635 and accounts for the 3-dimensionality of the flow.

Values of C_V as a function of the aspect ratio $\pi R/2h$ are obtained from fig.A5.2.

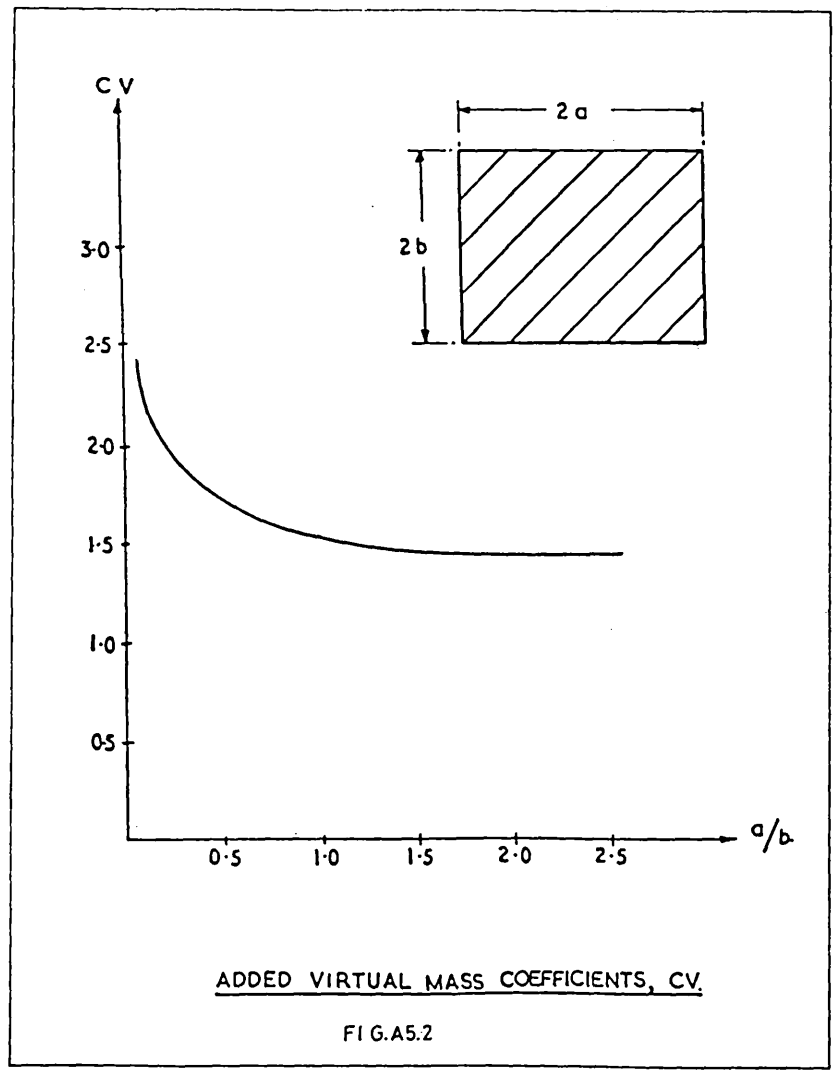

ADDED VIRTUAL MASS COEFFICIENTS, CV.

FIG.A5.2

RESULTS OF AUTHORS PROGRAM FOR EIGEN SOLUTION

```
****WARNING -70313 LIBRARY NOT ADDED WITH EXECUTE ACCESS BECAUSE ALREADY
 CE.5508, MAL:7FEFFB5
 ************************************************************************
**********

 INTERNAL DATA

 NUMBER OF NODES          :    3
NUMBE    R OF ELEMENTS     :    2
 NUMBER OF SUPPORT NODES  :    1
 MOD   US OF ELASTICITY :  210000000000.
 DENSITY :                   7850.0000

 NODAL COORDI   ATES
       NODE      X          Y
         1      0.00       0.00
         2      0.50       0.00
         3      1.00       0.00

 ELEMENT CONNECTIVITY AND PROPERTIES
    ELEMENT   ST   ART NODE  END NODE     AREA     M. OF INERTIA
         1          1          2  0.1000E-03  0.8330E-09
...
         2          2          3  0.1000E-03  0.8330E-09

 BOUNDARY CONDITION DATA
                          STATUS
                    (0:PRESCRIBED, 1:FREE)
       NODE          U          RZ
         1           0          1
```

[K] =

0.139944E+04	-0.419832E+04	0.699720E+03	0.000000E+00	0.000000E+00
-0.419832E+04	0.335866E+05	0.000000E+00	-0.167933E+05	0.419832E+04
0.699720E+03	0.000000E+00	0.279888E+04	-0.419832E+04	0.699720E+03
0.000000E+00	-0.167933E+05	-0.419832E+04	0.167933E+05	-0.419832E+04
0.000000E+00	0.419832E+04	0.699720E+03	-0.419832E+04	0.139944E+04

[M] =

0.934524E-03	0.607440E-02	-0.700893E-03	0.000000E+00	0.000000E+00
0.607440E-02	0.291571E+00	0.000000E+00	0.504643E-01	-0.607440E-02
-0.700893E-03	0.000000E+00	0.186905E-02	0.607440E-02	-0.700893E-03
0.000000E+00	0.504643E-01	0.607440E-02	0.145786E+00	-0.102798E-01
0.000000E+00	-0.607440E-02	-0.700893E-03	-0.102798E-01	0.934524E-03

-0.3196E-09 | 0.5364E+05 | 0.6944E+06 | 0.4095E+07 | 0.1384E+08 ← LAMBDA

0.1955E+01	0.6160E+01	-0.1504E+02	0.3307E+02	0.2511E+02
0.9775E+00	0.1340E+01	0.5472E+00	-0.1274E+01	0.4913E+00
0.1955E+01	-0.3053E+01	0.1340E+02	0.1211E+02	0.3202E+02
0.1955E+01	-0.2283E+01	-0.2308E+01	-0.2564E+01	0.3815E+01

..

0.1955E+01	-0.8994E+01	-0.1828E+02	-0.3748E+02	0.7830E+02

RESULTS OF COMPUTER PROGRAM FOR EIGEN SOLUTION BY DR M^{c}NAMEE (GLASGOW UNIV)

```
 DFLINR

 MATRIX A
```

0.13994D+04	-.41983D+04	0.69972D+03	0.00000D+01	0.00000D+01
-.41983D+04	0.33587D+05	0.00000D+01	-.16793D+05	0.41983D+04
0.69972D+03	0.00000D+01	0.27989D+04	-.41983D+04	0.69972D+03
0.00000D+01	-.16793D+05	-.41983D+04	0.16793D+05	-.41983D+04
0.00000D+01	0.41983D+04	0.69972D+03	-.41983D+04	0.13994D+04

= [K]

```
 MATRIX B
```

0.93452D-03	0.60744D-02	-.70089D-03	0.00000D+01	0.00000D+01
0.60744D-02	0.29157D+00	0.00000D+01	0.50464D-01	-.60744D-02
-.70089D-03	0.00000D+01	0.18691D-02	0.60744D-02	-.70089D-03
0.00000D+01	0.50464D-01	0.60744D-02	0.14579D+00	-.10280D-01
0.00000D+01	-.60744D-02	-.70089D-03	-.10280D-01	0.93452D-03

= [M]

```
 EIGENSOLUTION    1
 LAMBDA       0.13842D+08
 EIGENVECTOR
     0.28433D+00
     0.55621D-02
     0.36256D+00
     0.43189D-01
     0.88644D+00

 EIGENSOLUTION    2
 LAMBDA       0.40950D+07
 EIGENVECTOR
     0.64197D+00
    -0.24728D-01
     0.23514D+00
    -0.49789D-01
    -0.72766D+00

 EIGENSOLUTION    3
 LAMBDA       0.69441D+06
 EIGENVECTOR
     0.55099D+00
    -0.20041D-01
    -0.49071D+00
     0.84518D-01
     0.66939D+00

 EIGENSOLUTION    4
 LAMBDA       0.53636D+05
 EIGENVECTOR
     0.52987D+00
     0.11524D+00
    -0.26257D+00
    -0.19635D+00
    -0.77360D+00

 EIGENSOLUTION    5
 LAMBDA       0.38217D-01
```

Results of independent programs for the solution of the eigenvalue equation for an articulated beam with 2 elements, 3 nodes and 2 d.o.f per node

APPENDIX 7.1

EXPERIMENTAL TEST RESULTS FOR ELASTIC VIBRATION OF MODEL ARTICULATED COLUMN

Wave Freq (Hz)	Ht (mm)	Top Displ	Mid Displ	Ratio (Mid/Top)	Steady Drift Top
TEST CONDITION 1					
4 Washers per node plus 17 on top. Freq 1.3Hz					
1.3 2V	14	5	13.3	2.66	3.48
1.3 3V	30	10.34	25.8	2.49	6.89
1.3 4V	47	19.8	39.58	1.99	17.2
1.3 5V	58	24.13	47.5	1.96	27.5
1.3 6V	60	25.0	50.0	2	37.93
1.3 7V	70	30.17	56.66	1.878	44.8
1.3 8V	80	31.03	60.83	1.96	51.7
TEST CONDITION 2					
5 Washers per node plus 18 on top. Freq 1.22Hz					
1.22 3V	33,33	8.33	25.6	3.07	5.17
1.22 4V	46.67	14.16	35.3	2.49	8.6
1.22 5V	60.0	20.0	45.0	2.25	23.27
1.22 6V	68.33	20.0	46.55	2.32	27.5
1.22 7V	76.67	26.67	55.08	2.06	34.48
1.22 8V	85.00	30.0	61.29	2.04	44.8
TEST CONDITION 3					
6 Washers per node plus 16 on top. Freq 1.18Hz					
1.18 3V	33.3	9.16	23.6	2.57	5
1.18 4V	46.67	15.83	35.25	2.23	12.5
1.18 5V	65.0	23.33	48.0	2.05	26.6
1.18 6V	70.0	30.83	54.75	1.77	30.0
1.18 7V	78.33	33.33	60.0	1.8	43.3
1.18 8V	86.67	34.16	66.0	1.93	60.0
TEST CONDITION 4					
7 Washers per node plus 17 on top. Freq 1.175Hz					
1.15	17				0
1.2	16				5.0
1.155	16				5.0
1.175	20	16/10	24/22	1.5	7.0
1.175	30	22/18	36/36	1.63	10.0
1.175	40	24/20	42/39	1.75	12.0
1.175	50	32/28	53/50	1.65	20.0
1.175	62	40/40	66/65	1.65	32.0

REFERENCES

1. 'The Challenge Offshore', Shell Briefing Service, Number One, 1983.

2. MILLER, N S and FAULKNER, D, 'The Development of the Offshore Engineering Industry in UK and Europe', University of Glasgow, Dept of Naval Architecture and Ocean Engineering, Report No NAOE-83-25, 1983.

3. PARKINSON, S T, and SAREN, M A, 'Offshore Technology: A Forecast and Review', Financial Times Business Information, 1981.

4. HALL, J E, and MANUEL, W S, 'Subsea and Process Controls for the Cadlao Floating Production System', OTC 4515, 1983.

5. PANICKER, N N, and YANCEY, I R, Deepwater Production Riser', OTC 4512, 1983.

6. FAULKNER, D, 'Design and Construction Concepts for Compliant Production Platforms in Exposed Deep Water Sites', WEMT, 1984.

7. BELLON de CHASSEY, C, FRANKHAUSER, H S and PICARD, J, 'Various Uses for the Articulated Column ELFOCEAN, A New Concept', OTC 1392, 1971.

8. NICHOLS, J H, and WESTBY, K A, 'Innovative Engineering Makes Maureen a Reality', European Offshore Petroleum Conf and Exhibition, EUR 231, 1980.

9. 'Statfjord C Output Shuttled to Shore', Offshore, Nov 84.

10. 'Offshore Engineer', p11, Feb 79; p10, Mar 79; p133/134, Apr 84.

11. 'Gravity Base SALS at Tazerka', Petroleum Engineer International, Oct 83.

12. TARTERA, M, DUMAZY, C, and DUPORT, B, 'Articulated Columns: The Key to Deep Water Development', World Oil, Jul 81.

13. SMITH, J R, and TAYLOR, R S, 'The Development of Articulated Buoyant Column Systems as an Aid to Economic Offshore Production', EUR 266, 1980.

14. FINN, L D, 'A New Deepwater Offshore Platform', OTC 2688, 1976.

15. OLBJORN, E H, and FOSS, I, 'Certification of New Concepts', Ocean Management, 1981.

16. BAKER, M J, PARKINSON, S T, and SAREN, M A, 'Offshore Inspection and Maintenance', Financial Times Limited, International Management Report, 1978

17. NEWMAN, J N, 'Marine Hydrodynamics', MIT Press, Camb, Mass, 1977.

18. PINKSTER, J A, 'Mean and Low Frequency Wave Drift Forces', Ocean Engineering, Vol 6, 1979.

19. DRAKE, K R, EATOCK-TAYLOR, R, and MATSUI, T, 'The Drift of an Articulated Column in Waves', University College London, Dept of Mech Eng Report, 1982.

20. KIRK, C L, and JAIN, R K, 'Response of Articulated Towers to Waves and Current', OTC 2798, 1977.

21. KIRK, C L, and JAIN, R K, 'The Dynamic Response of Double Articulated Offshore Loading Structure to Non-Colinear Waves and Current', Applied Mech Engrg Conf, Yale University, 1977.

22. KIRK, C L, 'Approximate Dynamic Analysis of Single Anchor Leg Storage System', Ocean Engineeering, 1984.

23. CHAKRABARTI, S K, and COTTER, D C, 'Transverse Motion of Articulated Tower', Jour of the Waterway, Port, Coastal and Ocean Div, WW1, Feb 80.

24. RAINEY, R C T, 'The Dynamics of Tethered Platforms', RINA Spring Meetings, 1977.

25. RICHARDSON, J R, 'Mathieu Instabilities and Response of Compliant Offshore Structures', NMI Report R49, 1979.

26. BISHOP, R E D, and PRICE, W G, 'Hydroelasticity of Ships', Cambridge, pp388-407, 1978.

27. HAVERTY, K F, McNAMARA, J F, and MORAN, B, 'Finite Dynamic Motions of Articulated Offshore Loading Towers', IMT 82, 110/01, 1982.

28. EATOCK-TAYLOR, R, DRAKE, K R and DUNCAN, P C, 'The Dynamics of a Flexible Articulated Column in Waves', Eng Structures, Vol 5, 1983.

29. VINCKEN, L M J, 'Design Philosophy of Floating Production Systems - Status and Future Trends', Shell International Petroleum, T-II/13, 1980.

30. 'Planning, Designing and Constructing Fixed Offshore Platforms, API, 1981.

31. 'Modern Production Risers', Petroleum Engineer International, Oct 80 on.

32. 'Modern Production Risers - Part 8', PEI, May 81.

33. 'Rules for the Design, Construction and Inspection of Offshore Structures', DnV, 1977.

34. SMITH, E,'On Nonlinear Random Vibrations', Norwegian Inst of Technology, Trondheim, Report No 78-3, Nov 78.

35. CHEN, P W, and ROBERTSON, L E, 'Human Perception Threshold of Horizontal Motion', ASCE, Jour of Structural Div, Aug 82.

36. SCHUMANN, E, 'Criteria for Human Reaction to Environmental Vibration on Naval Ships', DTNSRDC.

37. SARPKAYA, T and ISAACSON, M, 'Mechanics of Wave Forces on Offshore Structures', Van Nostrand, pp259/260, 1981.

38. McCAMY, R C and FUCHS, R A, 'Wave Forces on a Pile', Tech Memo 69, US Army Corps of Engineers, Beach Erosion Board, 1954

39. MORISON, J R, O'BRIEN, M P, JOHNSON, J W and SCHAAF, S A, 'The Force Exerted by Surface Waves on Piles', Petroleum Trans 189, 1950.

40. GARRISON, C J, 'Hydrodynamic Loading of Large Offshore Structures', Numerical Methods in Offshore Engineering, Wiley, 1979.

41. LIGHTHILL, J, 'Waves and Hydrodynamic Loading', BOSS 1979.

42. KEULEGAN, G H and CARPENTER, L H, 'Forces on Cylinders and Plates in Oscillatory Fluid', Jour of Research of NBS, Vol 60, No 5, May 58.

43. SARPKAYA, T, 'Vortex Shedding and Resistance in Harmonic Flow About Smooth and Rough Cylinders at High Reynolds Numbers', Report NPS-59SL76021, Naval Postgraduate School, CA, 1976.

44. SARPKAYA, T and ISAACSON, M, 'Mechanics of Wave Forces on Offshore Structures', Van Nostrand, p315, 1981.

45. STANDING, R G, DACUNHA, N M C, and MATTEN, R B, 'Mean Wave Drift Forces: Theory and Experiment', NMI, R124, 1981.

46. HAVELOCK, T H, 'The Drifting Forces on a Ship Among Waves', Phil Magazine, Vol 33, pp467-475, 1942.

47. MALHOTRA, A K and PENZIEN, J, 'Nondeterministic Analysis of Offshore Structures', ASCE, Jour of Engrg Mechs Div, Vol 93, EM6, Dec 70.

48. LAMBERT, J D, 'Computational Methods in Ordinary Differential Equations', Wiley, 1973.

49. CLOUGH, R W and PENZIEN, J, 'Dynamics of Structures', McGraw-Hill, 1982.

50. INOUE, Y, 'Slowly Varying Oscillations of Moored Vessels', BOSS, 1976.

51. KOKKINOWRACHOS, K and MITZLAFF, A, 'Dynamic Analysis of One and Multi-Column Articulated Structures', Symp Hydrodynamics in Ocean Engineering, Trondheim, 1981.

52. OGIHARA, K, 'Theoretical Analysis of the Transverse Motion of a Buoy by Surface Waves', Coastal Engineering, 1978.

53. HOGBEN, N and STANDING, R G, 'Experience in Computing Wave Loads on Large Bodies', OTC 2189, 1975.

54. SKJELBRIA, L and HENDRICKSON J,'Fifth Order Gravity Wave Theory and Tables of Functions', National Engrg Science Co, 1962.

55. LeMEHAUTE, B, 'An Introduction to Hydrodynamics and Water Waves', Springer Verlag, Dusseldorf, 1976.

56. EBBESMEYER, C C, 'Fifth Order Stokes Wave Profiles', Jour Waterways, Harbors and Coastal Eng Div, Vol 100, No WW3, pp264-265, 1974.

57. OHMART, R D and GRATZ, R C, A Comparison of Measured and Predicted Ocean Wave Kinematics', OTC 3276, 1978.

58. PEREGRINE, D H, 'Interaction of Water, Waves and Currents', Advances in Applied Mechanics, Academic Press, NY, Vol 16, pp9-117, 1976.

59. BISHOP, R E D and HASSAN, A Y, 'The Lift and Drag Forces on a Circular Cylinder Oscillating in a Flowing Fluid', Proc RS, London, Vol 277A, pp51-76, 1964.

60. BEARMAN, P W and CURRIE, I G, 'Pressure Fluctuation Measurements on an Oscillating Cylinder', Jour Fluid Mechs, Vol 91, Part 4, pp661-677, 1979.

61. WELLS, D A, 'Lagrangian Dynamics - Theory and Problems', McGraw-Hill, 1967.

62. 'NAG Mark 9 Manual, Numerical Algorithms Group Ltd, 1981.

63. BOLOTIN, V V, 'The Dynamic Stability of Elastic Systems', Holden-Day, 1964.

64. Ocean Industry Article, p58, Jan 76.

65. PINKSTER, J A, 'Low Frequency Second Order Wave Exciting Forces on Floating Structures', PhD Thesis, 1980.

66. ZIENKIEWITZ, O C, 'The Finite Element Method in Engineering Science', McGraw-Hill, 1971.

67. RAO, S S, 'The Finite Element Method in Engineering', Pergamon Press, 1982.

68. DESAI, C S and ABEL, J F,'Introduction to the Finite Element Method', Van Norstrand, 1972.

69. SEBASTIANI, G and BRANDI, R, 'Design of a New Concept of Single Point Mooring for Very Deep Water', OTC 4350, 1982.

70. PARUZZOLO, A and BUSETTO, G, 'The Monopile Deepwater Offshore Loading System. Theoretical Analysis versus Model Tests', 2nd Intl Symp Ocean Engrg and Ship Handling, Gothenburg, 1983.

71. RODNIGHT, T V, 'New Generation of Semis Improves Offshore Drilling Operations', Petroleum Engrg Intl, Oct 81.

72. WILSON, E L, FARHOOMAND, I and BATHE, K J, 'Non-linear Dynamic Analysis of Complex Structures', Intl Jour of Earthquake Engineering and Structural Dynamics 1, pp241-252, 1973.

73. McNAMARA, J F, 'Solution Schemes for Problems of Nonlinear Structural Dynamics', ASME, Paper No 74-PVP-30, Jul 74.

74. HUGHES, T J R and BELYTSCHKO, T, 'A Precis of Developments in Computational Methods for Transient Analysis', Jour of Applied Mechs, Vol 50, Dec 83.

75. McNAMARA, J F and MARCAL, P V, 'Incremental Stiffness for Finite Element Analysis of Non-Linear Dynamic Problems', Numerical and Computer Methods in Structural Mechanics, Academic Press, NY, pp353-376, 1973.